AD-A138 100 INVESTIGATION OF SHEATH PHENOMENA IN ELECTRONEGATIVE GLOW DISCHARGES(U) AIR FORCE INST OF TECH WRIGHT-PATTERSON AFB OH SCHOOL OF ENGINEERING G L DUKE 1/3

UNCLASSIFIED DEC 83 AFIT/DS/PH/83-6 F/G 20/3 NL

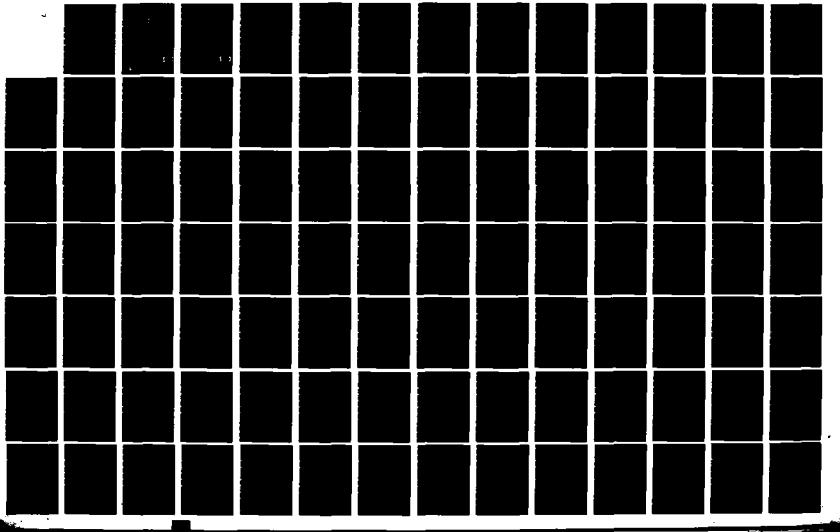

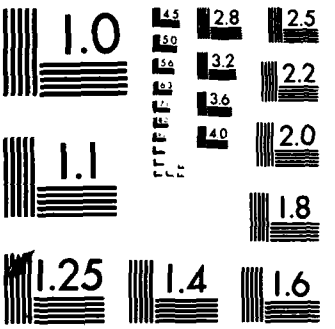

MICROCOPY RESOLUTION TEST CHART
NATIONAL BUREAU OF STANDARDS-1963-A

(1)

AIR FORCE INSTITUTE OF TECHNOLOGY

AIR UNIVERSITY
UNITED STATES AIR FORCE

INVESTIGATION OF SHEATH PHENOMENA IN

ELECTRONEGATIVE GLOW DISCHARGES

DISSERTATION

AFIT/DS/PH/83-6

Gary L. Duke
Captain USAF

SCHOOL OF ENGINEERING

WRIGHT-PATTERSON AIR FORCE BASE, OHIO

AFIT/DS/PH/83-6

INVESTIGATION OF SHEATH PHENOMENA IN ELECTRONEGATIVE GLOW DISCHARGES

DISSERTATION

AFIT/DS/PH/83-6

Gary L. Duke
Captain USAF

Approved for public release; distribution unlimited

REPORT DOCUMENTATION PAGE

1a. REPORT SECURITY CLASSIFICATION UNCLASSIFIED	1b. RESTRICTIVE MARKINGS NONE
2a. SECURITY CLASSIFICATION AUTHORITY	3. DISTRIBUTION/AVAILABILITY OF REPORT Approved for public release; distribution unlimited
2b. DECLASSIFICATION/DOWNGRADING SCHEDULE	
4. PERFORMING ORGANIZATION REPORT NUMBER(S)	5. MONITORING ORGANIZATION REPORT NUMBER(S)
6a. NAME OF PERFORMING ORGANIZATION Air Force Institute of Technology 6b. OFFICE SYMBOL (If applicable)	7a. NAME OF MONITORING ORGANIZATION
6c. ADDRESS (City, State and ZIP Code) AFIT/EN Wright-Patterson AFB, OH 45433	7b. ADDRESS (City, State and ZIP Code)
8a. NAME OF FUNDING/SPONSORING ORGANIZATION AF Aero Propulsion Laboratory 8b. OFFICE SYMBOL (If applicable)	9. PROCUREMENT INSTRUMENT IDENTIFICATION NUMBER
8c. ADDRESS (City, State and ZIP Code) AFWAL/POOC-3 Wright-Patterson AFB, OH 45433	10. SOURCE OF FUNDING NOS. PROGRAM ELEMENT NO.: 61102F PROJECT NO.: 2301 TASK NO.: S2 WORK UNIT NO.: 12
11. TITLE (Include Security Classification) Investigation of Sheath Phenomena in Electronegative Glow Discharges	
12. PERSONAL AUTHOR(S) Duke, Gary L., Capt, USAF	
13a. TYPE OF REPORT Dissertation 13b. TIME COVERED FROM _____ TO _____	14. DATE OF REPORT (Yr., Mo., Day) 1983 December 15. PAGE COUNT 218
16. SUPPLEMENTARY NOTATION	Approved for public release: IAW AFR 190-17. LYNN E. WOLAVER 7 Feb 84 Dean for Research and Professional Development Air Force Institute of Technology (AIC)

17. COSATI CODES			18. SUBJECT TERMS (Continue on reverse if necessary and identify by block number)
FIELD	GROUP	SUB. GR.	
20	9	4	Anode Fall, Argon, Attachment, Boltzmann Transport Equation,
20	3	2-6	Cathode Fall, Cathode Fall Voltage, Cathode Fall Length, Drift Velocity, Electron Kinetics, Electronegative Gas,

19. ABSTRACT (Continue on reverse if necessary and identify by block number)

Two different methods of analyzing the cathode fall region of low pressure glow discharges were developed and applied to three different electronegative gas mixtures. One method was based on a self-consistent numerical solution to Poisson's equation, the current continuity equations for electrons and negative ions, and the current conservation equation. This method assumes the electrons are always in equilibrium with the electric field. The other method was based on a self-consistent numerical solution of the Boltzmann transport equation for electrons, Poisson's equation, and the current conservation equation. This method allows the electrons not to be in equilibrium with the field. Comparing these two methods revealed that nonequilibrium prevails throughout the cathode fall region.

The electronegative gas mixtures investigated were small concentrations (less than 10%) of hydrogen chloride in helium, argon, or xenon. The electric field, Townsend ionization and attachment coefficients, electron and negative ion current densities, and electron, positive ion, and negative ion number densities are plotted as functions of

20. DISTRIBUTION/AVAILABILITY OF ABSTRACT UNCLASSIFIED/UNLIMITED ☐ SAME AS RPT. ☒ DTIC USERS ☐	21. ABSTRACT SECURITY CLASSIFICATION UNCLASSIFIED
22a. NAME OF RESPONSIBLE INDIVIDUAL Gary L. Duke, Capt, USAF	22b. TELEPHONE NUMBER (Include Area Code) (513) 255-2168 22c. OFFICE SYMBOL AFWAL/POCE

Item 18. Equilibrium, Glow Discharge, Helium, Hydrogen Chloride, Ionization, Negative Ion, Nonequilibrium, Poisson's Equation, Self-consistent, Similarity Rules, Sheath, Xenon

Item 19. distance through the cathode fall region. Discharge current densities, cathode fall lengths, and voltages are compared to other theoretical and experimental data through a scaling relationship. The experimentally observed contraction of the cathode fall length in electronegative gases with helium as a buffer is described and not predicted for argon or xenon mixtures. Other regions such as the negative glow and anode fall are also briefly discussed.

AFIT/DS/PH/83-6

INVESTIGATION OF SHEATH PHENOMENA IN ELECTRONEGATIVE GLOW DISCHARGES

DISSERTATION

Presented to the Faculty of the School of Engineering
of the Air Force Institute of Technology
Air University
in Partial Fulfillment of the
Requirements for the Degree of
Doctor of Philosophy

by
Gary L. Duke, B.A., M.S.
Capt USAF

AFIT/DS/PH/83-6

INVESTIGATION OF SHEATH PHENOMENA IN ELECTRONEGATIVE GLOW DISCHARGES

by

Gary L. Duke, B.A., M.S.
Captain USAF

Approved:

Allan Gerscadden.	7th Dec, 1983
Chairman	
John Jones Jr.	8 Dec, 1983
Michael Stamm	8 DEC 1983
Lillian F. Bailey	8 Dec., 1983

Accepted:

J S Przemieniecki	9 Dec. 1983
Dean, School of Engineering	

Preface

Glow discharges have a wide variety of applications such as in excimer lasers, thyratrons, or in plasma reactors for the deposition of thin films or for plasma etching. Many of these discharges of current interest now contain reactive electronegative gases. It is hoped that this study has provided a better understanding of the cathode fall region and the influence of attachment within this region.

A number of people have provided guidance and encouragement to me during the course of this study. In particular, thanks are given to: Dr Alan Garscadden for his patience and many critical discussions; the other members of my committee, Lt Col William Bailey, Maj Michael Stamm, and Dr John Jones for insuring a quality and administratively correct document; Colonels George Strand (ret) and James Johnson for their encouragement and the time they gave me to pursue my research and to put this document together; Marge Phillips and Rita Jackson, two excellent typists; Bill Bateson for assistance in plotting the graphs; and especially my wife Mary and sons Brian and Eric, who helped me keep my perspective throughout the ordeal.

Gary L. Duke

Contents

Contents (Continued)

List of Figures

List of Figures (cont.)

List of Figures (cont.)

List of Tables

Abstract

Two different methods of analyzing the cathode fall region of low pressure glow discharges were developed and applied to three different electronegative gas mixtures. One method was based on a self-consistent numerical solution to Poisson's equation, the current continuity equations for electrons and negative ions, and the current conservation equation. This method assumes the electrons are always in equilibrium with the electric field. The other method was based on a self-consistent numerical solution of the Boltzmann transport equation for electrons, Poisson's equation, and the current conservation equation. This method allows the electrons not to be in equilibrium with the field. Comparing these two methods revealed that nonequilibrium prevails throughout the cathode fall region.

The electronegative gas mixtures investigated were small concentrations (less than 10%) of hydrogen chloride in helium, argon, or xenon. The electric field, Townsend ionization and attachment coefficients, electron and negative ion current densities, and electron, positive ion, and negative ion number densities are plotted as functions of distance through the cathode fall region. Discharge current densities, cathode fall lengths, and voltages are compared to other theoretical and experimental data through a scaling relationship. The experimentally observed contraction of the cathode fall length in electronegative gases with helium as a buffer is described and not predicted for argon or xenon mixtures. Other regions such as the negative glow and anode fall are also briefly discussed.

Chapter I. Introduction

Introduction and Definition of Terms

An understanding of the role of negative ions in low pressure gas discharges is important in several fields such as electric discharge lasers, high power switches, and plasma deposition of thin films. Discharges such as these which contain negative ion densities in addition to the usual electron and positive ion densities are termed electronegative discharges. They are so named since the attaching gas yielding negative ions is referred to as an electronegative gas. Discharges containing only electrons and positive ions are termed electropositive discharges.

Both types of discharges are characterized by the distinctive luminous and dark regions shown in Fig I-1. The actual position of the various regions depends upon the gas or gas mixture, pressure, and current or voltage across the discharge. Starting at the cathode there is sometimes visible a very narrow dark space termed Aston's dark space followed by a feeble layer of light called the cathode glow. However, the term cathode glow often includes the total region from the cathode to the beginning of the negative glow. The region between the cathode glow and negative glow is not totally dark, but only appears so to the eye in comparison to its luminous neighboring regions and is termed the cathode dark space. The negative glow is probably the most luminous region of the discharge. A sharp luminous boundary exists with the cathode nonluminous space, but the boundary on the anode side is diffuse and gradually grows dimmer as it merges into the relatively dark Faraday dark space. This is normally followed by a long luminous

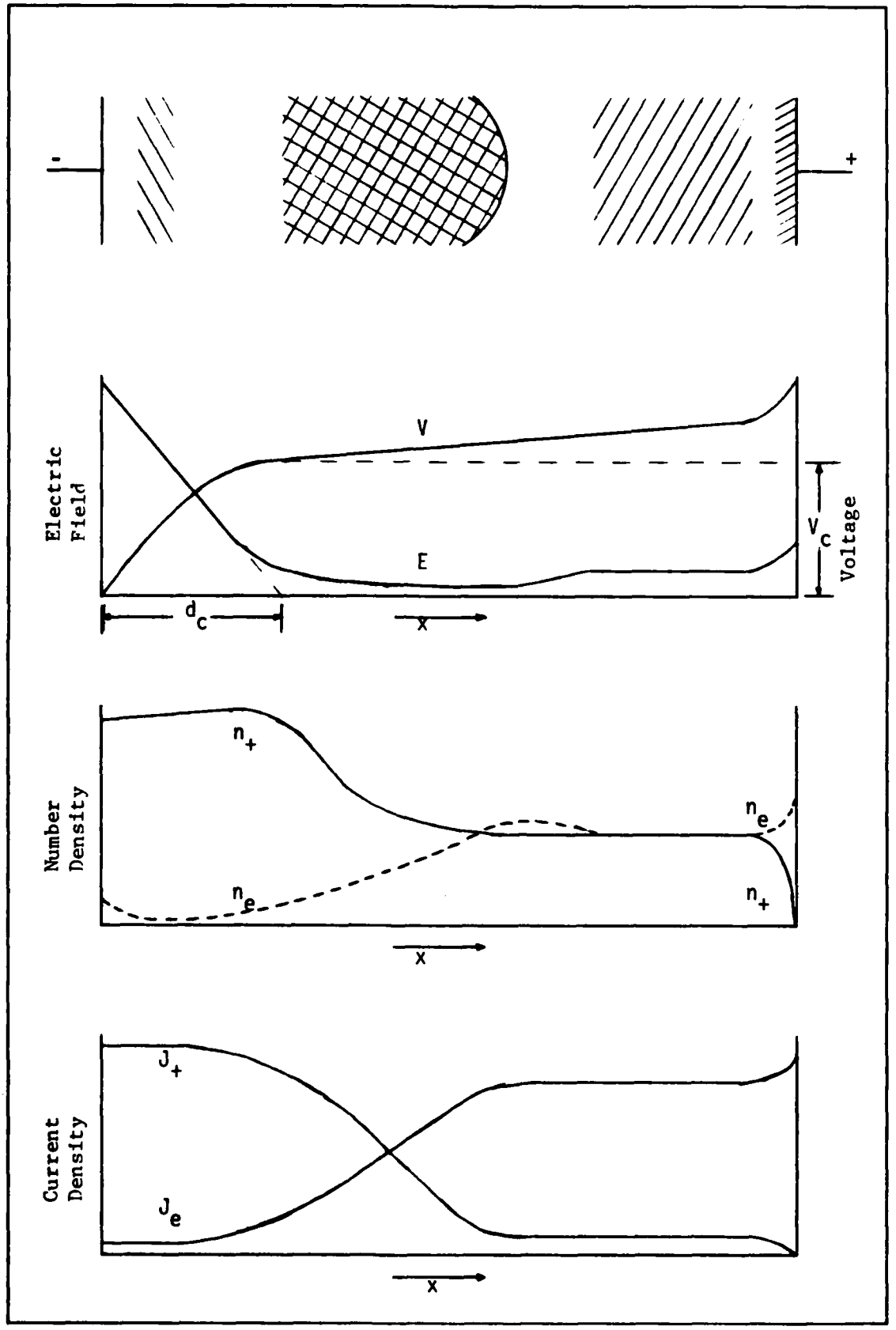

FIG I-1 Discharge Parameters as a Function of Discharge Length

positive column region extending up to the anode glow. The anode glow appears adjacent to the anode surface. Depending on the distance between the electrodes, only Aston's dark space, the cathode glow, and the cathode dark space are necessary for a discharge to exist.

It has been observed that the presence of negative ions can spatially alter the above regions and in some gases such as iodine, negative ions can become the dominant negative charge carrier through most of the discharge regions. Formation of negative ions in the positive column of the discharge often results in striations which can cause fluctuations in the light output of the positive column. The most undesirable effect of negative ions is in causing severe radial construction of the positive column limiting the efficient usage of the available container volume. Up to now, however, the exact role negative ions play in the cathode fall region of a discharge was unknown. The literature frequently cites experimental evidence indicating that the cathode fall region contracts longitudinally with the addition of even a trace of an attaching gas. This was interpreted to mean that the electronegative gas can have a significant impact in the region. The original question which initiated this study was if the formation of negative ions in the cathode fall led to the longitudinal contraction of the cathode fall region.

Before proceeding further, definitions of equilibrium and non-equilibrium are necessary to alleviate any confusion. 'Equilibrium' in high pressure discharges is termed local thermodynamic equilibrium (LTE) and means that all states of the charged and neutral species can be described by one temperature. In contrast at low pressures, the term 'equilibrium', more properly called 'field equilibrium', means

that the electron energy distribution function is characterized by the local value of E/N (E is the electric field, N is the gas number density) and the species in the volume element of interest. The electron distribution function need not be Maxwellian, as long as it can be defined in terms of E/N. Nonequilibrium at low pressures occurs when the above criterion for field equilibrium does not apply. For example, electrons are not in equilibrium in large spatial gradients where the mean velocity of the electrons would not be equal to the mean velocity of electrons in an equivalent, but spatially uniform field.

Basic analytical analysis (ref 20, 21, 60, 79, 86) now indicates that the electrons are not in equilibrium with the electric field in the cathode fall region. Since the electrons are being accelerated across the cathode fall region, they are gaining energy from the field faster than they lose energy to elastic scattering or inelastic processes in the gas. The electrons leave the cathode at low energies of few electron volts where the field is actually the highest. The electrons approach the negative glow with a multi-peaked distribution function as the field is approaching a minimum. Since the electrons are not in equilibrium with the field, their multiplication cannot be described by the usual Townsend ionization coefficient. This coefficient is measured in uniform fields where the energy gained by the electrons from the field is balanced by their energy losses to various elastic and inelastic processes with the gas molecules. By analogy, the equilibrium attachment coefficient also is not expected to correctly describe the formation of negative ions across the cathode fall region. The attachment coefficient is expected to be large adjacent to

cathode and then to decrease as the electrons are accelerated to higher energies. The formation of negative ions in this nonequilibrium sheath region has not been studied either analytically or experimentally. Concentrations of negative ions could alter the space charge in the sheath region and thus affect the voltage drop across the cathode fall region. This phenomena of nonequilibrium in the cathode fall region requires a 'nonequilibrium theory', such as calculating the electron energy distribution function as a function of distance in order to properly model the electron number density and ionization and attachment coefficients. However, 'equilibrium theory' has often been applied to describe the electric field, voltage drop, and electron current because its results have agreed fortuitously with the macroscopic parameters that have been able to be measured across the cathode fall region.

Objectives of This Study

This analytical study investigates the role small concentrations of an attaching gas play in the cathode fall region of a glow discharge. To do this, a new equilibrium model based on current continuity equations and Poisson's equations was developed. Additionally, a nonequilibrium model based on the Boltzmann transport equation and Poisson's equation was modified to be self-consistent, include negative ions and be more flexible The electron energy distribution function was calculated as a function of distance through the cathode fall region and the effects of negative ion formation were examined. The first and most important objective was to examine the effects in the cathode fall region resulting from the addition of small amounts of an

attaching gas such as HCl to a rare gas discharge. The second objective was to model the nonequilibrium behavior of the three charged particle densities through the cathode fall region. The third objective was to compare and contrast the equilibrium and nonequilibrium approaches and determine their regions of applicability.

Overview of Contents and Results

Chapter I describes the purpose and objective of this study, defines the regions of a discharge, and outlines the contents of the remaining chapters.

In Chapter II, the sufficient condition for the existence of a discharge is described in terms of electron multiplication in the cathode fall region. A historical review is presented on how trace amounts of negative ions affect an electropositive discharge. A qualitative theory is described which simplistically describes the result of negative ion formation in glow discharges.

Chapter III critically reviews the previous equilibrium theories of the cathode fall region, primarily for electropositive gases. These equilibrium theories are based on continuity type equations coupled with Poisson's equation. Boundary conditions are also discussed. A new equilibrium model of the cathode fall region allowing for negative ion formation is described and numerical results are presented.

In comparison to the equilibrium approaches described in Chapter III, Chapter IV critically reviews the previous nonequilibrium theories of the cathode fall region based on calculating the electron distribution as a function of position through the cathode fall region. A numerical technique for calculating the electron distribution as a

function of position in the cathode fall is described. This study extends this technique to include attachment, the presence of negative ions in the relevant equations, gas mixtures with a variable number of collision processes, and the calculation of the Townsend ionization and attachment rates from the distribution function. A convergent technique was developed which leads to a self-consistent solution between Poisson's equation and the electron distribution function. The boundary conditions, electron and ion kinetics, and the self-consistency of the solution are discussed. Characteristic cathode fall parameters are calculated as a function of distance and percentage of attaching species.

Chapter V compares the equilibrium theory with the nonequilibrium theory and discusses the discrepancies between the two theories in the cathode fall region. The anode fall region is also discussed.

Finally, Chapter VI summarizes the new results of this study and presents some considerations for future study.

Chapter II. Review of Qualitative Theory

Description of the Cathode Fall Region

The regions of a discharge were identified in Fig I-1. Of these, the cathode fall region is the most important segment of the discharge in that the largest potential drop per unit distance usually occurs there. However, it is probably the region least understood theoretically. It is the region of the discharge closest to the cathode and consists of the three subregions identified in the previous chapter as the primary dark space or Aston's dark space, the cathode glow, and the cathode dark space. The properties of the cathode fall region are almost independent of the rest of the discharge, since a discharge can exist without a positive column, Faraday dark space, or negative glow. A discharge cannot exist, however, without a cathode dark space (ref 6). Specifically, the length of the cathode dark space, the voltage drop across this distance, and the discharge current do not depend on any other external physical parameters such as the length of the discharge (providing the anode is not so small as to inhibit the axial current). The cathode dark space is the longest of the three cathode fall regions.

The essential processes in the cathode fall region are as follows. The purpose of the cathode is to provide electrons to maintain the discharge. Several processes exist by which the cathode can emit electrons. Direct processes include thermionic emission and field emission. For applied voltages up to several thousand volts these processes can be ignored. Indirect emission of electrons, usually

called secondary emission, results from bombardment of positive ions, photons, excited and neutral molecules on the cathode. Due to the low collision rate of excited and neutral molecules with the cathode in most discharges, the physical processes contributing most to the emission of electrons from the cathode are ion and photon bombardment. The electrons produced by secondary emission are accelerated across the cathode dark space, whereupon they begin to excite and ionize the gas creating new electrons and positive ions. The positive ions in turn are accelerated back towards the cathode where they produce new electrons. For every (M-1) electrons produced through ionization in the gas, γ electrons are released at the cathode. The maintenance condition for a self sustained discharge becomes

$$\gamma(M-1)=1 \quad \text{or} \quad M=1+\frac{1}{\gamma} \tag{II-1}$$

The multiplication M of electrons depends upon the nature and pressure of the gas. It is commonly expressed (in an electropositive gas) as

$$M=\exp\int_0^d \alpha(x)\,dx \tag{II-2}$$

where $\alpha(x)$ is Townsend's ionization coefficient. The number of electrons released at the cathode per incident particle (γ) is influenced by the size and energy of the ion or photon as well as the cathode material and the state of its surface. Thus, the cathode fall region is where processes essential to the maintenance of the rest of the discharge occur. The next section describes the scaling relationships for glow discharges.

Similarity Rules

Although the various parameters describing a glow discharge are all interrelated and often depend on each other through complex relationships, the parameters describing two different discharges can be related to each other using similarity or scaling rules. Two discharges are said to be similar if they are identical in one or two parameters and different in others. For example, two discharges in the same gas, at the same gas temperature, with the same electrode material, and with the same potential difference between the electrodes are similar even if all the corresponding linear dimensions differ by a constant factor. This includes the vessel dimensions, the electrode dimensions, and the properties of the gas such as the mean free path. Francis (ref 6) has comprehensively derived a set of similarity rules which result in several invariant quantities. If the discharge voltage, current, and gas temperature are the same for both discharges, he has shown that the following quantities are also invariant:

E/p - electric field/pressure

pd - pressure * distance

J/p^2 - current density/pressure^2

These parameters remain invariant for respective points in the discharges as long as the following processes dominate the kinetics.

a) Single stage processes such as electron impact ionization, attachment, or detachment.

b) Penning ionization

c) Charge transfer

d) Drift and diffusion from a volume

If two stage processes, photoionization, or recombination are the

dominant processes in the discharge, then the similarity rules will not be followed and the scaling parameters above may no longer be appropriate. The above invariant quantities apply both to the whole discharge as well as to specific regions of the discharge. For example, given two discharges with the same discharge voltage, current, and gas temperature, the invariant quantities for the cathode fall region would be:

V_c - cathode fall voltage drop

E/p - ratio of electric field to pressure at respective positions in the cathode fall

pd_c - pressure * cathode fall length

J/p^2 - current density/(pressure)^2

Basically, given V, I, and T, then V_c, E/p, pd_c, and J/p^2 are constants and relate how the electric field, cathode fall length and current density scale with pressure. The next section describes the experimental effects observed and attributed to negative ions in low pressure glow discharges including the cathode fall region.

Effects Attributed to Negative Ions in Gas Discharges

Several authors have reviewed the effects of adding small amounts of negative ions to a glow discharge (ref 5, 6, 8), but all agree with the initial description advanced by Emeleus and Sayers in 1938 (ref 42). Emeleus, et al. observed the effects on the discharge when a trace of an attaching gas such as chlorine was added to a neon discharge containing a little helium. With the addition of a trace of chlorine, the fluorescence from the pure neon discharge illustrated in Fig II-1a changed to that illustrated in Fig II-1b. The following

results were observed at a pressure of 2 torr and discharge potential of 800v:

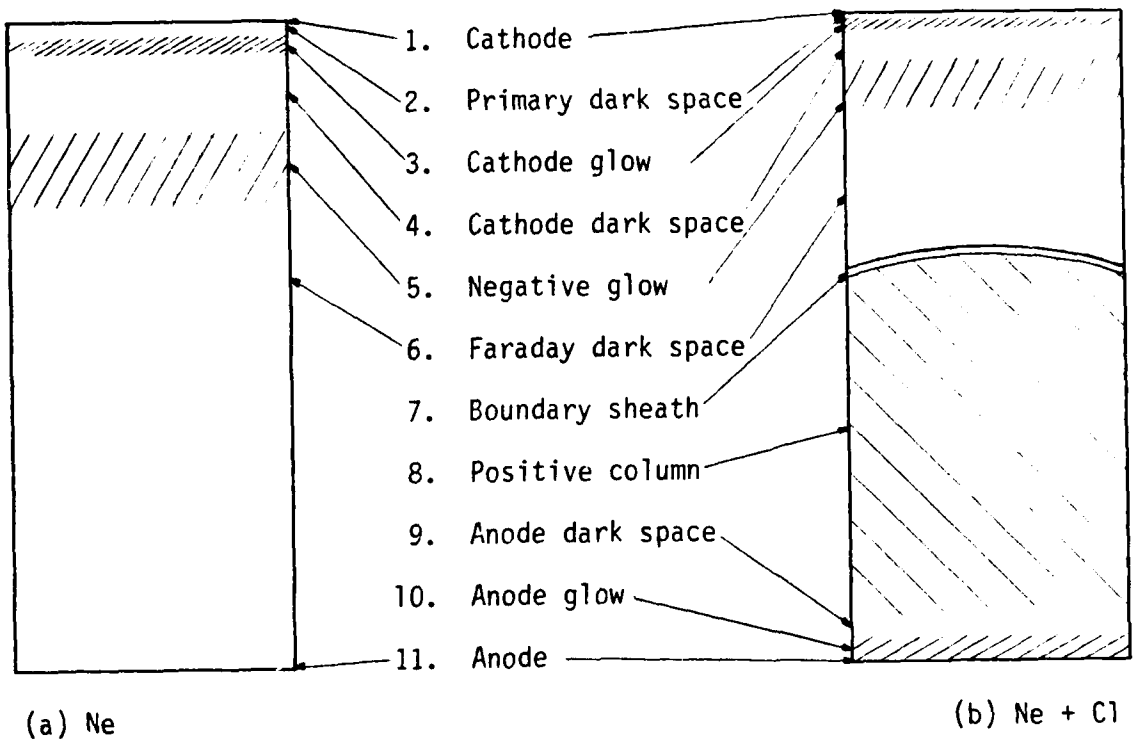

Fig II-1 Effect of Adding an Electronegative Gas to a Rare Gas Discharge

a. All the negative zones (cathode dark space, 4; cathode glow, 3; negative glow, 5; and Faraday dark space, 6) contracted towards the cathode such that Aston's dark space, or the primary dark space, 2, became so small as to be unobservable.

b. Curved striations appeared in the positive column, 8, often accompanied by an increase in the potential gradient.

c. A new dark sheath, 7, appeared between the Faraday dark space, 6, which was moderately luminous and the positive column, 8.

d. A new dark sheath, 9, also appeared between the positive column, 8, and anode glow, 10.

Spencer-Smith (ref 81) and more recently, Davis and King (ref 34) observed similar but more pronounced effects in pure iodine discharges, and in helium containing a trace of iodine. The positive column was observed to constrict radially to either a stationary form or a mobile ribbon. This type of constricted positive column has often been found in other discharges containing electronegative gases.

Following the discussion by Emeleus and Sayers (ref 39), the origin of the characteristic effects of electronegative gases was attributed to the decrease in the average mobility of the negative charge carriers as electrons are converted to heavier negative ions. Three almost independent effects ensue:

a. Creation or addition of negative ions corresponds to an increase in pressure in an electropositive discharge. The reduction of the drift velocity of the electrons by their attachment to gas molecules is equivalent to the more continuous retardation caused by more frequent collisions from an increase in gas pressure. The contraction of the negative zones, the occurrence of striations in the positive column, and the constriction of the positive column are all characteristics of an electropositive discharge at higher pressures, for example 100 torr compared to 1 torr.

b. Since negative ions are more massive than electrons, they diffuse more slowly from regions of space charge. Thus regions of space charge tend to grow once negative ions have formed. This leads to the formation of double space charge layers of positive ions next to negative ions. The high field gradient between these layers enhances the formation of stationary striations and thus the enhanced boundaries between dark and luminous regions. The axial field resulting from

these stationary double (+-) space charge regions accelerates electrons to sufficient energy to produce maximum excitation of the gas atoms and molecules leading to increased light emission. The dark sheaths, 7, between the positive column, 8, and the Faraday dark space, 6, and the anode glow, 9, are believed to be the result of space charge due to negative ions created in previous regions of the tube (ref 5, 6, 42).

c. Since some of the electrons become attached to gas molecules, the radial distribution of negative charge carriers will change. Due to the lower negative ion mobility, the negative ions will be less likely to diffuse away from the slightly positive axis in the positive column. Since detachment of electrons from negative ions can often be an inefficient process in many gases, large concentrations of negative ions can build up near the axis. This causes positive ions also to drift to the axis to balance the total charge resulting in a constricted discharge.

The above description is based mainly on qualitative observations which have been reviewed in reference 5. Several quantitative measurements have been made most of which have been accomplished since 1938, confirming the above hypotheses. These will be reviewed briefly.

Spencer-Smith (ref 81) and Woolsey (ref 96) used probe measurements and magnetic methods for measuring charge to mass ratios to investigate the negative glow and positive column regions of low pressure iodine discharge. Probe measurements in the presence of large quantities of negative ions are very difficult to interpret, but Spencer-Smith found the positive and negative ion concentration in the negative glow to be about equal, and about 100 times larger than the electron concentration. In the positive column, the ratio of positive

ions to electrons remained about the same, but the absolute concentrations were lower. Spencer-Smith also found the electron temperature in the negative glow to be normal (~1 to 1.5 eV) for E/N ≃ 620Td. The electron temperature in the positive column was much greater, ~13 eV. This can be accounted for by some of the electrons being accelerated through several potential drops as a result of striations. However, the conventional concept of electron temperature under such nonequilibrium circumstances probably is not valid. Woolsey's results were similar to Spencer-Smith's in that he found the ratio of negative ions to electrons to be 200 in both the negative glow and the positive column. Woolsey also determined the radial distribution of negative charge carriers to be much flatter than the normal zero order Bessel function found in the negative glow. The number of negative ions was found to be much larger and more concentrated around the axis in the positive column than the negative glow, in agreement with Emeleus and Sayer's speculation. In both experiments the positive column fluorescence about the center of the discharge tube was constricted. In a similar experiment using probes, Zimmermann (ref 98) found the positive ion concentrations more than fifty times greater than the electron concentration in the constricted positive column of a hot cathode discharge in hydrogen chloride vapor.

Lunt and Gregg (ref 63), and Thompson (ref 84), have investigated oxygen discharges. Again using probes and mass analysis, Lunt and Gregg found the concentration of O^- in the positive column with an E/N ≃ 250 Td to be about equal to the concentration of electrons. In the Faraday dark space and negative glow, however, hardly any negative ions were detected (<1%). Thompson used a radio frequency mass spec-

trometer probe to measure the particle concentrations. He found the concentration of O^- was about equal to the concentration of O_2^+, thus confirming Lunt and Greg's observation that O^- was the most abundant negative ion. Thompson also measured negative particle energy distributions in various regions of the discharge and compared them to the electron energy distributions in the same regions in a pure nitrogen discharge. The energy distributions in oxygen contained an apparent large low energy peak due to negative ions, as expected. He determined the radial space potential in the positive column to be much flatter for oxygen than for nitrogen and the axial space potential changed much more abruptly through a striation than in nitrogen. Although both discharges contained standing striations, the striations in the oxygen discharge were much closer together. The radial distribution of the electron concentration in the oxygen discharge was almost constant whereas the radial variation of positive and negative ions both decreased almost to zero supporting the idea that the positive and negative ions would concentrate near the axis.

More recently Davis and King (ref 4) observed the striations formed in a He-I_2 glow discharge laser. They calculated the ratio of negative ions to electrons to be on the order of 20-110 for a current density of 100 amp/m² and on the order of 2-11 for a current density of 10^4 amp/m². The negative ions with their lower mobility readily led to the formation of both stable and unstable stationary and moving striations as well as the constriction of the positive column when small quantities (<.1 torr) of iodine was admitted to pure helium discharges (2-10 torr). The forward wave (anode to cathode) striations

occurred at a 10kHz frequency and results in a partial modulation of the laser intensity. The radius of the constricted positive column decreased with an increase in iodine pressure. Even when the column remained stable, it was not always axially symetric, but often adopted a twisted configuration in the discharge tube caused by fluctuations in the local wall temperature and iodine density. Thus constricted discharges are undesirable for laser applications, since they prevent efficient usage of the available resonator volume. The instabilities which result in these striations and constriction of the positive column has been investigated extensively by Nighan and Wiegand (ref 70). This topic will not be investigated in this study. The occurrence of negative ions in the negative glow and positive column is, however, relevant to the cathode fall region and the boundary conditions relating these regions.

Chapter III. Electron Kinetics in the Cathode Fall Region: Equilibrium Analysis

Review of Equilibrium Theories

There are several theories for the cathode fall region in an electropositive gas which relate the cathode fall voltage (V_c), the discharge current (J), and the cathode fall distance (d_c). These theories will be referenced later as they are discussed. In comparison, there is a distinct lack of any kind of analytical analysis for electronegative discharges. These theories for the cathode fall region can be divided into equilibrium analyses based on Poisson's equation and hydrodynamic current continuity equations, and nonequilibrium analyses based on calculating an electron distribution function. The equilibrium analyses will be critically analyzed and expanded upon in this chapter. The nonequilibrium analyses will be considered in the next chapter.

The equilibrium analyses are of two types; those which regard the cathode dark space as an isolated independent unit considered separate from the negative glow and those which include the negative glow so that together their processes sustain the discharge. These theories of glow discharges are thoroughly summarized, but not necessarily critically reviewed in several references (ref 6, 7, 89). The cathode fall current-voltage relationship derived by von Engel and Steenbeck (ref 90) for a self-sustaining glow discharge has provided a benchmark for all following papers and will be briefly reviewed first. The emphasis will then be on results presented since 1975.

The von Engel and Steenbeck theory assumed the electric field in

the cathode fall to be a linearly decreasing function, of the form

$$E = E_o\left(1 - \frac{x}{d_c}\right) \qquad \text{(III-1)}$$

where E_o is the electric field at the cathode and d_c is the cathode fall distance. The ion flow to the cathode is assumed to be mobility limited so that

$$v_+ = \mu_+ E \qquad \text{(III-2)}$$

where v_+ is the positive ion velocity and μ_+ their mobility. The boundary conditions that von Engel and Steenbeck used set the positive ion current to zero at the cathode fall-negative glow boundary and assumed each positive ion incident on the cathode produced γ electrons, yielding

$$J_+(d) = 0 \qquad \text{(III-3)}$$

and

$$J_e(0) = \gamma J_+(0) \qquad \text{(III-4)}$$

equation (III-3) is not entirely correct in that the positive ion current does decrease at the cathode fall-negative glow boundary but does not necessarily to to zero. The question of whether the number of positive ions entering the cathode fall from the negative glow is significant or not has developed into an area of controversy and is described later.

Using the empirical form of Townsend's ionization coefficient,

$$\frac{\alpha}{p} = A \exp\left(-\frac{Bp}{E}\right) \qquad \text{(III-5)}$$

they derived equations relating the total current J, the cathode fall voltage V_c, and the cathode fall width d_c. The cathode fall thickness is derived by applying the maintenance condition, equation II-1, to the cathode fall region resulting in

$$\overline{\alpha}\, d_c = \int_0^d \alpha(x)\, dx = \ln\left(1 + \frac{1}{\gamma}\right) \qquad \text{(III-6)}$$

Definition of the width of the cathode fall is not exact but it is usually defined as the distance from the cathode to the point in the discharge where the electric field is extrapolated to zero. The voltage is determined from the electric field.

$$V_c = \int_0^d E(x)\, dx \approx \frac{E_0 d_c}{2} \qquad \text{(III-7)}$$

if E(x) is given by equation III-1. Since the ion current to the cathode is generally mobility limited, they derived a current-voltage relationship for the cathode fall from the high pressure space-charge-limited current voltage relationship yielding

$$\frac{J}{p^2} = (1+\gamma)\, \frac{9\varepsilon_0 \mu_+ p}{8} \frac{V_c^2}{(pd)^3} \qquad \text{(III-8)}$$

Equations III-6, III-7, and III-8 uniquely describe the cathode fall region and obey the similarity or scaling rules described in Chapter I. Solving these equations numerically for a linearly decreasing electric field, provides good agreement with experiment over a wide range of

conditions in electropositive gases. Helium is an exception and one reason may be that the Townsend ionization coefficient cannot be fitted with an exponential form like equation III-5. However, the above assumptions have recently become controversial areas (ref 7).

Druyvesteyn and Penning (ref 38) pointed out that if a significant number of positive ions entered the cathode fall region from the negative glow, the maintenance condition for the discharge was altered to the following:

$$\bar{\alpha} d_c = \ln \frac{1 + \frac{1}{\gamma}}{1 + \delta} \qquad \text{(III-9)}$$

where δ is the ratio of the positive ion current to the electron current at the cathode fall-negative glow interface. Thus the value of $\bar{\alpha} d_c$ could be reduced if the positive ion current was comparable to the electron current at the cathode fall-negative glow boundary.

Little and Von Engel (ref 59) refute the idea that a significant number of ions enter the cathode fall region from the negative glow. A linear electric field requires a constant net space charge density in the cathode fall, whereas if a significant number of positive ions originated in the negative glow, then the positive ion density would be expected to decrease towards the cathode. As Ingold (ref 7) pointed out, these are not conclusive arguments, since such field measurements are very difficult and any slowly varying field would appear approximately linear to the experimentalist. Reviews by Francis (ref 6) and Weston (ref 93) survey many attempts to measure the electric field in the cathode fall region. The weight of the evidence suggests an electric field decreasing linearly through the cathode dark space becoming almost zero in the negative glow. Several recent theoretical

papers have tried to show the electric field to be linear in the cathode fall. These papers will be reviewed later, in chronological order.

The other area of controversy is the concept of Townsend's ionization coefficient (α) and the assumption that the electrons are in equilibrium with the field. α is the number of ionizing collisions per centimeter of path length and is usually determined from drift tube experiments. These experiments assume the electrons are in equilibrium with a uniform electric field. This condition probably is not met in the cathode fall where the electric field changes rapidly. Evidence of this appears in the nonequilibrium analyses of the cathode fall by Long (ref 60) and Tran Ngoc An (ref 86) which are discussed in Chapter IV. Thus the theoretical models based on the concept that the electron distribution function is in equilibrium with the field may not be valid. As von Engel noted about his own theory, the equilibrium theories give "physically the correct picture, but the numerical agreement with observations is largely fortuitous" (ref 89:224). This observation is also discussed later in Chapter V where the equilibrium and nonequilibrium results are compared.

Returning to the review of the literature, since 1975, Ul'yanov (ref 87) analytically investigated the effect of the positive ion contribution from the negative glow. He based his approach on experimental evidence of Gunthershultze (ref 46) indicating that as the anode approaches the plasma side of the cathode sheath, the potential drop across the cathode fall increases. This indicates that some of the positive ions required to carry the current in the cathode fall region originate in the negative glow. Ul'yanov solved the following set of

equations for both high and low ion mobility cases, defined below

$$\frac{dE}{dx} = \frac{e n_e}{\epsilon_0} \qquad \text{(III-10)}$$

$$\frac{dJ_e}{dx} = (J - J_+)\,\alpha(E) \qquad \text{(III-11)}$$

$$\alpha(E) = A_p\, e^{-\left(\frac{Bp}{E}\right)} \qquad \text{(III-12)}$$

$$J_+ = e n_+ \mu_+ E \quad \text{(low field case)} \qquad \text{(III-13a)}$$

$$J_+ = e n_+ k_+ E^{\frac{1}{2}} \quad \text{(high field case)} \qquad \text{(III-13b)}$$

The boundary conditions which neglect any potential drop in the negative glow are given by

$$E(d) = 0 \qquad \text{(III-14)}$$

$$J_+(d) = \delta J_0 \qquad \text{(III-15)}$$

where δ was a variable parameter representing in his theory the ratio of positive ion current density to electron current density at the cathode fall-negative glow boundary. For both mobility cases, his final transcendental equations contained integrals which had to be solved numerically. His results indicated that if the fraction of ion current coming from the negative glow (δ) decreases, then the electric field at the cathode increases. For a given secondary emission coefficient (α), he determined that the normal cathode fall potential (V_N),

normal current density (J_N), and normal cathode fall length (x_N) changed quite slowly over a wide range of δ values. He found the greatest discrepancy between his theory and von Engle's theory at small δ where a singularity existed in his equations for V_N and J_N. His equations for V_N, J_N, and x_N depended only on gas, cathode parameters, and δ, once the transcendental equation for the electric field was solved. From the fact that V_N, J_N, and x_N were a function of δ, he concluded that a complete theory for the cathode fall normal glow discharge must take into account ion production in the negative glow.

Neuringer (ref 69) made an analytical investigation of the cathode fall region in high-voltage low-current discharges. He determined that to first order the electric field decreased linearly in the cathode fall region, the voltage drop depended on the two-thirds power of J/p^2 and the cathode fall thickness was independent of the operating current and varied inversely with pressure. His model combined the electron current continuity equation,

$$\frac{dJ_e}{dx} = \alpha(E(x))\, J_e(x) \qquad \text{(III-16)}$$

Poisson's equation,

$$\frac{dE}{dx} = \frac{-1}{\varepsilon_0}\left[\frac{J_+(x)}{V_+(E(x))} - \frac{J_e(x)}{V_e(E(x))}\right] \qquad \text{(III-17)}$$

with the requirement for total current conservation.

$$\nabla \cdot J = 0 \quad \text{or} \quad J = J_+ + J_e = \text{constant} \qquad \text{(III-18)}$$

J_e and J_+ are the electron and positive ion current densities and v_e and v_+ are the electron and positive ion drift velocities. He used Townsend's ionization coefficient (equation III-5), Ward's (ref 92) modified formula for the positive ion velocity for ions in a high field,

$$v_+ = k_+ (E/p)^{\frac{1}{2}} \tag{III-19}$$

and the fact that $v_+/v_e \ll 1$ throughout the cathode fall to obtain a differential equation separable in J_e and E. This equation

$$\frac{dJ_e}{dE} = -\alpha \varepsilon_0 v_+ \left(\frac{J_e}{J-J_e}\right) = -\varepsilon_0 A p e^{-\left(\frac{Bp}{E}\right)} k_+ (E/p)^{\frac{1}{2}} \left(\frac{J_e}{J-J_e}\right) \tag{III-20}$$

can be integrated assuming the electric field goes to zero and the electron current density is equal to the total current density at the cathode fall-negative glow boundary.

$$E(d) \approx 0 \tag{III-21}$$

$$J_e(d) \approx J \tag{III-22}$$

He was able to derive an expression for the electric field as a function of distance by assuming $J_e \ll J$ close to the cathode. Keeping only first order terms, he derived

$$E = E_0 - \frac{p^{\frac{1}{2}} J x}{k_+ \varepsilon_0 E_0^{\frac{1}{2}}} \tag{III-23}$$

Assuming no externally initiated electron current density, such that

$$J_e = \left(\frac{\gamma}{1+\gamma}\right) J \qquad \text{(III-24)}$$

he also obtained

$$\frac{E_o}{p} = \left[\frac{\frac{3}{2}\log\left(\frac{\gamma+1}{\gamma}\right)}{\varepsilon_o k_+ A}\right]^{\frac{2}{3}} \left(\frac{J}{p^2}\right)^{\frac{2}{3}} \qquad \text{(III-25)}$$

The derivation of equation III-23 is important because it was the first time the linear functional dependence of the electric field on distance had been derived, and not assumed. He claims good agreement with experimental results quoted in Francis' article (ref 6) and with a computer model using a differential equation solver technique which was previously developed by Ward (ref 92) to solve equations III-16 and III-17. Even though he uses valid boundary conditions (equations III-21 and III-22), his model is correct only in region very near the cathode since he has assumed $v_+ \simeq k_+(E/p)^{\frac{1}{2}}$ and $J_e << J$ in order to drop terms. Additional analysis in the next section includes negative ions and reveals that the first order approximations do not have to be made. Nevertheless, his results add credence to von Engel's assumption that the electric field decreases linearly in the cathode fall region.

Davies and Evans (ref 32) extended Neuringer's analysis and showed it could be applied to the whole discharge by changing the boundary conditions and assuming the ratio of positive ion to electron mobility to be a constant.

$$r = \frac{\mu_+}{\mu_e} \qquad \text{(III-26)}$$

This assumption was found to breakdown only at electric fields for which $1 - J_e \ll rJ_e$, which normally was not the case. The boundary condition at the cathode was the same as Neuringer's i.e. equation III-24, but the other boundary condition was changed to represent the electric field at the anode or to specify a particular applied voltage.

$$E(d) = E_a \tag{III-27}$$

$$V = \int_0^d E(x)\,dx \tag{III-28}$$

Based upon combining Poisson's equation III-17 and the electron current continuity equation III-16 into a transcendental type of equation, including the above changes, they developed a new, fast numerical technique for predicting the variation of E and j_e as a function of distance from cathode to anode. Although equation III-16 is true in the cathode fall region where ionization is the dominant process and the electrons are scattered predominantly in the forward direction, it is not correct in the positive column region where the electrons are scattered isotropically and the gain of electrons is balanced by losses to radial diffusion, recombination, or attachment. In essence, when r is held constant, this is tantamount to including diffusion in the positive column. However, diffusion was not included as a loss process in the electron current continuity equation. In addition to this discrepancy, the anode fall voltage appears to be much too small. Estimating from their Fig 1, the anode fall in helium appears to be

less than 5 volts which is much less than the nominal value of 26 volts (ref 6:148). Later in this chapter the same problem was encountered when this method was used. Further discussion of the anode fall is reserved for Chapter V.

Recently, Mitchell, Kline, and Denes (ref 67) calculated the electric field, particle fluxes, and particle densities as a function of position in the cathode and anode regions of a high pressure glow discharge containing an attaching gas mixture. They used a one dimensional steady state continuity equation model including Poisson's equation. The following boundary conditions were used:

Cathode	Anode	Positive Column	
$J_e = \gamma J_+$	$n_e = n_+ = n_- = 0$ $J_+ = 0$	$\frac{dJ}{dx} = \frac{dn}{dx} = \frac{dE}{dx} = 0$	(III-29)

where J_e/J_- and E were adjustable initial parameters. They reported that the cathode sheath characteristics are insensitive to variations in the concentrations of the attaching species, whether diffusion of electrons were included or not. However, the anode sheath was affected by the inclusion of electron diffusion as well as the attaching concentration. However, as will be shown in the next section, the boundary condition for the positive column in equation III-29 may not lead to a unique solution. Thus there remains some question on the convergence and hence self-consistency of their solutions.

New Equilibrium Analysis of the Cathode Region Including Negative Ions

This section expands Neuringer's analysis of the cathode fall region to include negative ions. Since the ratio of positive ions to electron mobility is held constant, the transverse diffusion of electrons was added to the electron continuity equation. A one-dimensional steady state distribution is assumed so all quantities are functions of the distance x from the cathode surface and not of the transverse geometry. When attachment and transverse diffusion processes are included, the equations governing the steady-state discharge are:

Poisson's equation

$$\frac{dE}{dx} = \frac{-1}{\varepsilon_0}\left[\frac{J_+}{V_+} - \frac{J_e}{V_e} - \frac{J_-}{V_-}\right] \qquad \text{(III-30)}$$

the electron current continuity equation

$$\frac{dJ_e}{dx} = \left(\alpha - \eta - \frac{D_e}{\lambda^2 V_e}\right) J_e \qquad \text{(III-31)}$$

the negative ion current continuity equation

$$\frac{dJ_-}{dx} = \eta J_e - \frac{k_r J_- J_+}{e V_- V_+} \qquad \text{(III-32)}$$

and the total current conservation equation

$$\nabla \cdot J = 0 \quad \text{or} \quad J = J_+ + J_e + J_- \qquad \text{(III-33)}$$

where E is the electric field strength, J_+, J_e, J_- and J are the positive ion, electron, negative ion and total current densities respectively, v_+, v_e, and v_- are the positive ion, electron, and negative ion drift velocities, ε_0 is the permittivity of free space, α and η are Townsend's first ionization and attachment coefficients, D_e is the electron free diffusion coefficient (cm^2/sec), λ is the electron mean free path, k_r is the ion-ion recombination rate (cm^3/sec), and x is the distance from the cathode to the anode. These equations differ from Davies and Evan's equations in that negative ions have been added to Poisson's equation, attachment and electron diffusion have been added to the electron continuity equation, the negative ion current continuity equation is now required, and the negative ion current density has been added to the total current conservation equation.

Normalizing the current density to unity implies:

$$J_e = \frac{J_e}{J} \qquad J_- = \frac{J_-}{J} \tag{III-34}$$

Then dividing equation III-30 by III-31 and using III-34 to eliminate the positive ion current density yields

$$\frac{dE}{dJ_e} = \frac{-J}{\varepsilon_0 v_+}\left[1 - \left(1 + \frac{v_+}{v_e}\right)J_e - \left(1 + \frac{v_+}{v_-}\right)J_-\right]\frac{1}{\left(\alpha - \eta - \frac{D_e}{\lambda^2 v_e}\right)J_e} \tag{III-35}$$

Equations III-31, III-32, and III-35 are the set which will be analyzed instead of the original system of equations III-30, III-31, and III-32. Because α, η, v_+, v_e are strong functions of the electric field, this system of coupled equations is highly nonlinear. The system becomes solvable if the following assumptions are made:

$$\frac{v_+}{v_e} = r \quad \text{and} \quad \frac{v_+}{v_-} \simeq 1 \tag{III-36}$$

The variation in r with the electric field is very small and becomes

significant only when $J_+ >> rJ_e$. Thus these are good assumptions over the complete range of E. Making use of these assumptions, separating variables and using the boundary conditions $E/p = E_o/p$ and $j_e = j_{eo}$ at the cathode results in the following integral equation

$$\int_{E/p}^{E_o/p} \left(\alpha - \eta - \frac{D_e r}{\lambda^2 V_+}\right) V_+ p \, d(E/p) = \frac{-J}{\varepsilon_o} \int_{j_e}^{j_{eo}} \left[1 - (1+r) J_e - 2 J_-\right] \frac{d J_e}{J_e} \qquad \text{(III-37)}$$

The Townsend first ionization coefficient that was used, was the more general form given by

$$\frac{\alpha}{p} = A e^{-\left(B(p/E)^s\right)} \qquad \text{(III-38)}$$

where A and B are empirically determined constants characteristic of the gas, and s=1, for molecular gases and s=½ for monatomic gases. Similarly, the attachment coefficient can be expressed as an exponential

$$\frac{\eta}{p} = C e^{-\left(D(E/p)^t\right)} \qquad \text{(III-39)}$$

or as a series

$$\frac{\eta}{p} = a_o + \sum_{i=1}^{n} a_i (E/p)^i \qquad \text{(III-40)}$$

where C, D, and t or a_i are empirically determined constants depending on the attaching gas. These are good assumptions provided the electrons are in equilibrium with the field. The ion drift velocity in a high field region can be described by Ward's modified formula.

$$V_+ = k_+ (E/p)^{\frac{1}{2}} \qquad \text{(III-41)}$$

Substituting for α , η, and v_+, equation III-37 becomes:

$$\int_{E/\rho}^{E_0/\rho}\left[A_p e^{-B(p/E)^s} - C_p e^{-D(E/\rho)^t} - \frac{D_e r}{\lambda^2 k_+ (E/\rho)^{\frac{1}{2}}}\right] k_+ (E/\rho)^{\frac{1}{2}} \rho\, d(E/\rho) = \frac{-J}{\ell_0}\int_{J_e}^{J_{e0}}\left[\frac{1}{J_e} - (1+r) - 2\frac{J_-}{J_e}\right] dJ_e \quad \text{(III-42)}$$

Changing variables by letting $\psi = B(p/E)^s$, the first term on the left side of the equation becomes the difference of the two incomplete gamma functions.

$$\int_{E/\rho}^{E_0/\rho} A_p e^{-B(p/E)^s} k_+ (E/\rho)^{\frac{1}{2}} \rho\, d(E/\rho) = A_p \rho^2 k_+ B^{\frac{3}{2s}} \int_{\psi}^{\psi_0} \frac{1}{\psi^{\frac{3}{2s}+1}} e^{-\psi}\, d\psi$$

$$= \frac{A_p \rho^2 k_+ B^{\frac{3}{2s}}}{s}\left[\Gamma\left(-\tfrac{3}{2s}, B(p/E_0)^s\right) - \Gamma\left(-\tfrac{3}{2s}, B(p/E)^s\right)\right] \quad \text{(III-43)}$$

Where $\Gamma(a,x) \equiv \int_x^\infty e^{-t} t^{a-1} dt$ (ref 9:260). Similarly changing variables so that $\phi = D(\ /p)^t$, the second term becomes:

$$-C_p \rho^2 k_+ \int_{E/\rho}^{E_0/\rho} (E/\rho)^{\frac{1}{2}} e^{-D(E/\rho)^t} d(E/\rho) = \frac{-C_p \rho^2 k_+}{t D^{\frac{3}{2t}}} \int_{\phi}^{\phi_0} \phi^{\frac{3}{2t}-1} e^{-\phi}\, d\phi$$

$$= \frac{C_p \rho^2 k_+}{t D^{\frac{3}{2t}}}\left[\Gamma\left(\tfrac{3}{2t}, D(E_0/\rho)^t\right) - \Gamma\left(\tfrac{3}{2t}, D(E/\rho)\right)\right] \quad \text{(III-44)}$$

The third term integrates easily to yield

$$-\int_{E/\rho}^{E_0/\rho} \frac{D_e r \rho}{\lambda^2}\, d(E/\rho) = -\frac{D_e r \rho}{\lambda^2}\left[E_0/\rho - E/\rho\right] \quad \text{(III-45)}$$

Integrating the right hand side of III-42, yields

$$-\frac{J}{\ell_0}\int_{J_e}^{J_{e0}}\left[\frac{1}{J_e} - (1+r) - 2\frac{J_-}{J_e}\right] dJ_e = \frac{J}{\ell_0}\left[\ln\left(\frac{J_e}{J_{e0}}\right) + (1+r)(J_{e0} - J_e) + 2\int_{J_e}^{J_{e0}} \frac{J_-}{J_e}\, dJ_e\right] \quad \text{(III-46)}$$

Therefore III-42 can now be rewritten as

$$\frac{A B^{\frac{3}{2s}}}{s}\left[\Gamma\left(-\frac{3}{2s}, B(E/\rho)^{t}\right]+\frac{C}{t D^{\frac{3}{2t}}}\left[\Gamma\left(\frac{3}{2t}, D(E/\rho)^{t}\right]-\frac{D_{c} r}{\lambda^{s} k_{+} \rho} E/\rho=\frac{A B^{\frac{3}{2s}}}{s}\left[\Gamma\left(-\frac{3}{2s}, B(E_{o}\right)\right]+\right.$$

$$\left.\frac{C}{t D^{\frac{3}{2t}}}\left[\Gamma\left(\frac{3}{2t}, D(E/\rho)^{t}\right]-\frac{D_{c} r}{\lambda^{s} k_{+} \rho}(E/\rho)-\frac{J}{k_{+} \rho^{s} \varepsilon_{o}}\left[\ln\left(\frac{J_{o}}{J_{\infty}}\right)+(1+r)(J_{\infty}-J_{o})+2\int_{J_{o}}^{J_{\infty}}\frac{J}{J_{o}} d J_{o}\right]\right. \tag{III-47}$$

The gamma functions can be simplified for numerical calculations with the help of the following recurrence relation (ref 15:457).

$$\Gamma(a+1, x)=a \Gamma(a, x)+x^{a} e^{-x} \tag{III-48}$$

For s = $\frac{1}{2}$, Γ(3/2s, x) reduces to

$$\Gamma(-3, x)=\frac{-1}{6}\left[E_{1}(x)-e^{-x}\left(\frac{1}{x}-\frac{1}{x^{2}}+\frac{2}{x^{3}}\right)\right] \tag{III-49}$$

where $E_{1}(x) \equiv \int_{x}^{\infty} \frac{e^{-t}}{t} dt$, the exponential integral (ref 9:228). For numerical calculations $E_1(x)$ can easily be represented by polynomial approximation (ref 9:231). For s = 1, Γ(3/2s, x) reduces to

$$\Gamma\left(-\frac{3}{2}, x\right)=\frac{4}{3} \sqrt{\pi} \operatorname{erfc} \sqrt{x}+\frac{2}{3} e^{-x}\left(\frac{1}{x^{\frac{1}{2}}}-\frac{2}{x^{\frac{1}{2}}}\right) \tag{III-50}$$

where $\operatorname{erfc}(x) \equiv \frac{2}{\sqrt{\pi}} \int_{0}^{\infty} e^{-t^{2}} dt$ is the complementary error function for which there are tables.

Similarly for t = 1, Γ(+3/2t, x) reduces to

$$\Gamma\left(\frac{3}{2}, x\right)=\frac{\sqrt{\pi}}{2} \operatorname{erfc} \sqrt{x}-\frac{e^{-x}}{\sqrt{x}} \tag{III-51}$$

These simplifications for the gamma functions above were used in the numerical calculations to ease computation. Error functions, exponentials, and square roots were more accessible in computer libraries than incomplete gamma functions.

These terms still form a trancendental equation involving j_e and E. Given j_e at the cathode, various mathematical methods can be used to find E which is a root to the equation. This field can then be used in solving the continuity equations, III-31 and III-32, very near the cathode. Iteratively, one can spatially step from the cathode to the anode by alternatively solving for $E(j_e)$ and j_e. This method eliminates the integration problems conventional differential equation solvers have in solving the original set of equations, which included Poisson's equation explicitly. $E(j_e)$ is a smooth function and can be determined using successive numerical approximations to solve the transcendental equation III-47. See Fig III-1.

An expression for the variation of the electric field can be obtained by first taking the derivative of equation III-47. The derivative of each of the terms in III-47 is given below.

$$\frac{d}{dx}\left[\frac{AB^{\frac{1}{s}}}{s}\Gamma\left(\frac{-3}{2s}, B(E/\rho)^s\right)\right] = A(E/\rho)^{\frac{1}{2}} e^{-B(E/\rho)^s}\frac{d(E/\rho)}{dx} \qquad \text{(III-52)}$$

$$\frac{d}{dx}\left[\frac{C}{t\,D^{3/2t}}\Gamma\left(\frac{3}{2t}, D(E/\rho)^t\right)\right] = -C(E/\rho)^{\frac{1}{2}} e^{-D(E/\rho)^t}\frac{d(E/\rho)}{dx} \qquad \text{(III-53)}$$

$$\frac{d}{dx}\left[\frac{D_e r\, E/\rho}{\lambda^2 k_0 \rho}\right] = \frac{D_e r}{\lambda^2 k_0 \rho}\frac{d(E/\rho)}{dx} \qquad \text{(III-54)}$$

$$\frac{d}{dx}\left[\frac{J}{k_0\rho^2\varepsilon_0}\left(\ln\left(\frac{j_e}{j_\infty}\right)+(1+r)(j_\infty - j_e)+2\int_{j_e}^{j_\infty}\frac{j}{j_\infty}dj_e\right)\right] = \frac{I}{k_0\rho^2\varepsilon_0}\left[\frac{d\ln j_e}{dx}-(1+r)\frac{dj_e}{dx}+2\frac{d}{dx}\int_{j_e}^{j_\infty}\frac{j}{J}dj_e\right] \qquad \text{(III-55)}$$

The derivatives involving j_e can be eliminated by substituting in

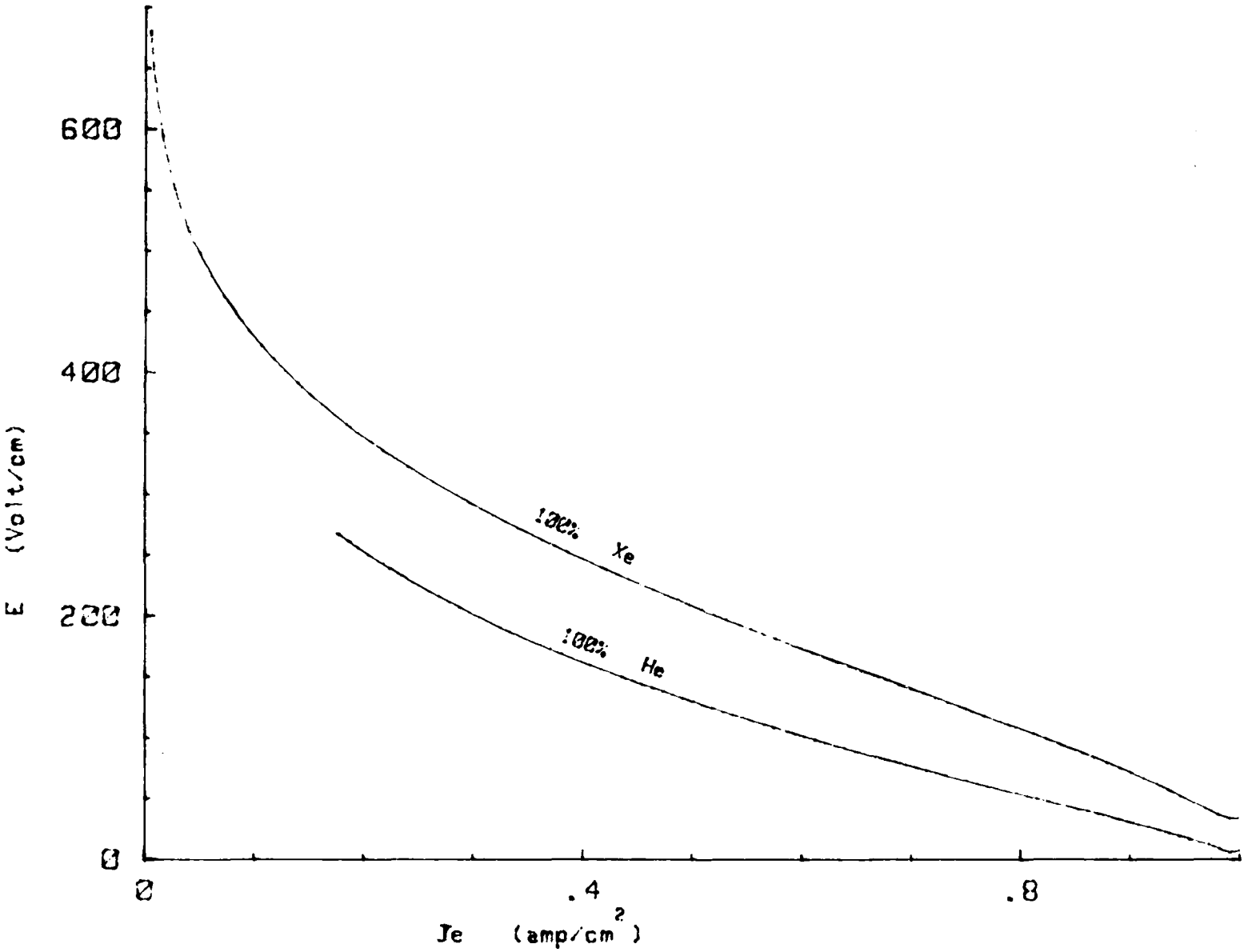

FIG III-1 ELECTRIC FIELD AS A FUNCTION OF ELECTRON CURRENT DENSITY

equation III-31 in normalized form yielding

$$\left(E/p\right)^{\frac{1}{2}}\frac{d\left(E/p\right)}{dx} = -\frac{J}{k_+ p^2 \varepsilon_0}\left[1-(1+\gamma)j_e + \frac{2}{\left(\alpha-\eta-\frac{D_e r}{p\lambda^2 k_+ (E/p)^{\frac{1}{2}}}\right)}\frac{d}{dx}\int_{j_e}^{j_{e\infty}}\frac{j_-}{j_{e\infty}}\,dj_e\right] \qquad \text{(III-56)}$$

In an electropositive gas, $j_- = 0$ and $j_e \ll 1$ very near the cathode so the last two terms in III-56 are negligible. Integrating equation III-56 under these conditions yields

$$\left(E/p\right)^{\frac{3}{2}} = \left(E_0/p\right)^{\frac{3}{2}} - \frac{3Jx}{2k_+ p\varepsilon_0} \qquad \text{(III-57)}$$

or taking the first two terms in a binomial expansion yields

$$E/p \approx E_0/p - \frac{Jx}{k_+ p\varepsilon_0 (E/p)^{\frac{1}{2}}} \qquad \text{(III-58)}$$

This is the same result Neuringer obtained, III-23, using many more approximations in his derivation. He retained only the first term in equation III-46 as he assumed $j_e \ll J$ near the cathode. This resulted in an equation similar to III-57 which contained terms proportional to $(E/p)^{\frac{1}{2}}$ which he conveniently dropped. The binomial expression leading to equation III-58 converges as long as $(E_0/p)^{\frac{1}{2}} > \frac{3Jx}{2k_+ p\varepsilon_0}$. This inequality holds in the cathode fall region but may not hold in the negative glow or positive column region where E_0/p becomes very small and no longer a linearly decreasing function.

Returning to equation III-56, the dominant terms for an electropositive gas are

$$\frac{J}{k_+ p^2 \varepsilon_0}\frac{(1-j_e)}{(E/p)^{\frac{1}{2}}} = \frac{J j_+}{k_+ p^2 \varepsilon_0 (E/p)^{\frac{1}{2}}} = \frac{J n_+ e}{\varepsilon_0 p^2} \qquad \text{(III-59)}$$

which is consistent with Poisson's equation and the fact that the field in the cathode fall region is determined primarily by the positive ion

number density.

In an electronegative gas, the situation is more complex. However very near the cathode even in an electronegative gas, $j_- << j_e$ and $j_e << 1$. Thus the field there is determined primarily by the positive ion current in both electronegative and positive gases. As one proceeds across the cathode fall, the electron and negative ion current densities increase in a related manner given by III-32. This has the affect of increasing the slope of the electric field as can be seen from the following analysis.

It was found from the results of the next section that the negative ion current density through the cathode fall region could be related to the electron current density by an exponential function of the following form,

$$j_- = e^{m j_e} - c \qquad \text{(III-60)}$$

where c is a constant determined by the boundary condition that $j_- = 0$ at the cathode and m is an empirically determined constant. Results of the nonequilibrium analysis in the next Chapter also confirm that equation III-60 is a good approximation throughout the cathode fall region except for a very small region a few electron mean free paths in length in front of the cathode. Using this approximation, the derivative of the integral on the right side of III-56 becomes

$$\frac{d}{dx}\int_{j_e}^{j_{eo}} \frac{j_-}{j_e}\, dj_e = \left(\alpha - \eta - \frac{D_e r}{p \lambda^2 k_+ (E/p) t}\right)\left(c - e^{m j_e}\right) \qquad \text{(III-61)}$$

After integrating III-56 and using this expression, one can solve for

the field as a function of distance

$$\left(E/p\right)^{\frac{3}{2}} = \left(E_o/p\right)^{\frac{3}{2}} - \frac{3J}{2k_{iz}p\,\epsilon_o}\left[x(1+2c) - (1+r)\int_0^x j_e\,dx - 2\int_0^x e^{m}\,dx\right] \qquad \text{(III-62)}$$

Taking the first two terms in a binomial expansion as before yields

$$E/p \approx E_o/p - \frac{J}{k_{iz}p\,\epsilon_o\left(E_o/p\right)^{\frac{1}{2}}}\left[x(1+2c) - (1+r)\int_0^x j_e\,dx - 2\int_0^x e^{m}\,dx\right. \qquad \text{(III-63)}$$

In the electronegative case, the field is shifted higher at each corresponding x near the cathode by the factor (1 + 2c). This shift is small but can be observed in the results presented in the next section as well as the results of the nonequilibrium analysis in Chapter IV for mixtures of Xe and HCl. Thus this analysis predicts that the attaching gas slightly lengthens the cathode fall and slightly increases the cathode fall voltage. As the electron current density grows with respect to distance the integral terms become larger and have the effect of increasing the field in the positive column region of the discharge. Thus increasing the amount of an attacher also increases the field in the positive column region in an attempt to balance the gain and loss of electrons.

Returning to equation III-56 and solving for the minimum slope of the electric field yields

$$\left.\frac{d(E/p)}{dx}\right|_{min} = 0 = \frac{-J}{k_{iz}p\,\epsilon_o\left(E/p\right)^{\frac{1}{2}}}\left[1 - (1+r)\,j_e + 2(c - e^{m})\right] \qquad \text{(III-64)}$$

The minimum field in an electropositive gas occurs when j_e = 1/1+r. In

the electronegative case, the minimum field occurs when

$$J_e = \frac{1+2(c-e^{-mL})}{(1+r)} = \frac{(1-2L_-)}{(1+r)} \qquad \text{(III-65)}$$

Both of these expressions are equivalent to charge neutrality.

$$n_+ = n_e + n_- \qquad \text{(III-66)}$$

Description of Program GLOW

The GLOW program was developed during this study to provide a fast, yet complete description of the electric field in a gas discharge from cathode to anode, similar to the Davies and Evan's model (ref 32). This type of model was chosen because it can give a complete description of the electric field as a function of distance from cathode to anode. The advantage of this type of technique is that it minimizes the number of boundary conditions. This code differs from most other approaches including Davies and Evans by starting at the cathode and proceeding towards the anode. Most other approaches start at the anode or positive column and work back towards the cathode due to stability problems. This method is sufficiently stable to start at the cathode where the boundary conditions on the negative ion current are well known. The theory upon which the model is based has already been described in the preceding section. This section will describe the boundary conditions and the iteration techniques in detail.

The boundary conditions used at the cathode and anode are ones on which there is fair agreement. The boundary conditions used at the

cathode are

$$J_e(0) = \frac{\gamma}{1+\gamma} J \qquad \text{(III-67)}$$

$$J_-(0) = 0 \qquad \text{(III-68)}$$

where γ is the secondary emission coefficient at the cathode. The other boundary condition requires current continuity at the anode such that

$$J_e + J_- = J \quad \text{or} \quad J_+ = 0 \qquad \text{(III-69)}$$

Other techniques such as starting in the positive column using a differential equation solver and starting toward the cathode usually require one or more boundary conditions in addition to equation III-67 and III-68 to match solutions for each region being described.

The code is based on a shooting technique which varies the electric field at the cathode to converge upon a calculated value of the electric field at the anode. The value of the electric field at which the electron current density plus the negative ion current density equals the total discharge current density was found to converge very quickly to a constant value. This value of the electric field, at which the anode boundary conditions hold was the field that was the target in the shooting technique. After each iteration from cathode to anode the target value of the electric field at the anode was updated with a refined value for which equation III-69 holds. If E(d) was too

high such that

$$J_e + J_- > J \tag{III-70}$$

then E(0) was decreased. If E(d) was too low, or the calculation did not reach the anode, then E(0) was increased. Fig III-2 shows the electric field as the program converged. For the second and twelfth iterations in Fig III-2, no solution existed for the transcendental equation past the points plotted. This implies that this technique converges not only to a solution which satisfies the boundary equations, but is also the lowest voltage for the discharge for the initial conditions.

Any numerical technique for finding the roots of an equation could be used in solving the transcendental equation, such as the method of halving the interval. However, a modified linear interpolation method (ref 45:10-11) was used since it is supposed to be sligthly faster than the halving the interval method. The only requirement was that the first two estimates for E(0) should bound the solution, i.e. one estimate be too large and the other too small. Rapid convergence to 4-6 digit accuracy was achieved within 20 iterations from electric fields differing as much as 10-20v/cm at the cathode. Numerical calculations were terminated when the target, E(d), was within 10% of the calculated value.

Within each of these iterations from cathode to anode, a differential equation solver, and this modified linear interpolation method was used to solve the system of current continuity equations, III-31 and III-37, and find the root to the transcendental equation, III-47, respectively. The variable order Adams predictor-corrector method

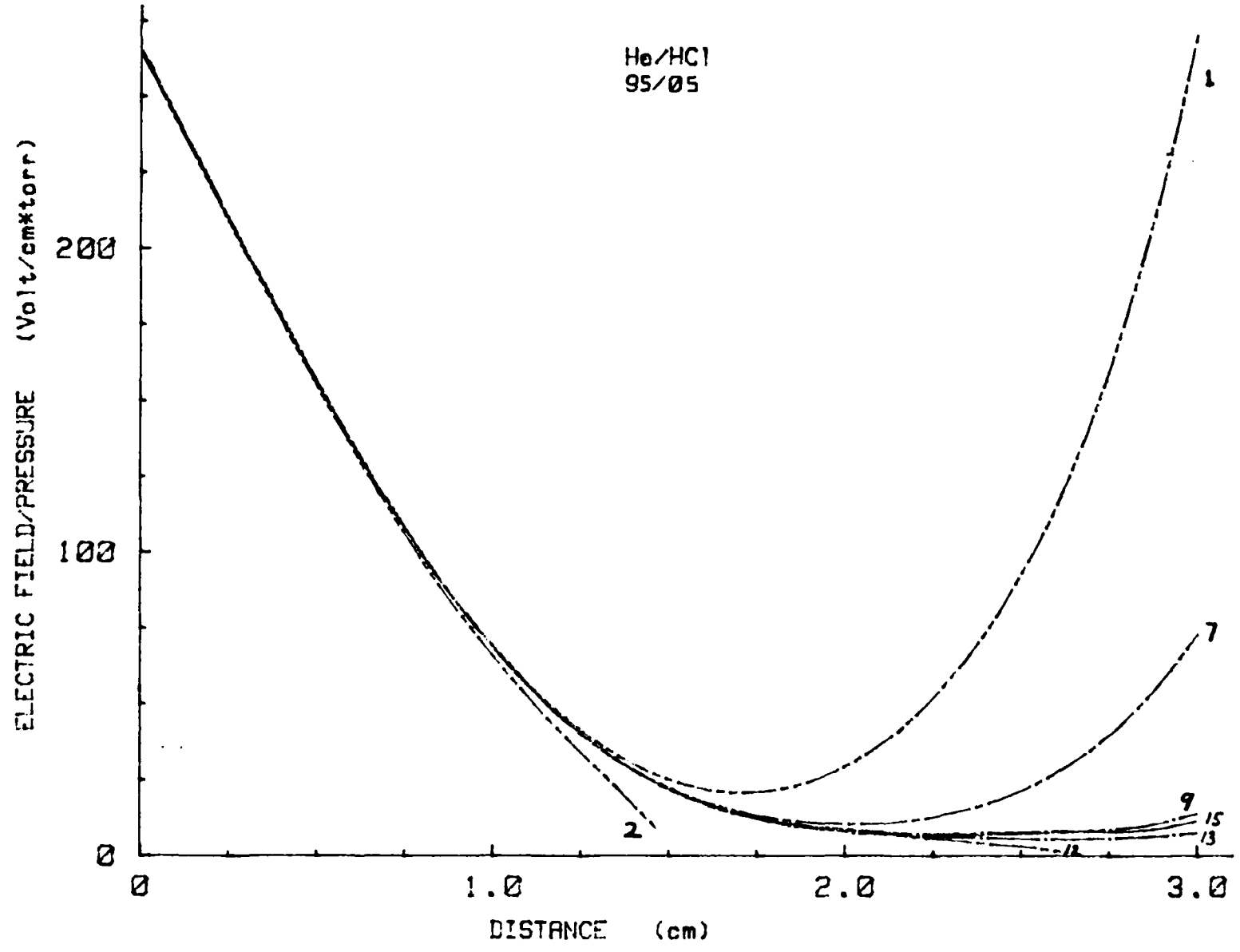

FIG III-2 CONVERGENCE OF THE GLOW CODE TO THE LOWEST VOLTAGE

which was part of a differential equation solver package called DGEAR (ref 36) for solving stiff differential equations was used to solve for j_e given an electric field. The overall iteration scheme from cathode to anode went as follows:

a. Given E(0), DGEAR was called to solve the set of equations III-31 and III-32 for $j_e(x)$ a short distance from the cathode.

b. Given this value of $j_e(x)$, the modified linear interpolation method was used to find the root or equilibrium value for E(x) from the transcendental equation, III -47.

c. Given this value of E(x), DGEAR was called again to solve for a new $j_e(x)$ at the next small increment in space. The spatial step size h was usually picked such that $(E(0) - E(h))/E(0) < 1\%$. This cycle of calculating $j_e(x)$ and E(x) was repeated as the program stepped from cathode to anode.

The program can be run without the help of the differential equation solver, using the field at the last step to calculate the field from equation III-47. However, this method was very sensitive to the spatial step size used. The addition of a differential equation solver to predict the electron current density at the next step where the transcendental equation III-47 was to be solved next, enabled much larger steps to be taken with a savings in computer time.

The GLOW program, incorporating both a differential equation solver and the modified linear interpolation method was usually run on a Cyber 750 computer system. Each iteration took on an average less than 4 sec of execution time for 250-300 spatial steps. It required less than 52k of memory to load and run. Parameters used in the numerical calculations are described in Appendix C.

To establish a baseline and verify the accuracy of the technique, Davies and Evans' boundary conditions and initial values were used and the resultant field plotted in Fig III-3. They set the electron current density equal to the total discharge current and then varied the electric field at the anode until a fixed value of the field was obtained at the cathode. By starting at the anode, γ was not required as a boundary condition. The GLOW code was first run from anode to cathode to determine γ at the cathode. The code was then run from cathode to anode using this value of $\gamma = .293$. In this instance, γ was fixed and the field at the cathode was varied until the electron current density equaled the total discharge current density at the anode. As can be seen form Fig III-3, very good agreement of the GLOW code (cathode to anode) is obtained with Davies and Evan's result (anode to cathode).

Results of Numerical Calculations

This section presents the results of calculations using the GLOW code in various mixtures of rare gases with HCl. All data presented for He and Ar was obtained for a gas pressure of 1 torr. The data for Xe was calculated for a gas pressure of 100 torr. However, it was found that for all three rare-gas mixtures, the results at different pressures obeyed the following pressure scaling relationships.

$$V_c = \text{constant}$$

$$J/p^2 = \text{constant}$$

$$pd = \text{constant}$$

This finding is in accordance with the similarity rules or scaling laws

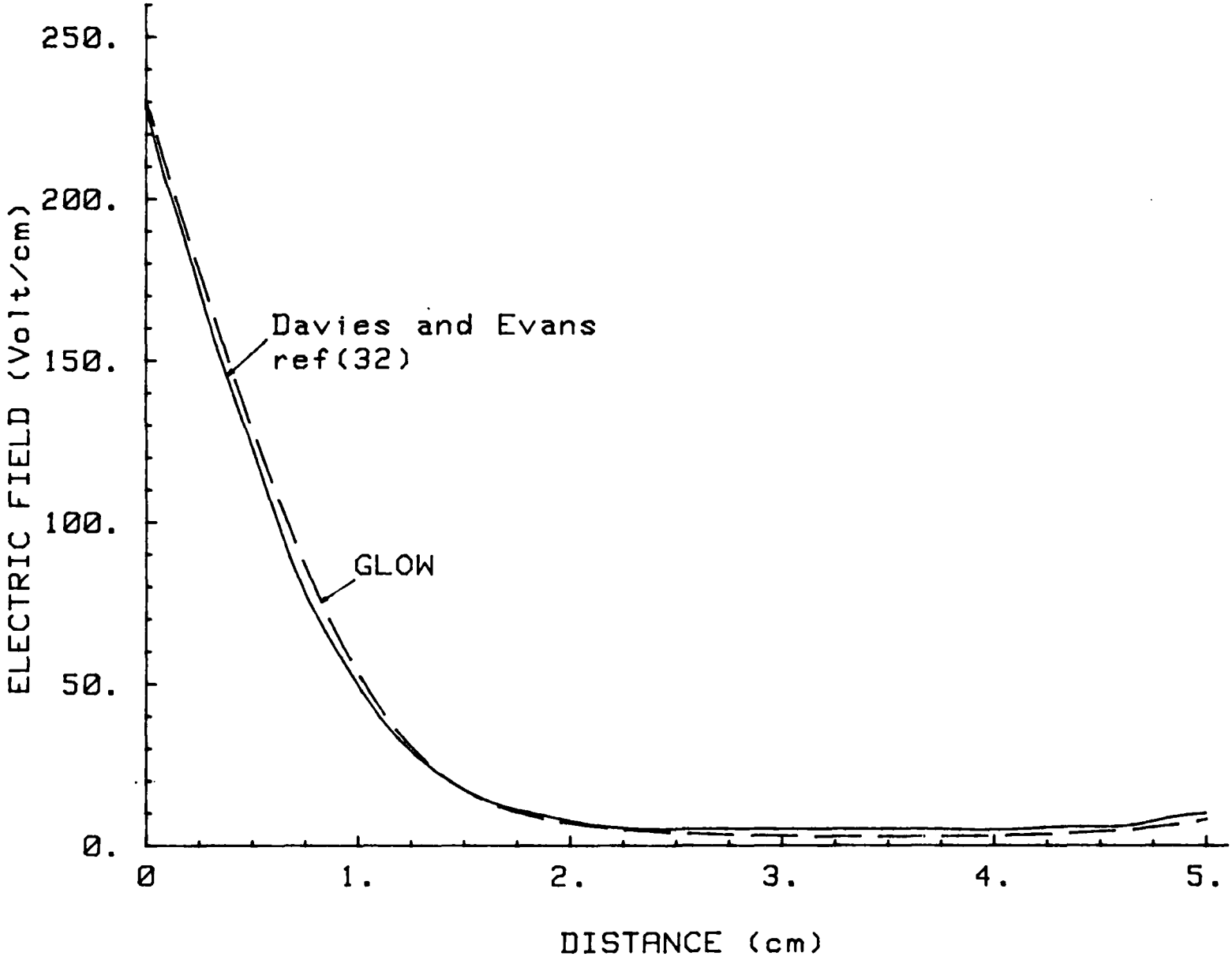

FIG III-3 COMPARISON OF THE ELECTRIC FIELD WITH OTHER DATA

for gas discharges discussed in Chapter I. Data was taken at 1, 10, and 100 torr for two gas mixtures and was found to deviate less than .01% from these scaling relationships.

A current-voltage relationship, similar to equation III-8 can be derived for the high field case where the positive ion velocity is proportional to the square root of the field. Following von Engel and Steenbeck's derivation, but using equation III-41 for the ion drift velocity results in the following current-voltage relationship.

$$J/p^2 = 1.4344\,\epsilon_0 k_+ (1+\gamma)\frac{V_c^{\frac{3}{2}}}{(pd)^{\frac{1}{2}}} \qquad \text{(III-71)}$$

Thus, this new scaling function

$$SF(\gamma, k_+) = \frac{J/p^2 (pd)^{\frac{1}{2}}}{V_c^{\frac{3}{2}}} \qquad \text{(III-72)}$$

is a constant for a given γ and k_+ in the high field case. This scaling relationship is useful in comparing data at different voltages and currents.

Results will be presented in the sequence He mixtures, Ar mixtures, and then Xe mixtures. Results will be discussed in this section for the cathode fall and positive column regions, but not for the anode fall region. At present the GLOW code does not adequately describe the anode region. The anode fall region is discussed in Chapter V.

Helium Mixtures

This section presents the results obtained for He/HCl mixtures,

given p = 1 torr, d = 3cm, J = 1.6E-5 amp/cm², and γ = .2. A summary of numerical values for the following figures is given in Table III-1 for E_o/p, E_{min}/p, pd_c, J/p^2, and V_c. E_o is the electric field at the cathode, E_{min} is the minimum electric field which in these calculations occurs in the positive column, p is the total gas pressure, d_c is the length of the cathode fall region, J is the total current through the discharge, and V_c is the cathode fall voltage. Consistent with the somewhat arbitrary but common scheme for calculating the cathode fall distance, the linear cathode field region was extrapolated to zero to determine the cathode fall length d_c. The cathode fall voltage was obtained from the voltage between the cathode and this point. (Other definitions can be used, but for the comparison with other published models this definition was applied. Experimental comparisons would have slightly lower values). The last column in Table III-1 is the scaling function (SF) given in equation III-72. This scaling relationship helps to put in perspective the various data on cathode fall parameters. The value of $SF(\gamma, k_+)$ for 100% He agrees only within 62.5% of Ward's data (ref 92). This discrepancy is largely due to the different approximation for the positive ion drift velocity which he used:

$$V_+ = \mu_+ E/p\,(1 - C\,E/p) \qquad E/p \le W_1 \qquad \text{(III-73a)}$$

$$V_+ = k_+ (E/p)^{\frac{1}{2}} \left(1 - \frac{D}{(E/p)^{\frac{1}{2}}}\right) \qquad E/p > W_1 \qquad \text{(III-73b)}$$

Table III-1

Summary of GLOW Code Results for He/HCl Mixtures

Ratio Ar/HCl		or Cathode Material	E_o/p volt / cm-torr	E_{min}/p volt / cm-torr	pd_c (torr-cm)	J/p^2 μ amp / cm^2-$torr^2$	V_c (volt)	SF (γ, k_+) $X10^{-9}$ amp $torr^{\frac{1}{2}}cm^{\frac{1}{2}}$ / $volt^{\frac{1}{2}}$
100/0								
Experimental	i	Mg	-	-	1.45	3.	125.	5.43
	i	Fe	-	-	1.3	2.	150.	2.10
	i	Ni	-	-	-	2.	158.	-
	i	Pt	-	-	-	5.	165.	-
	i	Al	-	-	1.32	-	140.	-
	i	Other Materials	-	-	-	-	59.-204.	-
Theoretical	ii	.2	-	-	2.6	1.6	143.	10.20
	iii	.2	274.3	5.4	1.26	16.	183.4	11.48
	iv	.293	230.	4.5	1.1	15.	-	-
	iii	.293	229.9	2.7	1.16	15.	141.1	12.97
99/1								
Theoretical	iv	.2	272.5	5.7	1.25	16.	180.8	11.49
95/5								
Theoretical	iv	.2	265.8	6.7	1.21	16.	171.7	11.45

i Data was taken from a summary presented in ref 6.
ii Data was taken from ref 92.
iv Data was taken from ref 32.
iii Data was calculated in this study.

(where for He $\mu_+ = 8.E3$ cm²-torr/volt-sec,

$k_+ = 4.1E4$ cm$^{\frac{3}{2}}$-torr$^{\frac{1}{2}}$/volt$^{\frac{1}{2}}$-sec, $C = 8.E\text{-}3$ torr-cm/volt,

$D = 27.44$ volt$^{\frac{3}{2}}$/cm$^{\frac{3}{2}}$-torr$^{\frac{3}{2}}$ and $W_1 = 25$v/cm-torr).

At 200v/cm-torr, Ward's approximation yields a positive ion velocity that is only 1% larger, whereas at 30 v/cm-torr it is 17% larger. Since the slope of the electric field is inversely proportional to the positive ion drift velocity, the cathode fall length and voltage are also sensitive functions of the positive ion drift velocity and largely accounts for the above discrepancy. Very good agreement is reached with Davies and Evans data (ref 32) for $\gamma = .23$. Care should be taken in comparing the values of $SF(\gamma,k_+)$ since this 'constant' is proportional to $(1 + \gamma)$.

Fig III-4 shows a 3% decrease in the electric field through most of the cathode fall region (0.-1.26 cm) as the amount of HCl is increased from 0 to 5%. This is contrary to the results that might be anticipated from equation III-63. However, HCl has an ionization potential approximately half of that for He (12.74eV as compared to 24.59 eV), the HCl contributes more electrons through ionization than the discharge loses to attachment to HCl resulting in a slightly reduced cathode fall voltage of up to 5% for the 95/5 He/HCl mixture. There is also a trend for the cathode fall width and voltage to decrease: 1% and 1.4% respectively for 99/1 mixture and 5% and 6.3% for the 95/5 mixture. In the positive column region (around 2.5 cm) the electric field is 5% higher for 99/1 mixture, and 25% higher for a 95/5 mixture of He/HCl as a result of the increase in the number of attaching molecules. The fields in the positive column region are consistent with the value of the field required to have the electron gain and loss

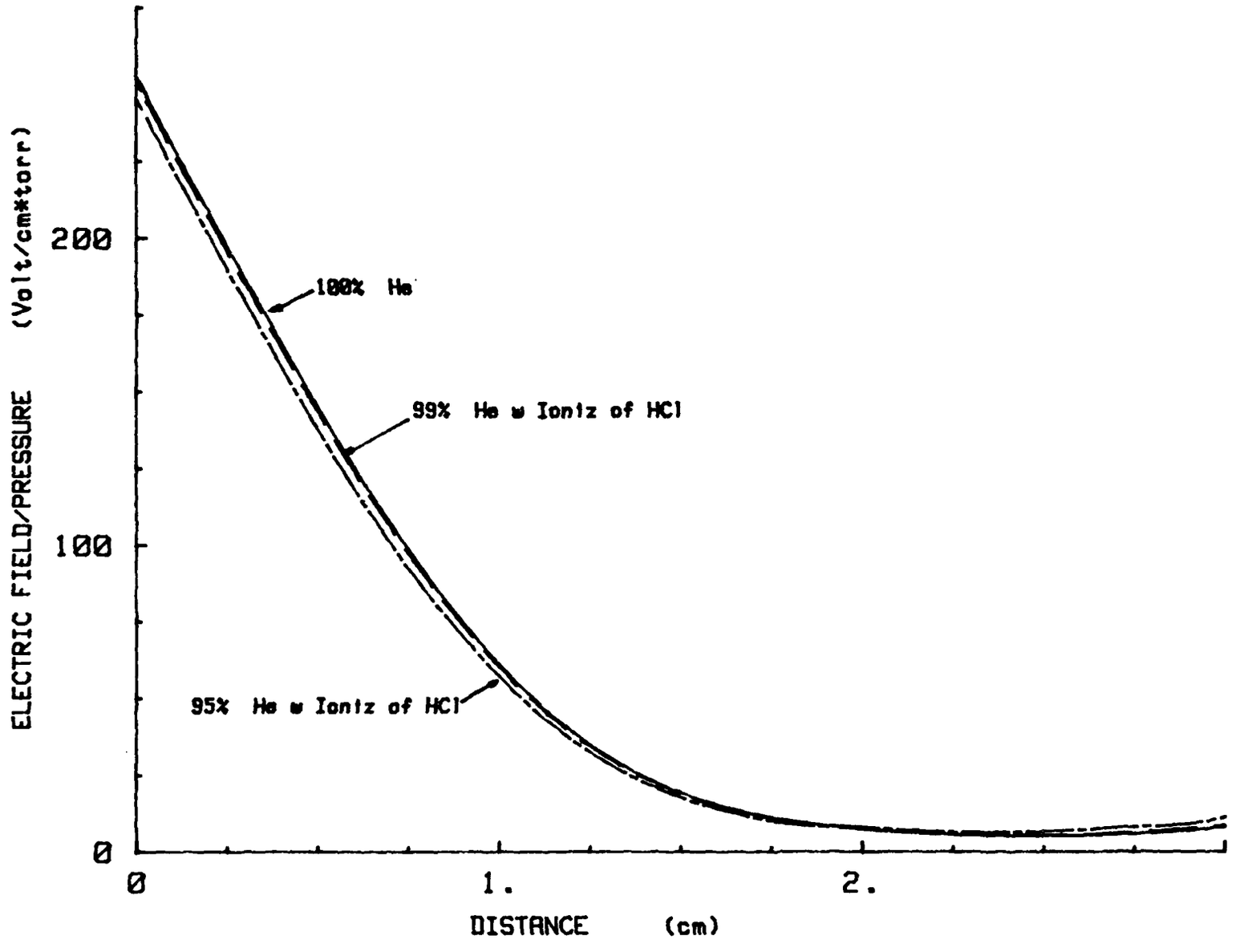

FIG III-4 ELECTRIC FIELD IN He/HCl MIXTURES

processes equal. In the nearly uniform field region of the positive column any additional loss of electrons must be balanced by an increase in ionization in order to maintain constant current.

Fig III-5 shows the same calculation in 95/5 He/HCl with and without the contribution of ionization from HCl. As expected, the electric field is increased in the cathode fall region when ionization of HCl is not included. This additional ionization in the cathode fall region as the percentage of HCl is increased results in a small relative increase in the electron current density in Fig III-6 in the cathode fall region. The current densities plotted in Fig III-6 and III-7 have been normalized as in equation III-34. The electron current density decreases in the positive column region as the percentage of HCl is increased indicating electrons are being lost to the formation of negative ions. As expected the negative ion current density shown in Fig III-7 becomes a larger fraction of the discharge current density through both the cathode fall region and the positive column region. However it still contributes less than 1% to the total discharge current.

Argon

The results for Ar/HCl mixtures will be presented next where p=1torr, d = 1.5cm, J = 1.E-5 amp/cm^2 and γ = .04167. A summary of numerical values for the following figures is given in Table III-2 as was done for He/HCl mixtures.

In 100% Ar the value of SF(γ, k_+) agrees very well with Ward's

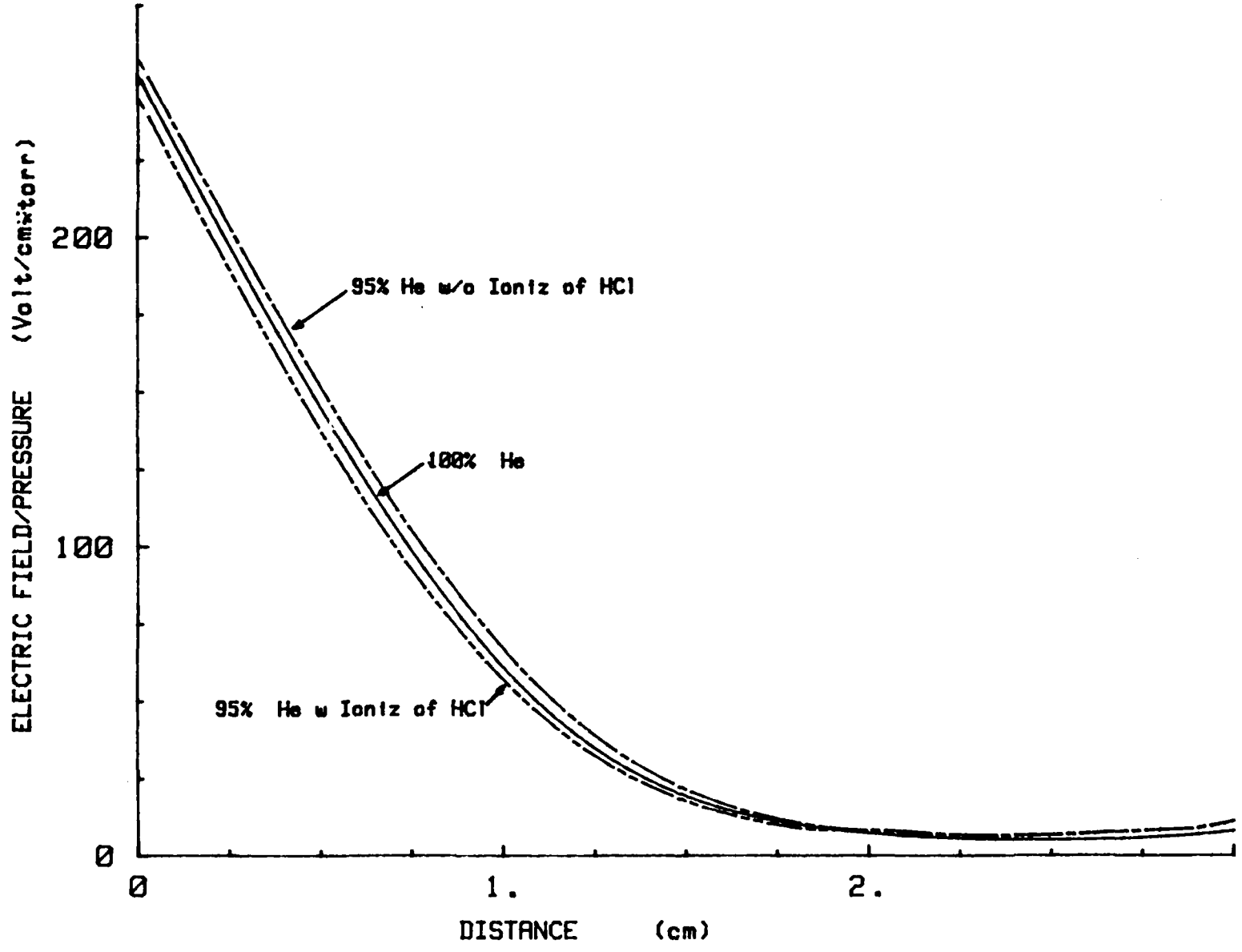

FIG III-5 EFFECT OF IONIZATION OF HCl IN He/HCl MIXTURES

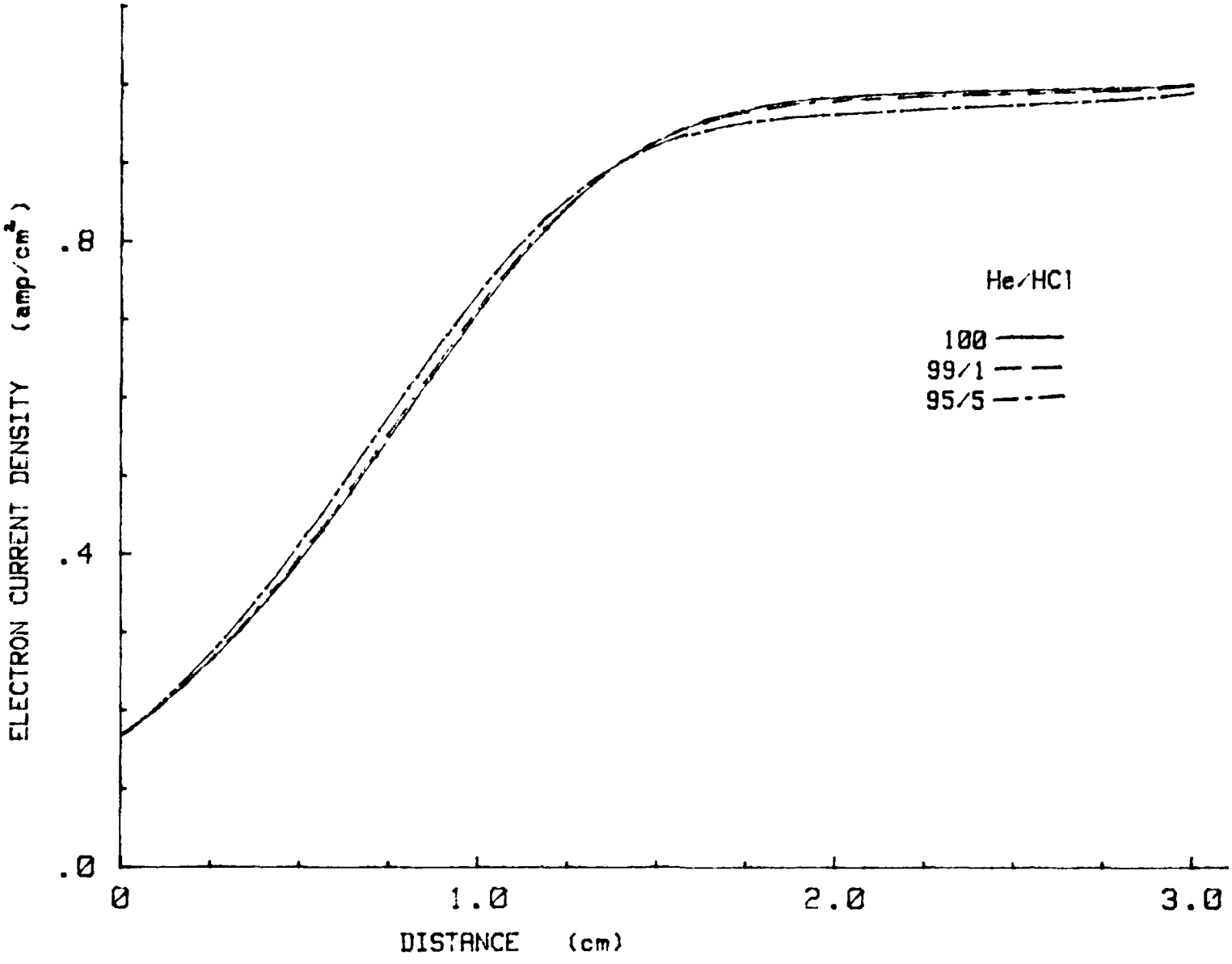

FIG III-6 NORMALIZED ELECTRON CURRENT DENSITY IN He/HCl MIXTURES

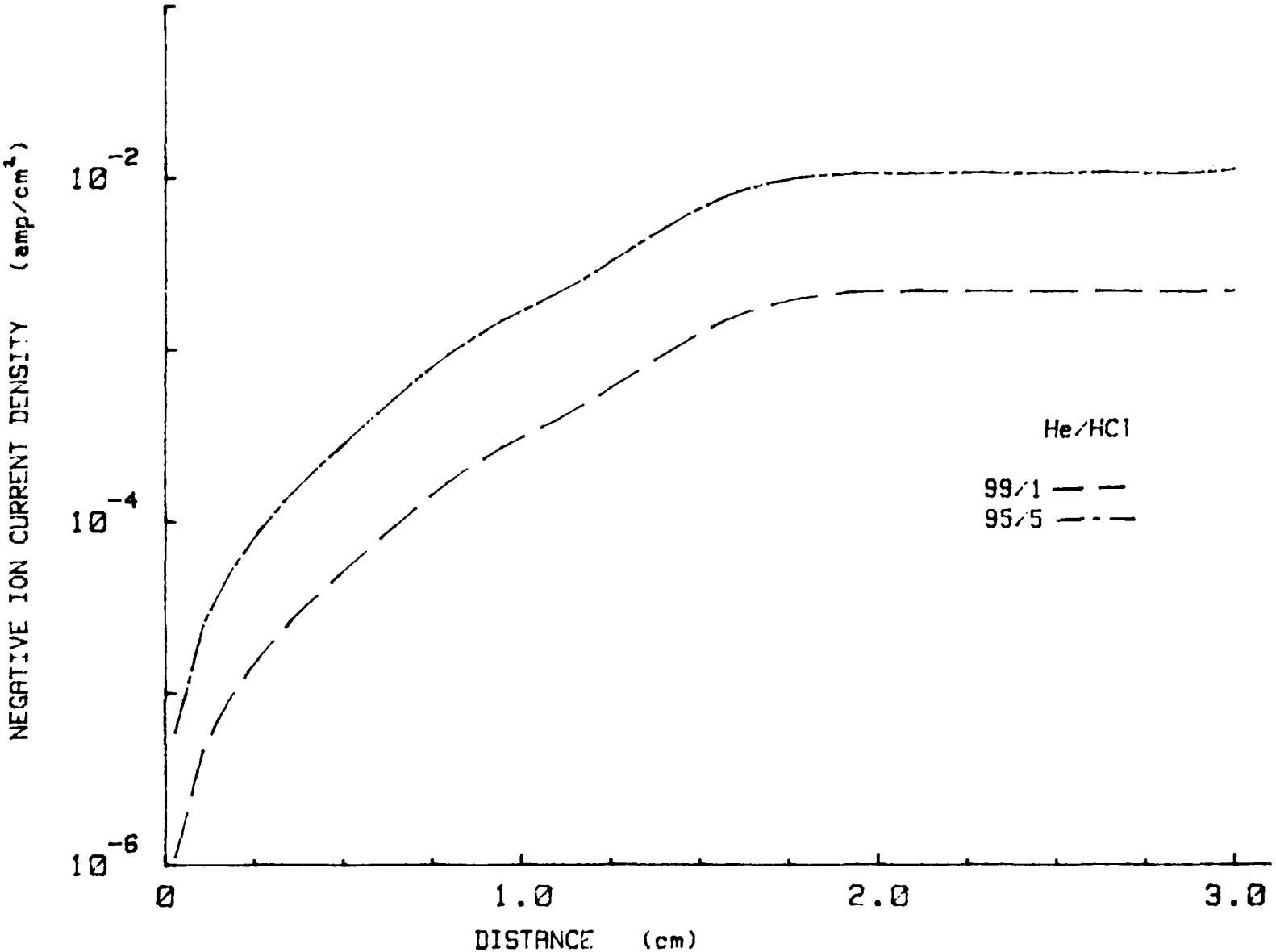

FIG III-7 NORMALIZED NEGATIVE ION CURRENT DENSITY IN He/HCl MIXTURES

value, within 1%. Better agreement is achieved in Ar than in He because the slope of the electric field is steeper in Ar resulting in less error in the cathode fall length and voltage. Approximately the same discrepancy exists in the positive ion drift velocity in Ar as in He. At 400v/cm-torr, Ward's approximation in equation III-73 (where for Ar μ_+ = 1.E3cm²-torr/volt-sec, k_+ = 8.25E3 $cm^{\frac{3}{2}}$-$torr^{\frac{1}{2}}$/$volt^{\frac{1}{2}}$-sec, C = 2.22E-3 torr-cm/volt, D = 86.52 $volt^{\frac{3}{2}}$/$cm^{\frac{3}{2}}$-$torr^{\frac{3}{2}}$, and W_1 = 60v/cm torr) yields a positive ion velocity that again is about 1% larger, whereas at 60v/cm-torr it is 18% larger.

Contrary to He mixtures there is a negligible effect on the electric field in the cathode fall region (0.-.66cm) in Fig III-8 when up to 5% HCl is added to an Ar discharge. In this case, since HCl has a slightly lower ionization potential than that for Ar (12.7eV as compared to 15.7eV), the small additional ionization due to the small percentage of HCl is insufficient to be seen as any effect on the electric field in the cathode fall region. Fig III-9 shows the same calculation in 95/5 Ar/HCl with and without the contribution of ionization from HCl. As expected, the electric field is increased, but not as much as for the He/HCl case since the thresholds for ionization are much closer. Similarly no change is seen in Fig III-10 in the electron current density in the cathode fall region. The negative ion current density in Fig III-11 never becomes a significant fraction of the total discharge current density. The negative ion density increases much more slowly than for the He case, since the fields in the cathode fall and positive column are higher in Ar than in He.

Table III-2

Summary of GLOW Code Results for Ar/HCl Mixtures

Ratio Ar/HCl		γ or Cathode Material	E_o/p $\frac{\text{volt}}{\text{cm-torr}}$	E_{min}/p $\frac{\text{volt}}{\text{cm-torr}}$	pd_c (torr-cm)	J/p^2 $\frac{\mu\text{ amp}}{\text{cm}^2\text{-torr}^2}$	V_c (volt)	SF (γ, k_+) $\frac{\times 10^{-9}\text{ amp}^{\frac{1}{2}}\text{torr}^{\frac{1}{2}}\text{cm}^{\frac{1}{2}}}{\text{volt}^{\frac{3}{2}}}$
100/0								
Experimental	i	Mg	-	-	-	20	119	-
	i	Fe	-	-	.33	160	165	4.72
	i	Ni	-	-	-	160	131	-
	i	Pt	-	-	-	150	131	-
	i	Al	-	-	.29	-	100	-
	i	Other	-	-	-	-	64.-196.	-
Theoretical	ii	.04	-	-	.9	4.5	146.	1.96
	iii	.04167	427.39	14.52	.656	10.	147.78	1.94
99/1								
Theoretical	iii	.04167	427.42	14.99	.657	10.	147.87	1.95
95/5								
Theoretical	iii	.04167	427.52	16.21	.657	10.	148.11	1.94

i Data was taken from a summary presented in ref 6.
ii Data was taken from ref 85.
iii Data was calculated in this study.

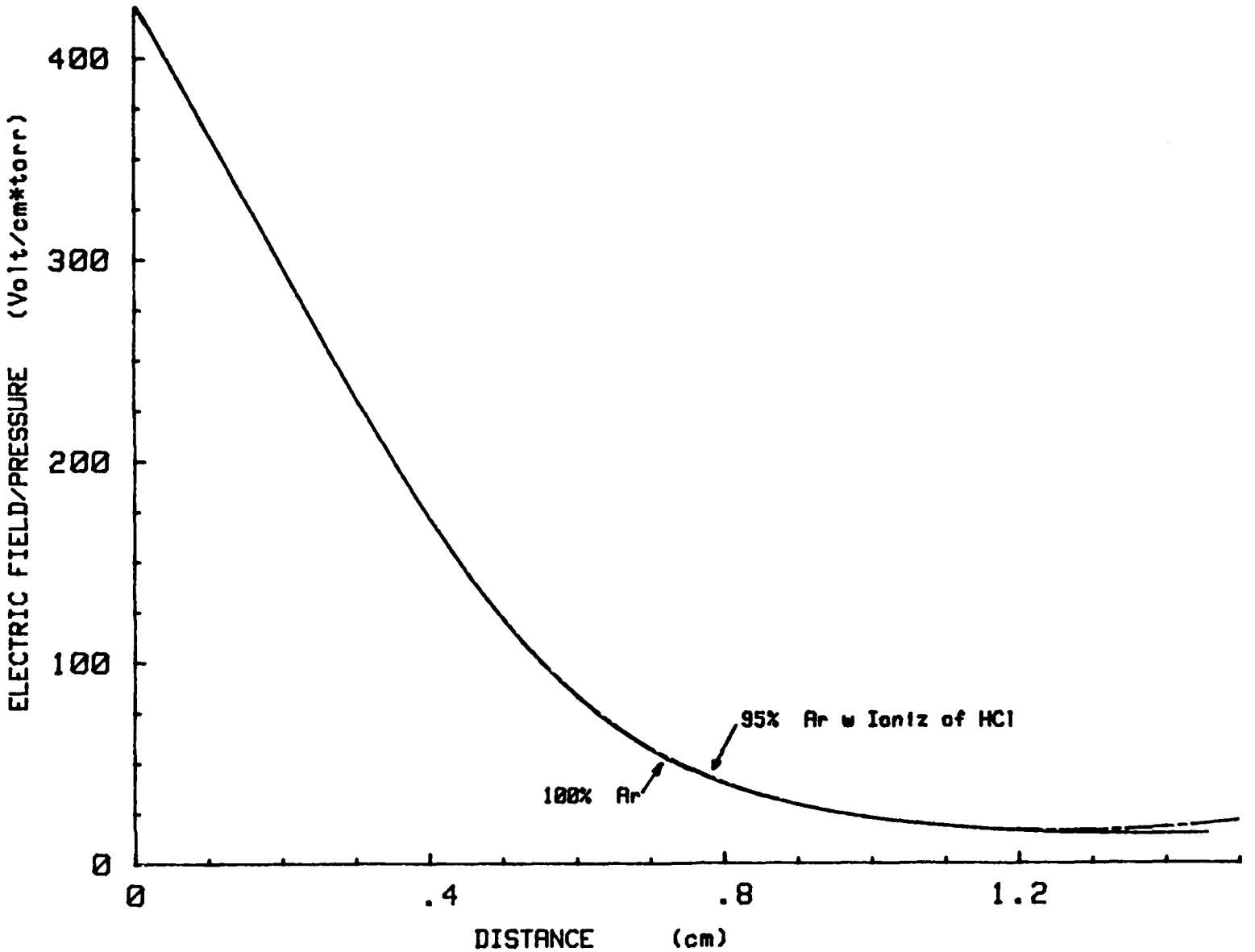

FIG III-8 ELECTRIC FIELD IN Ar/HCl MIXTURES

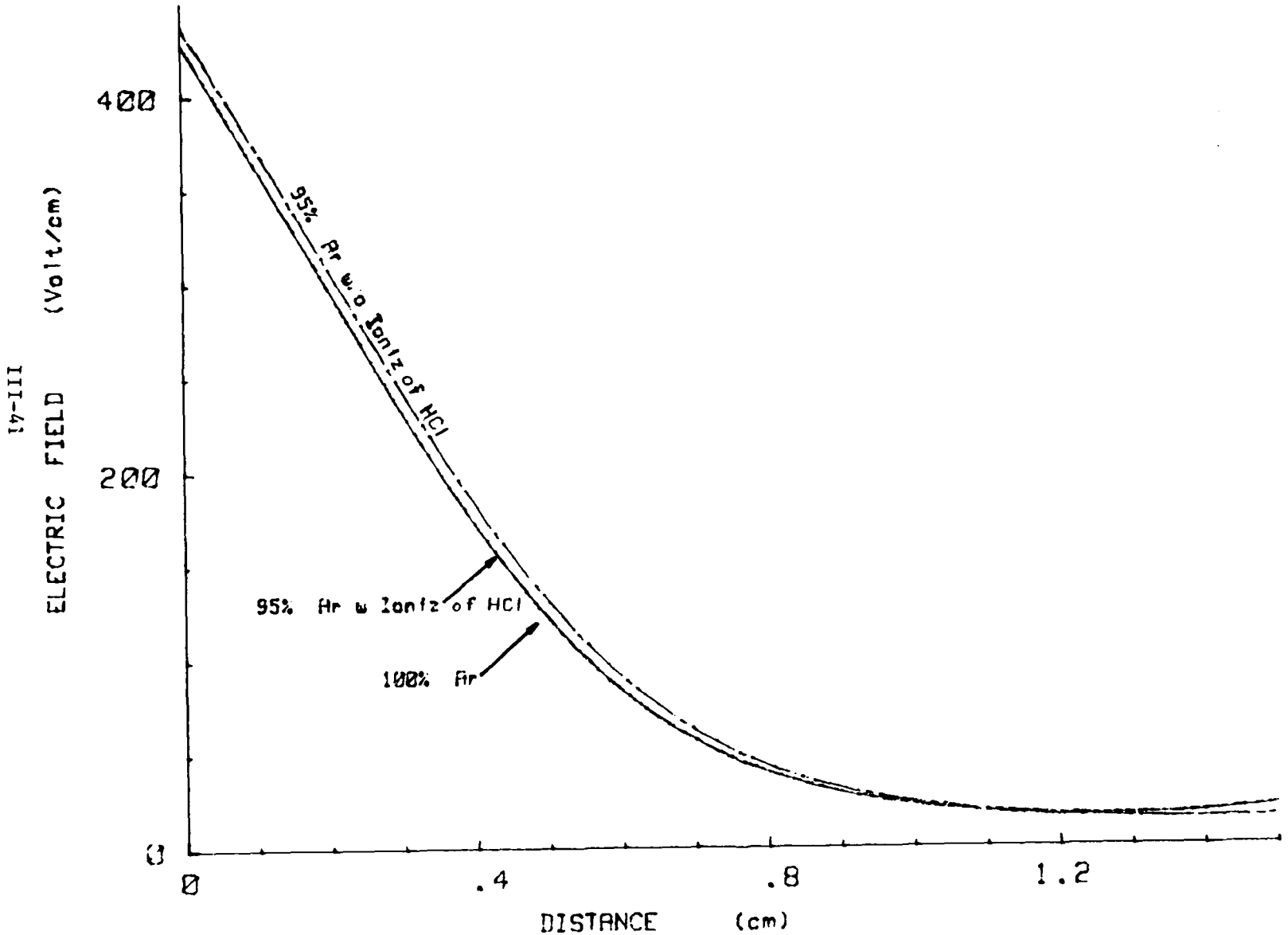

FIG III-9 EFFECT OF IONIZATION OF HCl IN Ar/HCl MIXTURES

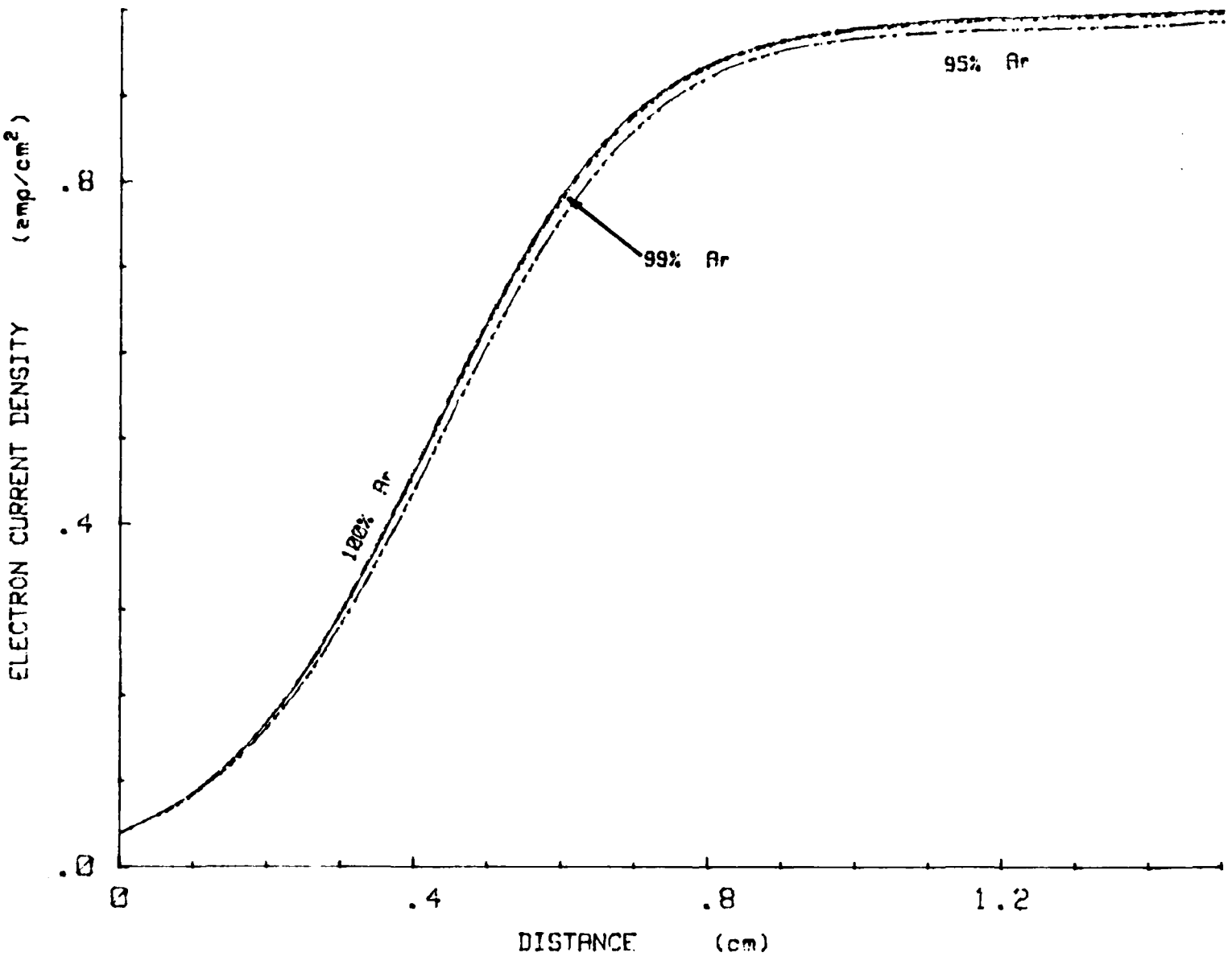

FIG III-10 NORMALIZED ELECTRON CURRENT DENSITY IN Ar/HCl MIXTURES

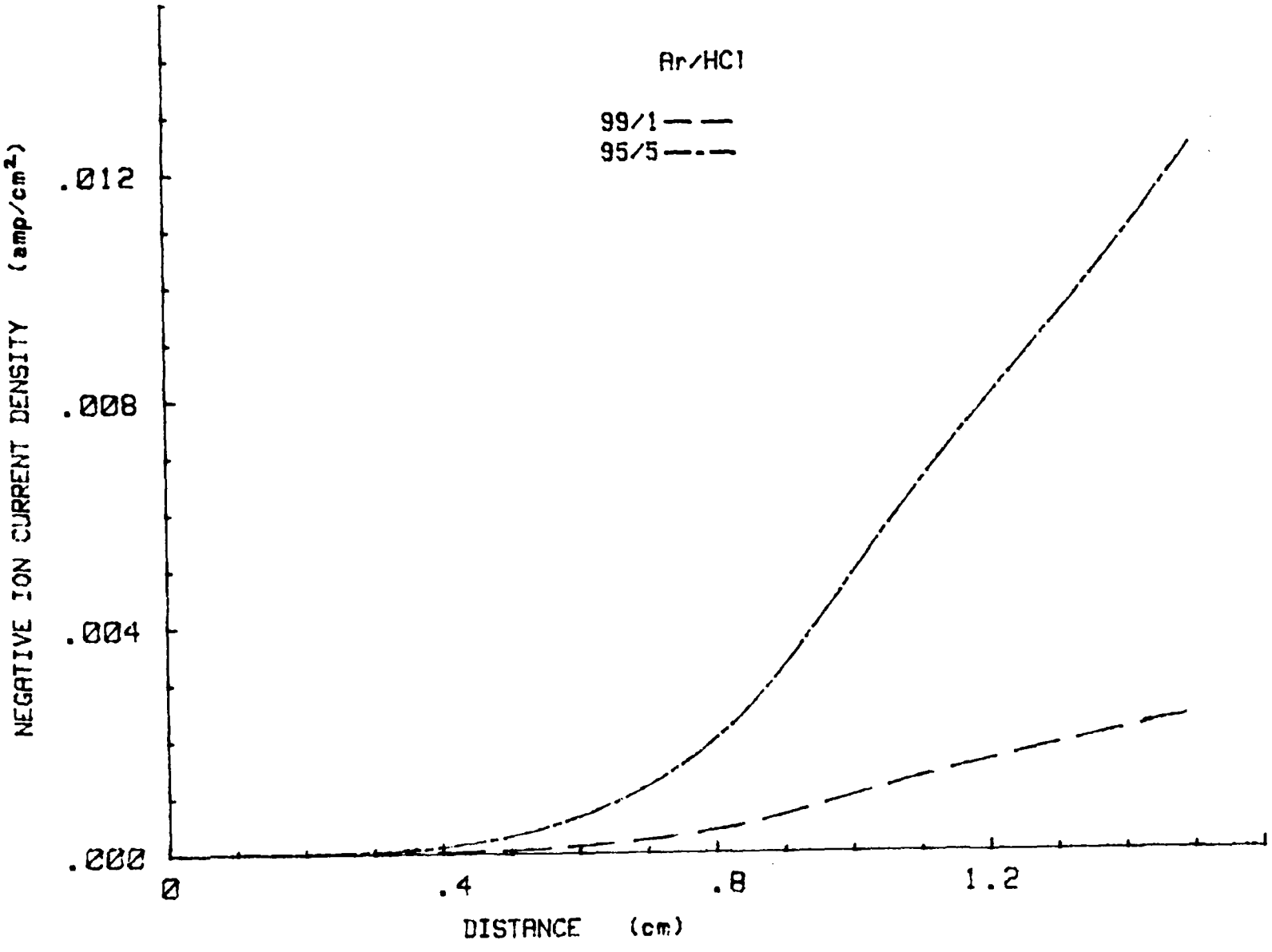

FIG III-11 NORMALIZED NEGATIVE ION CURRENT DENSITY IN Ar/HCl MIXTURES

In the positive column (around 1.2cm) the electric field is increased approximately 3% for a 99/1 Ar/HCl mixture (not plotted) and almost 12% increase for a 95/5 mixture. Again this is the result of an increase in the number of attaching molecules in the positive column region.

Xenon

The results for Xe/HCl mixtures with p = 100 torr, d = .01cm, J = .1 amp/cm^2, and γ = .004 will be presented next. This value of γ was chosen so results could be compared with Ward's results (ref 85). A summary of numerical values for the following figures is given in Table III-3 as was done for the previous mixtures.

In 100% Xe, there is apparent agreement (6%) between the scaling factors calculated from Wards data and the data from the GLOW code. Approximately the same discrepancy exists in the positive ion drift velocity as in the previous rare gases. At 690 v/cm-torr, Ward's approximation using equation III-73

(where in Xe μ_+ = 4.E2 cm torr/volt-sec,
k_+ = 4.E3 cm$^{\frac{3}{2}}$-Torr$^{\frac{1}{2}}$/volt$^{\frac{1}{2}}$-sec, C = 2.25E-3 torr-cm/volt,
D = 225 volt$^{\frac{3}{2}}$/cm$^{\frac{3}{2}}$-torr$^{\frac{3}{2}}$, and W_1 = 100 v/cm-torr)

yields a positive ion velocity that is about 1% larger, whereas at 100 v/cm-torr, it is 23% larger.

In Xe mixtures there is a very slight trend for the electric field to increase in the cathode fall region (0.-.6cm) as the percentage of HCl is increased. This is observable in Fig III-12. Xe/HCl mixtures

Table III-3

Summary of GLOW Code Results for Xe/HCl Mixtures

Ratio Ar/HCl		or Cathode Material	E_o/p volt / cm-torr	E_{min}/p volt / cm-torr	pd_c (torr-cm)	J/p^2 μamp / cm^2-$torr^2$	V_c (volt)	SF (γ, k_+) 10^{-11} amp $torr^{\frac{1}{2}}cm^{\frac{1}{2}}$ / $volt^{\frac{3}{2}}$
100/0								7.583
Experimental	i	Fe	-	-	.23	16	306	7.58
Theoretical	ii	.004	-	-	.7	6.2	212	82.3
	iii	.004	690.7	33.26	.592	10.	212	87.4
99/1								
Theoretical	iii	.004	693.6	33.76	.594	10.	213.2	87.3
95/5								
Theoretical	iii	.004	695.3	34.46	.598	10.	215.9	87.2
90/10								
Theoretical	iii	.004	722.4	36.22	.604	10.	219.5	87.2

i Data was taken from a summary presented in ref 6.
ii Data was taken from ref 85.
iii Data was calculated in this study.

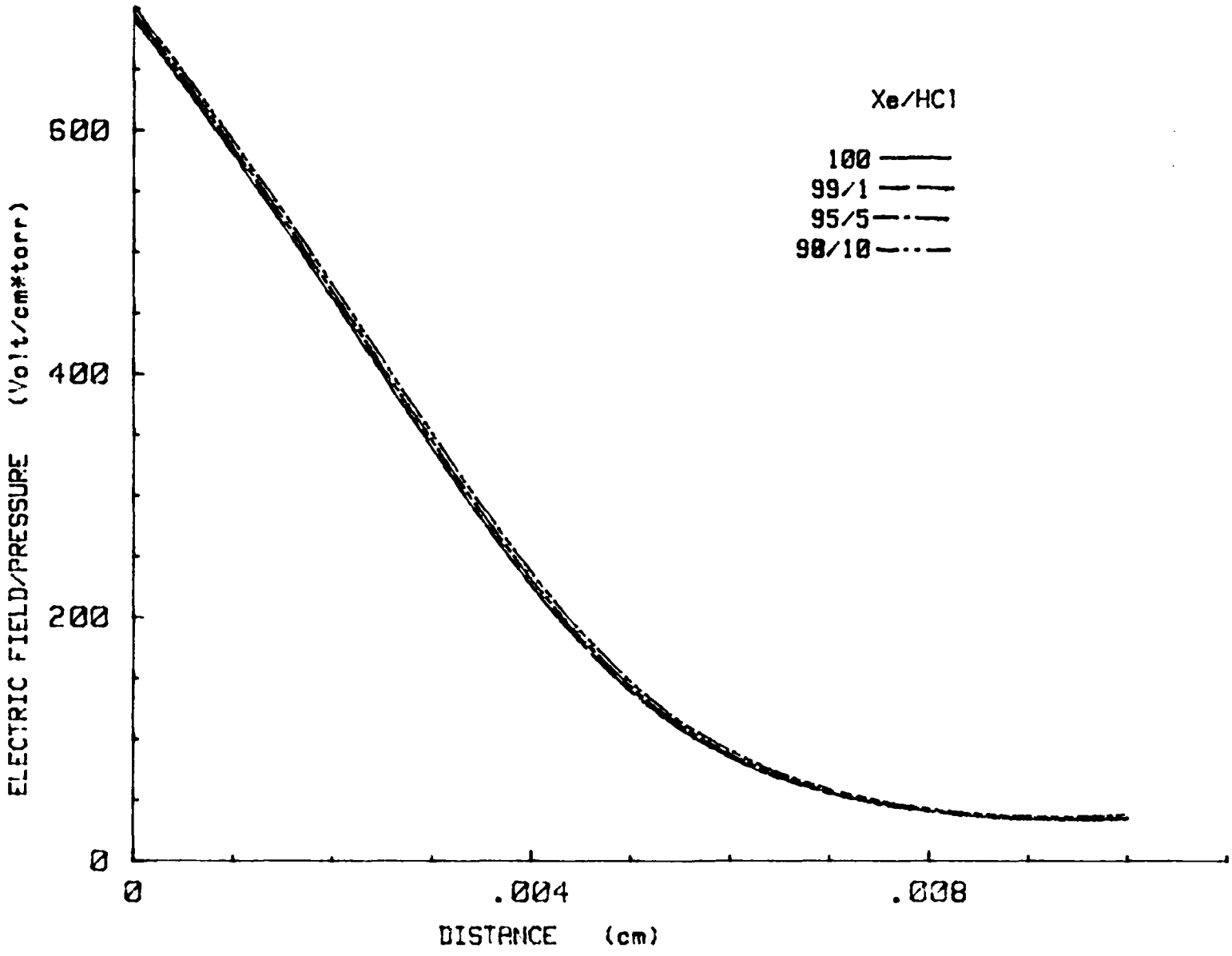

FIG III-12 ELECTRIC FIELD IN Xe/HCl MIXTURES

are unique in that both constituents have almost the same ionization potential (12.74eV for HCl and 12.13eV for Xe). Thus only effects of attachment are observed and the results agree with the analytical description given earlier. The effect of attachment is to raise the field slightly throughout the cathode fall region.

Even though the field increases as HCl is added to Xe, the electron current density decreases slightly throughout most of the cathode fall region in Fig III-13 due to the pure loss of electrons to attachment. As in Ar mixtures, the negative ion current density in Fig III-14 grows very slowly near the cathode but begins to grow rapidly as the electric field levels off into the positive column. It is still insignificant in comparison to the contribution from the electron and positive ion current densities to the total discharge current density.

In the positive column (around .009 cm) the electric field increases approximately 2% for 99/1 mixture, 4% for 95/5 mixture, and 9% for 90/10 mixture. Again this is the result of an increase in the number of attaching species in the positive column and the imposed boundary condition of constant current.

In summary, the above calculations, which implicitly assumed that the electrons were in equilibrium with the local field, have shown that:

a. The formation of small amounts of negative ions in the cathode fall region is not the reason that the cathode a length contracts in the axial direction.

b. The observed contraction of the cathode full length is a result of the increased ionization from the more efficient ionization of the attaching gas in some gas mixtures. The contraction will only

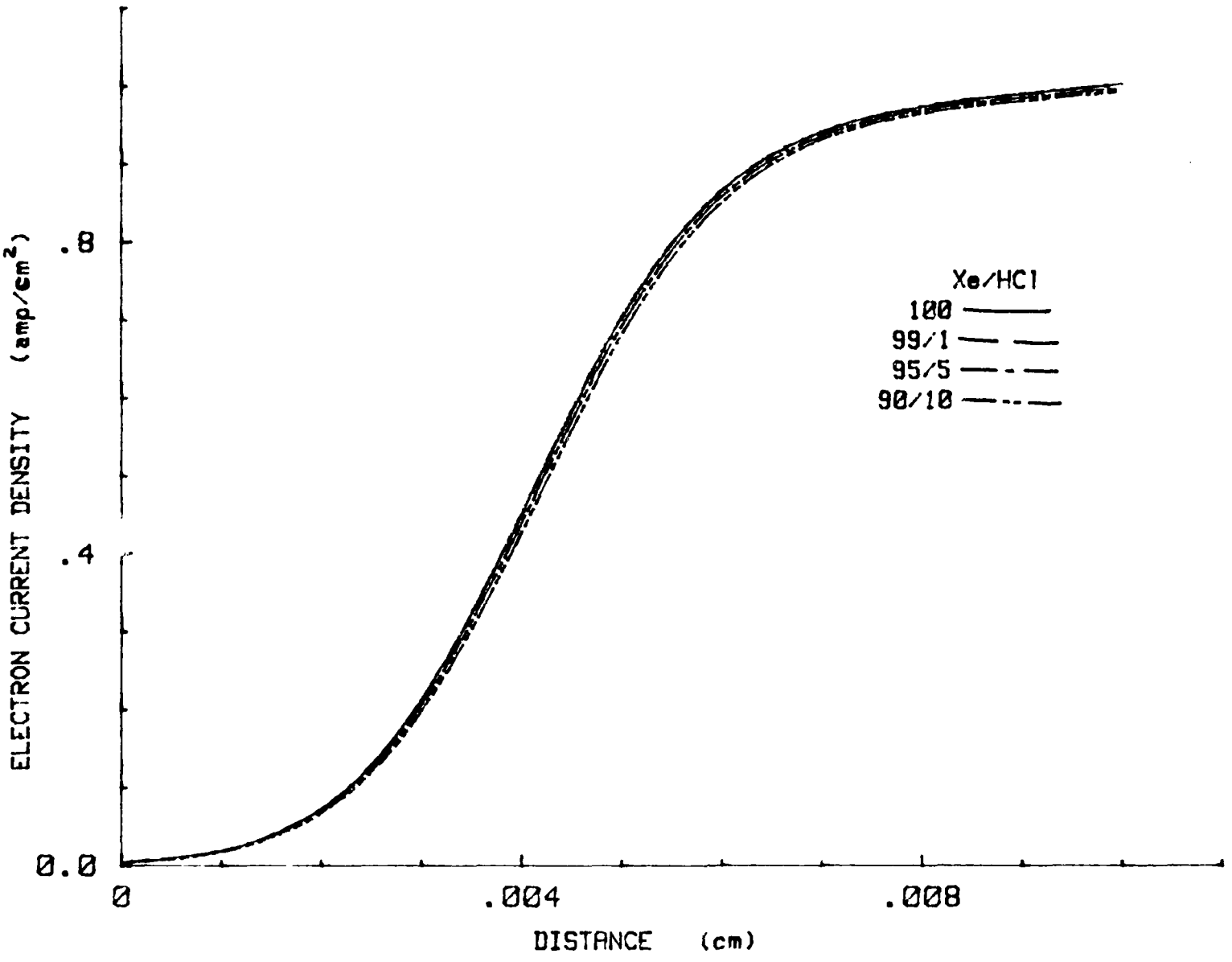

FIG III-13 NORMALIZED ELECTRON CURRENT DENSITY IN Xe/HCl MIXTURES

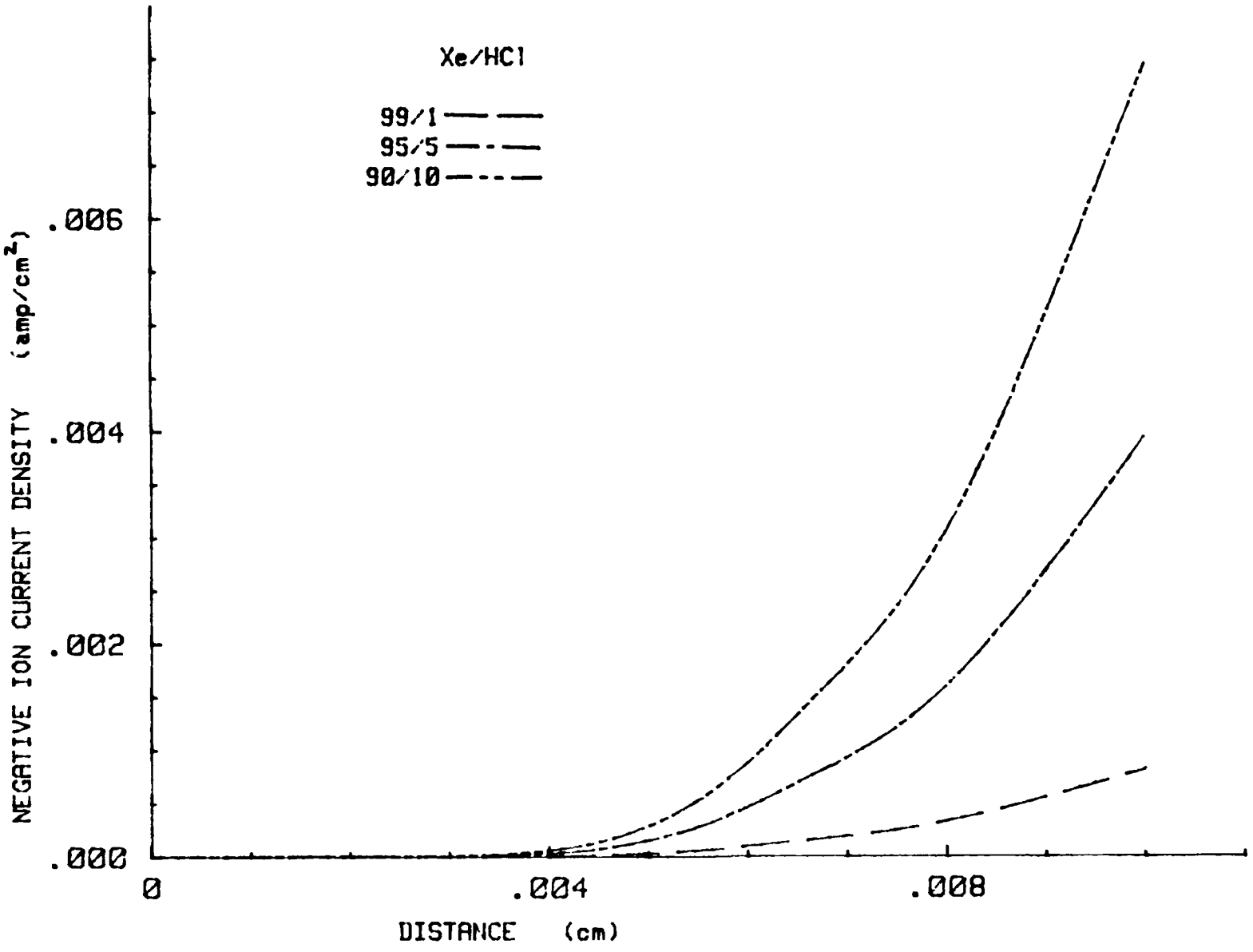

FIG III-14 NORMALIZED NEGATIVE ION CURRENT DENSITY IN Xe/HCl MIXTURES

appear in gas mixtures in which the ionization rate of the attaching gas is larger than that of the background gas.

c. When the ionization rates and thresholds of both gases in the mixture are similar, then the formation of negative ions tends to increase the voltage drop across the cathode fall region and to increase the field at the cathode.

d. The field in the positive column region increases as the percentage of attacher is increased. This is required in order to balance the electron gain and loss processes and to maintain a constant current.

Chapter IV. Electron Kinetics in the Cathode Fall Region: Nonequilibrium Analysis

Review of Nonequilibrium Analyses

The analyses in Chapter III were all based on Poisson's equation and current continuity or flux equations. These analyses presuppose that the electron energy distribution function is in equilibrium with the local electric field. As mentioned in Chapter I, there is analytical evidence that the electrons are not in equilibrium with the electric field in the cathode fall region. Since the electron current or flux is an average over the product of the electron number density times the electron velocity, <nv>, it is not possible to derive n or v from this average unless the nonequilibrium electron energy distribution function is known. There are two methods of calculating the electron energy distribution function:

1) by using a Monte Carlo simulation of the electrons as they drift from cathode to anode, or

2) by calculating the distribution function from the Boltzmann equation.

This chapter will critically review and, where appropriate, point out defects in the few papers that have investigated the nonequilibrium electron kinetics using either of these two methods. The new results of this study, which used a self-consistent Boltzmann method and included dissociative attachment, will be presented at the end of the chapter.

First, a comparison will be made between the Monte Carlo method and the Boltzmann method. Although both methods should yield similar

results, there are important computer and scientific differences. The Monte Carlo method is much more costly in terms of computer time. In order to obtain good statistics, a large number of collisions are required, typically 10^5 or greater. The advantage of the Monte Carlo method lies in its ease of implementation as a computer code. However, the Boltzmann method normally enables a greater insight into the physics of the situation. The sensitivity to changes in inputs is more easily investigated primarily due to the shorter run time. This enables approximate analytical solutions to be found which illustrate the dependence on the relevant parameters. In uniform electric fields, the agreement between Monte Carlo results and Boltzmann analyses have been excellent (ref 62, 72, 77).

The theory and first calculation of the electron distribution function as a function of distance through the cathode fall region was reported by Allis and co-workers (ref 13, 14) in 1975 and 1977. Their approach involved transforming Boltzmann's equation into energy space where the new variables are the electron potential energy, $\phi = e\int E(x)dx$ and the electron kinetic energy $\xi = \frac{1}{2}mv^2$. In addition, they treated the cathode fall region as a separate entity allowing for no flux of positive ions from the negative glow and forcing the electric field to zero at the anode. Their calculations were based on an 'ideal' gas defined as having a constant momentum transfer cross section and constant excitation and ionization cross sections with thresholds of 8eV and 16eV respectively. In addition their calculations are not considered self-consistent, meaning the calculations of the electron number density and electric field were not iterated on successively to converge to a self-consistent solution. The nonequilibrium phenomena

which their calculations demonstrated included:

a. A dip in the electron number density adjacent to the cathode. This results from the electrons being accelerated away from the cathode and not yet having sufficient energy for ionization.

b. A peaked ionization coefficient which is small near the cathode where the field is highest and peaking between one half and two thirds the total cathode fall length.

This technique of transforming Boltzmann's equation into energy space has become the basis of several investigations discussed later.

Almost simultaneously with Allis, Tran Ngoc, et al. (ref 86) used a one dimensional Monte Carlo method to investigate the nonequilibrium electron kinetics of the cathode fall. They began by assuming a linearly decreasing electric field. Although no attempt was made to correct the field through Poisson's equation, their results did give a good physical picture of the nonequilibrium process occurring in a high field gradient. They found the electron distribution function evolved from a sharply peaked distribution near the cathode to a multiply peaked distribution entering the negative glow. This was the first theoretical prediction of the three groups of electrons observed experimentally by Pringle and Farvis (ref 73) in the negative glow (high energy electrons which have undergone few collisions, intermediate energy electrons which form the bulk of the distribution, and low energy electrons which were primarily a result of ionization processes). Tran Ngoc, et al. concluded that the use of Townsend's ionization coefficient given by equation III-38 was inappropriate in the cathode fall region since the electrons never reached equilibrium with the field. In addition they determined that the major features of the cathode fall are actually determined by a

small number of inelastic collisions and that elastic collisions play only a subsidiary role.

The most definitive work using a Boltzmann analysis was accomplished by Long (ref 60). It was based upon an approach outlined by Allis (ref 13) of a direct solution of the Boltzmann equation without the conventional expansion methods. Long simplified Allis' result by simplifying the angular dependence of the distribution function in the cathode fall region. His method of solution was first to estimate the distribution function and, to use this in the collision terms to integrate the distribution function along the various energy characteristics. The distribution function was iterated until there was less than .2% change in the distribution function at each energy bin and then the electron number densities and electron current densities were calculated from the distribution function as a function of distance. He attempted to use these values to solve Poisson's equation for the electric field before repeating the process to converge on a self-consistent solution. Long's results and conclusions for mercury and argon agreed very well with those of Tran Ngoc for helium. However, in his integration of Poisson's equation for the electric field, he failed to include any change in the ion drift velocity due to changes in the electric field that occurred from assuming current continuity. This limited the convergence of his code to unique cases where the anode was placed inside the cathode sheath. The resolution of this problem and further improvements of Long's computer code are described in the following section. His program required 202K of memory to load and run. Run times were typically 5-10sec per field iteration on a CDC 6600 computer.

More recently Segur, et al. (ref 79) coupled a Boltzmann solution

for the electrons with an analytical approximation to the Boltzmann equation for positive ions in the cathode fall region for various helium-mercury mixtures. They assumed the electron collisions were isotropic and only considered charge transfer collisions with a constant cross section for the positive ions. They did not have to use conservation of current to calculate the positive ion density as a function of position as Long had done. Segur, et al. initially assumed a linearly decreasing electric field vanishing at the anode. Within 3-4 iterations of calculating the electron and ion densities, followed by solving Poisson's equation for the field, their numerical technique achieved a stable convergence. Thus their technique was self-consistent. As the percentage of mercury was increased from 0% to 9.1%, the peak of the ionization coefficient increased and the threshold for ionization shifted towards the cathode. This is due to the fact that mercury atoms have a larger ionization cross section as well as a lower ionization threshold than helium atoms. They found the ionization in the cathode fall region took place in two stages: mercury is ionized first near the cathode and helium is ionized slightly further away from the cathode. Eventually both processes exist together during the remaining part of the discharge. Since the mobility of the mercury atoms is much lower than helium atoms, they also found a smaller ionic current near the cathode and a larger ionic current near the anode when mercury was added.

At the same time, Boeuf, et al. (ref 21) investigated the cathode fall in a helium discharge using a self-consistent Monte Carlo technique. They also investigated some features in an oxygen discharge. They performed one Monte Carlo calculation for positive ions and found

that the positive ion drift velocity reached equilibrium with the field in less than 10^{-2} cm. Thereafter they assumed that the ions drifted towards the cathode with their equilibrium drift velocity. In their self-consistent iterations between the number density and the field, their calculations normally reached convergence after 5 iterations. They concluded from their ionization coefficient and electron drift velocity data that the nonequilibrium region in a helium discharge extends just over half (54%) of the cathode fall length which agreed with the previous investigations.

A three dimensional Monte Carlo calculation was accomplished very recently by Boeuf, et al. (ref 20). They made extensive use of the null collision technique using a fictitious total cross section to maintain a pseudo-constant collision frequency so that numerical integrations could be avoided in determining the time interval between two collisions. This allowed them to calculate a three-dimensional electron distribution function more efficiently taking angular scattering into account. Radial fields were not included and no attempt was made to iterate successively on the electron number density and electric field. Thus their calculations were not self-consistent. They examined two cases: 1) a normal glow discharge in helium at one torr with an absorbing anode placed in the negative glow, and 2) an abnormal discharge in helium at one torr. They found that there is little error if isotropic scattering is assumed and the momentum transfer cross section is used as the elastic cross section instead of assuming angular scattering and using the elastic differential cross section. Boeuf et al. showed that the original assumption of forward scattering made by Tran Ngoc (ref 86) led to too high of electron energies in the latter two thirds of the

cathode fall. As a result of all the electrons being directed in the same direction and at too high of energy, the Townsend ionization coefficient for the forward scattering case was as much as 25% too low through most of the latter two thirds of the cathode fall region. They calculated the Townsend ionization coefficient by integrating the ionization cross section and electron distribution function. Its maximum occurred somewhat beyond the maximum of the mean energy distribution. They concluded that as a result of the bimodal character of the electron distribution function,the mean energy and ionization coefficient were not related to the same part of the distribution function. Finally, their angular distribution functions show that the high energy segment of the distribution function is largely forward directed, while that of the low energy part is much more isotropic. As a function of distance through the cathode fall region, this trend became much more evident close to the negative glow. This concludes the critical review of nonequilibrium techniques.

Description and Modifications to Program SHEATH

The SHEATH program was developed by W. H. Long to solve the Boltzmann equation for electrons in non-uniform fields without requiring the electron distribution function to be in equilibrium with the local field. The collisional Boltzmann equation describes the evolution of a swarm of electrons in both space and time, and is given by

$$\frac{\partial f}{\partial t} + \bar{v} \cdot \bar{\nabla} f + \bar{a} \cdot \bar{\nabla} f = \frac{\partial f}{\partial t}\Big)_{col} \qquad \text{(IV-1)}$$

where $f = f(\bar{r},\bar{v},t)$ is the electron distribution function which represents a complete statistical description of the electron in a weakly ionized gas. The variable t is time, $\bar{v}$ is the electron velocity vector, $\bar{r}$ is the electron spatial vector, $\bar{a} = -e/m\ (\bar{E} + \bar{v} + \bar{B})$ is the acceleration of the electrons due to electric and magnetic fields. $\left(\frac{\partial f}{\partial t}\right)_{col}$ represents the change in the distribution function due to elastic and inelastic electron collisions.

Considering only spatial variations in the direction of the electric field, then IV-1 reduces to

$$v_x \frac{\partial f}{\partial x} + \frac{e}{m} E(x) \frac{\partial f}{\partial v_x} = \left(\frac{\partial f}{\partial t}\right)_{col} \qquad \text{(IV-2)}$$

Dividing both sides by v_x and $eE(x)$, equation IV-2 can be transformed into energy space.

$$\frac{\partial f}{\partial \phi} + \frac{\partial f}{\partial \xi} = \frac{1}{e v_x E(x)} \left(\frac{\partial f}{\partial t}\right)_{col} \qquad \text{(IV-3)}$$

where $\phi = e \int E(x)dx$ is the electron potential energy and $\xi = \frac{1}{2}mv_x^2$ is the electron kinetic energy in the field direction. By defining the total kinetic energy as $\varepsilon = \xi + \eta$, then f can be represented as the sum of two functions, $f_-(\varepsilon, \xi, \phi)$ which is the distribution of electrons with $v_x < 0$ moving against the field and $f_+(\varepsilon, \xi, \phi)$ which is the distribution of electrons with $v_x > 0$ moving with the field. The variable η represents the electron random kinetic energy. Equations IV-2 and IV-3 can be used to mathematically define equilibrium and nonequilibrium regions. Equilibrium can be defined as occurring when $\frac{\partial f}{\partial \phi} < \frac{\partial f}{\partial \xi}$ or when $\frac{\partial f}{\partial \xi} \approx \frac{1}{e v_x E(x)} \left(\frac{\partial f}{\partial t}\right)_{col}$. Thus the kinetic energy gained from the field is balanced by the loss of energy to collisions. In nonequilibrium regions, the decrease in the potential energy of the

electrons is converted predominantly into an increase in their kinetic energy. In equation IV-2, equilibrium can similarly be defined as occurring when $v_x \frac{\partial f}{\partial x} < \frac{eE(x)}{m} \frac{\partial f}{\partial v_x}$ or when $\frac{\partial f}{\partial v_x} \approx \frac{m}{eE(x)} \frac{\partial f}{\partial t}\Big)_{coll}$. In other words, equilibrium exists when the distribution function changes faster in velocity space than it does as a function of position. This was the definition used in Chapter I.

In the absence of collisions, f is constant along the energy characteristics, $\xi - \phi$ = constant. These characteristics correspond to electron trajectories in the two-dimensional energy space (ξ, ϕ). The right hand term in equation IV-3 represents the change in f along the energy characteristics when collisions are included. This collision term is a complicated function involving f, and the cross-sections for all the various collision processes. The theory and derivation of this term is described in Long's report (ref 60:12-21). He showed that IV-3 can be put in operator form

$$\frac{\partial f}{\partial \phi} + \frac{\partial f}{\partial \xi} = \frac{1}{e\, E/N(\phi)} \left(\frac{\varepsilon}{\xi}\right)^{\frac{1}{2}} (K - Q(\varepsilon)) f \qquad \text{(IV-4)}$$

where K is an integral operator representing a sum over all collisional processes and $Q(\varepsilon)$ is the total cross section for electrons with total kinetic energy ε. Using this technique, the distribution function f does not need to be stored between iterations, only Kf must be retained. The collision term can be further simplified by assuming Kf is nearly isotropic in velocity space and expanding Kf in Legendre polynomials, $P_1(\cos\theta)$ for example.

$$Kf = \sum_{l=0}^{\infty} A_l(v)\, P_l(\cos\theta) \qquad \text{(IV-5)}$$

where $$A_l(v) = \frac{2l+1}{2} \int_{-1}^{+1} \frac{1}{Nv} \left(\frac{\partial f}{\partial t}\right)_{col} P_l(\cos\theta)\, d(\cos\theta)$$

This expansion is quite different from the usual two term expansion of Boltzmann's equation in spherical harmonics. This expansion is an expansion of the product of the integral operator times f, and not an expansion of f. Assuming that the secondary electrons are emitted isotropically and neglecting superelastic electron collisions and the recoil term for electrons, Long derived the following form of the Boltzmann equation in terms of the total electron energy:

$$\frac{\partial f}{\partial \phi} + \frac{\partial f}{\partial \xi} = \frac{1}{e E_N(\phi)} \frac{1}{\cos\theta} \left[\sum_{l=0}^{\infty} \frac{1}{2l+1} \left\{ f_l(\varepsilon,\phi)\, Q_l^e(\varepsilon) \right.\right.$$

$$\left. + \sum_h \frac{\varepsilon+\varepsilon^h}{\varepsilon} f_l(\varepsilon+\varepsilon^h,\phi)\, Q_l^h(\varepsilon+\varepsilon^h) + \int_{\varepsilon+\varepsilon_i}^{\infty} \frac{\varepsilon'}{\varepsilon} f_l(\varepsilon',\phi)\, Q_l^i(\varepsilon',\varepsilon)\, d\varepsilon' \right\} P_l(\cos\theta) \qquad \text{(IV-6)}$$

$$\left. - f(\varepsilon,\xi,\phi) \left\{ Q_o^e(\varepsilon) + \sum_h Q_o^h(\varepsilon) + \int_0^{\frac{\varepsilon-\varepsilon_i}{2}} Q_o^i(\varepsilon,\varepsilon')\, d\varepsilon' + Q_o^a(\varepsilon) + \frac{n_+}{N} Q(\varepsilon) \right\} \right]$$

where

$$\cos\theta = \pm \left(\frac{\xi}{\varepsilon}\right)^{\frac{1}{2}}$$

$$f_l(\varepsilon,\phi) = \frac{2l+1}{2} \int f(\varepsilon, \varepsilon\cos^2\theta, \phi)\, P_l(\cos\theta)\, d(\cos\theta)$$

$$Q_l(\varepsilon) = 4\pi \frac{2l+1}{2} \int \sigma(\gamma,\varepsilon)\, P_l(\cos\gamma)\, d(\cos\gamma)$$

ε_h = inelastic collision energy loss
ε_i = ionization energy loss
Q_o^i = collision cross section integrated over all scattering angles
superscript h refers to a sum over inelastic processes
superscript i refers to a sum over ionization processes
superscript e refers to a sum over elastic collision processes
superscript a refers to an attachment
superscript r refers to recombination
n_+ = positive ion density

Thus, in equation IV-4, the electrons scattered-in is represented by

$$Kf = \sum_{l=0}^{\infty} \frac{1}{2l+1} \left[f_l(\varepsilon,\phi) Q_l^e(\varepsilon) + \sum_h \frac{\varepsilon+\varepsilon^h}{2} f_l(\varepsilon+\varepsilon^h,\phi) Q_l^h(\varepsilon+\varepsilon^h) + \int_{\varepsilon+\varepsilon_i}^{\varepsilon'} \frac{\varepsilon'}{\varepsilon} f_l(\varepsilon',\phi) Q(\varepsilon,\varepsilon') d\varepsilon' \right] P_l(\cos\theta) \quad \text{(IV-7)}$$

and the electrons scattered-out is represented by

$$Q(\varepsilon)f = f(\varepsilon,\xi,\phi) \left\{ Q_o^e(\varepsilon) + \sum_h Q_o^h(\varepsilon) + \int_0^{\frac{\varepsilon-\varepsilon_i}{2}} Q_o^i(\varepsilon,\varepsilon') d\varepsilon' + Q_o^a(\varepsilon) + \frac{n_t}{N} Q_o^r(\varepsilon) \right\} \quad \text{(IV-8)}$$

Equation IV-4 is solved numerically using an iterative technique for evaluating Kf. It is assumed initially that there is no contribution from scattered in electrons, ie Kf = 0 and equation IV-6 is then integrated both for forward moving electrons and backward moving electrons for each value of $\eta=\varepsilon-\xi$. This yields a first approximation to the distribution function from which a new Kf can be calculated. The procedure is repeated until convergence is reached, typically when there is less than .2% change in the distribution function. By performing the integration in a specific order the same array can be used to store both the old and the new values of Kf, thus minimizing computer storage requirements. The arrays for Kf_+ and Kf_- are trapezoidal in shape since $f_{\pm}(\varepsilon,\xi,\phi) = 0$ for $\xi > \phi+\xi_0$, where ξ_0 is the initial kinetic energy in the field direction of the electrons leaving the cathode. Fig IV-1 shows how the arrays for Kf are arranged in core to further minimize storage requirements. The total area of the array in Fig IV-1 is $48{,}240_{10}$ ($136{,}160_8$) words. For a 200V cathode fall, these dimensions give a 1eV energy resolution. The storage of only Kf prevents the distribution function from being known as a function of distance, except at the cathode and anode where it is stored in sepa-

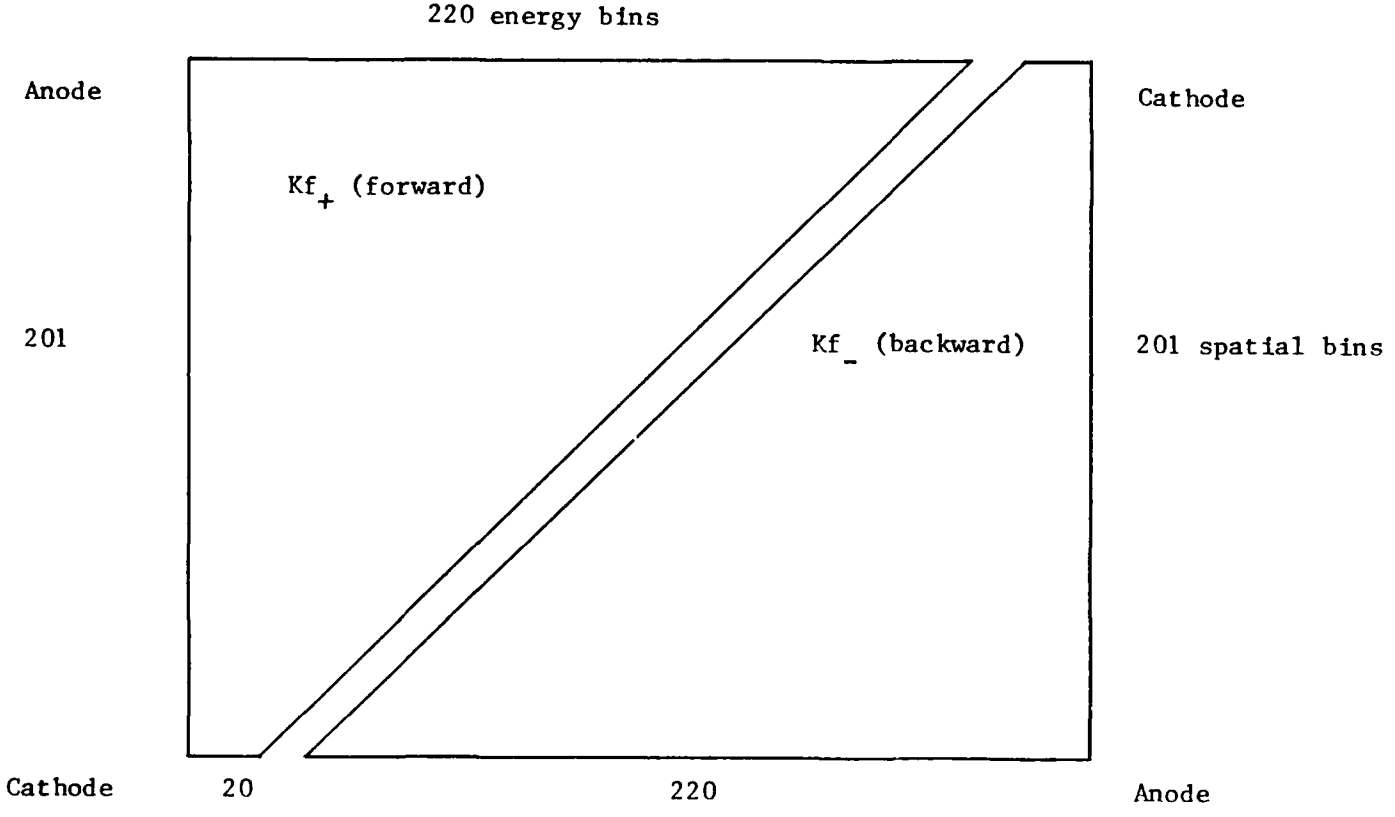

FIG IV-1 STORAGE ARRAY FOR COLLISION INTEGRAL IN SHEATH CODE

rate arrays.

Boundary conditions are usually specified at the cathode and anode. At the cathode, the energy distribution of electrons, $f_+(\varepsilon,\xi,0)$ is a variable input. The function $f_-(\varepsilon,\xi,\phi)$ can represent the distribution of electrons at the head of the positive column when $\phi = \phi_{max} = V_c$, the voltage drop across the cathode fall, negative glow and Faraday dark space, or it can represent the distribution of electrons at the anode then $f_- = 0$, or it can represent the distribution along an axis of symmetry such that $f_- = f_+$. Along the locus of turning points where the electron kinetic energy in the field direction $\xi = 0$, the forward and backward fluxes are equal, $f_+(\varepsilon,0,\phi) = f_-(\varepsilon,0,\phi)$.

The algorithm used in Long's code for the numerical integration of equation IV-6 is second order and stable. The distribution function is calculated via

$$f_{i+1} = \frac{C_{i+1} + C_i\left(\frac{2}{\Delta\xi} - \frac{Q_i}{E/N_i}\right) f_i}{\left(\frac{2}{\Delta\xi} + \frac{Q_{i+1}}{E/N_{i+1}}\right)} \qquad \text{(IV-9)}$$

where $C = \frac{1}{\varepsilon E/N}\left(\frac{\varepsilon}{\xi}\right)^{\frac{1}{2}} Kf$ and $\Delta\xi$ is the energy step. The relative error at each step is

$$E_{error_{rel}} = \frac{C}{2}\left(\frac{\Delta\xi}{2}\right)^2 + \frac{2}{3}\left(\frac{\Delta\xi}{2}\frac{Q}{E/N}\right) \qquad \text{(IV-10)}$$

which implies that the error is small as long as

$$\Delta\xi \leq \frac{2E}{NQ} \qquad \text{(IV-11)}$$

Near the cathode this condition is easily satisfied since $\frac{E}{NQ} << \varepsilon_i$ which is typically 20eV or less.

In the negative glow and Faraday dark space however the field becomes very small. In this region of the discharge, the distribution function is changing more rapidly with respect to position (x) than it is with respect to potential (ϕ). Thus ϕ is no longer an appropriate variable, and x becomes the variable of choice. Changing variables, equation IV-4 becomes

$$\frac{\partial f}{\partial x} + eE(x)\frac{\partial f}{\partial \varepsilon} = N(x)\left(\frac{\varepsilon}{\varepsilon}\right)^{\frac{1}{2}}\left(K - Q(\varepsilon)\right) f \qquad \text{(IV-12)}$$

To correctly determine f through these regions, the code first starts with coordinates (ε, ξ, ϕ) and iterates on equation IV-5. When $\Delta\xi > 2E/NQ$, then the coordinates are changed to (ε, ξ, x) and equation IV-12 is then iterated on until convergence.

The code is presently configured to calculate the electron energy distribution function as a function of distance from the cathode to the anode. The electrons are constrained to move either with or against the field, i.e. all integrations are in the plane $\eta = 0$. This simplification significantly reduces computer run time.

The electron number density is normalized to the electron number density at the cathode such that

$$n_e(\phi) = n_{eo}\frac{\int_0^\infty \left(f_+(\varepsilon,\phi) + f_-(\varepsilon,\phi)\right)\varepsilon^{-\frac{1}{2}}\,d\varepsilon}{\int_0^\infty \left(f_+(\varepsilon_o,\phi_o) + f_-(\varepsilon_o,\phi_o)\right)\varepsilon^{-\frac{1}{2}}\,d\varepsilon} \qquad \text{(IV-13)}$$

where subscript 0 indicates the boundary condition at the cathode.

Similarly the electron current density is normalized to the electron current density at the cathode and is given by the following

$$J_e(\phi) = J_{eo} \frac{\int_0^\infty (f_+(\varepsilon,\phi) - f_-(\varepsilon,\phi))\, d\varepsilon}{\int_0^\infty (f_+(\varepsilon_o,\phi_o) - f_-(\varepsilon_o,\phi_o))\, d\varepsilon} \qquad \text{(IV-14)}$$

Townsend rates for the various inelastic processes including ionization are normalized to the electron current density at the cathode as well

$$\alpha(\phi) = N(\phi) \frac{\int_0^\infty (f_+(\varepsilon,\phi) + f_-(\varepsilon,\phi))\, \sigma_i(\varepsilon)\, d\varepsilon}{\int_0^\infty (f_+(\varepsilon,\phi) - f_-(\varepsilon,\phi))\, d\varepsilon} \qquad \text{(IV-15)}$$

In order to obtain a completely self-consistent solution in which Poisson's equation is obeyed in addition to the boundary conditions at the cathode and anode, successive calculations for the electron distribution function, electron number density and the resulting electric field were accomplished.

Long attempted to do this for the case where the anode is just inside the cathode fall-negative glow boundary. By integrating the electron distribution function he obtained the electron number density and electron current density and obtained the positive ion number density using current conservation.

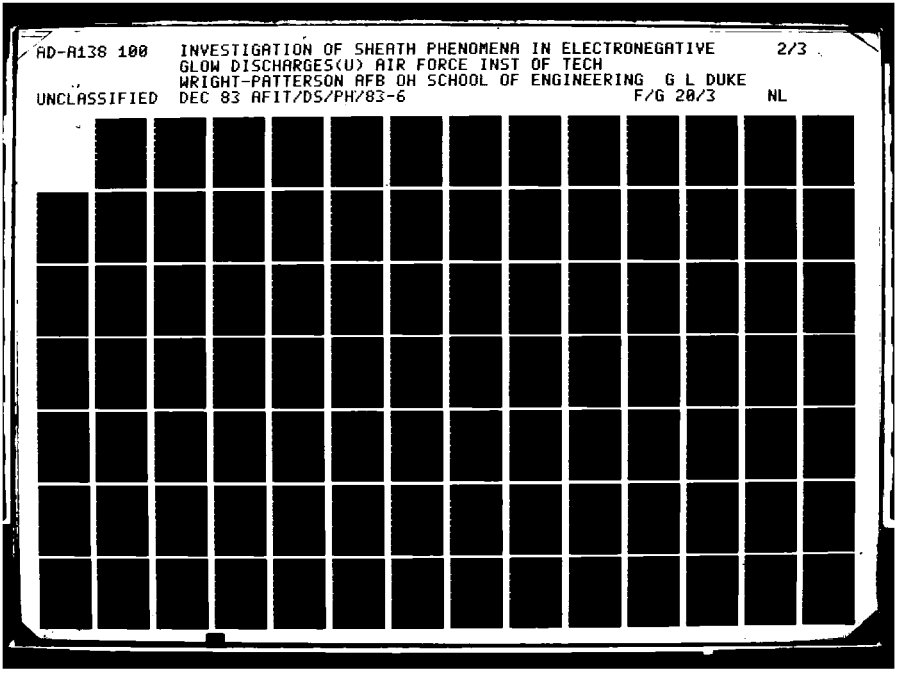
AD-A138 100 INVESTIGATION OF SHEATH PHENOMENA IN ELECTRONEGATIVE 2/3
GLOW DISCHARGES(U) AIR FORCE INST OF TECH
WRIGHT-PATTERSON AFB OH SCHOOL OF ENGINEERING G L DUKE
UNCLASSIFIED DEC 83 AFIT/DS/PH/83-6 F/G 20/3 NL

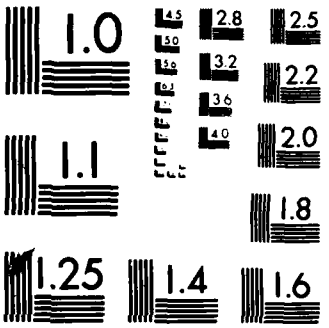

$$n_+(x) = \frac{J - J_e(x)}{e V_+(x)} \qquad \text{(IV-16a)}$$

$$V_+(x) = \mu_+ E(x) \qquad \text{(IV-16b)}$$

In this calculation, however he had to use his initial guess for the electric field, so the ion drift velocity ($\mu_+ E$) was not consistent with the new calculation of the field.

He normalized his number densities, not through the previous definitions, but by the ratio of E_0/E_1 where

E_0 = electric field at the cathode prior to the calculation of the distribution function

and

$E_1 = \int_{x_1}^{x_0}(n_+ - n_e)dx$ which is the electric field at the cathode after the unnormalized densities are known. x_1 is the spatial point at which the field is zero.

This approach does not permit the secondary emission coefficient to be used as an input parameter, however the coefficient was calculated via the following equation:

$$\gamma = \frac{1}{\frac{J_e(E=0)}{J_{eo}} - 1} \qquad \text{(IV-17)}$$

This normalization gave good results and converged as long as the anode was at the boundary or within the cathode fall region.

It was found by this study that Long's technique diverged when the anode was more realistically placed outside the cathode fall, so a new

technique to reach a self-consistent solution was derived. This technique is based on putting Poisson's equation in difference form so the value of the field at each point is based on the value at the previous increment with the field at the cathode given as a boundary condition. Writing Poisson's equation in difference form yields.

$$E_j = E_{j-1} - \frac{e}{\varepsilon_0}\left(n_{+j} + n_{+j-1} - n_{ej} - n_{ej-1} - n_{-j} - n_{-j-1}\right)\frac{(x_j - x_{j-1})}{2} \qquad \text{(IV-18)}$$

where n_{+j}, n_{ej}, n_{-j} are the positive ion, electron, and negative ion number densities at position j, and x_j is the spatial point corresponding to increment j. The positive ion number density can be written in terms of the current conservation such that

$$n_{+j} = \frac{(J - J_{ej} - J_{-j})}{e k_+ \left(E_j/p\right)^{\frac{1}{2}}} \qquad \text{(IV-19)}$$

The negative ion number density can be calculated from the negative ion current density.

$$J_{-j} = \int_0^x \eta_j J_{ej}\, dx_j \qquad \text{(IV-20)}$$

$$n_{-j} = \frac{J_{-j}}{e k_- \left(E_j/p\right)^{\frac{1}{2}}} \qquad \text{(IV-21)}$$

where η is the attachment rate. Equations IV-21 and IV-19 can be substituted into IV-18. This results in a fifth order polynomial whose solution can be found by numerical means.

$$X^5 + \left(\frac{b\Delta y}{E_{j-1}^{\frac{1}{2}}} - E_{j-1} - c\Delta y\right)X^3 + a\Delta y X^2 - \left(\frac{b\Delta y}{E_{j-1}^{\frac{1}{2}}} - E_{j-1} - c\Delta y\right) = 0$$

where $a = \frac{(J - J_{e_j} - 2J_{-_j})p^{\frac{1}{2}}}{\varepsilon_0 k_+}$ $\qquad$ $b = \frac{(J - J_{e_{j-1}} - 2J_{-_{j-1}})p^{\frac{1}{2}}}{\varepsilon_0 k_+}$ $\qquad$ (IV-22)

$$c = \frac{e}{\varepsilon_0}(n_{e_j} + n_{e_{j-1}}) \qquad X = E_j^{\frac{1}{2}}$$

Steinman's method (ref 66) was used in this study to solve for the roots. Thus E is calculated based on n_e, j_e, j_- and the previous value of the electric field. This technique converged after successive iterations of first calculating $f(\varepsilon)$, n_e, j_e and then E(x). Fig IV-2 gives an example of the convergence as the electric field and electron distribution are successively iterated.

The initial discharge parameters, E_0, E_{min}, and d_c, were varied to achieve the best convergence. These parameters describe the initial field distribution according to the formulas

$$E(x) = E_0\left(1 - \frac{x}{d_c}\right) \qquad x < d_c \qquad \text{(IV-23a)}$$

$$E(x) = E_{min} \qquad x \geq d_c \qquad \text{(IV-23b)}$$

It was observed that the optimum convergence was achieved when the initial E_{min} was slightly greater than (what was later found to be) the converged E_{min} and the initial slope E_0/d_c was equal to or slightly shallower than the shallowest slope of the converged curve. This generally was the slope occurring between E_0 and $3E_0/4$ or $7E_0/8$.

Fig IV-3 shows the effect of changing the value of the electric field at the cathode. Note that if E_0 is assumed too low, in this case for $E_0 \leq 757$v/cm, then the solution to equation IV-22 becomes imagi-

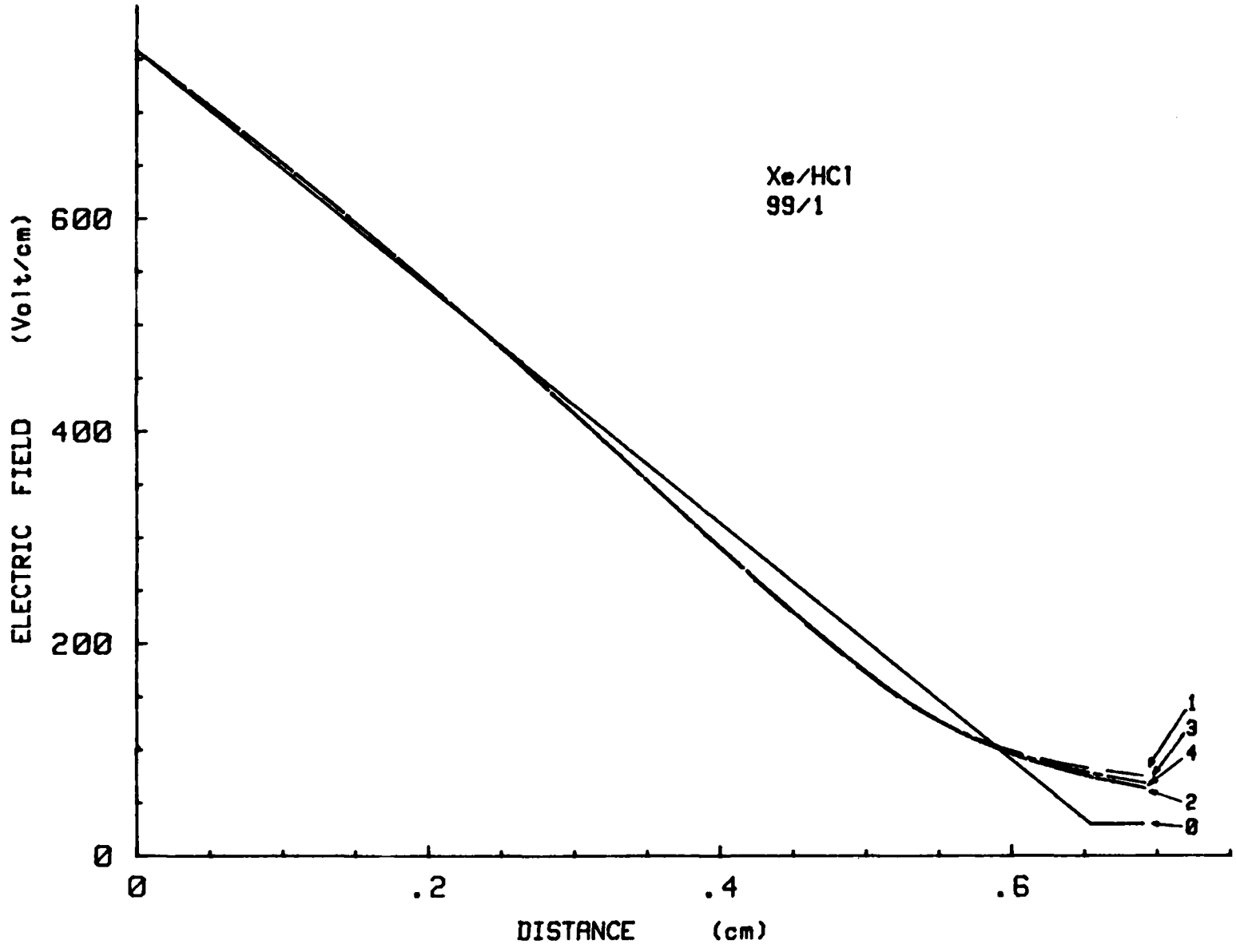

FIG IV-2 CONVERGENCE OF THE SHEATH CODE TO A SELF-CONSISTENT ELECTRIC FIELD

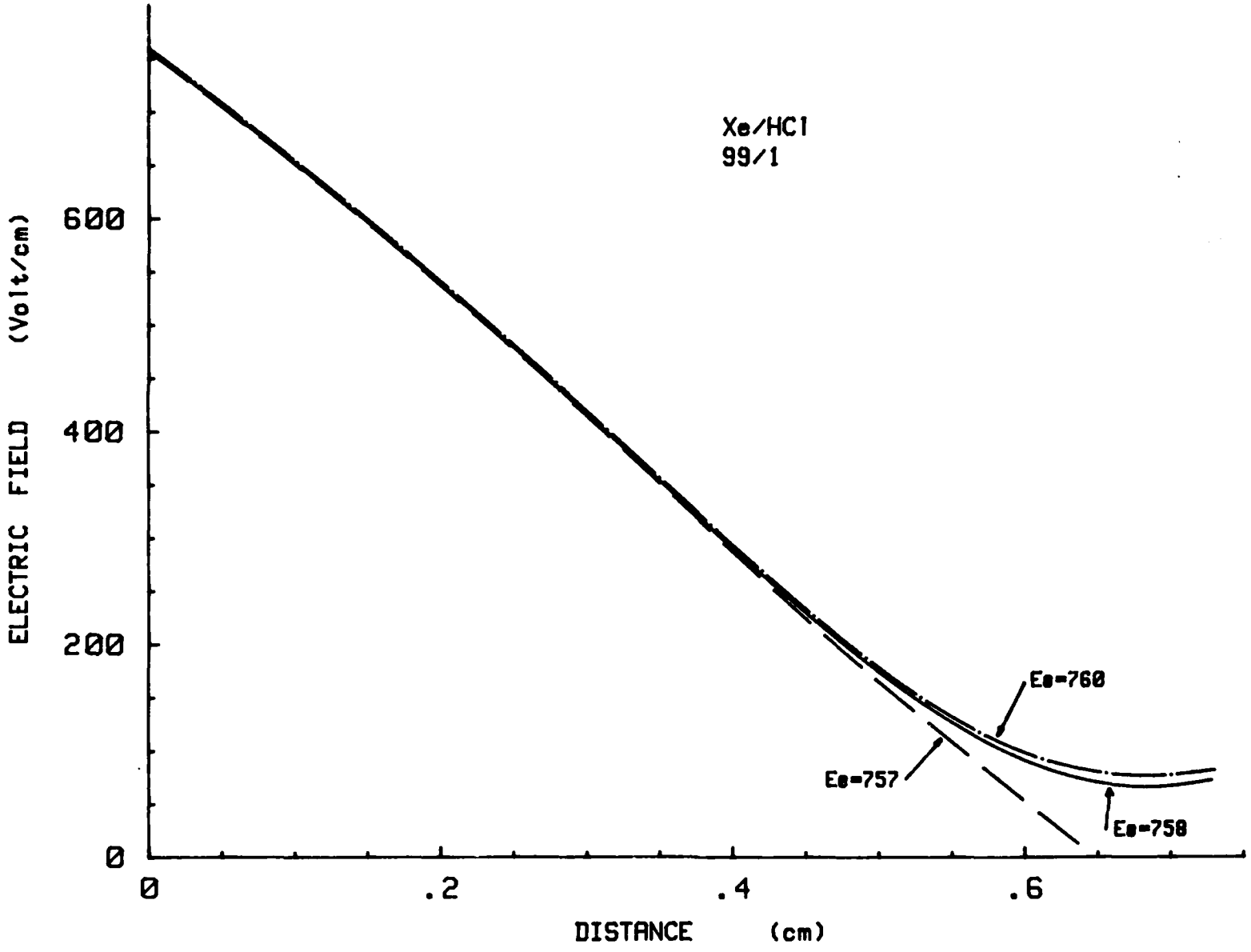

FIG IV-3 CONVERGENCE OF THE SHEATH CODE TO THE LOWEST VOLTAGE

nary, representing an unphysical solution for the field between the electrodes. This corresponds quite closely to the phenomena seen in the convergence of the previous GLOW model (Fig III-2). The calculation for E_0 = 758v/cm was deemed to be the solution most representative of a discharge since it represented the lowest voltage in which a complete real solution existed from cathode to anode. Although E_0 was varied manually, a technique similar to the modified linear interpolation or halving the interval technique could be programmed to converge to the lowest value of E_0 for which a complete solution exists.

Summarizing the changes made since Long published his report, this study has added attachment as an electron loss process in the numerical calculation of the distribution function, modified the code to include a variable number of gases, and modified the code to include a variable number of collision processes per gas. The original program was limited to analyzing a pure gas with one momentum transfer, one excitation, and one ionization cross section. The Townsend ionization and attachment rates are now calculated from the distribution function, instead of a net ionization rate from the electron current continuity equation. In addition, in the calculation of the positive ion drift velocity, Long had assumed it was proportional to the field. This has been changed so that the positive ion drift velocity is more appropriately represented at high fields by equation III-41 in which it is proportional to the square root of the field. Also a new self-consistent technique was found for calculating the electric field from the electron density, the electron current density, and the negative ion current density.

The SHEATH program was normally run on a Cyber 74 computer system.

Each iteration to converge to a solution for a given E_o took an average of 15sec. Normally 4 to 6 iterations were required to reach three significant figure convergence in E(d). The code required 216K of memory to load and run. The majority of this space was taken up by the 220 x 201 array described earlier.

Results of Numerical Calculations

This section presents the results of calculations using the SHEATH code in the same rare gas-HCl mixtures as in the previous chapter. All the data presented was obtained for a gas pressure of 1 torr. Again the results for He will be be presented first, followed by Ar mixtures, and then Xe mixtures.

Only the cathode fall region will be discussed because the anode was placed just outside the cathode fall region where the electric field leveled off to a constant value as in an obstructed discharge. The SHEATH code, while improved, still had difficulty converging at very low electric fields where the code transformed from integrations over energy to integrations over position. This transformation was discussed in the preceding section. All the SHEATH data presented in this study was obtained before this transformation of variables occurred, ie. while integrations are conducted in energy space. Further comments on the anode fall will be made in Chapter V.

Helium

This section presents the results of the nonequilibrium calculations for He/HCl mixtures. A summary is given in Table IV-1 of the same scaling parameters listed in tables in the previous chapter. The

Table IV-1

Summary of SHEATH Code Results for He/HCl Mixtures

Ratio He/HCl		γ or Cathode Material	E_o/p $\frac{volt}{cm\text{-}torr}$	E_{min}/p $\frac{volt}{cm\text{-}torr}$	pd_c torr-cm	J/p^2 $\frac{\mu\ amp}{cm^2\text{-}torr^2}$	V_c volt	SF (γ,k_+) $\frac{X10^{-9}\ amp\text{-}torr^{-\frac{1}{2}}cm^{\frac{1}{2}}}{volt^{\frac{3}{2}}}$
100/0								
Experimental	i	Mg	-	-	1.45	3.	125.	5.43
	i	Fe	-	-	1.3	2.	150.	2.10
	i	Ni	-	-	-	2.	158.	-
	i	Pt	-	-	-	5.	165.	-
	i	Al	-	-	1.32	-	140.	-
	i	Other Materials	-	-	-	-	59.-204.	-
Theoretical	ii	-	-	-	1.3	2.84	150.	2.98
	iii	.086	220.	37.	1.3	2.2	-	-
	iv	-	231.	1.	1.3	3.	150.	3.15
	v	.2	177.	1.5	2.	5.	180.	11.71
	vi	.2	353.	8.1	1.73	16.	309.4	11.57
99/1								
Theoretical	vi	.2	338.	8.1	1.62	16.	277.4	11.57
95/5								
Theoretical	vi	.2	301.	17.5	1.37	16.	209.	11.63

i Data was taken from a summary presented in ref 6.
ii Data was taken from ref 86 (not self-consistent).
iii Data was taken from ref 79.
iv Data was taken from ref 20 (not self-consistent)
v Data was taken from ref 21
vi Data was calculated in this study

cathode fall width and voltage was calculated from the electric field in the same manner as in Chapter III for the GLOW model.

There is a wide range of values for $SF(\gamma, k_+)$ in Table IV-1. Some of these differences are due to the differences in input data, such as the Townsend secondary emission coefficient or the cross section set used. Also, there were different approximations used for the positive ion drift velocity dependence on the electric field. However, there were also important model differences that influenced the results as well. The data from calculations by Boeuf and Marode (ref 20) and Tran Ngoc et al. (ref 86) are not self-consistent. They picked values of pd, J/p^2, and V_c which agreed well with experiment and assumed a linearly decreasing field before calculating the electron distribution function as a function of distance through the cathode fall using a Monte Carlo technique. Segur et al. (ref 79) calculated the positive ion density and current from the Boltzmann equation for ions, so an analytical fit to experimental data was not used for the positive ion drift velocity. Boeuf et al. (ref 21) used a Monte Carlo technique for both electrons and positive ions. The positive ion "nonequilibrium drift velocity" predicted by the Monte Carlo technique was within 20% of experimental data which had been measured in equilibrium. In the SHEATH code, equation III-41 was used to calculate the positive ion drift velocity. This analytic approximation agrees more closely with the drift velocity predicted by the Monte Carlo results of Boeuf et al. than the experimental data they presented. As a result, the scaling factor $SF(\gamma,k_+)$ for the data from the Monte Carlo technique and the SHEATH code agree within 1%. This agreement with the Monte Carlo technique was used as a benchmark in comparing the accuracy of the

SHEATH model to other nonequilibrium techniques. Note that SF(γ, k_+) changes very little for the different He/HCl mixtures, indicating that SF(γ, k_+) is still an invariant even when the ionization efficiency of the gas changes. These changes in the ionization coefficients will be seen in later figures. The observation that SF (γ, k_+) is not a function of the ionization coefficient is consistent with equation III-72. The variation in SF (γ, k_+) in this author's results is due to round off and extrapolation errors in pd_c and V_c.

The SHEATH program predicts a 15% decrease in the electric field in the cathode fall region as the amount of HCl is increased form 0 to 5%. See Fig IV-4. This corresponds to a 32% decrease in the cathode fall voltage. This trend agrees with the results of the GLOW model including the linearity of the field near the cathode in both cases. The shift in the electric field, however, is much greater in the SHEATH model and can be observed in the GLOW model in Fig III-4. A more detailed comparison of the two techniques will be described in the next chapter. This decrease in the field and voltage as a function of HCl is due to the increase in the Townsend ionization coefficient which can be seen in Fig IV-5. The increase in the peak region which corresponds to the cathode glow region is due to the fact that HCl is much easier to ionize than He. HCl has an ionization threshold of 12.74eV which is about half of that for He whose ionization threshold is 24.59eV. Note that the spatial threshold for the Townsend ionization coefficient is halved when HCl is added corresponding to the change in the ionization cross section threshold. This indicates that very close to the cathode, the HCl is being ionized before the He. These results are consistent with the results of Segur, et al. with Hg in He. The decrease in

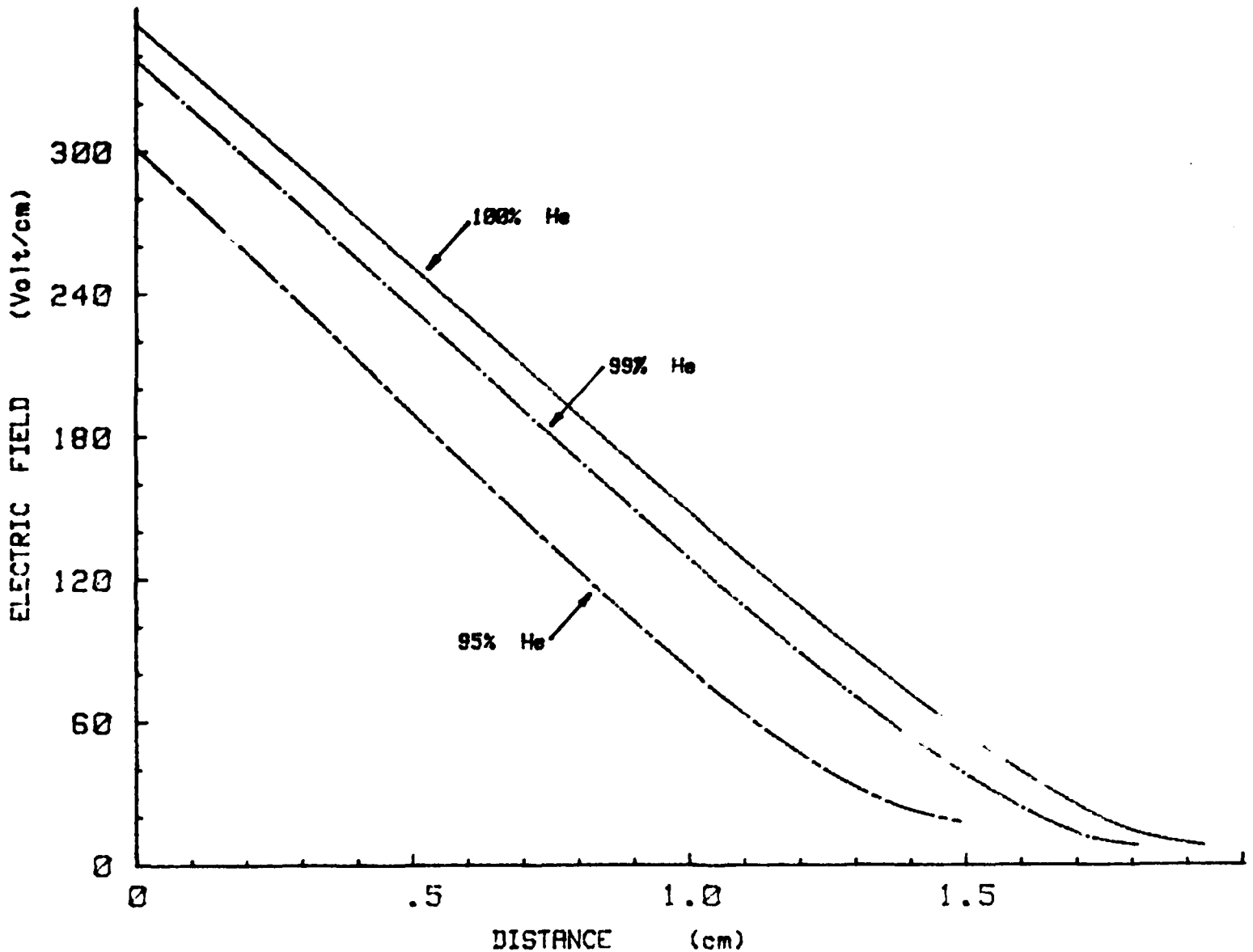

FIG IV-4 ELECTRIC FIELD IN He/HCl MIXTURES

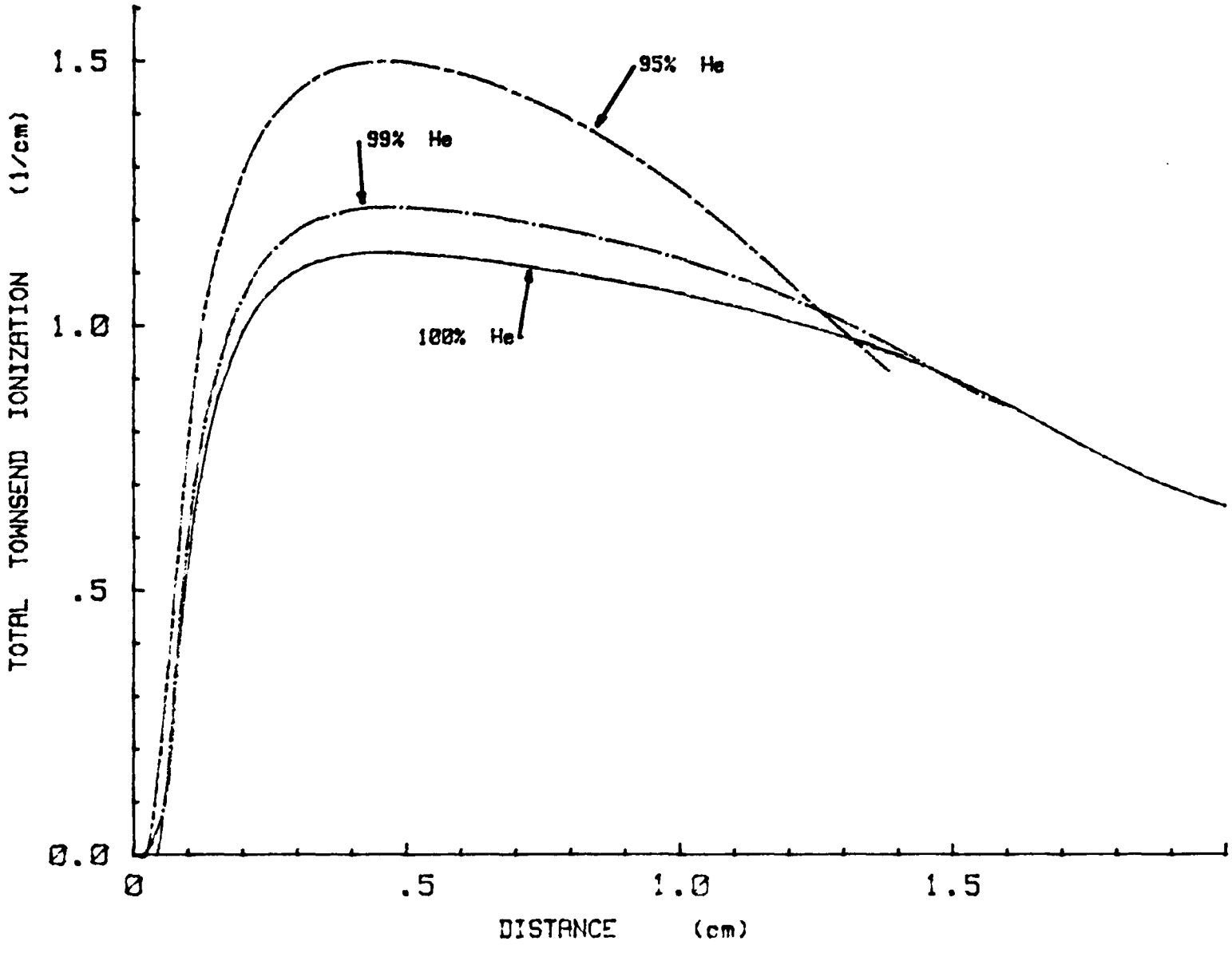

FIG IV-5 COMPARISON OF TOWNSEND IONIZATION COEFFICIENT IN He/HCl MIXTURES

the linear electric field with the addition of HCl results in similar decreases in the cathode fall length, decreasing 6.4% for the 99/1 mixture and 21% for the 95/5 mixture. These results are summarized in Table IV-1.

The curves for the various electric fields in Fig IV-4 are almost parallel because the slope of the electric field is determined through Poisson's equation by the positive ion density. The positive ion density at the cathode is determined by γ, J, and the positive ion drift velocity. Since these variables and relations remained constant for the various HCl mixtures, the slopes of the electric fields remained constant.

Fig IV-6 and IV-7 compare the Townsend ionization and attachment coefficients as a function of distance for 99/1 and 95/5 concentrations of He/HCl. The magnitude of the attachment rate is much smaller than the ionization rate throughout the cathode fall region as one would expect, except immediately in front of the cathode. In this region which corresponds to the Primary dark space, the electrons have just left the cathode at a few eV of energy and are not yet in equilibrium with the field. The second peak seen in the attachment curve at 1.cm is probably due to the electron distribution function first reaching the ionization energy and producing a new crop of slow secondary electrons.

Fig IV-8 and IV-9 display the electron and negative ion current densities as a function of distance and as a function of percent of HCl. The increase in the ionization rate also manifests itself in an increase in the electron current density throughout the cathode fall region. The electron current density stays constant for the first few mean free

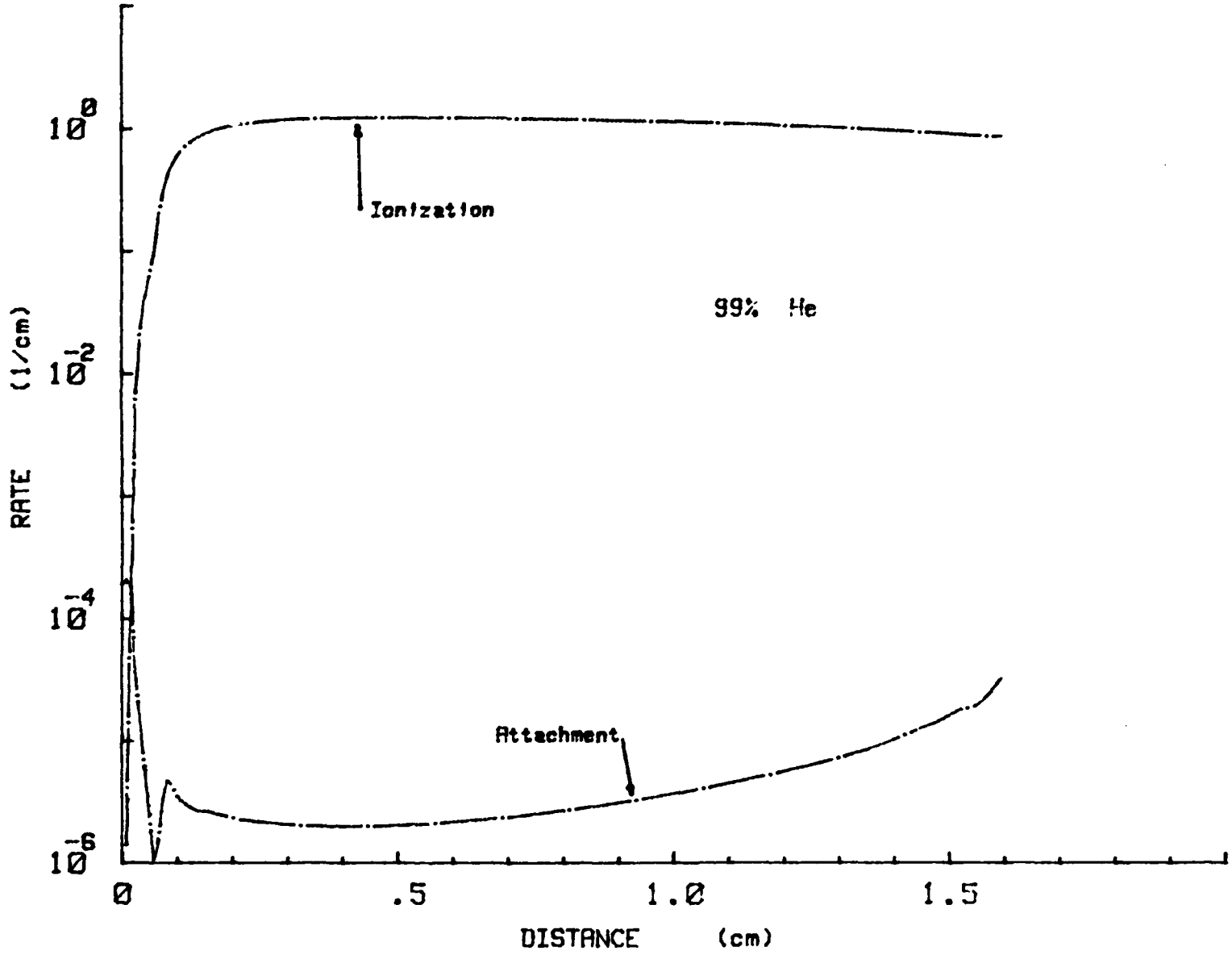

FIG IV-6 COMPARISON OF IONIZATION AND ATTACHMENT COEFFICIENT IN 99/1 He/HCl

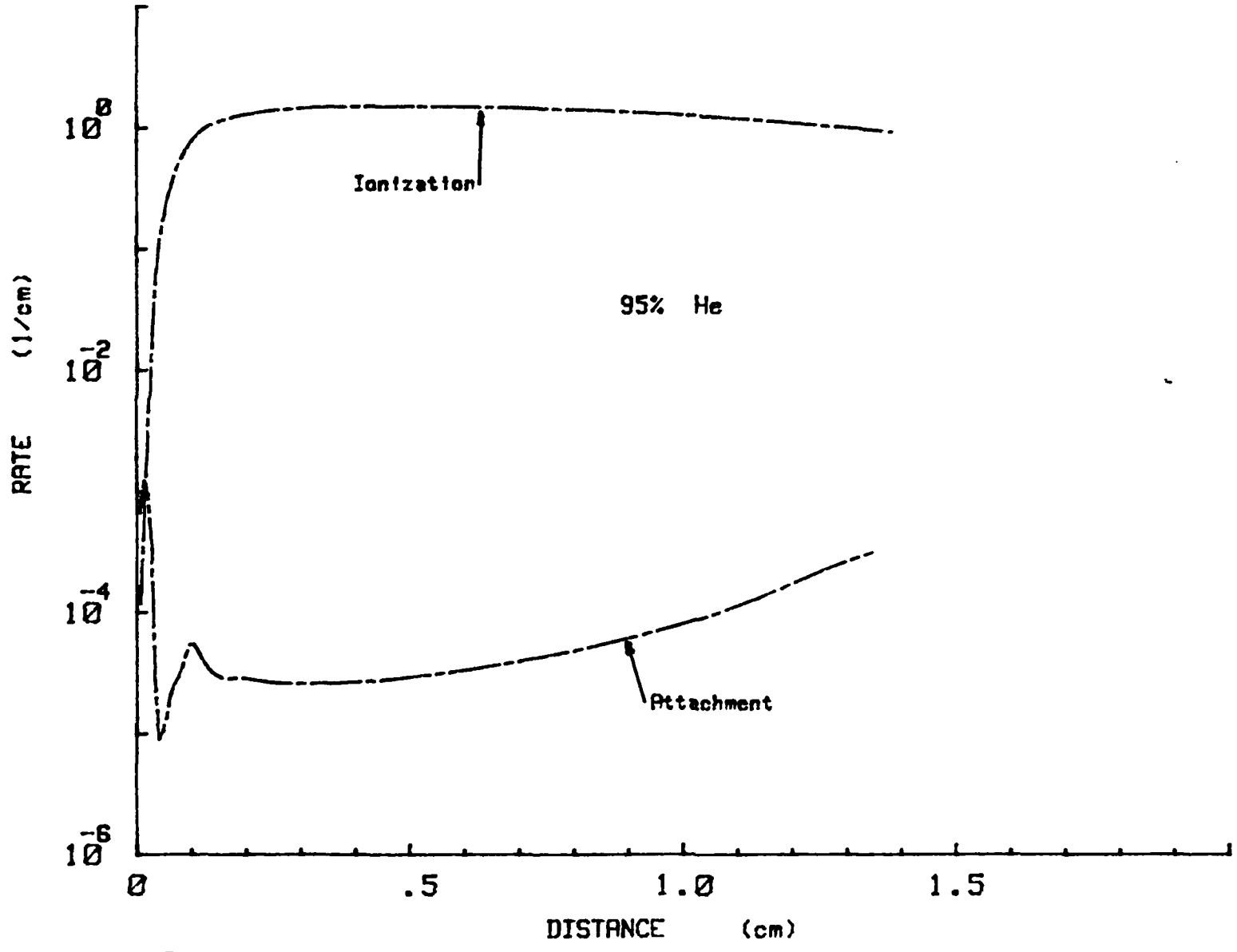

FIG IV-7 COMPARISON OF IONIZATION AND ATTACHMENT COEFFICIENT IN 95/5 He/HCl

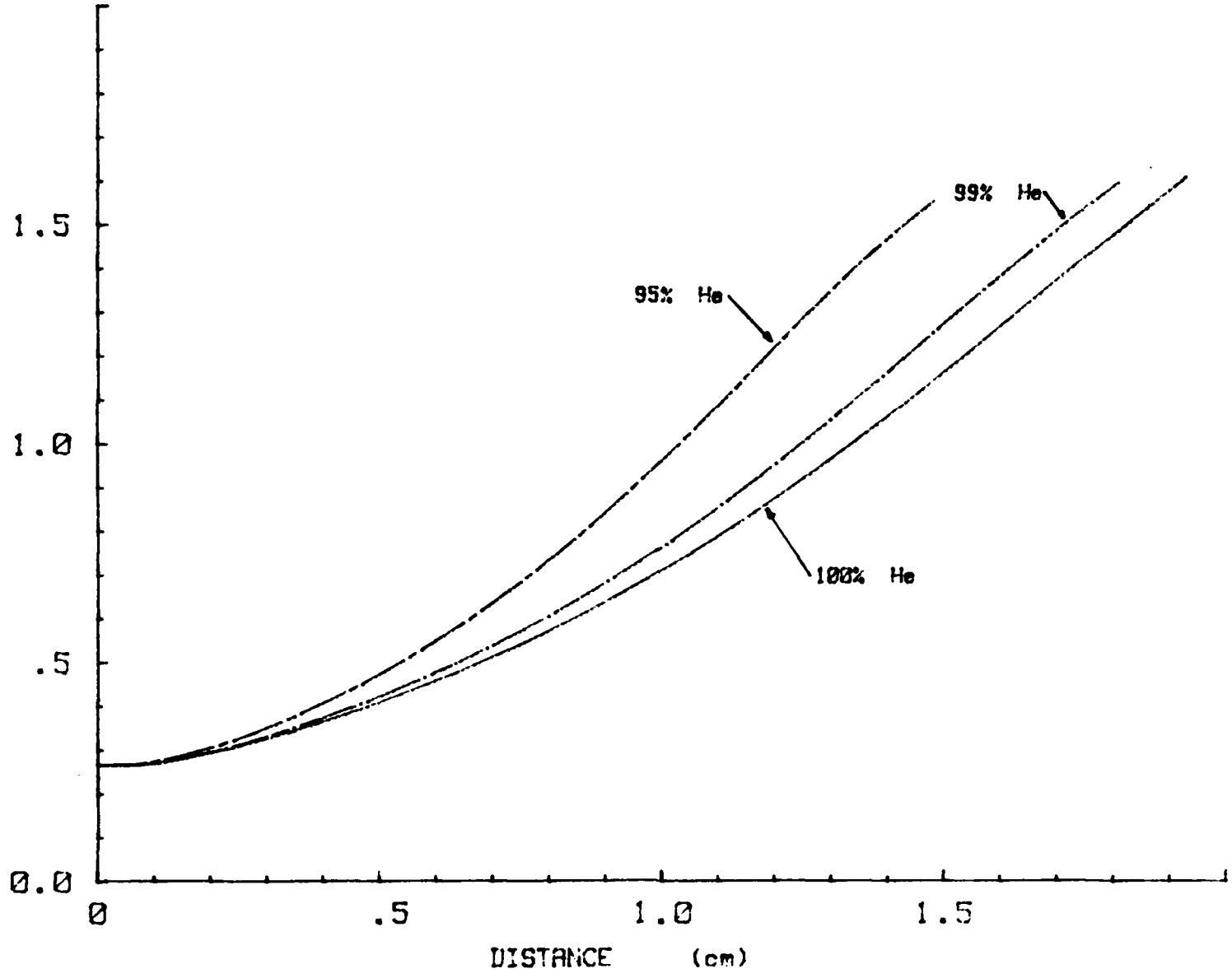

FIG IV-8 ELECTRON CURRENT DENSITY IN He/HCl MIXTURES

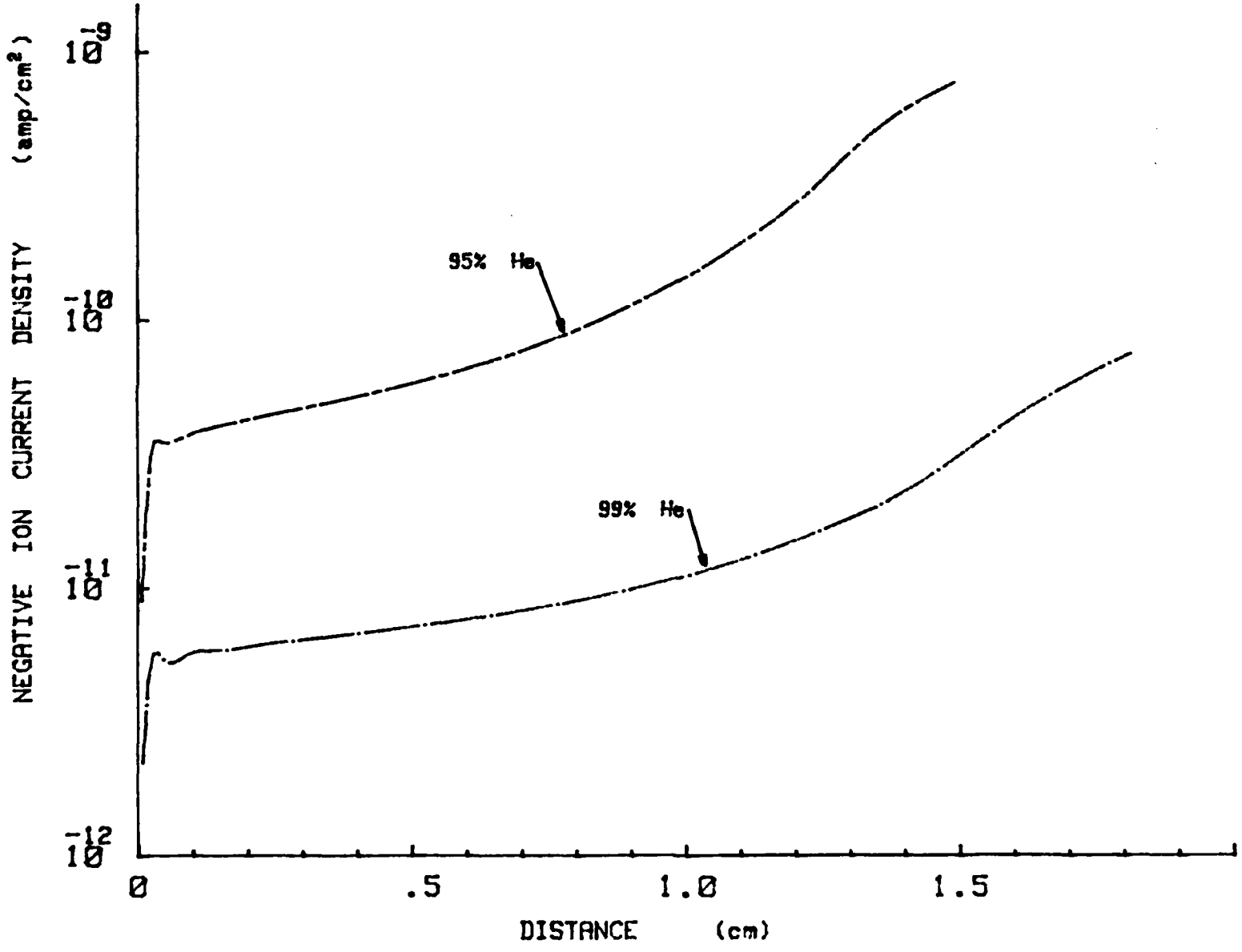

FIG IV-9 NEGATIVE ION CURRENT DENSITY IN He/HCl MIXTURES

paths as the electrons are being accelerated up to the ionization potential. It then increases almost exponentially through the remainder of the cathode fall. As expected, the negative ion current density in Fig IV-9 increases as the proportion of HCl increases. It is characterized by a very steep onset due to the large attachment rate near the cathode. As the total distribution of electrons is accelerated away from the cathode, they reach the ionization threshold of the gas. Most electrons are then past the peak region of the attachment cross section and the negative ion current density grows at a much slower rate. Note the logarithmic scale, indicating the growth of the negative ion current density is still slightly faster than an exponential function of distance.

Fig IV-10, IV-11, and IV-12 display the electron, positive ion, and negative ion number densities as a function of distance through the cathode fall region. The result of nonequilibrium electron kinetics is easily seen in these figures. The electron density initially decreases because the electrons are rapidly accelerated away from the cathode. Just before they have gained sufficient energy for ionization, their density reaches a minimum and begins to increase. The fact that by mid-cathode fall the field has also decreased substantially allows the electron density to increase. Similarly the positive ion density increases away from the cathode since there is very little ionization close to the cathode and the positive ions are being accelerated towards it. Although negative ions are present throughout the cathode fall region in Fig IV-11 and IV-12, their density is generally much too small to affect the net space charge to any significant degree. Note that the negative ion density is more than four orders of magnitude smaller than

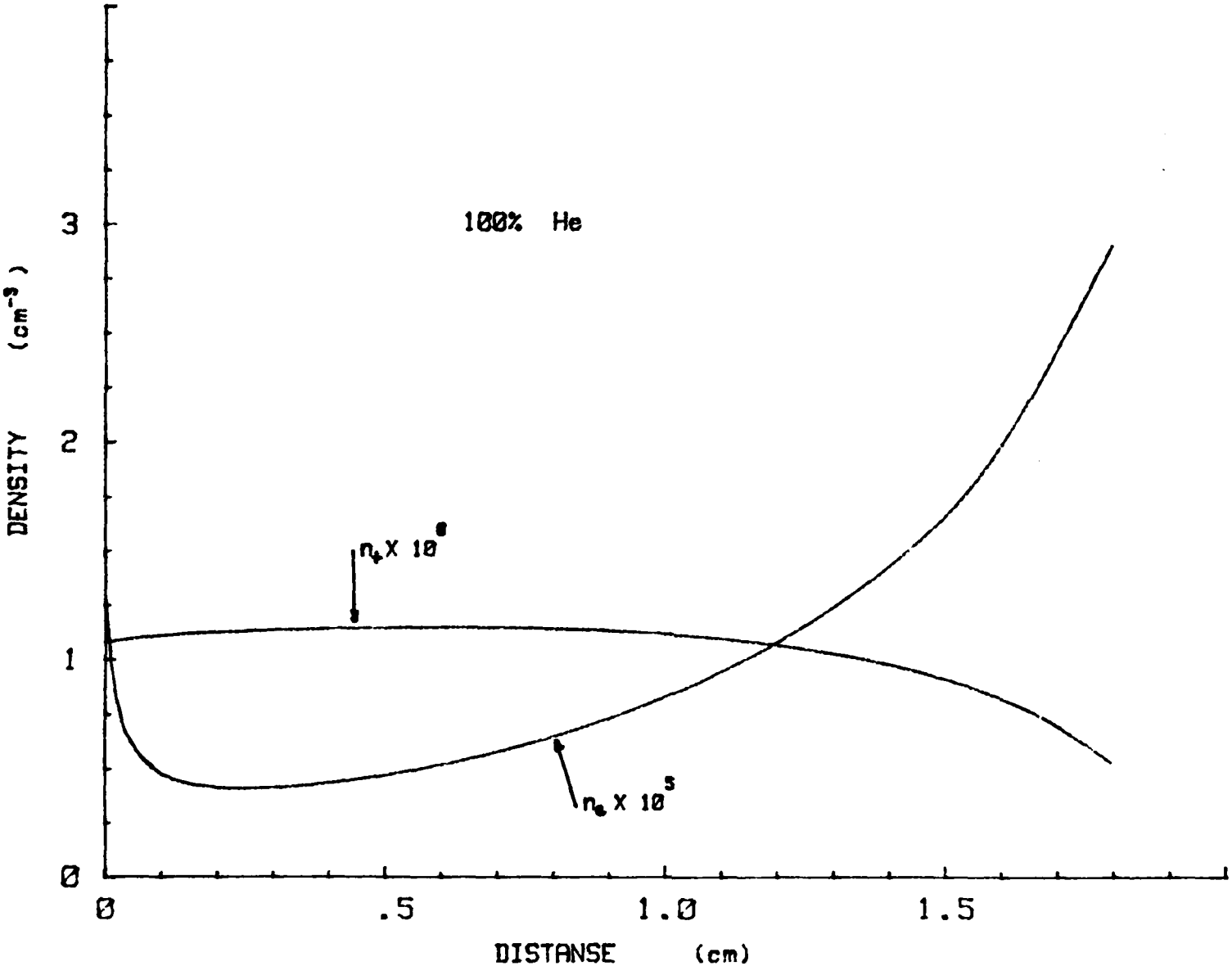

FIG IV-10 CHARGED PARTICLE DENSITIES IN 100% He

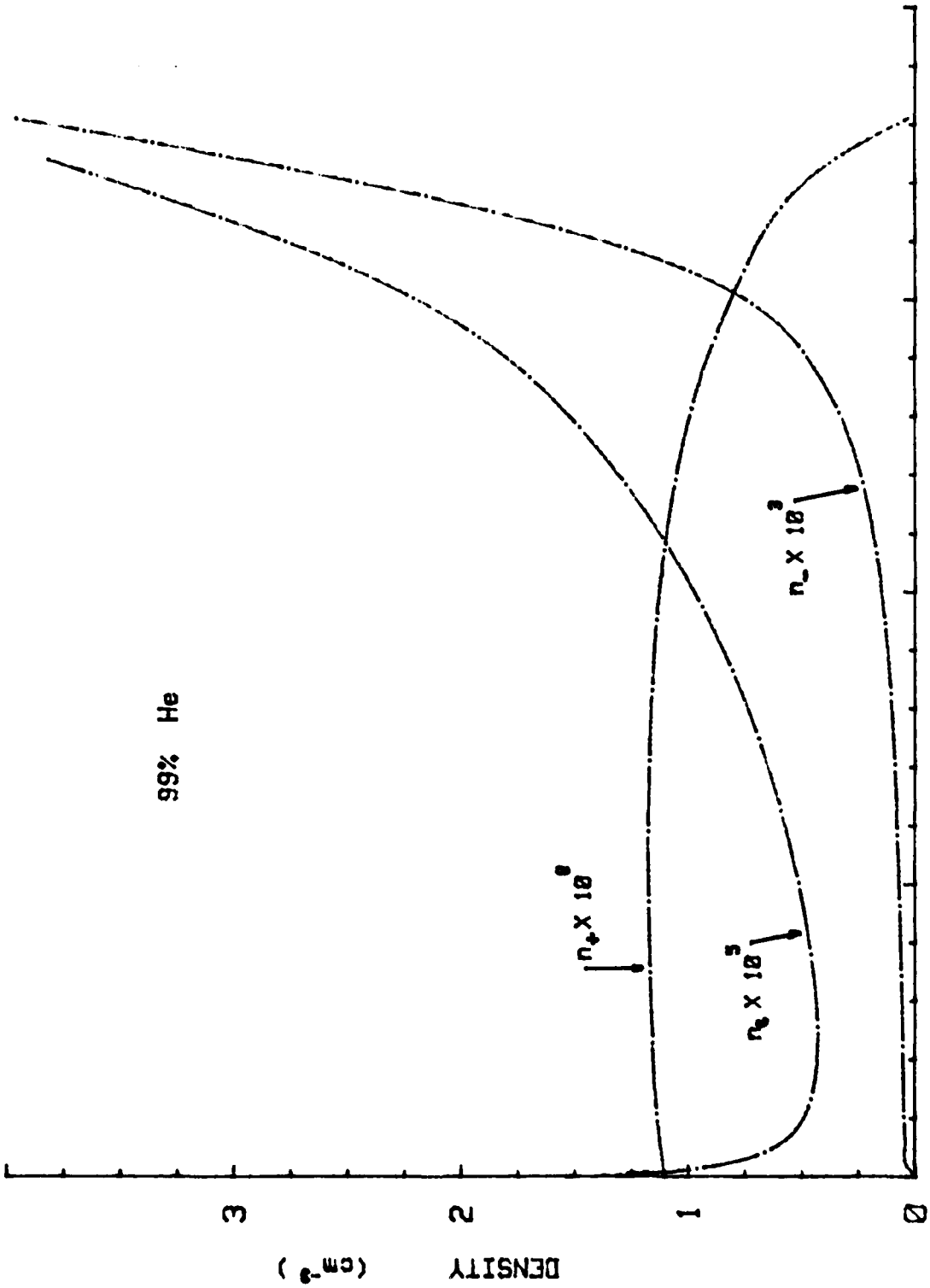

FIG IV-11 CHARGED PARTICLE DENSITIES IN 99/1 He/HCl

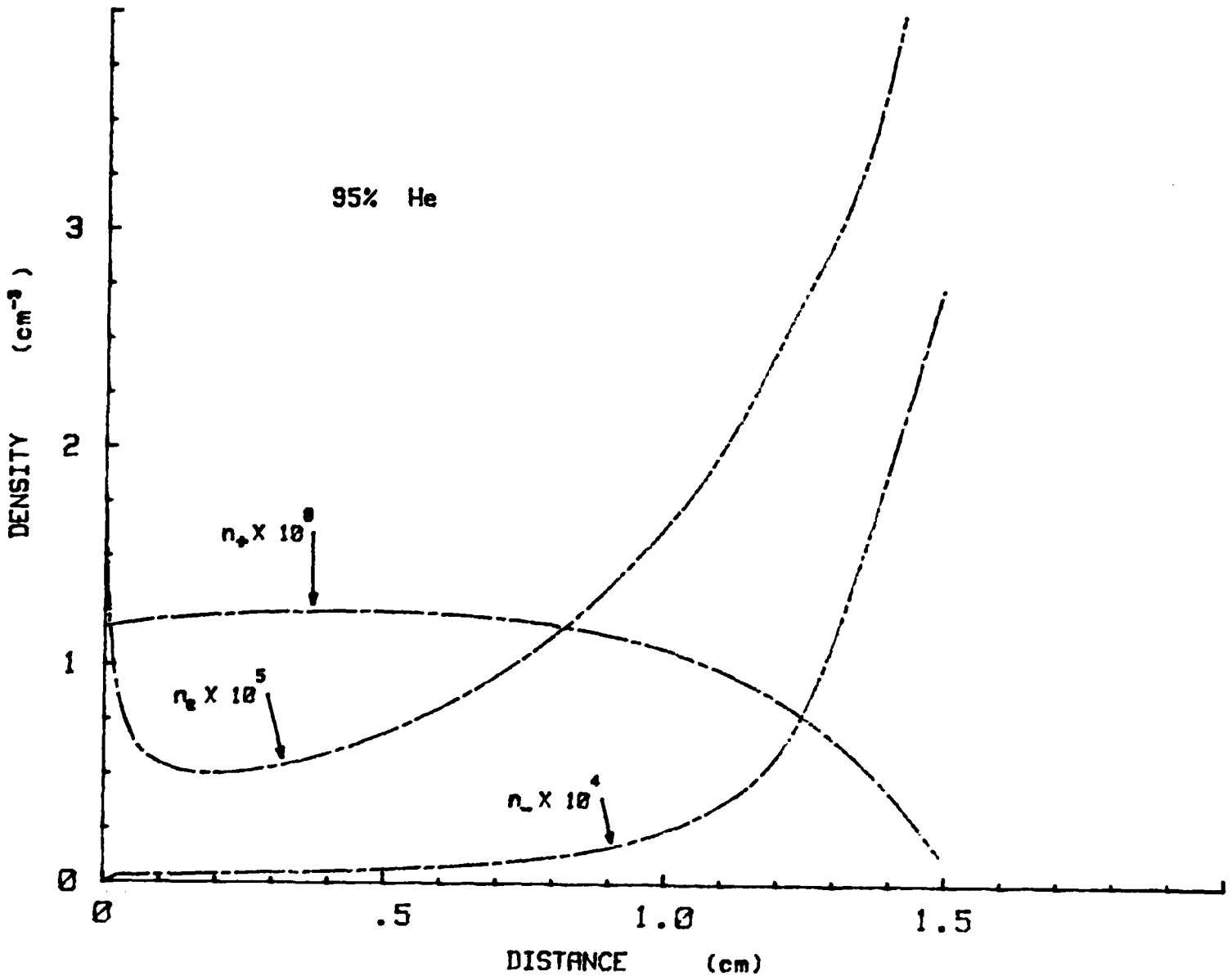

FIG IV-12 CHARGED PARTICLE DENSITIES IN 95/5 He/HCl

the positive ion density. The positive ion density actually determines the slope of the field throughout the cathode fall. The magnitude of the electron density approaches that of the positive ion density only after the negative glow is reached or, in these examples just prior to the anode. Equilibrium is never reached in these figures because a slightly bimodal electron distribution still exists at the anode.

Since the cathode fall voltage decreases as HCl is added, the ions arrive at the cathode at a lower velocity. Similarly, the electrons are not accelerated away as quickly, so both electron and positive ion densities increase near the cathode (20% and 8% respectively for up to 5% HCl). The opposite trend can be seen in Fig IV-10, IV-11, and IV-12 near the cathode glow-negative glow boundary (1.5-1.75 cm). The electron density increases as a function of HCl in this region due to the increase in the ionization coefficient closer to the cathode. Since the field is lower in this region and the ionization coefficient is lower, the positive ion density decreases as the percentage of HCl is increased, which in a self-consistent (or interrelated) manner causes the cathode fall region to contract.

Argon

The results for Ar/HCl mixtures are summarized in Table IV-2 as was done for previous mixtures. As in He, there is a wide range of values for SF(γ, k_+) in Table IV-2 for Ar. The only other nonequilibrium data available for Ar is that of Long (ref 60) which was not entirely self-consistent. The lack of self-consistency of his method was discussed earlier in this Chapter. Also, he had assumed the positive ion drift velocity was proportional to the field. This assumption

Table IV-2

Summary of SHEATH Code Results for Ar/HCl Mixtures

Ratio Ar/HCl		γ or Cathode Material	E_o/p $\frac{volt}{cm\text{-}torr}$	E_{min}/p $\frac{volt}{cm\text{-}torr}$	pd_c torr-cm	J/p^2 $\frac{\mu\ amp}{cm^2\text{-}torr^2}$	Vc volt	SF (γ,k_+) $\frac{X10^{-9}\ amp^{\frac{1}{2}}torr^{\frac{1}{2}}\text{-}cm^{\frac{1}{2}}}{volt^2}$
100/0								
Experiment	i	Mg	-	-	-	20.	119.	-
	i	Fe	-	-	.33	160.	165.	4.72
	i	Ni	-	-	-	160.	131.	-
	i	Pt	-	-	-	150.	131.	-
	i	Al	-	-	.29	-	100.	-
	i	Other Materials	-	-	-	-	64.-196.	-
Theoretical	ii	-	-	-	.36	100.	100.	7.78
	iii	.04	480.	37.7	.75	10.	183.8	1.95
99/1								
Theoretical	iii	.04	480.	31.6	.75	10.	183.8	1.95
95/5								
Theoretical	iii	.04	481.	42.8	.76	10.	186.8	1.97

i Data was taken from a summary presented in ref 6.
ii Data was taken from ref 60 (not self-consistent).
iii Data was calculated in this study.

is only appropriate in the low field region, i.e. E/p<60v/cm-torr. Note that as in He mixtures the scaling factor SF(γ, k_+) remains almost constant as the concentration of HCl increases.

In contrast to He mixtures, there is a negligible effect on the electric field in the cathode fall region when up to 5% HCl is added. This can be seen in Fig IV-13 and these results agree with the GLOW model. This electric field distribution through the cathode fall corresponds to approximately a 184v potential drop across the cathode fall region. With 1% HCl, the difference in total ionization is too small to have any observable effect on the electric field. The ionization thresholds for Ar (15.7eV) and HCl (12.7eV) are much closer than for He and HCl. This difference is too small to be observed in Fig IV-14 in the Townsend ionization coefficient. With 5% HCl, there is sufficient HCl to increase the ionization rate about 1.6% throughout most of the cathode fall region. Fig IV-15 and IV-16 compare the Townsend ionization and attachment coefficients as a function of distance for 99/1 and 95/5 concentrations in Ar/HCl. As in He/HCl mixtures, the attachment rate is larger than the ionization rate only for a few electron collisions close to the cathode where the electrons have insufficient energy for ionization.

Fig IV-17 and IV-18 display the electron and negative ion current densities as a function of distance and concentration of HCl. Again very little change is observed in the electron current density since the change in HCl concentration had only a minor effect on the ionization coefficients in Fig IV-14. The electron current density stays constant as the electrons are accelerated up to the ionization potential. Again the negative ion current density in Fig IV-18 i. charac-

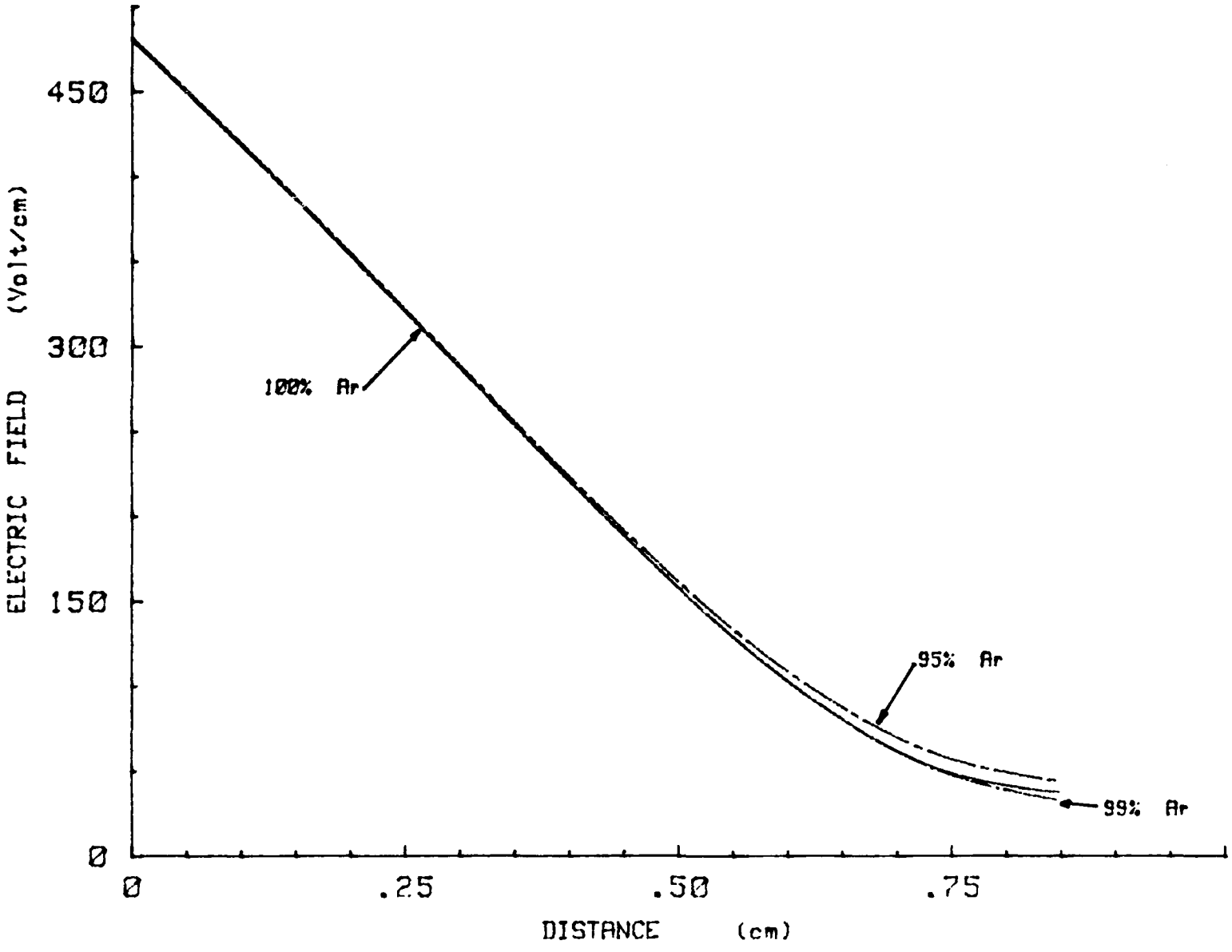

FIG IV-13 ELECTRIC FIELD IN Ar/HCl MIXTURES

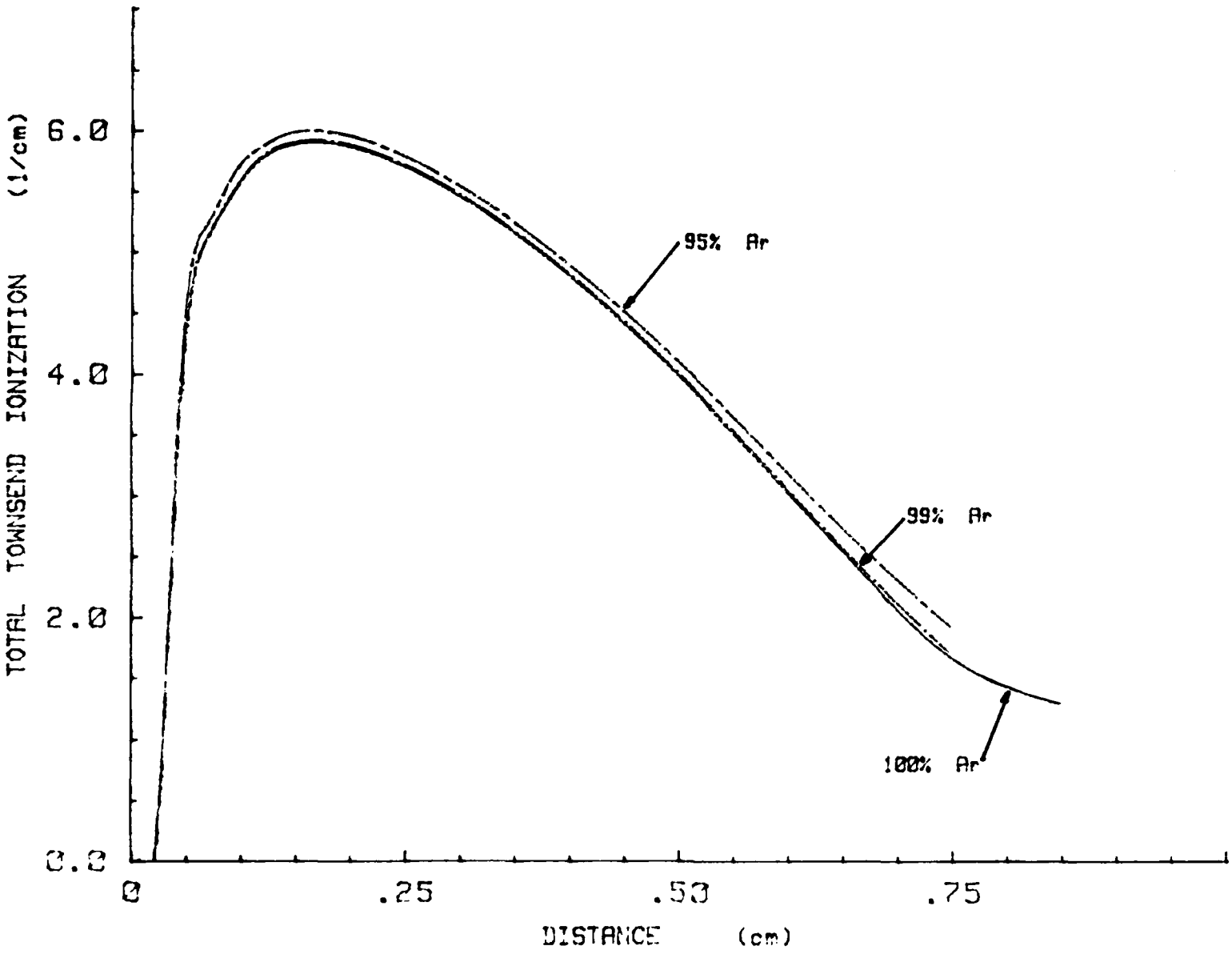

FIG IV-14 COMPARISON OF TOWNSEND IONIZATION COEFFICIENTS IN Ar/HCl MIXTURES

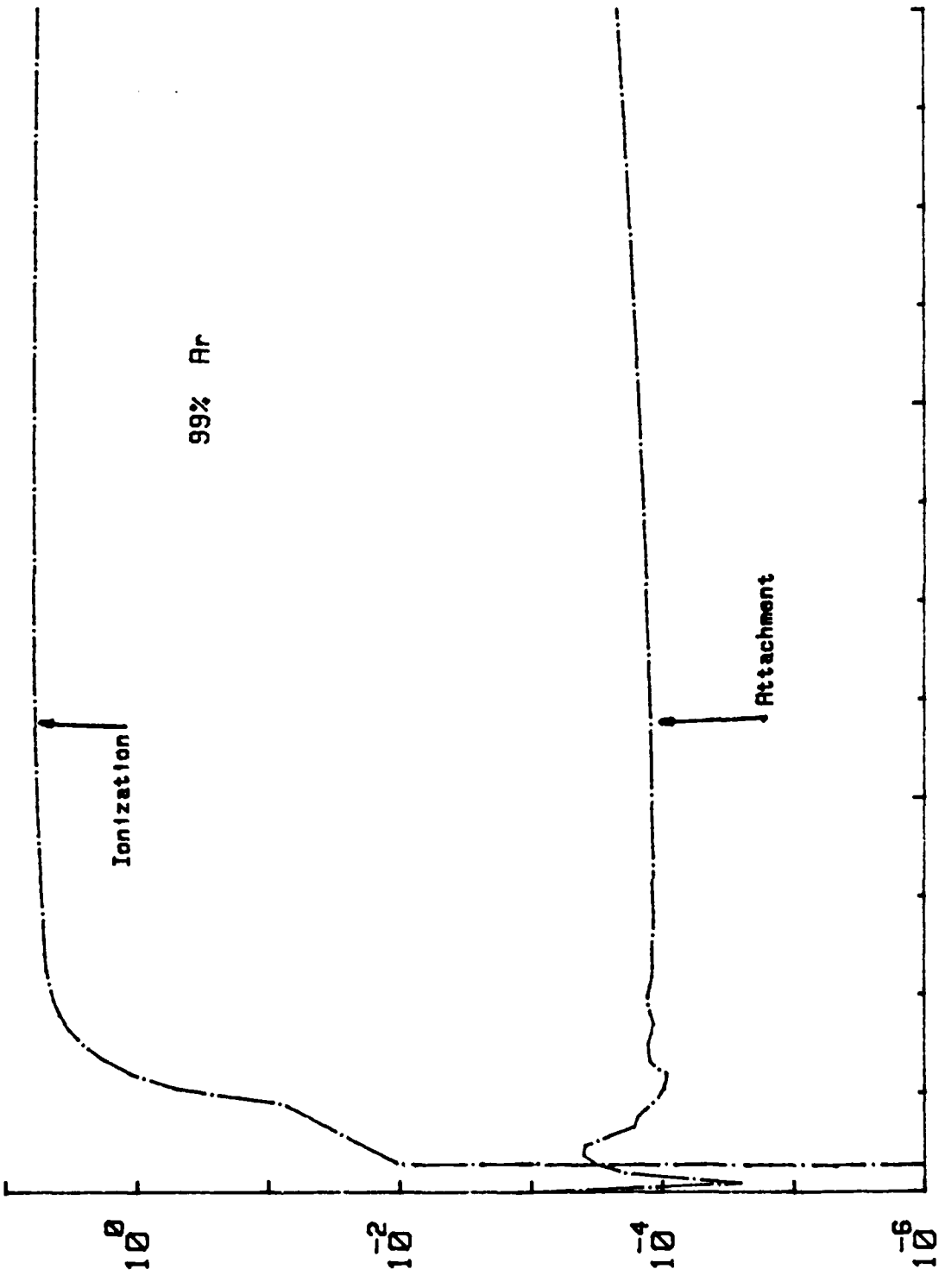

FIG IV-15 COMPARISON OF IONIZATION AND ATTACHMENT COEFFICIENTS IN 99/1 Ar/HCl

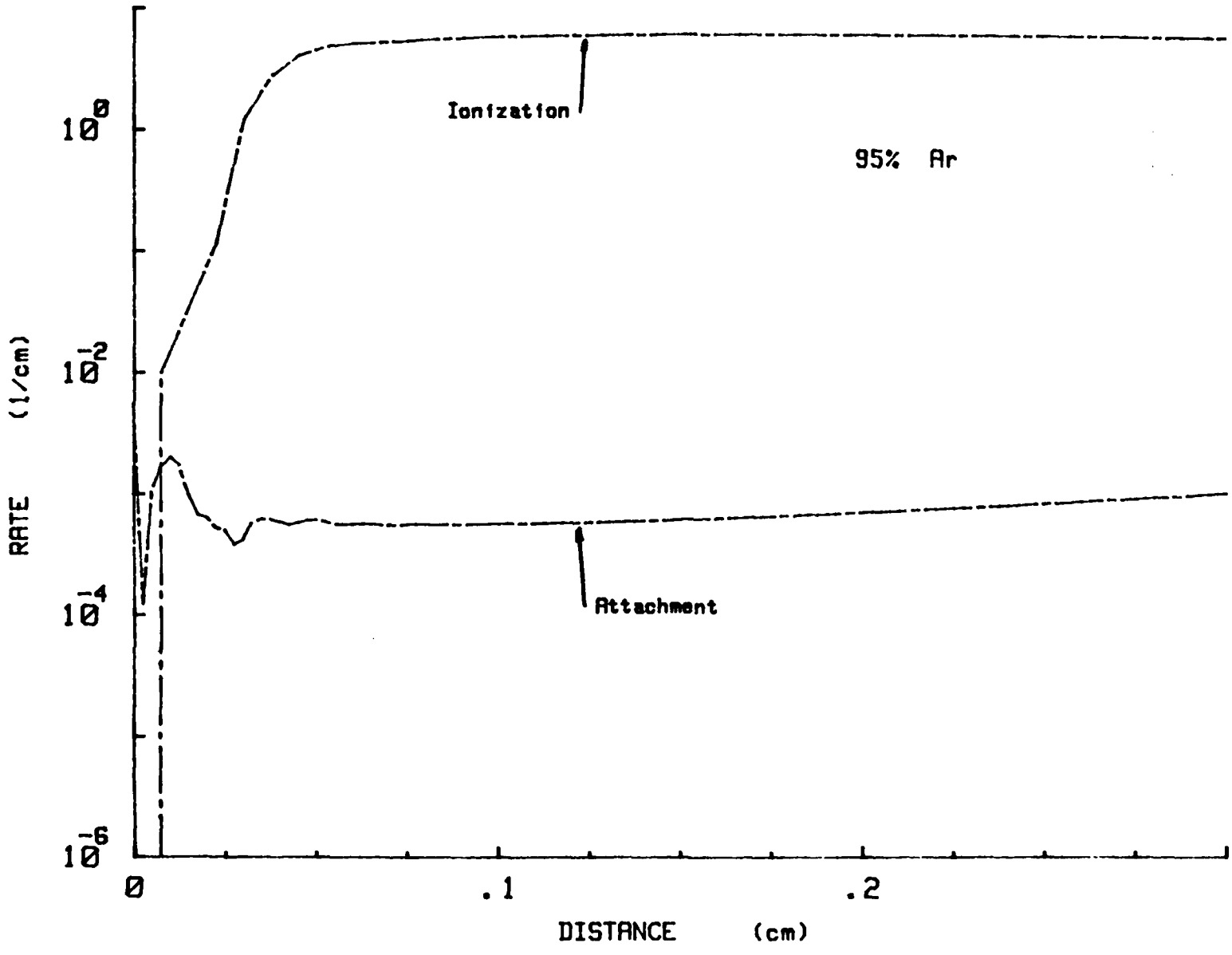

FIG IV-16 COMPARISON OF IONIZATION AND ATTACHMENT COEFFICIENTS IN 95/5 Ar/HCl

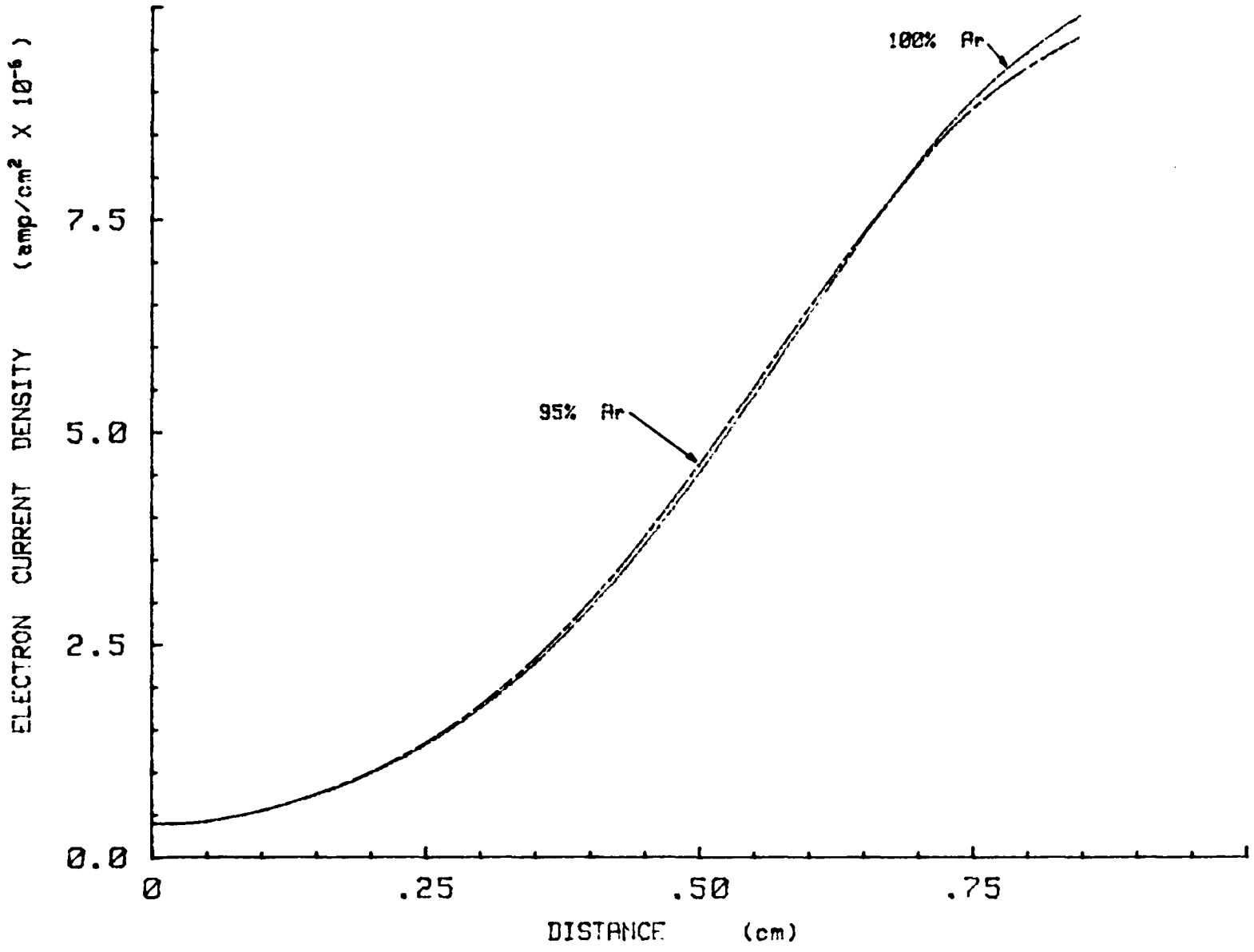

FIG IV-17 ELECTRON CURRENT DENSITY IN Ar/HCl MIXTURES

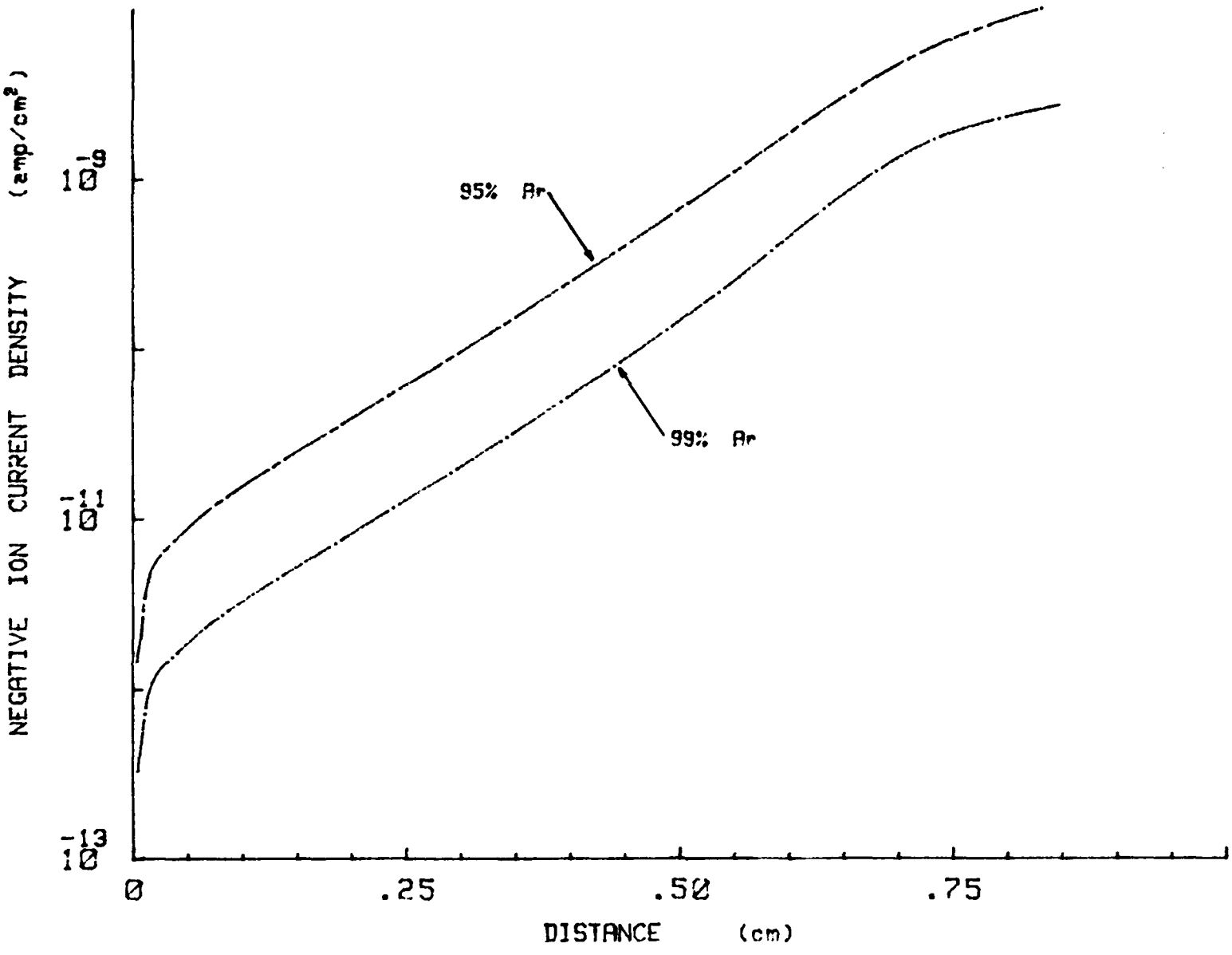

FIG IV-18 NEGATIVE ION CURRENT DENSITY IN Ar/HCl MIXTURES

terized by a very steep onset followed by a slightly faster than exponential growth through most of the cathode fall region. Even though the negative ion current density increases with HCl concentration, its contribution to the total discharge current through the cathode fall is still negligible.

The same nonequilibrium phenomena that occurred in He mixtures in the number densities can be observed in Ar mixtures in Fig IV-19, IV-20 and IV-21. The positive ion density increases in the direction moving away from the cathode, while the electron number density initially decreases. The number of negative ions is more than two orders of magnitude smaller than the number of positive ions, and actually their density does not begin to grow exponentially until the cathode fall begins to merge into the negative glow.

Since there is very little difference in the fields adjacent to the cathode, there is very little difference in the electron and positive ion number densities in this region. The positive ion density is still several orders of magnitude larger than the electron and negative ion densities and thus determines the slope of the electric field. Only in the last third of the cathode fall length (.5-.75 cm) is there a change when Fig IV-19, IV-20, and IV-21 are compared. As in He/HCl mixtures, the electron number density increases and the positive ion number density decreases but to a lesser degree since there is less change in the Townsend ionization coefficient.

Xenon

The results for Xe/HCl mixtures are summarized in Table IV-3.

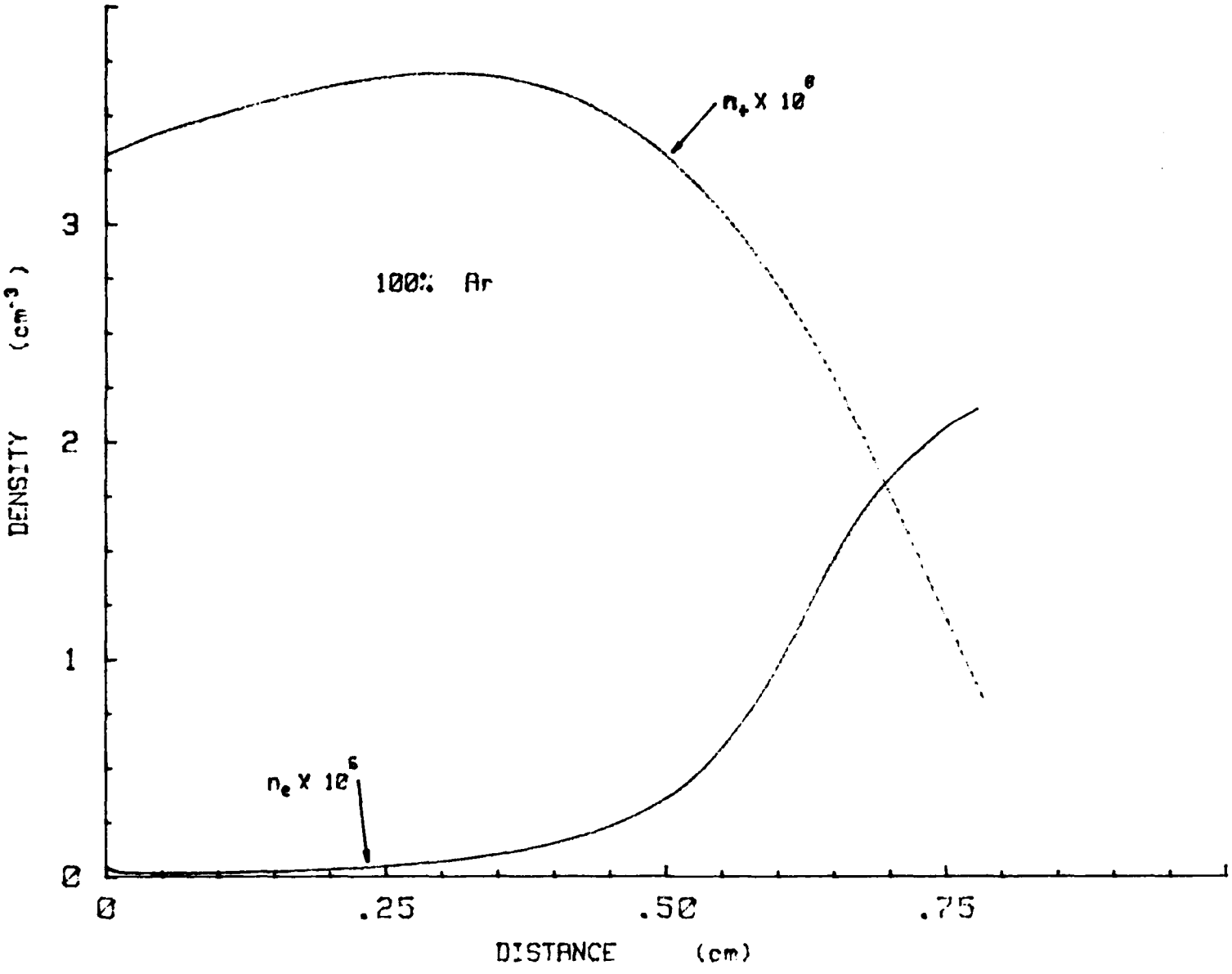

FIG IV-19 CHARGED PARTICLE DENSITIES IN 100% Ar

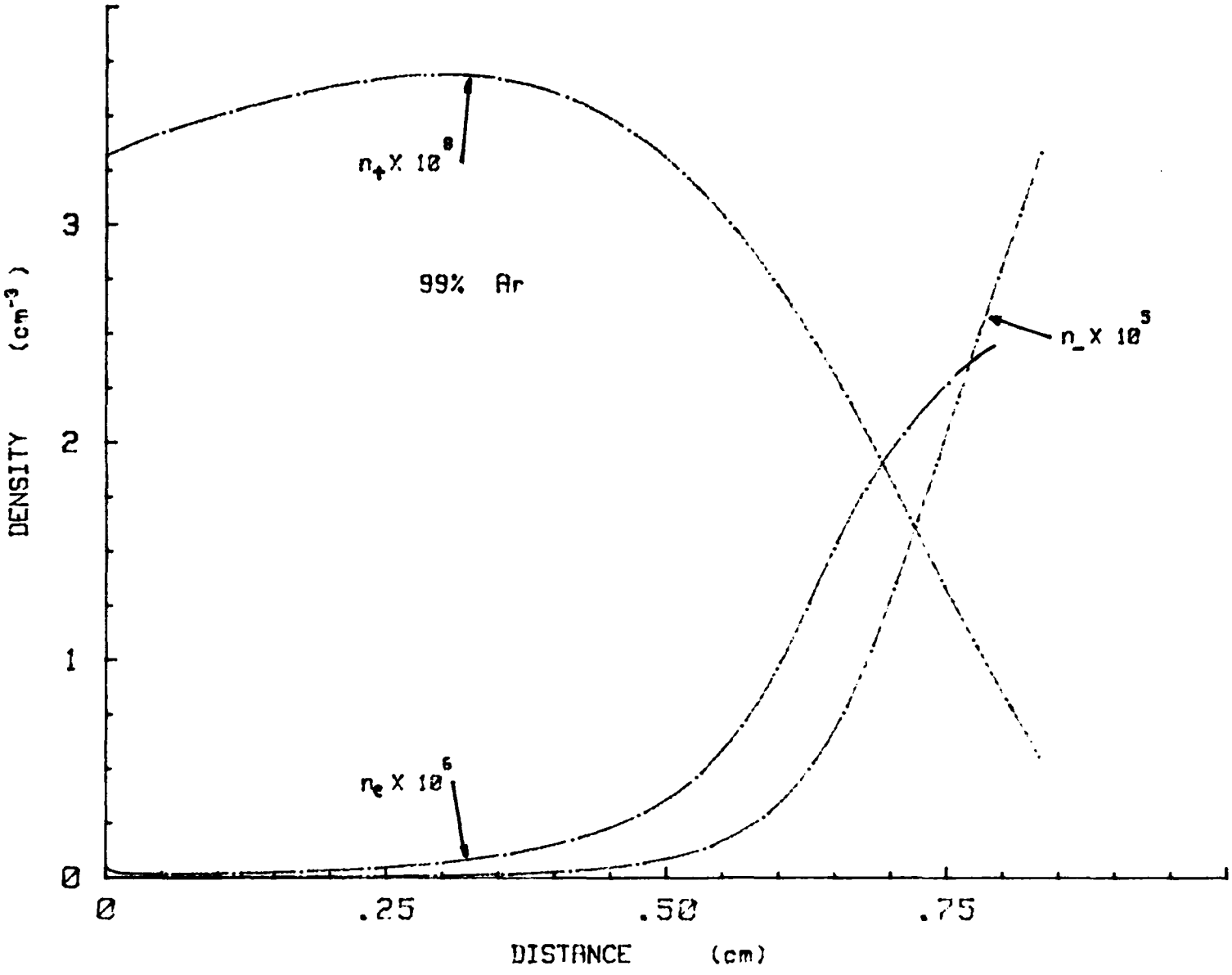

FIG IV-20 CHARGED PARTICLE DENSITIES IN 99/1 Ar/HCl

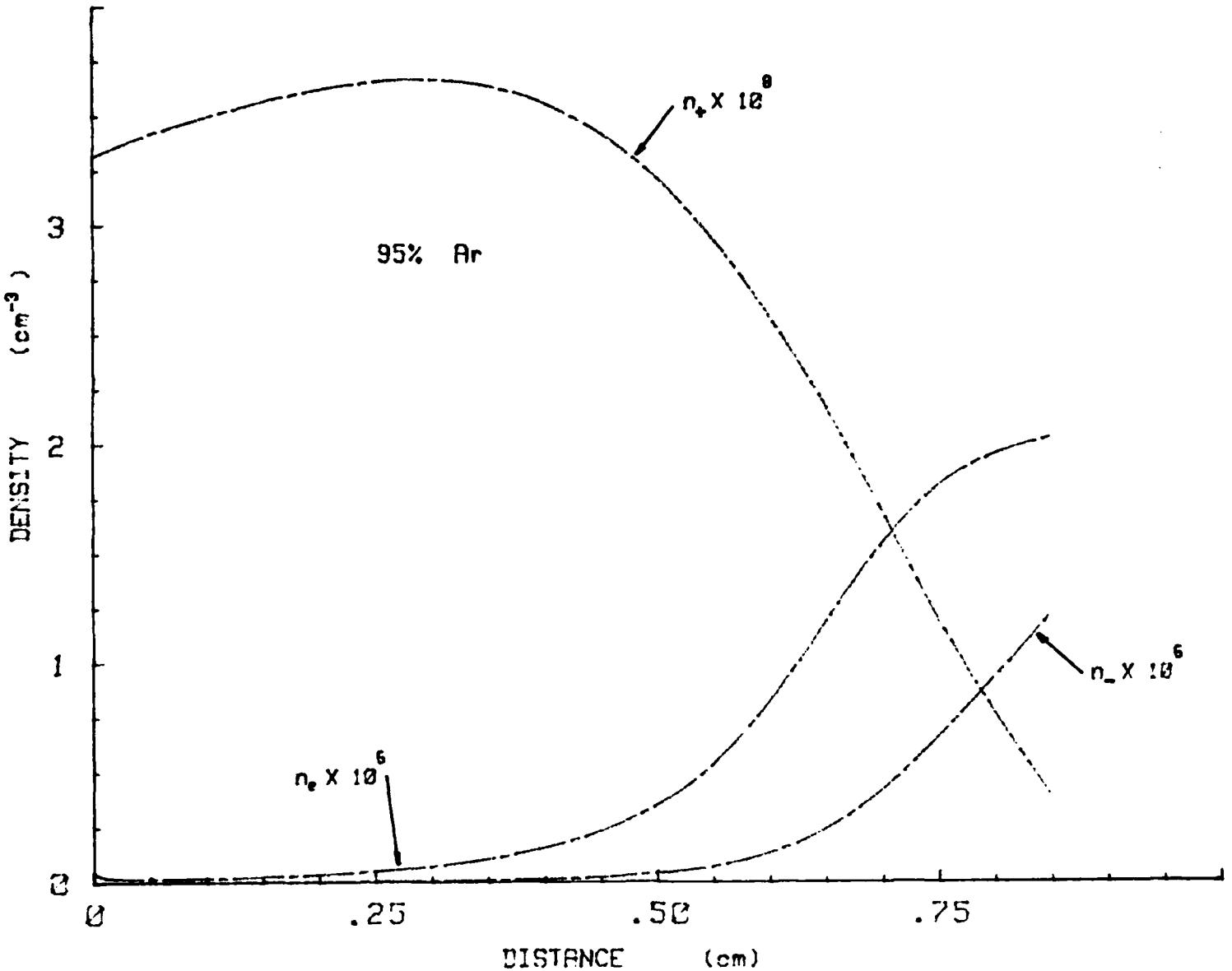

FIG IV-21 CHARGED PARTICLE DENSITIES IN 95/5 Ar/HCl

Table IV-3

Summary of SHEATH Code Results for Xe/HCl Mixtures

Ratio Xe/HCl		γ or Cathode Material	E_o/p $\frac{\text{volt}}{\text{cm-torr}}$	E_{min}/p $\frac{\text{volt}}{\text{cm-torr}}$	pd_c torr-cm	J/p^2 $\frac{\mu\text{ amp}}{\text{cm}^2\text{-torr}^2}$	Vc volt	SF (γ,k_+) $\frac{X10^{-11}\text{amp}_{\frac{1}{2}}\text{torr}^{\frac{1}{2}}\text{-cm}^{\frac{1}{2}}}{\text{volt}^2}$
100/0								
Experiment	i	Fe	-	-	.23	16.	306.	7.58
Theoretical	ii	.004	756.	60.2	.665	10.	252.2	90.04
99/1								
Theoretical	ii	.004	758.	66.4	.668	10.	254.4	89.88
95/5								
Theoretical	ii	.004	760.	61.8	.671	10.	256.2	89.94

i Data was taken from a summary presented in ref 6.
ii Data was calculated in this study.

There is very little data for comparison in Xe. The cathode fall voltage V_c and length d_c are sensitive functions of the secondary emission coefficient γ. The value of $\gamma = .004$ was chosen not to compare with an iron cathode but to be able to compare with the equilbrium results of the GLOW code which were compared with Ward's data. Even though this value of γ is low, it can not totally account for the large discrepancy between theory and experiment in $SF(\gamma,k_+)$. Of the three rare gases studied, the cross sections for Xe are probably the least well known. The derivation of the set of cross sections for Xe is described in Appendix C. The cross sections could be in error by as much as 20-25%. Since a parametric study of the cross section thresholds and initial slopes was not a part of this study, the magnitude of any change in the cross sections is as yet unknown. Since $SF(\gamma,k_+)$ is larger for the theoretical data, this implies that a smaller pd_c is required to make the theoretical data agree more closely with experiment. A reduction in pd_c, probably will also be accompanied by a decrease in V_c. Changing the excitation and ionization cross sections in order to make the Townsend ionization coefficient larger would tend to make pd_c and V_c smaller. Another source of error could be in the value of k_+. The value of k_+ was obtained from Ward (ref 92:2791) who subjectively fit equations III-71 to experimental data. He made no systematic effort to obtain the best parameters. In addition, only the first term in equation III-71b was used by the SHEATH model. In effect, a smaller positive ion drift velocity would result in a steeper slope for the electric field. This also would tend to make pd_c and V_c smaller. The minor variation in $SF(\gamma,k_+)$ in this author's results is due to round off and extrapolation errors in pd_c and V_c.

In contrast to He and Ar mixtures, there is a slight increase in the electric field in the cathode fall region when up to 5% HCl is added. This trend of the field shifting vertically can be seen in Fig IV-22. It results in a slight increase in the voltage which is summarized in Table IV-3. This trend is also the same as in Fig III-11 from the GLOW model. Slightly higher fields are required to obtain the same net ionization near the cathode. This results in a uniform vertical shift in the electric field throughout the cathode fall region. Note that even though the field is shifted to slightly higher values, there is no observable change in the ionization coefficient in the cathode fall region as illustrated in Fig IV-23. Again only near the minimum field region in the negative glow is a difference observed. Xe/HCl mixtures are unique in that both constituents have almost the same ionization potential (12.74 for HCl and 12.13 for Xe) and similar cross section magnitudes. A description of these cross sections occurs in Appendix C. Thus the slight expansion seen here is probably due to the formation of negative ions close to the cathode where there is a peak in the attachment rate. A loss of electrons close to the cathode is similar to the effect of reducing the secondary emission coefficient of the cathode. A decrease in γ similarly results in a higher cathode fall voltage. However, the slope of the electric field stays the same because the positive ions still dominate the other number densities. Thus the trend of the field shifting vertically with an increase in voltage would be expected to continue for larger concentrations of HCl in Xe. In this study the positive ion velocity of only the rare gas was included. For Xe/HCl mixtures, the addition of HCl would tend to increase the average positive ion drift velocity. This would result in

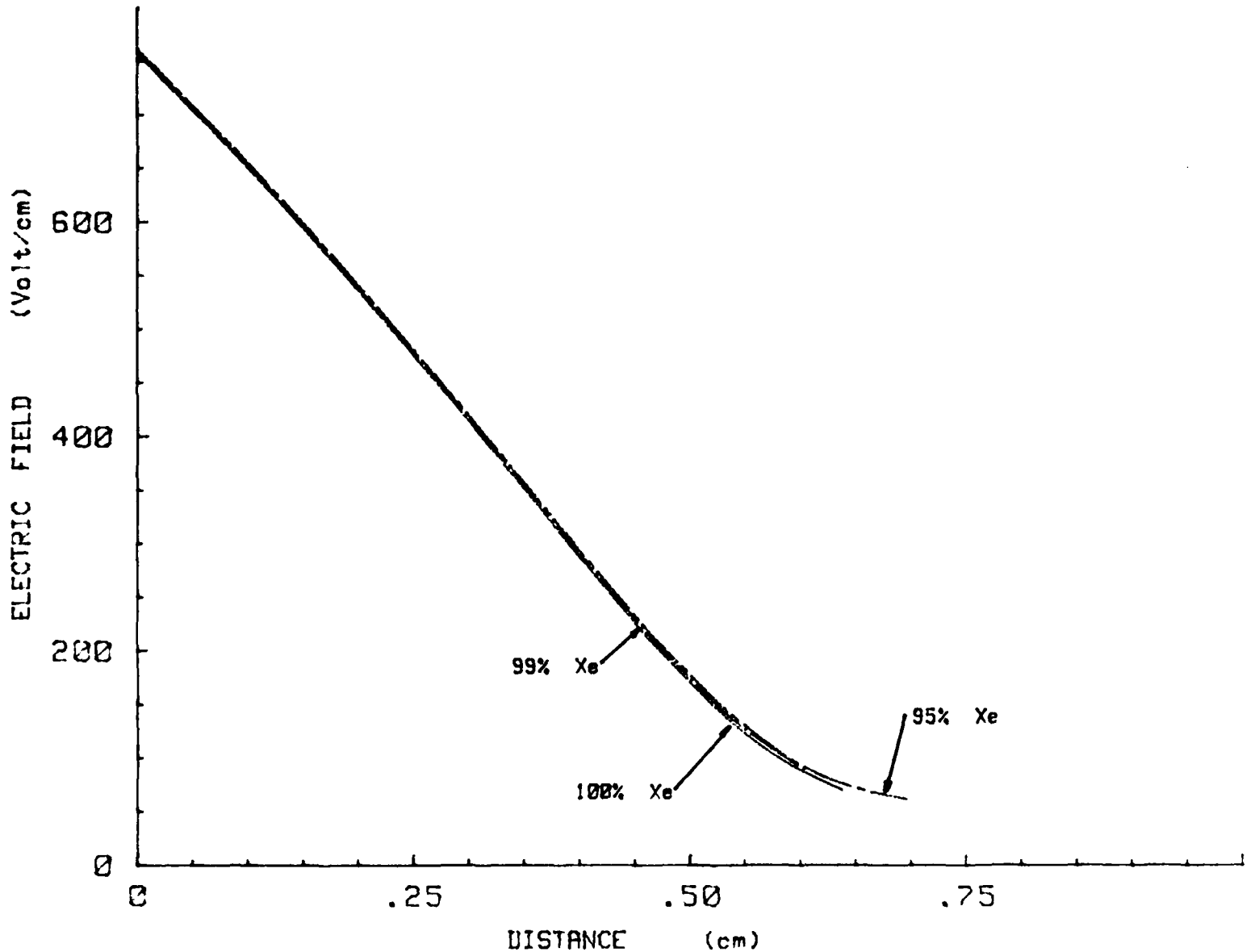

FIG IV-22 ELECTRIC FIELD IN Xe/HCl MIXTURES

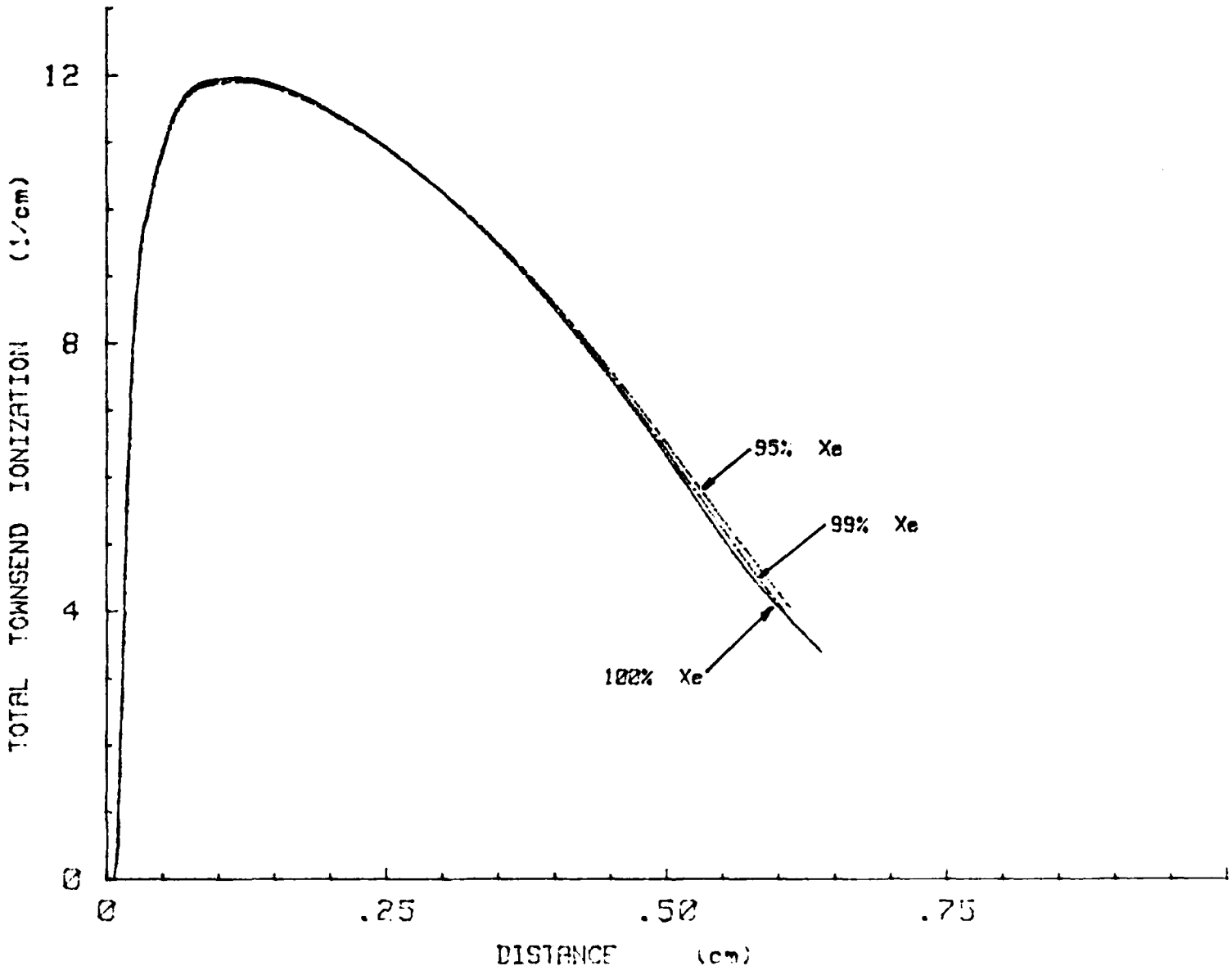

FIG IV-23 COMPARISON OF TOWNSEND IONIZATION COEFFICIENT IN He/HCl MIXTURES

a shallower slope of the electric field and a further expansion in pd_c.

Fig IV-24 and IV-25 compare the Townsend ionization and attachment coefficients as a function of distance for 99/1 and 95/5 concentrations in Xe/HCl. Again the attachment coefficient is much smaller than the ionization rate throughout the cathode fall region except immediately in front of the cathode. Note that the region where the attachment coefficient is greater than the ionization rate is smaller in Xe mixtures than in He or Ar mixtures. This is due to Xe having a lower ionization threshold than the other buffer gases. The first peak in the attachment coefficient is a result of the slow electrons leaving the cathode and the second peak is a result of the formation of slow electrons that have lost their energy to excitation or ionization. The first peak has the effect of reducing the secondary emission coefficient of the cathode.

Fig IV-26 and IV-27 display the electron and negative ion current densities as a function of distance and concentration of HCl. Very little change is observed in the electron current density until near the cathode glow-negative glow boundary. Here the electron current density is observed to decrease instead of increasing as a function of HCl concentration as in previous rare gas mixtures. This is another example of the effect of attachment in the cathode fall region. Even though the negative ion current density in Fig IV-27 increases significantly with HCl concentration, its contribution to the total discharge current is still negligible.

The same nonequilibrium phenomena that occurred in previous rare gas mixtures for the number densities can be observed in Xe mixtures. The results are illustrated in Fig IV-28, through IV-30. Again the

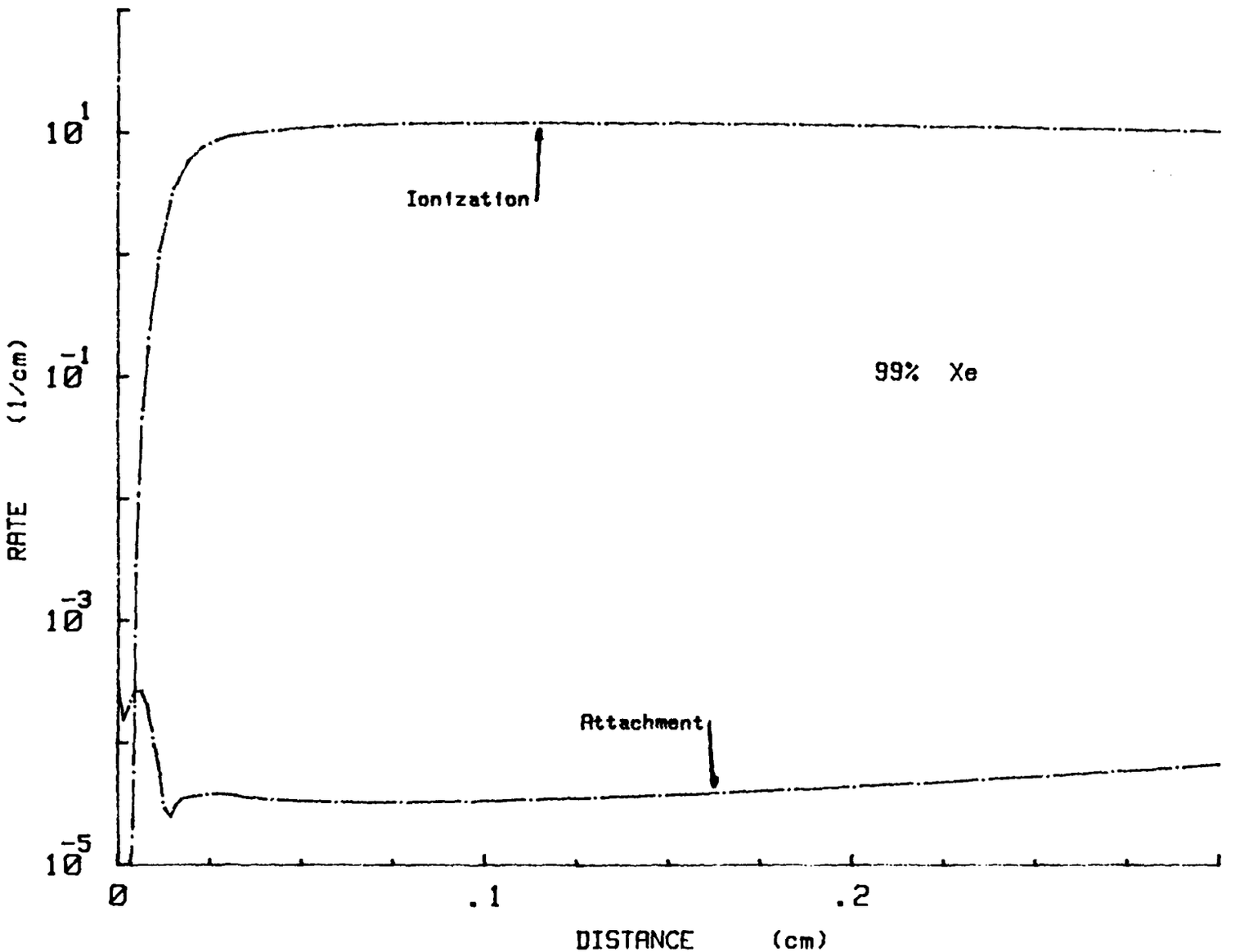

FIG IV-24 COMPARISON OF IONIZATION AND ATTACHMENT COEFFICIENT IN 99/1 Xe/HCl

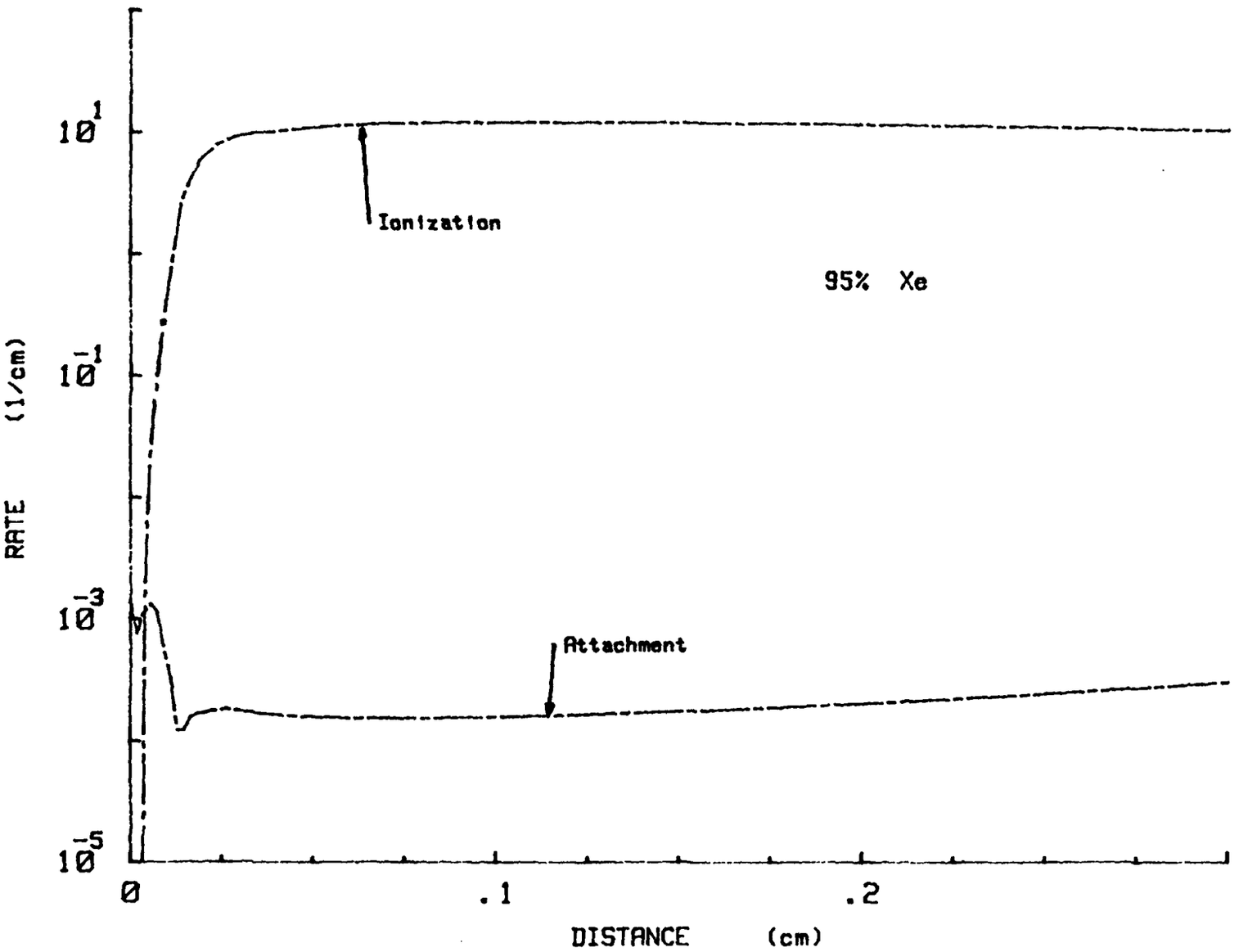

FIG IV-25 COMPARISON OF IONIZATION AND ATTACHMENT COEFFICIENT IN 95/5 Xe/HCl

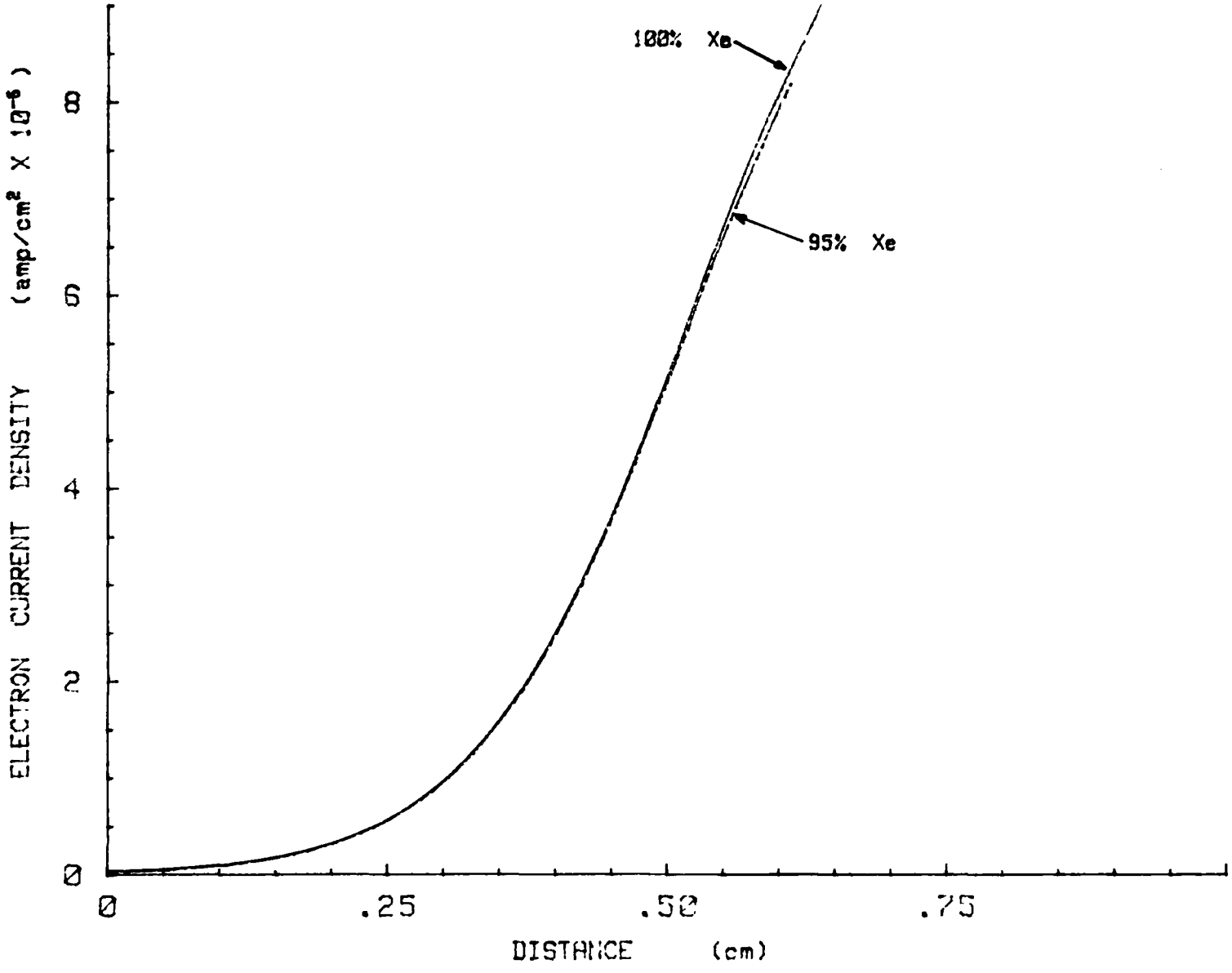

FIG IV-26 ELECTRON CURRENT DENSITY IN Xe/HCl MIXTURES

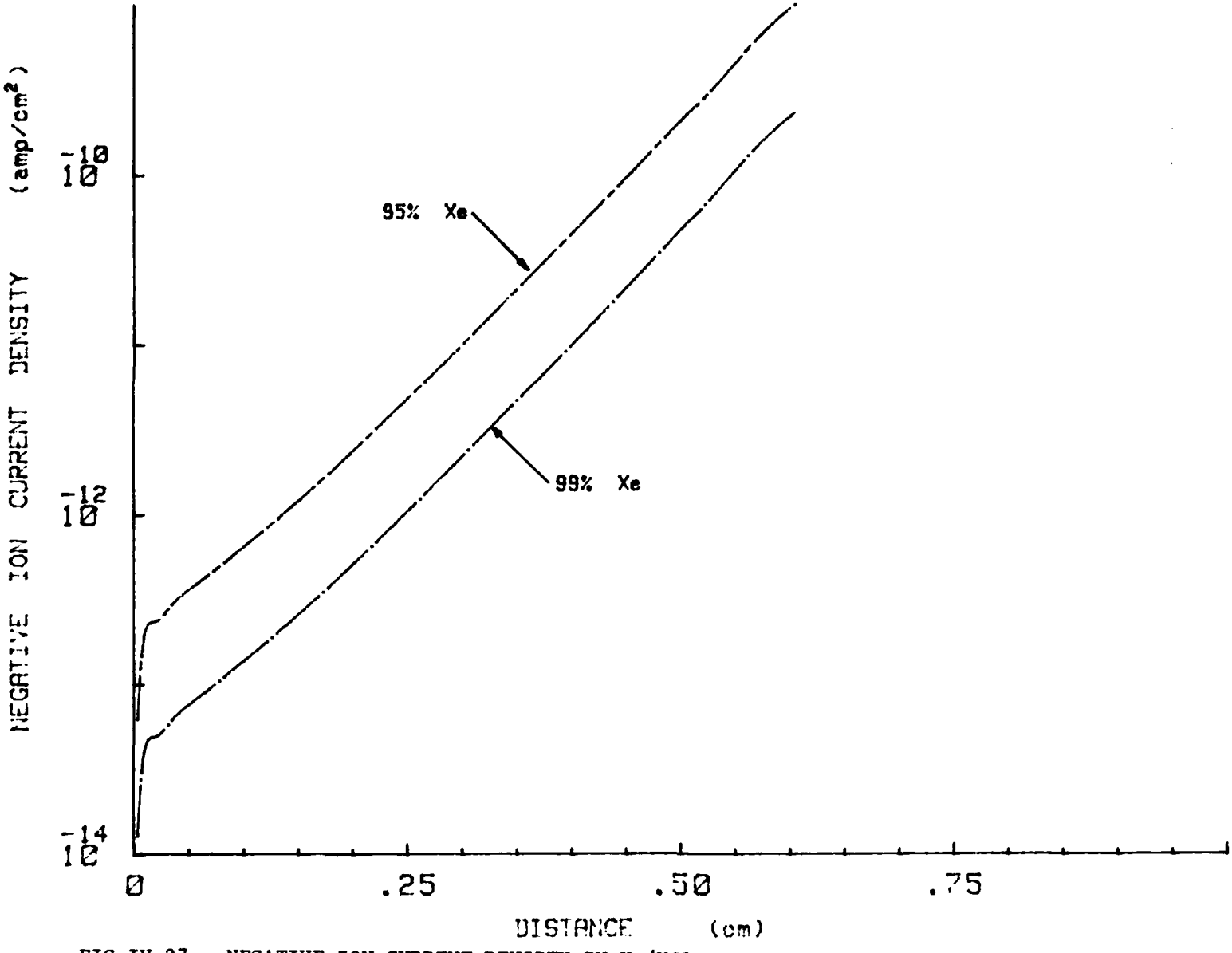

FIG IV-27 NEGATIVE ION CURRENT DENSITY IN Xe/HCl MIXTURES

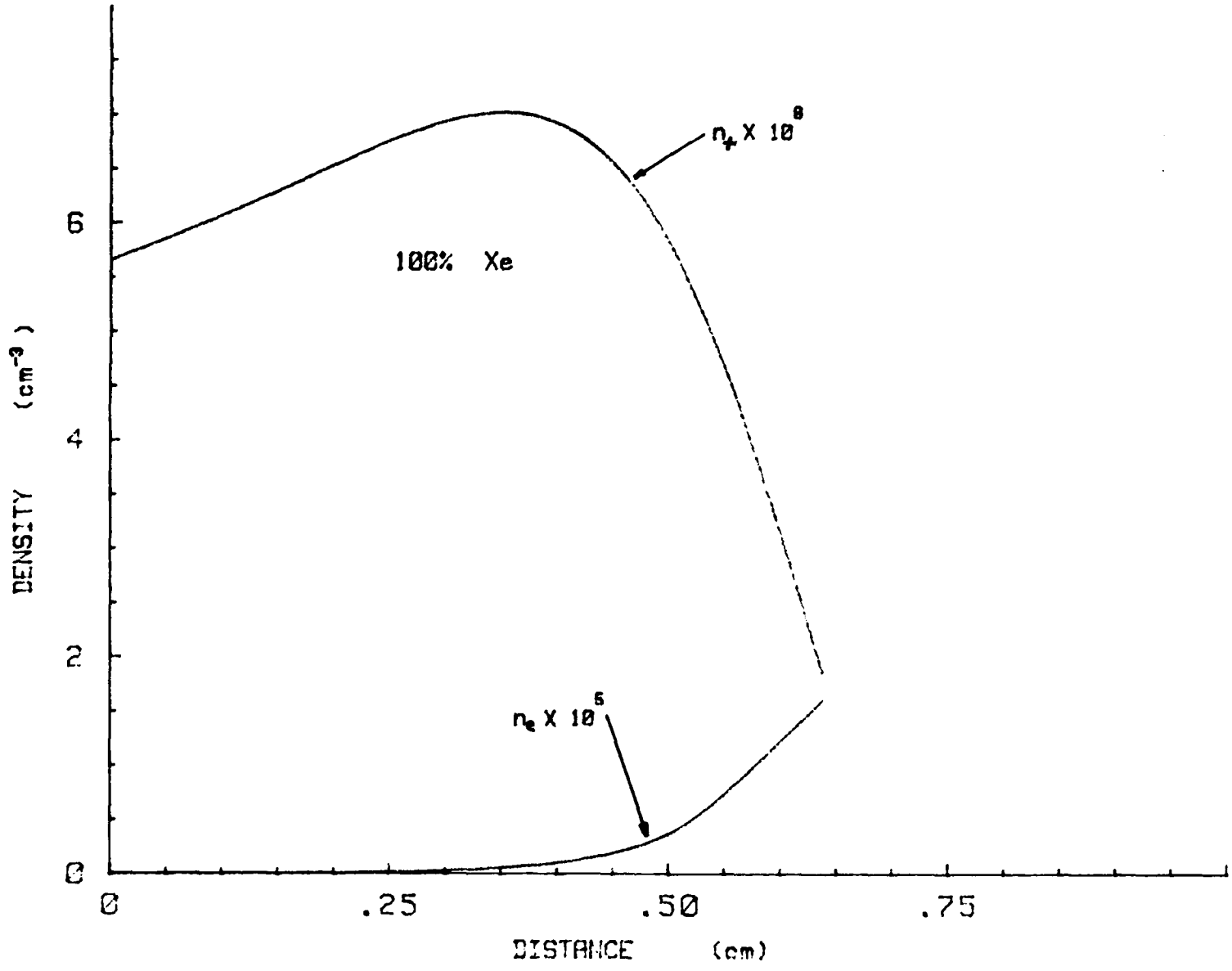

FIG IV-28 CHARGED PARTICLE DENSITIES IN 100 % Xe

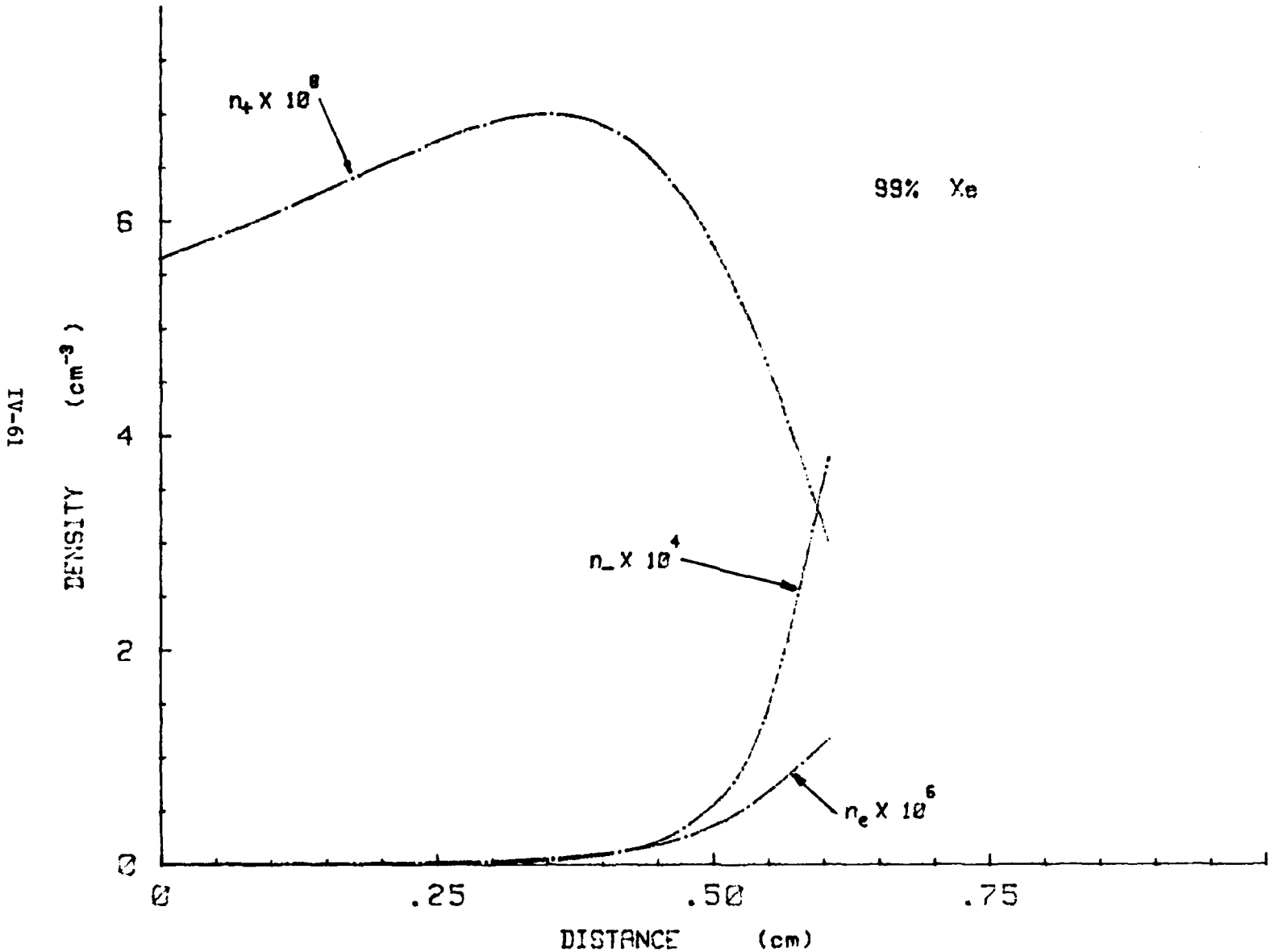

FIG IV-29 CHARGED PARTICLE DENSITIES IN 99/1 Xe/HCl

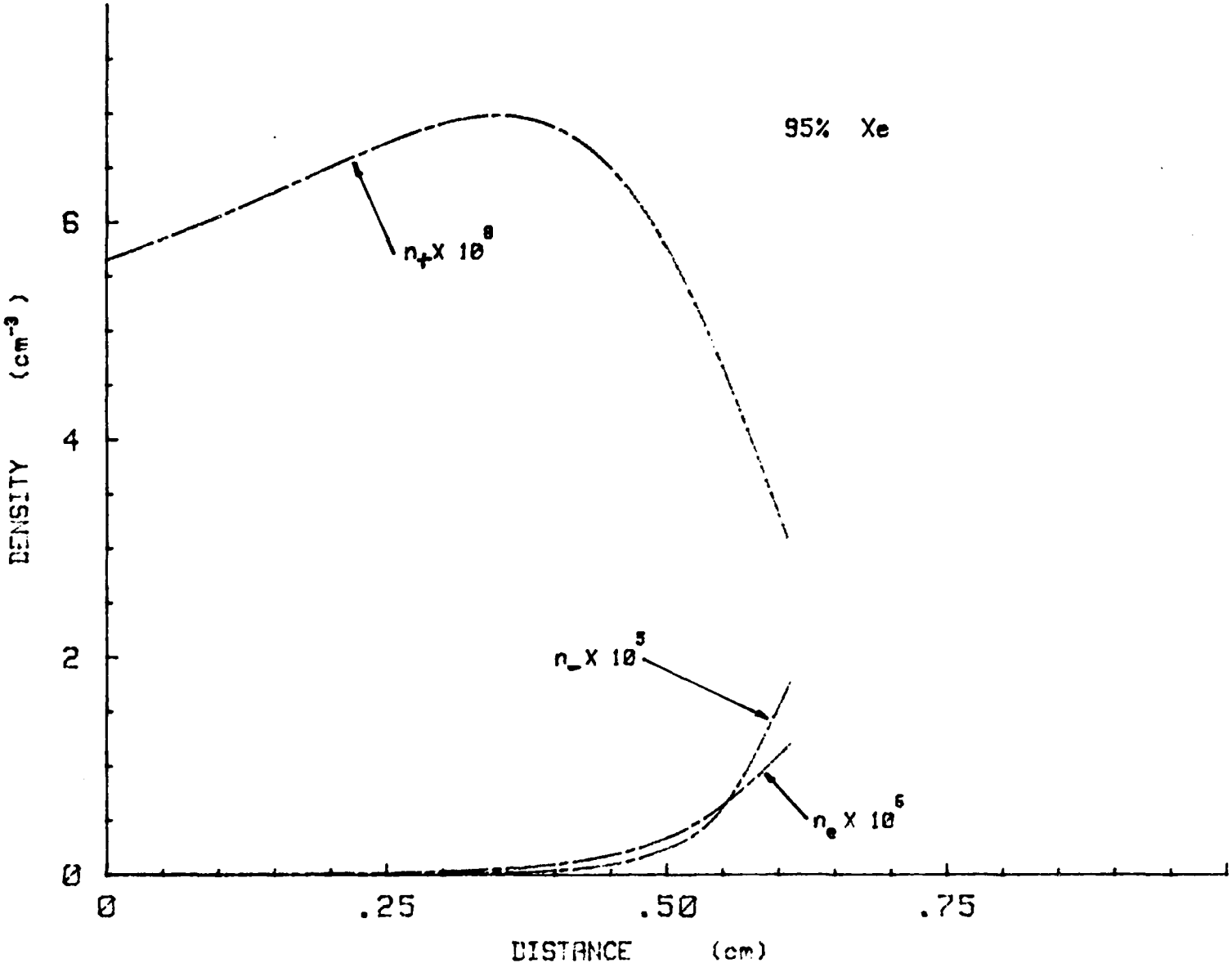

FIG IV-30 CHARGED PARTICLE DENSITIES IN 95/5 Xe/HCl

trends of each of the number densities is similar to the trends seen before. The positive ion density is still several orders of magnitude larger than the electron and negative ion densities and thus determines the slope of the electric field in Xe as well. The number of negative ions is more than three orders of magnitude smaller than the number of positive ions, and actually their density does not begin to grow exponentially until the cathode fall begins to merge into the negative glow. As in Ar, there is almost no difference in the number densities of electrons and positive ions adjacent to the cathode, since the field changes only slightly there when HCl is added. As in Ar, only in the last third of the cathode fall length (.45-.65cm) do the number densities differ as a function of HCl. This is a result of a change in the net ionization prior to this region.

In summary, we have examined three cases represented by He/HCl, Ar/HCl and Xe/HCl mixtures. In all three gas mixtures, there was a peak in the Townsend attachment coefficient as a result of electron nonequilibrium. However, throughout the cathode fall region the positive ion density dominates the other charge densities and so determines the slope of the electric field even in electronegative gas mixtures. He/HCl mixtures were characterized by a significant contraction of the cathode fall length and a decrease in the cathode fall voltage. This was a result of the HCl being easier to ionize than the He. As a result of HCl having a lower ionization cross section threshold than He, the threshold for the total Townsend ionization coefficient shifted closer to the cathode. There was a negligible effect in the electric field, cathode fall length, or cathode fall voltage when HCl was added to Ar mixtures. The Townsend ionization coefficient did increase

slightly with the addition of 5% HCl. This is because the ionization rate is very sensitive to the gas species and the shape of the electron energy distribution function. In contrast, in Xe/HCl mixtures, the electric field, cathode fall length, and cathode fall voltage increased slightly, probably as a result of the nonequilibrium electrons being attached to form negative ions in the primary dark space.

In conclusion, the formation of negative ions in the cathode fall region does not lead to a contraction of the sheath. The contraction that is often observed and that was seen by Emeleus and Sayers, was actually due to an increase in the ionization efficiency of the gas mixture when an electronegative gas is added.

Chapter V. Comparison of Results of the Equilibrium and Nonequilibrium Analyses

This section compares and contrasts the GLOW and SHEATH models. First, their equations and assumptions are briefly reviewed. Second, the results from these models are compared. In order to determine the influence of nonequilibrium without further complications due to negative ions, results for the pure rare gases will be emphasized. These results include the electric field, Townsend ionization and attachment coefficients, the electron current densities, and the charged particle densities. The trends predicted by both models are summarized along with a criticism of each technique on its applicability in the cathode fall region. Finally, the applicability of each model to the anode region is discussed.

Review of Basic Assumptions

The GLOW and SHEATH models are founded on two entirely different methods for describing the kinetics and fields in a glow discharge. As described in Chapter III, the GLOW model is based on a self-consistent solution to a set of equilibrium equations: Poisson's equation, the hydrodynamic current continuity equations for electrons and negative ions, and the current conservation equation. The SHEATH model described in Chapter IV is based on a solution of the Boltzmann transport equation for electrons as a function of distance coupled with Poisson's equation and the current conservation equation. The equations are listed in Table V-1 for comparison. The fundamental difference behind

Table V-1

Comparison of Basic Equations

	Basic Equations	Boundary Conditions	Variable Inputs	Equations Defining Parameters
GLOW	$\frac{dE}{dx} = \frac{-1}{\epsilon_0 v_+}(J_+ - rJ_e - J_-)$	$J_e(0) = \gamma J_+(0)$	E_o	$\frac{\alpha}{p} = A\, e^{-B(\frac{p}{E})^s}$
	$\frac{dJ_e}{dx} = \left(\alpha - \eta - \frac{D_e r}{\lambda^2 v_+}\right) J_e$	$J_-(0) = 0$	d	$\frac{\eta}{p} = C\, e^{-D(E/p)^t}$
	$\frac{dJ_-}{dx} = \eta J_e - \frac{k_r J_- J_+}{e v_+^2}$	$J_+(d) = 0$ or	p	$\frac{\eta}{p} = \sum_{i=0}^{n \text{ or } \infty} a_i (E/p)^i$
	$J = J_+ + J_e + J_-$	$J_e(d) + J_-(d) = J$		$v_+ = k_+ (E/p)^{\frac{1}{2}}$
SHEATH	$\frac{\partial f}{\partial \phi} + \frac{\partial f}{\partial \xi} = \frac{1}{e E/N}\left(\frac{\varepsilon}{\xi}\right)^{\frac{1}{2}}(K - Q(\varepsilon))f$	$J_e(0) = \gamma J_+(0)$	E_o	$\alpha(\phi) = N(\phi)\, \frac{e\int_0^\infty (f_+(\varepsilon,\phi) + f_-(\varepsilon,\phi))\sigma_i(\varepsilon)\,d\varepsilon}{\int_0^\infty (f_+(\varepsilon,\phi) - f_-(\varepsilon,\phi))\,d\varepsilon}$
	$\frac{dE}{dx} = \frac{-e}{\epsilon_0}(n_+ - n_e - n_-)$	$J_-(0) = 0$	d	
	$J = J_+ + J_e + J_-$	E is not imaginary	p	$\eta(\phi) = N(\phi)\, \frac{e\int_0^\infty (f_+(\varepsilon,\phi) + f_-(\varepsilon,\phi))\sigma_a(\varepsilon)\,d\varepsilon}{\int_0^\infty (f_+(\varepsilon,\phi) - f_-(\varepsilon,\phi))\,d\varepsilon}$
	$\frac{dJ_-}{dx} = \eta J_e$	$f_+(\varepsilon,\phi)$ at $x=0$ is described in Appendix C.	E_{min}	$v_+ = k_+ (E/p)^{\frac{1}{2}}$
	$J_e(\phi) = J_{e0}\, \frac{\int_0^\infty (f_+(\varepsilon,\phi) - f_-(\varepsilon,\phi))\,d\varepsilon}{\int_0^\infty (f_+(\varepsilon_0,\phi_0) - f_-(\varepsilon_0,\phi_0))\,d\varepsilon}$			

these equations is that the glow model assumes the electrons are in equilibrium with the field, whereas the SHEATH model does not. Since both methods are describing the same discharge, the boundary conditions in Table V-1 are almost identical.

In addition, both methods predict results that appear to scale according to equation III-71. In the equilibrium model, limited data was taken at 10 and 100 Torr to check the pressure scaling. There was also good agreement with other theoretical data when the same value of the secondary emission coefficient and the same relationship of the positive ion drift velocity to the electric field was used. In the nonequilibrium model, the scaling factor in Table IV-1 for 100% He agreed very well with the Monte Carlo results of Boeuf, et al. (ref 21). Scaling agreement of both models can be expected because both models support the assumptions used in deriving equation III-71, which are:

a. Positive ions dominate the other charged particle species through most of the cathode fall and therefore determine the slope of the electric field.

b. The positive ion drift velocity is proportional to the square root of the electric field.

c. The electric field can be approximated as a linearly decreasing function through most of the cathode fall region.

Despite the differences in assuming equilibrium or not assuming equilibrium, both models scale appropriately and predict the same trends in all three gas mixtures.

Comparison of Results

Comparing the results of the GLOW and SHEATH models from Chapters III and IV respectively indicates that both methods do predict the same trends for each gas mixture. In He mixtures both models predict a contraction of the cathode fall with the addition of HCl as seen in Fig III-3 and IV-4. Data from both models indicate this contraction is due to the more efficient ionization of the HCl in the mixture, rather than the formation of negative ions in the cathode fall as was speculated by Emeleus, et al. (ref 42). Similarly in Ar/HCl mixtures, both methods agree that the addition of up to 5% HCl has an insignificant effect on the cathode fall field or voltage. This can be observed in Fig III-7 and IV-13. In Xe/HCl mixtures a slight increase in electric field as well as voltage drop across the cathode fall was predicted by both models. This increase can be seen in Fig III-11 and IV-22. Data from both methods agree that this field enhancement is due to the loss of electrons to attachment near the cathode, although this is perhaps most easily seen from the theory described in section, "New Equilibrium Analysis of the Cathode Fall Region including Negative Ions" in Chapter III. This loss of electrons to attachment close to the cathode is analogous to reducing the electron secondary emission coefficient.

Fig V-1 through V-3 compare the distribution of the electric field through a discharge for He, Ar, and Xe. For each gas, the slope of the electric fields are approximately the same as a result of the same field relationship being used for the positive ion drift velocity. Also, the results of the SHEATH model are consistently higher than those of the GLOW model until the field begins to merge into the negative glow. This is a result of the nonequilibrium behavior of the

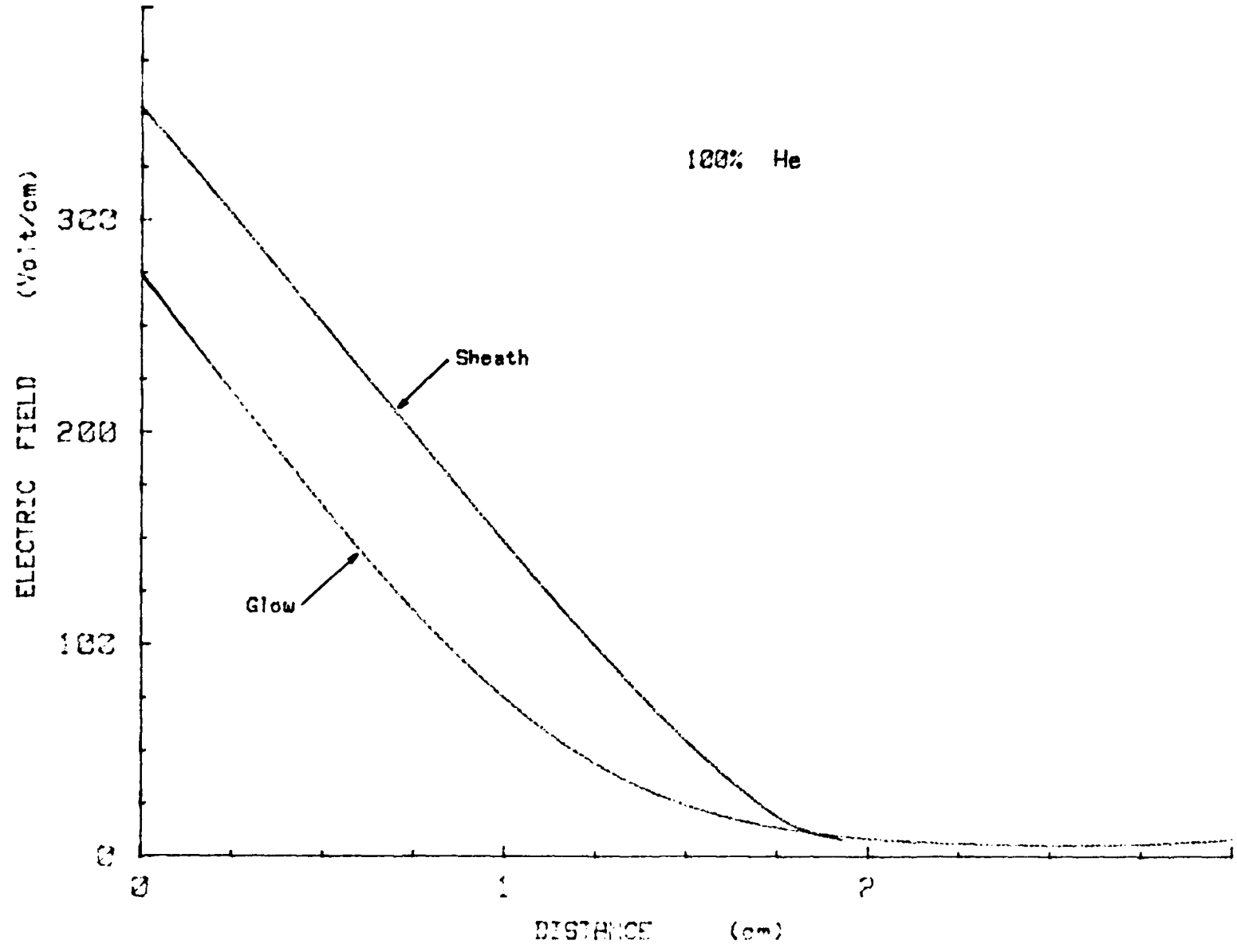

FIG V-1 COMPARISON OF ELECTRIC FIELDS FROM GLOW AND SHEATH CODES IN 100% He

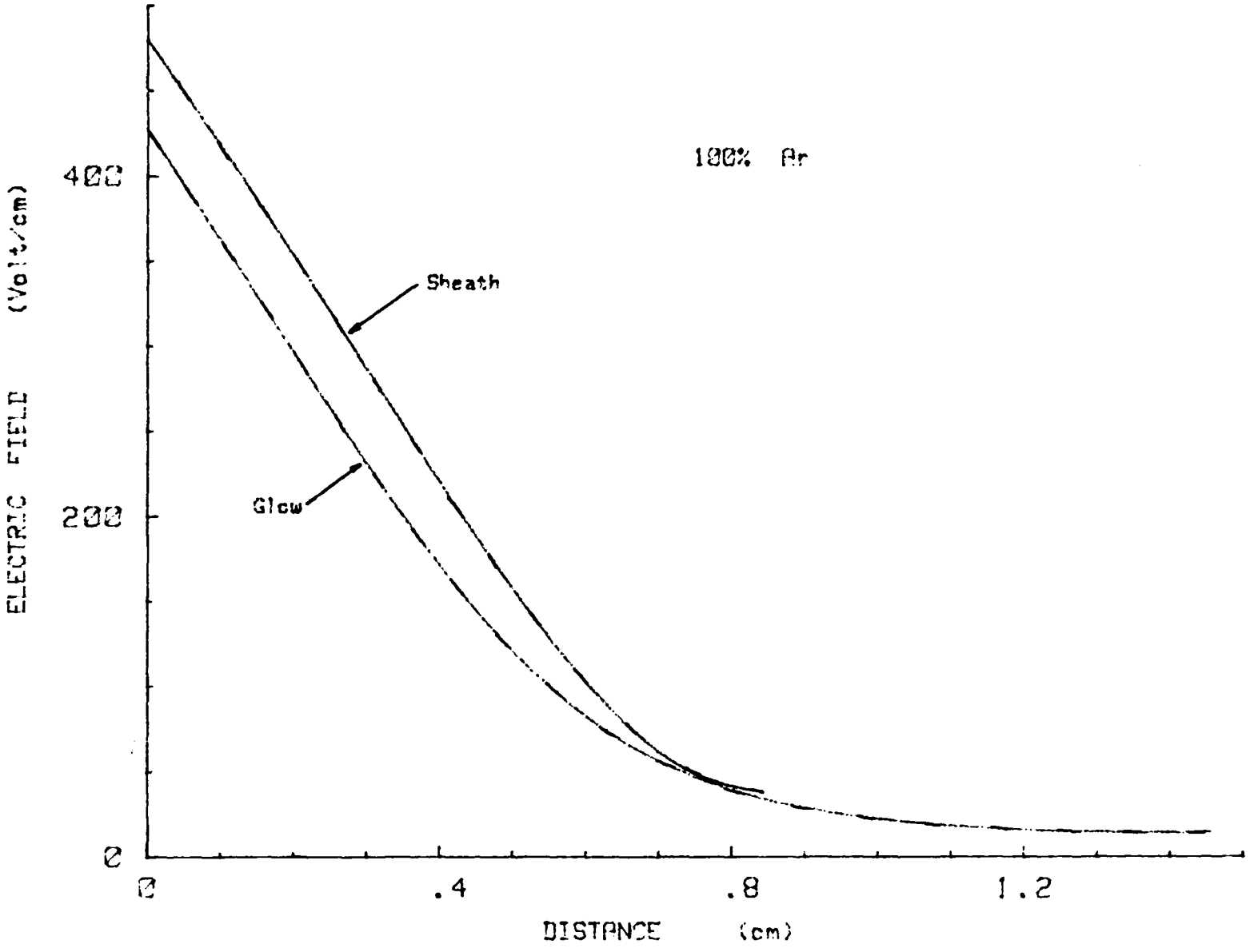

FIG V-2 COMPARISON OF ELECTRIC FIELDS FROM GLOW AND SHEATH CODES IN 100% Ar

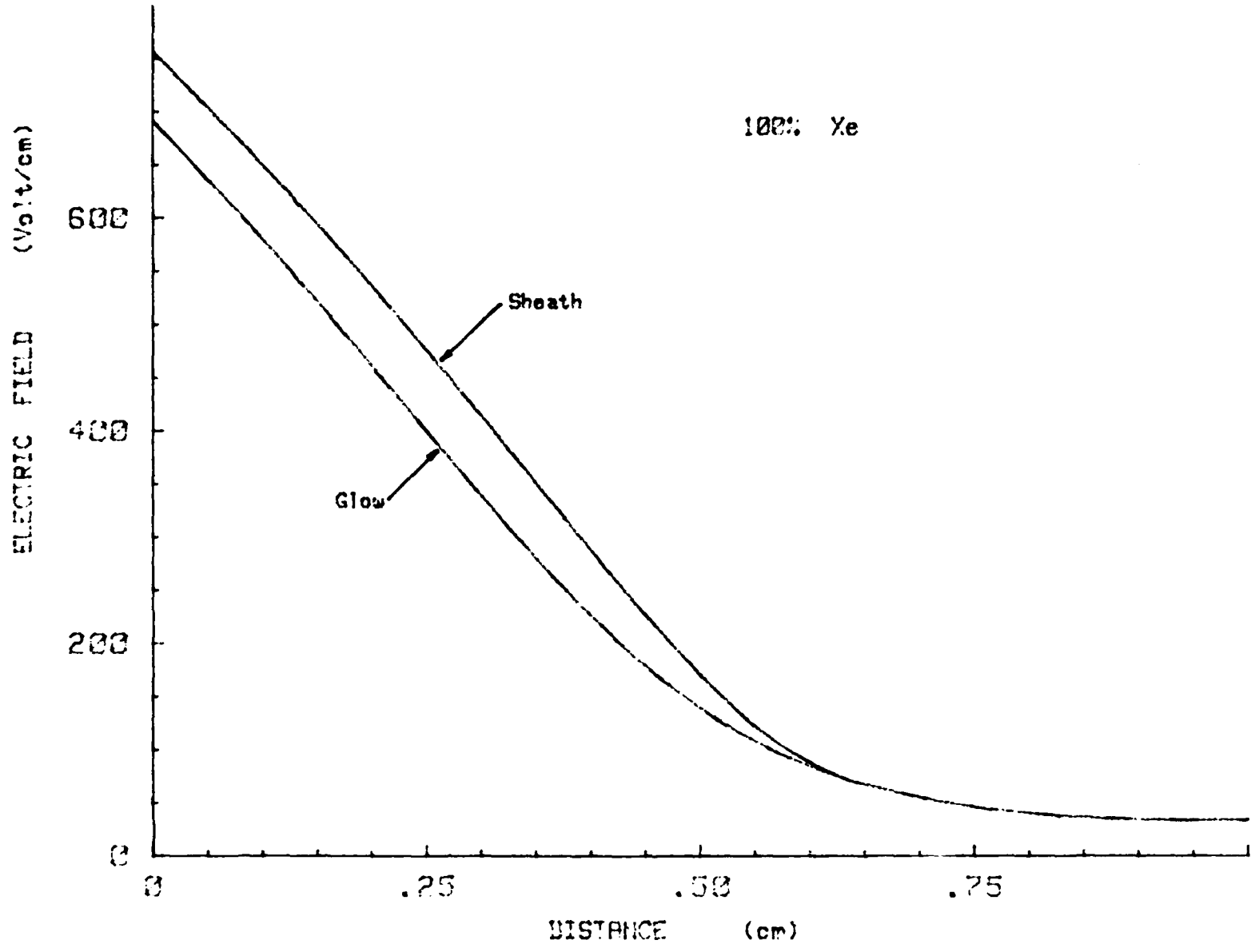

FIG V-3 COMPARISON OF ELECTRIC FIELDS FROM GLOW AND SHEATH CODES IN 100% He

electrons near the cathode. The best agreement is obtained for Xe and the worst for He, since the electrons have shorter mean free paths in Xe than in He and thus spatially reach equilibrium faster.

The Townsend ionization coefficient for each model is plotted in Fig V-4 along with the electric field calculated by the SHEATH model. These coefficients were calculated for the given electric field using the equations in Table V-1. As can be seen, the plots for these coefficients are not the same shape due to the nonequilibrium electron behavior in the cathode fall region. In the SHEATH model, the electrons require several mean free paths before they reach the ionization energy and can begin to multiply. This spatial delay in ionization results in a higher cathode fall voltage and higher field at the cathode. The ionization coefficient predicted by the SHEATH model actually lags the field, ie. the rate is low where the field is highest and then overshoots and is high where the field merges into the negative glow. The GLOW model assumes the electrons to be in equilibrium with the field and thus predicts the highest ionization at the highest fields adjacent to the cathode. Thus the cathode fall voltage required to produce sufficient ionization for the discharge maintenance condition (equation II-1) is lower for the equilibrium model than for the nonequilibrium model.

The Townsend attachment coefficient for each model is similarly plotted in Fig V-5 along with the electric field calculated by the SHEATH model. These coefficients were calculated for the given electric field using the equations in Table V-1. Again the plots for these coefficients are not the same shape due to the nonequilibrium electron behavior in the cathode fall. The electrons close to the cathode have

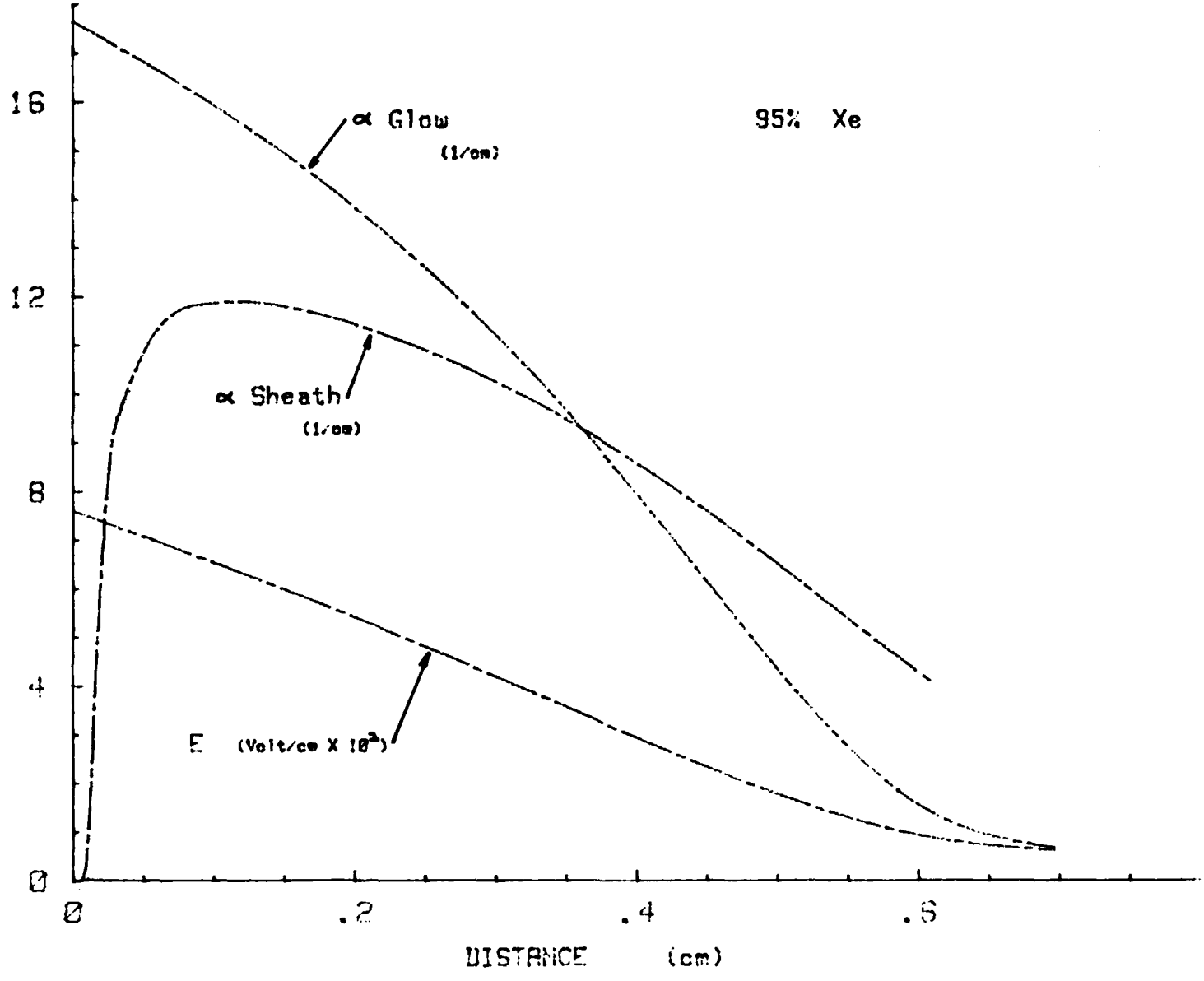

FIG V-4 COMPARISON OF IONIZATION COEFFICIENTS

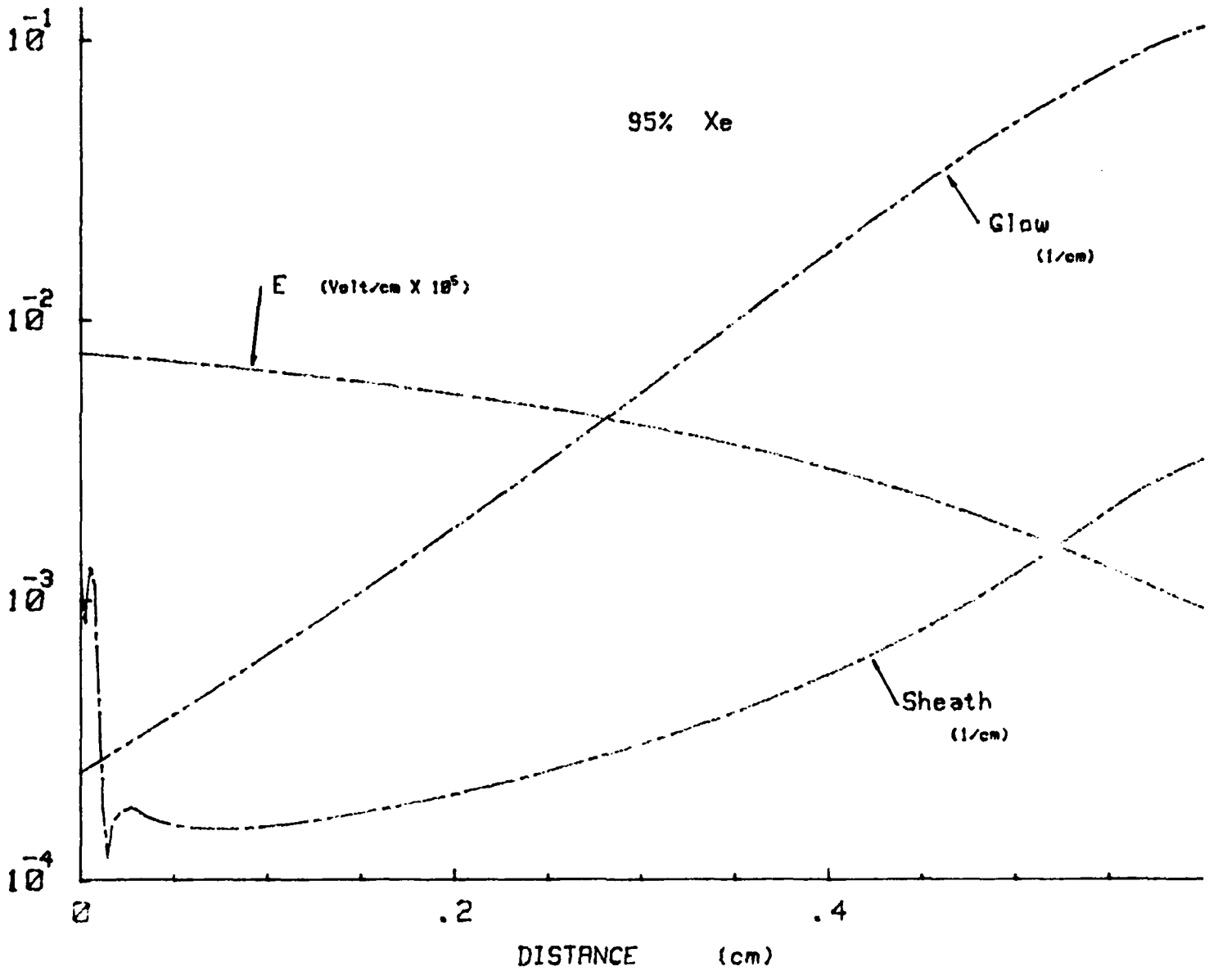

FIG V-5 COMPARISON OF ATTACHMENT COEFFICIENTS

a low energy and undergo several collisions before reaching the ionization energy of the gas. This results in a large peak in the attachment coefficient close to the cathode in the results predicted by the SHEATH model. The Townsend attachment coefficient predicted by the SHEATH model actually leads the field, i.e. the rate is high where the field is highest and then undershoots and rises again where the minimum field merges into the negative glow. Note that the attachment coefficient predicted by the nonequilibrium model is more than an order of magnitude smaller than that predicted by the equilibrium model except immediately in front of the cathode. Thus the ionization and attachment coefficients predicted by the equilibrium model do not represent the actual spatial distribution of the coefficients predicted by the SHEATH model.

The growth of the electron current density is portrayed for each of the rare gases in Fig V-6 through V-8. The GLOW model consistently predicts a faster rising electron current. This difference is again a result of the nonequilibrium behavior of the electrons close to the cathode. The electrons first have to be accelerated to the ionization potential of the gas before they can begin to multiply. This causes the electron current density predicted by the SHEATH model to lag the current density predicted by the GLOW model. To make the equilibrium model agree more closely with the nonequilibrium model, Tran Ngoc, et al. (ref 86) have suggested that the mean electron energy and the Townsend ionization coefficient be related through an energy balance equation. This yielded good agreement with their nonequilibrium ionization coefficient calculated by a Monte Carlo technique. Similarly, relating the Townsend ionization coefficient to the mean

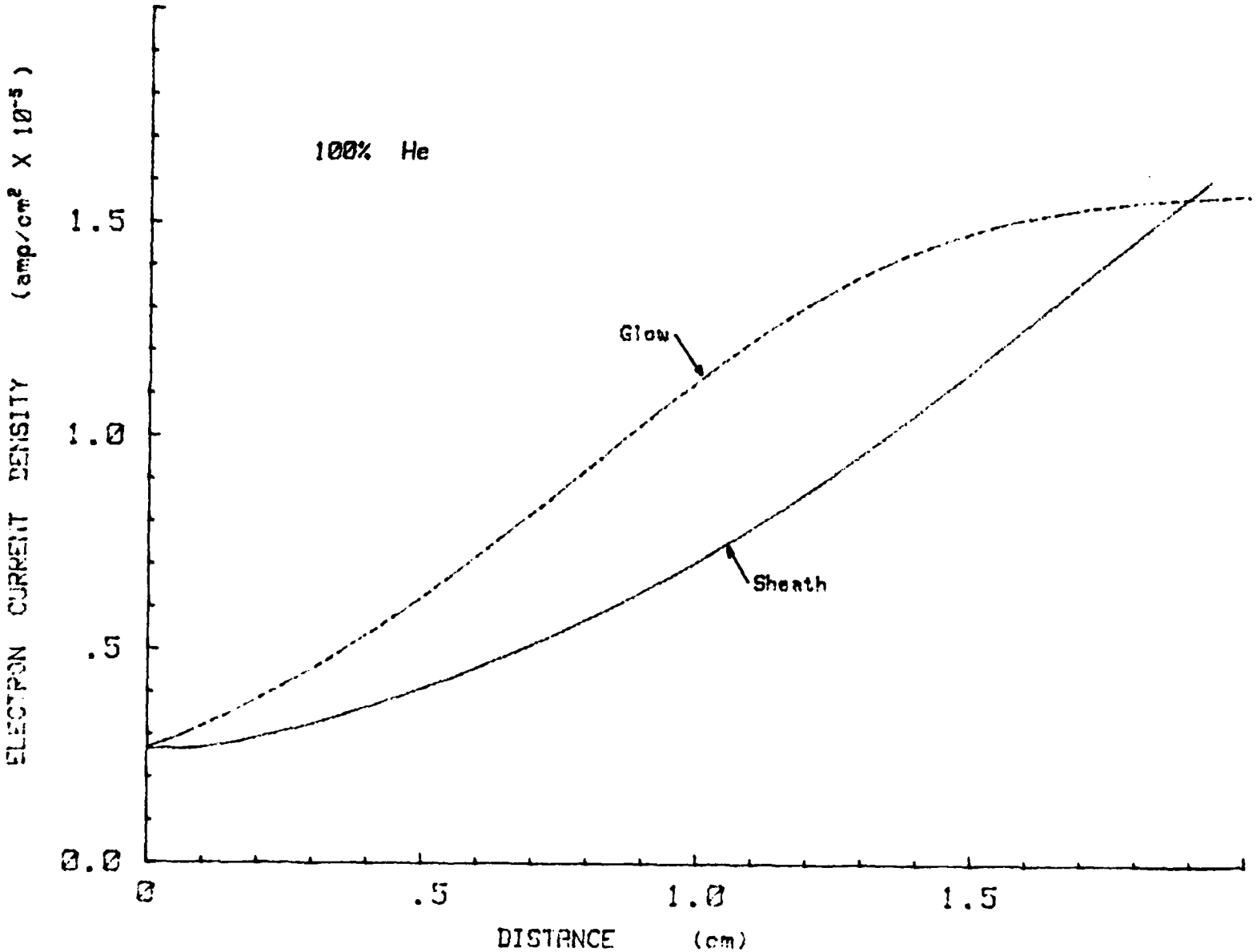

FIG V-6 COMPARISON OF ELECTRON CURRENT DENSITIES IN 100% He FROM GLOW AND SHEATH METHODS

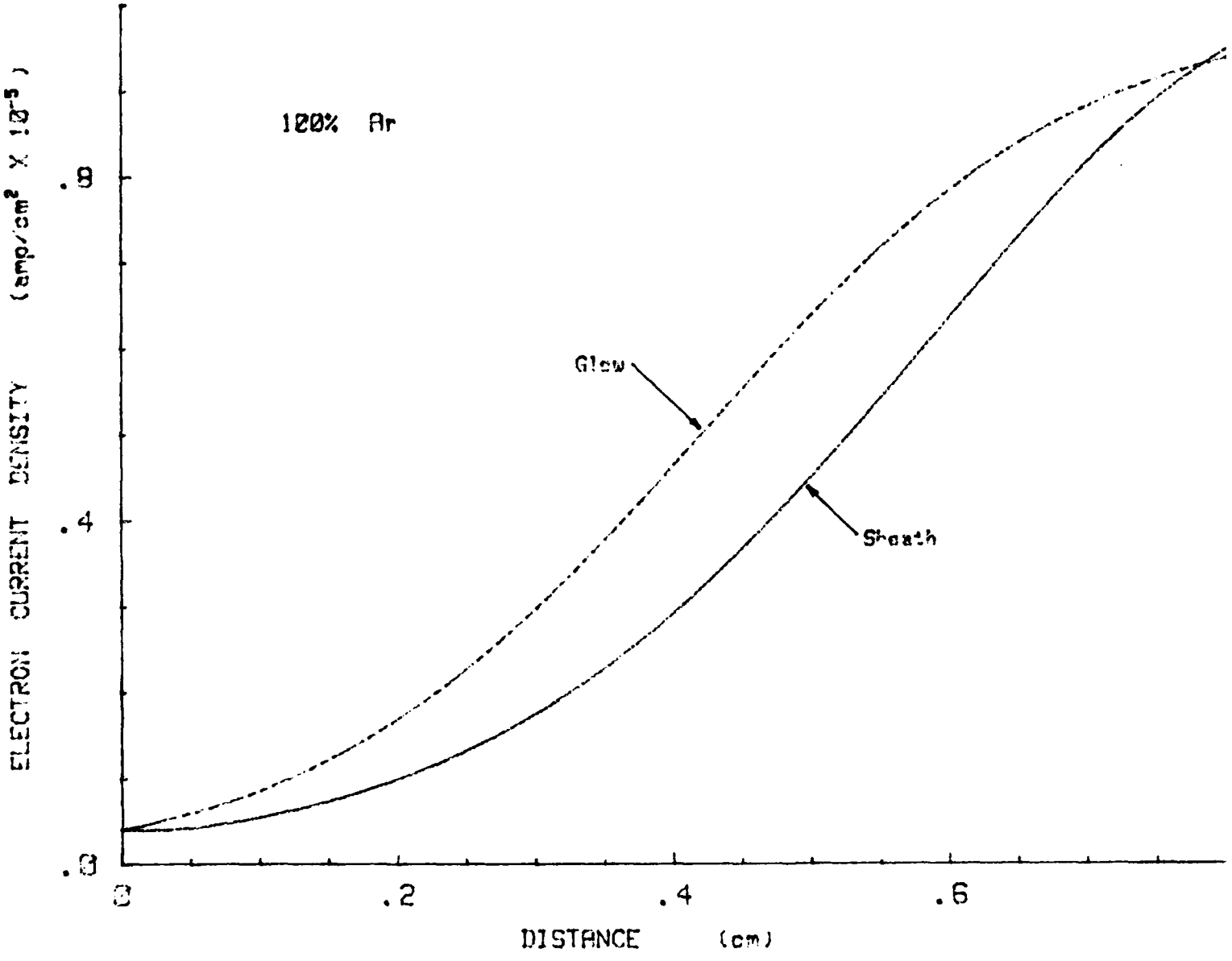

FIG V-7 COMPARISON OF ELECTRON CURRENT DENSITIES IN 100% Ar FROM GLOW AND SHEATH METHODS

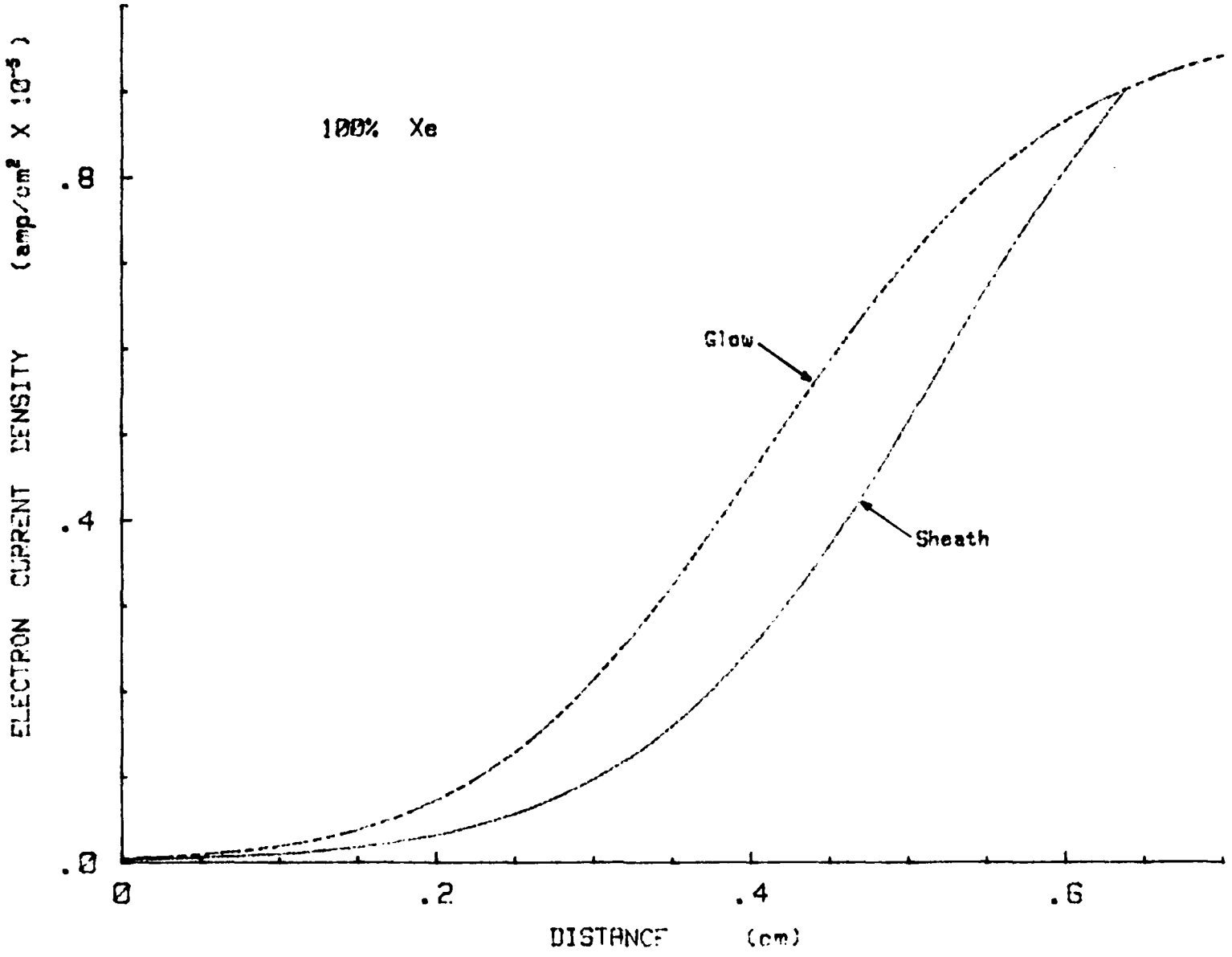

FIG V-8 COMPARISON OF ELECTRON CURRENT DENSITIES IN 100% Xe FROM GLOW AND SHEATH METHODS

electron energy should also predict a slower rising electron current density more closely approximating the nonequilibrium results.

Another example of the inability of the equilibrium model to describe the nonequilibrium behavior in the cathode fall region is shown in the plots of the charged particle densities in Fig V-9 through V-11. There is good agreement between the methods on the positive ion density near the cathode. The GLOW results agree within 13% for He, 6% for Ar, and 5% for Xe of the positive ion density predicted by the SHEATH model at the cathode. This agreement in positive ion density results in the electric fields being almost parallel in Fig V-1 through V-3. However, not as good agreement is obtained as the cathode fall transitions into the negative glow region. This is due to the different rates of growth of the electron density. The GLOW method consistently predicts an electron density that is higher than the SHEATH method even close to the cathode. At the cathode where the electron current densities agree for both methods, the electron density calculated by the GLOW method is larger than the SHEATH results because the electron drift velocity calculated by the GLOW model is lower than that calculated from the distribution function in the SHEATH model. The difference between the electron number densities calculated by the GLOW and SHEATH models does not affect the slope of the field until near the negative glow region because the electron density is 3-4 orders of magnitude less than the positive ion density. Thus the equilibrium theory is not capable of describing the particle densities as a function of distance through the cathode fall region. Through adjustment of boundary conditions such as the secondary emission coefficient and the electron drift velocity at the cathode better

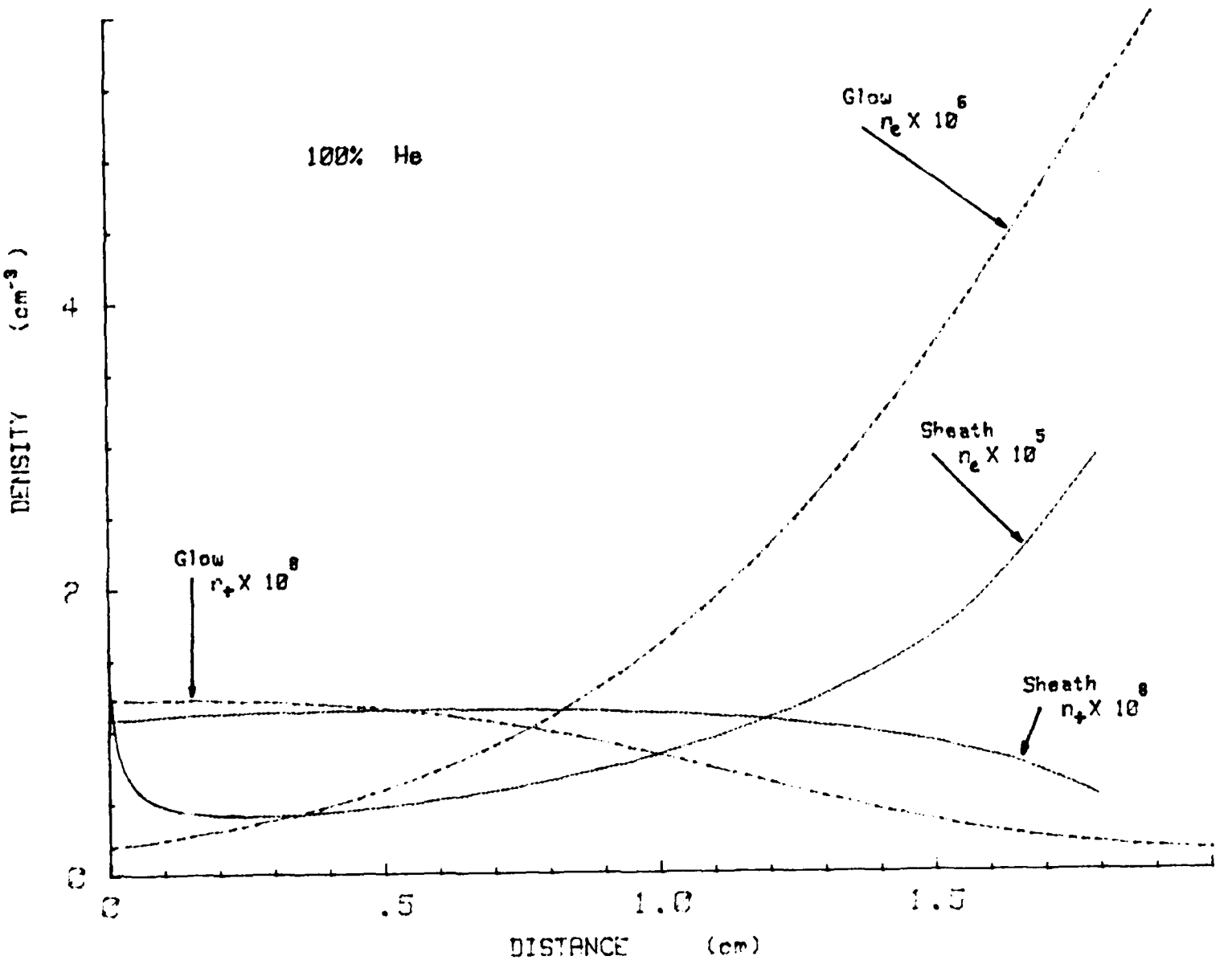

FIG V-9 COMPARISON OF POSITIVE ION AND ELECTRON DENSITIES IN 100% He FROM GLOW AND SHEATH METHODS

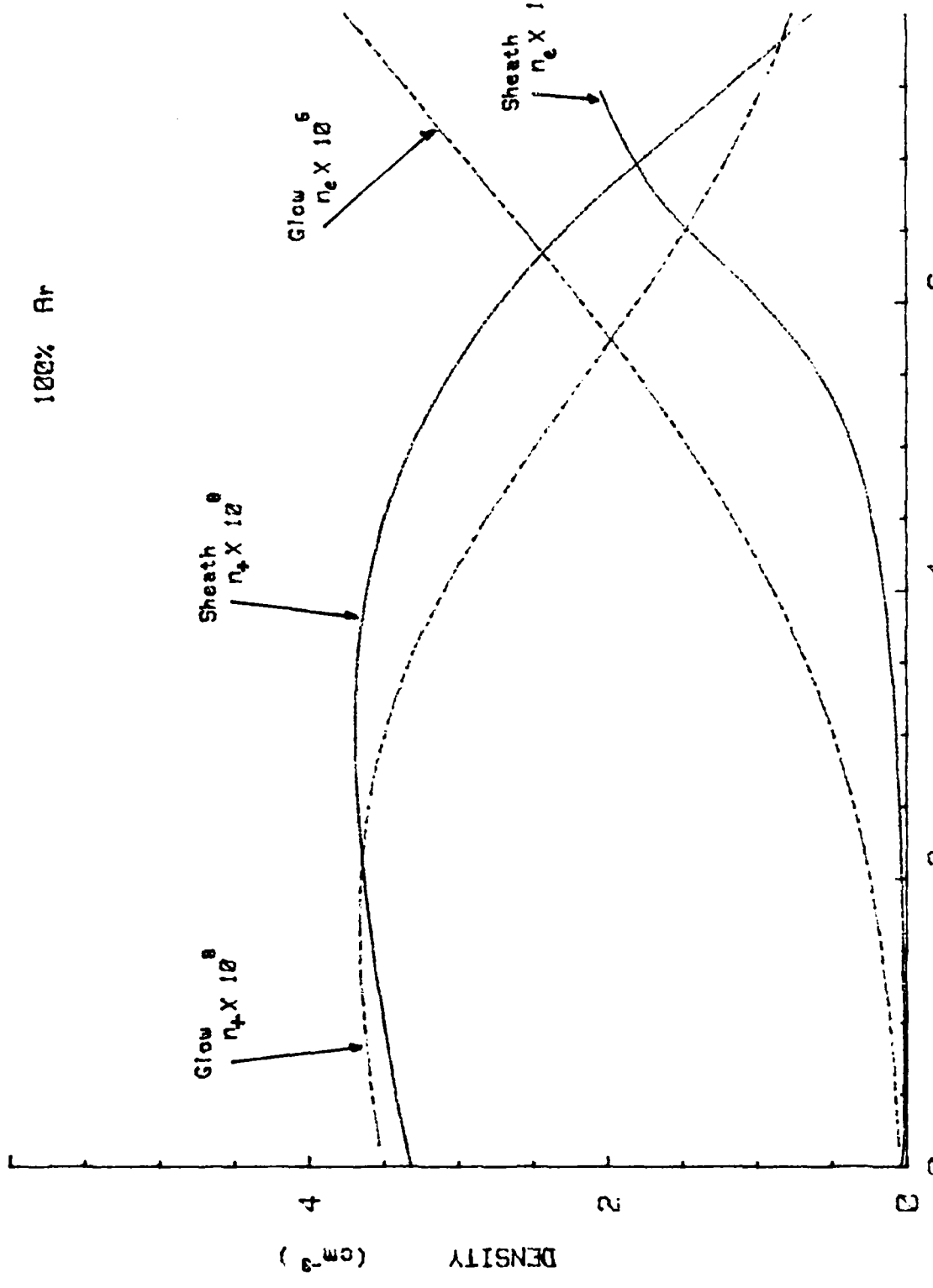

FIG V-10 COMPARISON OF POSITIVE ION AND ELECTRON DENSITIES IN 100% Ar FROM GLOW AND SHEATH METHODS

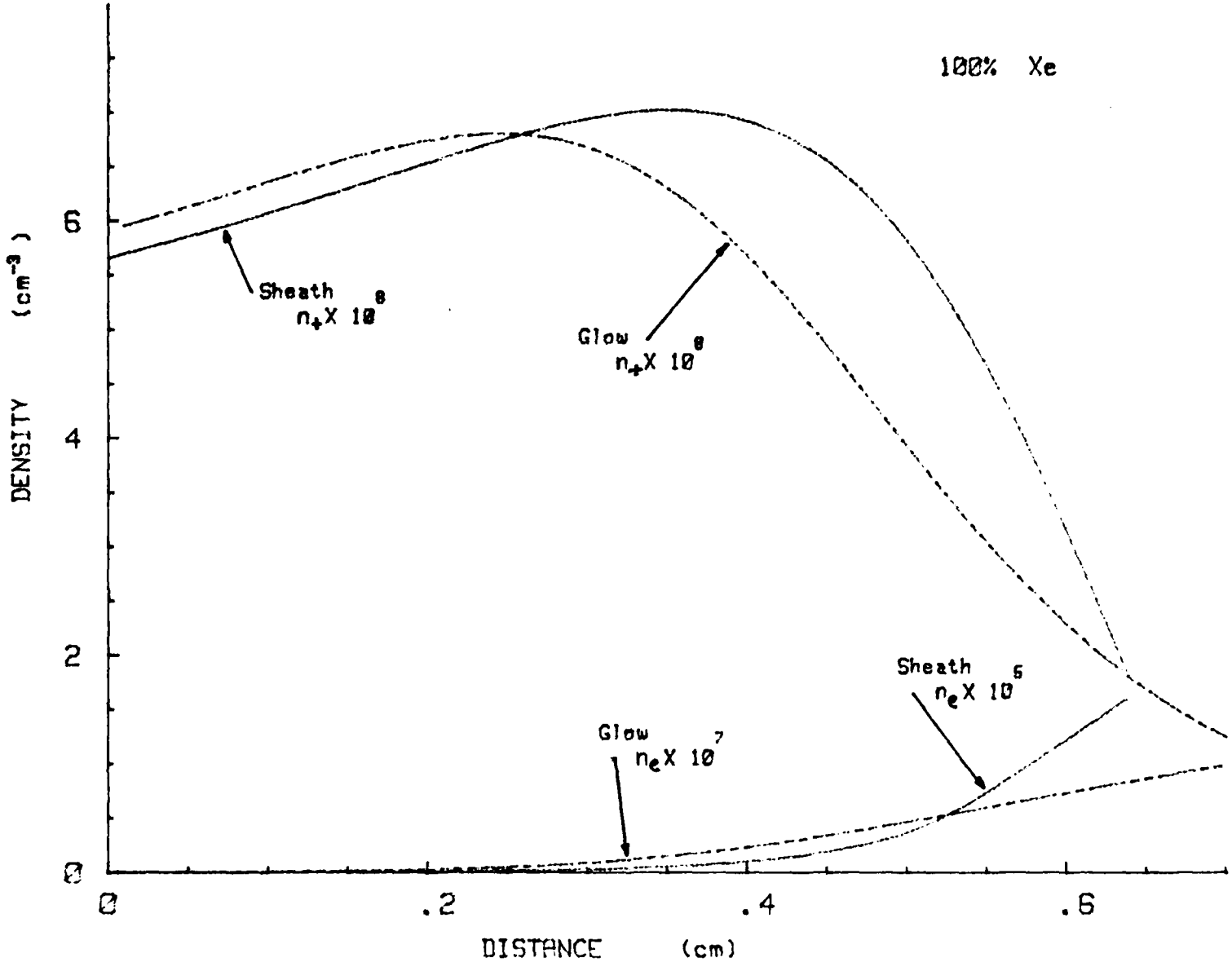

FIG V-11 COMPARISON OF POSITIVE ION AND ELECTRON DENSITIES IN 100% Xe FROM GLOW AND SHEATH METHODS

agreement with experimental results could probably be obtained, but it would still not represent the actual nonequilibrium kinetics involved there.

The macroscopic parameters such as discharge current, cathode fall voltage and length, and electric field each contain one or more averages or integrals over the electron distribution function. It was thought that these integrals might tend to dilute the effects of nonequilibrium on these macroscopic parameters. Thus good agreement on these macroscopic parameters should be expected between the GLOW and SHEATH models. This was found <u>not</u> to be the case. Table V-2 summarizes these macroscopic parameters for the GLOW and SHEATH models. The voltage and thus the electric field at the cathode are determined by the <u>net</u> multiplication of the electrons as they cross the cathode fall. For an electronegative gas, equation II-2 for the multiplication of the electrons becomes

$$M = \exp \int_0^d (\alpha(x) - \eta(x))\, dx \qquad \text{(V-1)}$$

From the results of the nonequilibrium analysis in Chapter IV, the attachment coefficient is always much smaller than the ionization coefficient except immediately in front of the cathode. The attachment rate for the cases examined was only a small perturbation on M in equation V-1. This also agrees with the results presented for Xe/HCl mixtures where the ionization coefficient effectively did not change as a function of gas mixture.

Returning to Fig V-4, the area under the ionization curves are different for the GLOW and SHEATH models. The GLOW model assumed the

TABLE V-2

Summary of Macroscopic Parameters from the GLOW and SHEATH Models

Gas Mixture	Model	E_o/p volt/cm-torr	E_{min}/p volt/cm-torr	pd_c torr-cm	J/p^2 μamp/cm^2-torr^2	V_c volt	$SF(\gamma, k_+)$ $X10^{-9}$ amp torr$^{\frac{1}{2}}$ cm$^{\frac{1}{2}}$ / volt$^{\frac{1}{2}}$
He/HCl							
100/0	GLOW	274.3	5.4	1.26	16.	183.4	11.48
	SHEATH	353.0	8.1	1.73	16.	309.4	11.57
99/1	GLOW	272.5	5.7	1.25	16.	180.8	11.49
	SHEATH	338.0	8.1	1.62	16.	277.4	11.57
95/5	GLOW	265.8	6.7	1.21	16.	171.7	11.45
	SHEATH	301.0	17.5	1.37	16.	209.0	11.63
Ar/HCl							
100/0	GLOW	427.4	14.5	.656	10.	147.8	1.94
	SHEATH	480.0	37.7	.75	10.	183.8	1.95
99/1	GLOW	427.4	15.0	.657	10.	147.9	1.95
	SHEATH	480.0	31.6	.75	10.	183.8	1.95
95/5	GLOW	427.5	16.2	.657	10.	148.1	1.94
	SHEATH	481.0	42.8	.76	10.	186.8	1.97
Xe/HCl							
100/0	GLOW	690.7	33.3	.592	10.	212.0	.874
	SHEATH	756.0	60.2	.665	10.	252.2	.900
99/1	GLOW	693.6	33.8	.594	10.	213.2	.873
	SHEATH	758.0	66.4	.668	10.	254.4	.899
95/5	GLOW	695.3	34.5	.598	10.	215.9	.872
	SHEATH	760.0	61.8	.671	10.	256.2	.899

electrons were in equilibrium with the field and results in the electrons being able to ionize immediately upon leaving the cathode. The SHEATH model allows the electrons to not be in equilibrium with the field. As a result, several electron collisions occur before the majority of the electrons have attained the energy necessary for ionization of the gas. Thus the nonequilibrium model predicts a higher cathode fall voltage than the equilibrium model in order to maintain the same net multiplication.

Analyzing this through the mathematical relationships, the slope of the electric field is determined by the mobility (k_+) of the positive ions through Poisson's equation. This is because the positive ion current density at the cathode is determined by the boundary conditions at the cathode involving the secondary emission coefficient and the total discharge current density. The length of the cathode fall is determined when the multiplication of the electrons is sufficient to maintain the discharge and equals $1 + 1/\gamma$ (equation II-1). The slope of the electric field and its extrapolated x-axis intercept (d_c) then determines the voltage for the cathode fall. Thus the difference in the macroscopic parameters in Table V-2 is a result of the nonequilibrium character of the electrons which alters the ionization coefficients from those predicted by the equilibrium (GLOW) model. Thus any agreement of the equilibrium method with experiment is entirely fortuitous as von Engel suggested (ref 89:224).

The scaling factor $SF(\gamma,k_+)$ listed in Table V-2 should be identical for both the SHEATH and GLOW models since they both used the same secondary emission coefficient and same field relationship for the positive ion drift velocity. The slight differences in the data between

the models are primarily due to extrapolation errors in determining d_c and to round off errors in d_c and V_c.

Although the inability of the GLOW model to describe nonequilibrium effects accounts for most of the disagreement in the preceding figures and in Table V-2, another factor affecting the agreement of the two methods is the use of two different data bases. The GLOW model bases its electron kinetics on curve fits of empirical data for the Townsend ionization and attachment coefficients. These coefficients are normally derived from drift tube experiments where a swarm of electrons drift between two electrodes and are in equilibrium with the field. The SHEATH model on the other hand bases its electron kinetics on scattering cross sections. Under ideal conditions both determinations of α, either from drift tube experiments or cross sections, should be consistent. Some attempt was made in Appendix C to correlate the sets of cross sections used, with measured transport properties using an equilibrium Boltzmann code. It was impossible, however, to correlate them over the whole range, since transport data was lacking at some high E/p's. In addition the equilibrium Boltzmann code was limited to calculations at low and medium fields because it did not include the newly created secondary electrons in the distribution function. Thus the data bases for E/p's less than about 160v/cm-torr differed less than 20% but for higher E/p values the difference could be more.

In summary, both the SHEATH and GLOW models predicted the same trends in He/HCl, Ar/HCl, and Xe/HCl mixtures and both models scale according to equation III-71. However, the discussion in this chapter has shown that the GLOW model should not be used to describe <u>any</u> of the

cathode fall parameters. In the cathode fall region, the electrons have been shown not to be in equilibrium with the field. As a result, the cathode fall voltage and length are larger in the SHEATH model than the GLOW model in order to compensate for the nonionizing region (Primary Dark Space) near the cathode where the electrons are being accelerated up to the ionization energy of the gas.

This investigation of the cathode fall region sets the stage for further investigations of the negative glow. Due to the slightly bimodal character of the electron distribution function at the cathode fall-negative glow boundary found in the SHEATH results, a nonequilibrium technique should also be used to investigate the negative glow. In this region, a small number of electrons, that have managed to traverse the cathode fall with one or no collisions, lose their energy in the negative glow forming new electrons and positive ions through ionization. In essence, the electron distribution function is still changing faster in coordinate space than it is in velocity space.

Anode Fall Region

This section discusses the applicability of both methods to the sheath region at the opposite end of the discharge near the anode. In the GLOW model calculations the anode was placed after a chosen length of positive column. However, due to a limitation of memory space the anode for the SHEATH cases was placed in the negative glow. This corresponds to an "obstructed discharge" (ref 6). The properties of the anode are very different when it is placed in a slightly negatively charged region such as the Faraday dark space as compared to being in contact with a neutral plasma such as the positive column. These prop-

erties are discussed further below.

The boundary conditions for the anode fall are fairly simple in the more usual case when the anode fall and positive column are adjacent. Sufficient electrons must be accelerated across the anode fall and create sufficient ionization such that the number of positive ions crossing the anode fall-positive column boundary is equal to the number crossing the positive column-Faraday dark space boundary.

It is commonly believed that each electron entering the anode fall must be accelerated to the ionization potential of the gas. Each electron has to create an ion before striking the anode in order to maintain charge neutrality in the positive column. It was found experimentally (data is summarized in ref 1 and 6) that the anode fall voltage was usually about the same magnitude as the ionization potential, except in electronegative gases. However, it is also known that the electrons in the positive column have an equilibrium distribution of energy, with a few having an energy greater than the energy equivalent to the ionization potential. Thus the potential is different for each electron to be accelerated to the ionization potential of the gas. In addition, charge neutrality and uniform density in the positive column are maintained by requiring that an ion enter the Faraday dark space each time one enters the positive column from the anode region. Similarly an electron is required to enter the positive column from the Faraday dark space each time one leaves the positive column and enters the anode fall region. Using these hypotheses, it is not necessary under ideal conditions for the anode fall voltage to always be equal to or slightly larger than the ionization potential.

The anode acts likes a probe collecting the random positive and

negative currents from the positive column and so its area is also very important. If the anode area is so small that the negative random current is less than that required by the external circuit, then a region of space charge forms to pull more negative charges from the positive column and make the collecting area of the anode larger. This requires a potential on the order of the ionization potential or less, since a potential much larger than the ionization potential would tend to create numerous electron-ion pairs reducing the effectiveness of the sheath. Anode fall voltages smaller than the ionization potential have been observed (ref 6) using large concave anodes. This type of anode reduces the losses to diffusion and enables more negative charges to be collected from the positive column.

The boundary conditions for the anode fall are more complicated when the anode is in the Faraday dark space. Near the negative glow boundary there may be sufficient fast electrons from the cathode fall to carry most of the discharge current. These electrons are already of sufficient energy that little or no acceleration is required for ionization to produce positive ions. In this case no anode fall exists and the field remains almost constant right up to the anode. As the electrode separation is increased, the anode fall region must of course eventually transition into the normal type previously described. Francis (ref 6) claims a normal anode fall develops suddenly at a critical distance from the cathode lying near where the Faraday dark space-positive column boundary would normally occur. This critical distance should be approximately equal to the stopping distance in a gas for an electron with an energy approximately equal to the cathode fall voltage.

Other factors described by Francis (ref 6) which affect the voltage across the anode fall are:

a) stepwise ionization. Stepwise ionization results in a smaller voltage since the electrons do not have to be accelerated to the full ionization potential in order to create an ion.

b) the electron current density. This is closely related to the anode geometry. Increasing the current density beyond what the anode can normally carry is tantamount to decreasing the anode area and hence increases the anode voltage. At high currents, regularly spaced spots form on the anode which are regions of high conductivity.

c) electronegative gases. Adding an electronegative gas to an electropositive gas may or may not cause the anode voltage to increase for the same reasons the cathode fall may or may not contract as discussed in previous chapters. The potential drop across the anode would depend upon the partial pressure averaged ionization potential of the gas mixture in addition to the loss of electrons to negative ion formation. Generally, a high coefficient of electron attachment greatly reduces the ionization efficiency. For example, anode fall voltages in the halogens have been observed to be several times the ionization potential.

d) artificially produced space charge. Specially coated anodes which yield positive ions upon electron impact obviously have smaller anode voltage. If the number of positive ions is more than that required for the flux entering the positive column, the fall can be negative.

e) proximity of side walls. Changing the distance of the side walls can change the rate of diffusion and radial fields which can

result in increasing or decreasing the anode fall voltage.

The anode fall in the GLOW code calculations was adjacent to a positive column region. The anode fall voltage in Fig III-3, III-7, and III-11 were in the range of 1-3v. These values were determined to be the difference in voltage at the anode and at the minimum electric field. This is much smaller than the normal anode fall voltage which is on the order of the ionization potential of the gas. The use of Ward's formula for the drift velocity (ref 92) could lead to a more correct anode fall voltage. Since the electric field near the cathode fall-positive column boundary is less, when Ward's formula is used, this would also result in a smaller electron current density entering the positive column. A broader anode fall region would then be required for the electron current density to reach the total discharge current limit. So even though the electric field gradient would also be less in the anode fall region, the fact that it would be over a longer distance could increase the anode fall voltage.

The anode in the SHEATH calculations was placed in the region of the negative glow. Any correlation in the data close to the anode is indeterminant due to the changing location of the anode in the negative glow region. This occurred because the cathode fall width changed while the electrode separation was held constant for each rare gas mixture.

In addition, the SHEATH code changes from constant energy bins to constant spatial bins very near or at the minimum in the electric field. At present, this change of variable is not smooth for all parameters calculated by the code, so any predictions by the SHEATH method on the anode fall will be held in reservation. Thus in their

present configuration, neither code properly describes a normal anode fall region.

In order for the SHEATH model to be able to correctly describe a normal anode fall, several new modifications would have to be made. The model could be changed to reflect the boundary conditions at the anode instead of the cathode, so that the calculation started at the anode and proceded towards the positive column.

$$J_+(d) = 0 \qquad \text{(V-2a)}$$

$$J_e(d) + J_-(d) = J \qquad \text{(V-2b)}$$

This also requires that E (d), j_-(d), and the electron distribution striking the anode be known. Potential problems with the point at which the code changes from equal energy increments to spatial increments could also occur again, since the energy gained in a mean free path is much less in the anode fall. Similarly there would be potential problems with greater than or less than statements when the sign convention was changed from x to -x.

If a new computer system is installed which has 2-3 times larger accessible memory space, it would also be feasible to expand the array so that discharges with larger electrode separations could be modeled. This is perhaps the easiest solution to modeling the anode fall using the SHEATH code.

Chapter VI. Conclusions and Some Considerations for Future Study

Conclusions

In the present study, two very different methods of analyzing glow discharges (GLOW and SHEATH) were developed and applied to three different cases represented by He/HCl, Ar/HCl, and Xe/HCl mixtures. Even though the two methods did use different input data bases founded on the prior work of different authors using different experimental approaches, the results of the two methods had the same trends and both models scaled according to equation III-71. The following conclusions are based on the results presented in Chapters III, IV, and the comparison of the models in Chapter V:

a) Electrons were found not to be in equilibrium with the electric field throughout the cathode fall region. Close to the cathode, the whole distribution is accelerated up to an energy equal to the ionization potential. This predominantly dark region is called the Primary dark space. Next the electron distribution function becomes bimodal as some of the electrons lose their energy to ionization and excitation. This luminous region is called the cathode glow. In this region, the majority of the electrons have a mean energy greater than the ionization energy. As more and more of the electrons lose energy to inelastic processes, the cathode glow merges into a relatively darker region called the cathode dark space. The energy difference between the decreasing number of fast and the increasing number of slow electrons gets larger as the fast electrons continue to be accelerated by the linearly decreasing electric field. As the electric field be-

comes very small and almost constant in the negative glow, the remaining fast electrons resemble an electron beam. They deposit their energy in the gas creating many highly excited species which cascade down and produce the bright luminescence characteristic of the negative glow region. As a result of this nonequilibrium, the GLOW or equilibrium model was found in Chapter V to be inadequate in describing both the microscopic parameters such as charged particle densities and ionization and attachment coefficients as well as macroscopic parameters such as cathode fall voltage, cathode fall length, electron current density and electric field. A model which allows the electrons to not be in equilibrium with the electric field such as the SHEATH model or Monte Carlo technique must be used to describe the parameters in the cathode fall region. The negative glow region should also be modeled by a technique which allows nonequilibrium. The model for the negative glow however could be simplified by separating the electron distribution function into a low energy component and a high energy component.

b) Better agreement between theory and experiment can be obtained for pure gases by a judicious choice of γ and k_+. Equation III-71 can be used to related γ and k_+ to experimental cathode fall voltage, currents, and cathode fall widths. These values of γ and k_+ should then be used as inputs in the SHEATH model since the SHEATH model was shown in Chapter IV to obey the scaling relationship given by equation III-72.

c) The slope of the electric field in the cathode fall is determined by the positive ion density. If Poisson's equation is written in terms of the ratios of the charged particle current density and drift velocity, then the slope of the field close to the cathode is deter-

mined by the mobility (k_+) of the positive ions. The positive ion current density is constant close to the cathode and is determined by the total discharge current density and γ. The length of the cathode fall is determined by the maintenance condition for the discharge involving the multiplication of electrons through the cathode fall (equations II-1 and V-1). The slope of the electric field and its extrapolated x-axis intercept (d_c) then determines the voltage drop across the cathode fall region.

d) The formation of small amounts ($n_- < n_e$) of negative ions in the cathode fall region was found not to be the reason that the cathode sheath length contracts in the axial direction. Actually, the formation of negative ions causes the cathode fall voltage to increase slightly which in turn results in a slight increase in the cathode fall length. These trends could be seen in the results of both the equilibrium and nonequilibrium analyses in Chapters III and IV.

e) When an attaching gas which has a low ionization potential is added to He or Ne, the observed contraction of the cathode fall length was found to be due to an increase in ionization in this region. This increase in ionization is a result of the lowering of the ionization threshold and the difference in cross section shape for the two gases in the mixture.

f) The SHEATH method which allowed the electrons to not be in equilibrium with the field predicted a Townsend attachment coefficient which contained a peak at the cathode, reached a minimum at the region where the electron mean energy and Townsend ionization peaked and then grew again as the field as well as the electron mean energy decreased. Thus the cathode fall in an electronegative gas mixture was found to be

characterized by a thin region close to the cathode in which attachment dominated, followed by a region in which ionization of HCl dominated the ionization of He or Ar but not Xe, before uniform ionization of the mixture began.

Although this analysis was mainly concerned with modeling phenomena in the cathode fall region, the conclusions d and e above could also be applied to the anode fall region. In contrast to the cathode fall region, the negative charge density is much larger than the positive charge density in the anode fall region. Thus the width of the anode fall would depend on how fast the electrons are accelerated to the ionization potential. Thus the relationship of the electron drift velocity to the field is more important in this region.

Theoretical Considerations for Future Study

In the course of this study several areas can be identified which warrant further theoretical investigation:

a) Since ionization of HCl caused the cathode fall to contract in He, further study of the effects resulting from changing the ionization cross-section would be of value. Both changes in the threshold and initial slope of the cross section should be examined to see which affects changes in the cathode sheath structure the most.

b) A parameter mapping of the secondary emission coefficient and positive ion mobility (k_+) is recommended. This has not been investigated using nonequilibrium techniques.

c) Using the present results from the cathode fall as inputs, the nonequilibrium method could be used to investigate the negative glow-Faraday dark space region provided the field does not go negative.

d) The linear analysis presented in this study can be expanded to describe the kinetics in different electrode geometries represented by thyratrons, plasma reactors for depositing thin films, or hollow cathode discharges.

e) The results of this study can also be applied to understanding the field variations and charged particle kinetics in striations. Different boundary conditions would be required for striations. The charged particle densities on each side of the striation would replace the boundary conditions on the current densities at the electrodes.

f) Hot cathodes could be modeled using either the GLOW or SHEATH techniques. Because the accelerating voltage is less in the cathode fall, there should be a smaller degree of nonequilibrium. Thus the GLOW model should give much better agreement in this case. In addition, the boundary condition at the cathode relating the positive ion to the electron current density would have to be replaced by a single source of electrons.

g) Due to limited computer storage space, the only electron collision processes calculated as functions of distance were the ionization and attachment coefficients. Further investigation of the other excitation coefficients and coefficients for vibrational excitation would be useful to complete the understanding of the cathode fall region.

h) Operation of the SHEATH code would be much more efficient as well as convenient if a numerical technique were added to converge to the lowest value of E_0 for which a complete solution exists, before the field is iterated for consistency with the electron distribution function. This technique could be similar to the modified interpolation

technique which was used in the GLOW code.

i) More detailed ion kinetics options would make the SHEATH model more universal. Electron-ion, and ion-ion recombination, detachment, and two step ionization could be added such that the ion or metastable densities could be updated after each calculation of the electron distribution function for a self-consistent solution. Recombination and detachment will be more important in the negative glow and Faraday dark space. These processes can not be incorporated in the present GLOW model because they are nonlinear with respect to j_e.

j) Cathodes can be coated with special films which emit negative ions. Further investigation of the effect of a cathode as a source of negative ions on the cathode fall voltage and width would be interesting. A further increase in voltage and perhaps width of the cathode fall should be anticipated according to the theory in Chapter III if negative ions are released at the expense of electrons.

Experimental Considerations for Future Study

Several experimental topics have also been identified in the course of this study which warrant further investigation. At present the first two topics are being pursued.

a) No experimental evidence could be found for the non-contraction of the cathode fall in mixtures of Ar or Xe with HCl or any other attaching gas. A small discharge tube is presently under construction in the Plasma Physics Group (AFWAL/POOC-3) which will allow confirmation of this phenomenon. A mass spectrometer will be used to monitor any change in the neutral particle chemistry.

b) It is now possible to consider measuring the electric field as

a function of distance through the cathode fall region. Some potential techniques are non-perturbing Doppler-free laser polarization, Doppler-free spectroscopy, or Stark induced mixing of different parity levels in an excited molecular electronic state.

c) The energy distribution of the electrons could be measured in an obstructed discharge by sampling the electrons through a small hole in the anode. These results could then be compared with theory.

d) Similarly the energy distribution of the positive ions could be sampled through a small hole in the cathode. Both major and minor ions should be sampled because of the differences in charge exchange cross sections. By knowing their energy and charge transfer rates, their origin in the cathode fall or negative glow could be determined and checked with theory.

e) Laser induced fluorescence could be used to search for fast neutral molecules which would be an indication that charge transfer has occurred. This technique would compliment those described in c and d above and could be accomplished simultaneously.

It is hoped that this study has provided a better understanding of the cathode fall and the influence of negative ions in this region. The generic results of this study can be applied to excimer lasers, thyratrons, or plasma reactors for the deposition of thin films. As a final guideline, it is just as important to understand the positive ion kinetics in the cathode sheath region as it is to understand the electron kinetics, because it is the ion mobility which determines the slope of the electric field.

BIBLIOGRAPHY

GENERAL REFERENCES

1. Brown, S. C., Basic Data of Plasma Physics Cambridge: Technology Press of the Massachusetts Institute of Technology (1959)

2. Cobine, J., Gaseous Conductors: Theory and Engineering Applications, New York: Dover Publications, Inc. (1958)

3. Emeleus, K. G., "Anode Glows in Glow Discharges, Outstanding Problems" Article preprint

4. Emeleus, K.G., "The Negative End of Cold Cathode Glow Discharges" Journal of Physics D: Applied Physics, 14:2179 - 87 (1981)

5. Emeleus, K. G. and G. A. Woolsey, Discharge in Electronegative Gases, London, Taylor and Francis (1970)

6. Francis, G., "The Glow Discharge at Low Pressure", Encyclopedia of Physics XXII, ed. by S. Flugge, Berlin: Springer-Verlag, p. 153-208 (1956)

7. Ingold, "Anatomy of the Discharge" Chapter 2 of Gaseous Electronics, Vol 1 ed by M. N. Hirsh, and H. J. Oskam, New York: Academic Press (1978)

8. Massey, H. S. W., Negative Ions, London: Cambridge University Press, 3rd ed. (1976)

Specific References

9. Abramowitz, M. and I. A. Stegun, Handbook of Mathematical Functions New York: Dover Publications Inc (1965)

10. Ahlsmann, G. "Some Remarks on the Anode Fall in the Faraday Dark Space". Proceedings of the Fifth International Conference on Ionization Phenomena in Gases" Vol I , ed. by H. Maecker, Munich, pp 306-14, 1961.

11. Aleskovskii, A., "Kinetic Theory of the Negative Low" Soviet Physics - Technical Physics 17:1458-62 (March 1973)

12. Allan, M. and S. F. Wong. "Effect of Vibrational and Rotational Excitation on Dissociative Attachment in Hydrogen", Physical Review Letters 41:1791-4 (December 1978)

13. Allis, W. P., "E'tude d'une De'charge a Haute Pression Ionise'e par un Faiscear d'Electrons a Haute Energie.", Revue de Physique Applque'e 10:97 (May 1975)

14. Allis, W. P., G. Fournier and D. Pigache, "Théorie Microsopique de la Chute Cathodique en Régime Luminescent" Journal de Physique, 38:915-20 (1977)

15. Arfken, G. Mathematical Methods for Physicists, 2nd ed, New York: Academic Press (1970)

16. Azria R., L. Roussier, R. Paineau, and M. Tronc "Attachment Electronique Dissociatif sur HCl et DCl" Revue de Physique Applique'e 9:469-473 (1974)

17. Bardsley, J. N. and J. M. Wadehra "Dissociative Attachment and Vibrational Excitation in Low Energy Collisions of Electrons with H_2 and D_2" Physical Review A 20:1398-1405 (October 1979)

18. Barkalou, A. and G. Gladush "Near - Electrode Phenomena in Discharge in Electronegative Gases and Their Effect on the Development of Domain Instability" Heat Physics of High Temperatures, (Translated from Teplofizika Vysokikh Temperatur, #3, 1981 by the Foreign Technology Division WPAFB), FTD-ID (RS) T-0743-82

19. Biondi, M. A. and R. E. Fox, "Dissociative Attachment of Electrons in Iodine. III Discussion" Physical Review 109:2012-4 (March 1958)

20. Boeuf, J. P. and E. Marode "A Monte Carlo Analysis of an Electron Swarm in a Nonequilibrium Field: The Cathode Region of a Glow Discharge in Helium" Journal of Physics D: Applied Physics, 15:2169-2187 (1982).

21. Boeuf, J. P., E. Marode, P. Segur, A. J. Davies, and J. G. Evans "Electron and Ion Behavior in the Cathode Region of a Discharge Studied by Monte Carlo Techniques "Proceedings of the 6th International Conference on Gas Discharges, Edinburgh, IEE Conference Publication 189, 2:63-66 (1980).

22. Buchel'nikova, I.S. "Cross Sections for the Capture of Slow Electrons by O_2 and H_2O Molecules and Molecules of Halogen Compounds" Soviet Physics JETP 35:783-91 (May 1959)

23. Chantry, P. J. "Attachment Measurements in Halogen Bearing Molecules" Westinghouse Electric Corporaton, Defense Documentation Center #AD B026570, Monitored by U.S. Army Ballistic Missle Defense Advanced Technology under Contract #DASG60-77-0023, (March 1978)

24. Christophorou, L. G., R. N. Compton and H. W. Dickson "Dissociative Electron Attachment to Hydrogen Halides and their Deuterated Analogs" Journal of Chemical Physics, 48:1949-55 (March 1968)

25. Christophorou, L. G., D. L. McCorkle, and V. E. Anderson, "Swarm-Determined Electron Attachment Cross Sections as a Function of Electron Energy "Journal of Physics B: Atomic and Molecular Physics, 4:1163-72 (September 1971)

26. Christophorou, L. G. and J. A. Stockdale, "Dissociative Electron Attachment to Molecules" Journal of Chemical Physics 48:1956-60 (March 1968)

27. Christov, N. "On the Potential Distribution in the Cathode Fall Region of a Glow Discharge" Plasma Physics 17:993-6 (1975)

28. Chutjian, A. and D. C. Cartwright, "Electron Impact Excitation of Electronic States in Argon at Incident Energies Between 16 and 100eV." Physical Review A 23:2178-93 (May 1981)

29. Compton, K. T. and C. C. Van Voorhis, "Probability of Ionization of Gas Molecules by Electron Impacts" Physical Review, 26:436-53 (1925)

30. Compton, R. N., and L. G. Christophorou "Negative-Ion Formation in H_2O and D_2O" Physical Review, 154:110-6 (February 1967)

31. Compton, R. N., J. A. Stockdale and P. W. Reinhardt "Electron-Impact Excitation and Negative-Ion Formation in NH_3 and ND_3" Physical Review, 180:111-120 (April 1969)

32. Davies, A., and J. Evans "An Analysis of the One Dimensional Steady-State Glow Discharge" Journal of Physics D: Applied Physics, 13:L161-6 (1980)

33. Davies, D. K., "Measurements of Swarm Parameters in Chlorine-Bearing Molecules" Westinghouse Electric Corporation, AFWAL-TR-82-2083 (August 1982)

34. Davis, C., and T. King "Processes in Electronegative Iodine - Helium Gas Laser Discharges" IEE Conference Publication 90:127-9 (1972)

35. de Heer, F. J., R. H. J. Jansen, and W. van der Kaay, "Total Cross Sections for Electron Scattering by Ne, Ar, Kr, and Xe" Journal of Physics, B: Atomic and Molecular Physics, 12:979-1002 (1979)

36. DGEAR and the associated nuclei are adaptations of a package designed by A. C. Hindmarsh, "GEAR: Ordinary Differential Equation System Solver", Lawrence Livermore Laboratory, Report UCID-30001, Revision 3. December 1974, based on C. W. Gears sub-routine DIFSUB described in Numerical Initial Value Problems in Ordinary Differential Equations, Engelwood Cliffs, New Jersey: Prentice Hall, (1971).

37. Dowell, J. T. "Production of Metastable Atoms by Electron Impact" University of California, UCRL - 14450 (December 1965)

38. Druyvesteyn, M. J. and F. M Penning, "The Mechanism of Electrical Discharges in Gases of Low Pressure" Reviews of Modern Physics 12:87-174 (April 1940)

39. Dutton, J. "A Survey of Electron Swarm Data" Journal of Physical and Chemical Reference Data 4:577-856 (1975)

40. Edgley, P. D. and A. von Engel, "Theory of Positive Columns in Electronegative Gases" Proceedings of the Royal Society of London A370:375-87 (1980)

41. Eggarter, E. "Comprehensive Optical and Collision Data for Radiation Action. II. Ar*" Journal of Chemical Physics 62:833-847 (February 1975)

42. Emeleus, K. G. and J. Sayers, "Negative Ions in Discharge Tubes" Proceedings of the Royal Irish Academy 44A:87-100 (1938)

43. Franklin, R. N. Plasma Phemomena in Gas Discharges Oxford: Clarendon (1976)

44. Ganas, P. S. and A. E. S. Green, "Electron Impact Excitation of the Rare Gases" Physical Review A 4:182-193 (July 1971)

45. Gerald, Curtis F. Applied Numerical Analysis, Chapter 1, 2nd ed., Reading, MA, Addison-Wesley Publishing Co. (1978)

46. Guntherschulze, A. "Die Behinderte Glimmentladung" Zeitschrift fur Physik, 61:1-14 (1930)

47. Harland, P. W. and J. L. Franklin, "Partitioning of Excess Energy in Dissociative Resonance Capture Processes" Journal of Chemical Physics 61:1621-36 (September 1974)

48. Hayashi, M. J. de Physique, 40-c7:45 (1979)

49. Hickman, A. "Approximation Scaling Formula for Ion-Ion Mutual Neutralization Rates" Journal Chemical Physics 70:4872-81 (1979)

50. Huang, S. and G. Freeman, "Electron Mobilities in Gaseous, Critical, and Liquid Xenon: Density, Electric Field, and Temperature Effects: Quasilocalization" Journal of Chemical Physics 68:1355-1362 (February 1978)

51. Huber, K. and G. Herzberg, Molecular Spectra and Molecular Structure, IV Constraints of Diatomic Molecules. New York: Van Nostrand Reinhold Company (1979)

52. Ingold, J. "The Glow Discharge Cathode Fall" Paper HB-1, 34th Annual Gaseous Electronics Conference, October (1981)

53. Jacob, J. H. and J. A. Mangano, "Total Electron Impact Excitation Cross Sections of Ar and Kr" Applied Physics Letters, 29:467-469 (October 1976)

54. Kieffer, L. J. "A Compilation of Electron Collision Cross Section Data for Modeling Gas Discharge Lasers." J. I. L. A. Information Center Report 13, September (1973)

55. Kline, L. E., D. K. Davies, C. L. Chen, and P. J. Chantry, "Dielectric Properties for SF_6 and SF_6 Mixtures Predicted from Basic Data" Journal of Applied Physics 50:6789-96 (November 1979)

56. Koniukov, M. V. "Concentration of Negative Ions in the Plasma of a Positive Column" Soviet Physics JETP 34:629-31 (October 1958)

57. Kurepa, M. V. and D. S. Belic' "Electron-Chlorine Molecule Total Ionization and Electron Attachment Cross Sections" Journal of Physics B: Atomic and Molecular Physics 11:3719-29 (November 1978)

58. Langmuir, I. "The Interaction of Electron and Positive Ion Space Charges in Cathode Sheaths" Physical Review 33:954-89 (1929)

59. Little, P.F., and A. von Engel, "The Hollow-Cathode Effect and the Theory of Glow Discharges" Proceedings of the Royal Society of London, 224:209-227 (1954)

60. Long, W. H. Jr., "Plasma Sheath Processes" Northrop Corporation AFAPL-TR-79-2038 (April 1979)

61. Long, W. H. Jr., "Program SHEATH User's Manual", Northrop Corporation Contract F33615-77-C-2048 / Project No. FY1455-77-00034, Northrop Corp. (April 1979)

62. Lucas, J. and H. T. Saelee, "A Comparison of a Monte Carlo Simulation and the Boltzmann Solution for Electron Swarm Motion in Gases", Journal of Physics D: Applied Physics, 8:640-50 (April 1975)

63. Lunt, R. W. and A. H. Gregg "The Occurrence of Negative Ions in the Glow Discharge through Oxygen and Other Gases" Transaction of the Faraday Society 36:1062-72 (1940)

64. MacNeil, K. A. G., and J. C. J. Thynme Journal of Chemical Physics 73:2960 (1969)

65. Makabe, T. and T. Mori, "Experimental and Theoretical Analysis of the Electron Energy Distribution Functions in Townsend Discharges in Xenon" Journal of Physics B: Atomic and Molecular Physics, 11:3785-3793 (1978)

66. Merritt, F. S. Mathematics Manual, New York: McGraw-Hill Book Company (1962)

67. Mitchell, R., L. Kline, and L. Denes, "Electrode Sheath Predictions for Attaching Gas Mixtures "Paper BB-4, 33rd Annual Gaseous Electronics Conference, October (1980)

68. Mott, N. F., and H. S. W. Massey, Theory of Atomic Collisions, 3rd ed. Oxford: Clarendom Press (1965)

69. Neuringer, J. "Analysis of the Cathode Fall in High Voltage Low-Current Gas Discharges" Journal of Applied Physics, 49:590-2 (1978)

70. Nighan, W. and W. Wiegand, "Influence of Negative-Ion Processes on Steady-State Properties and Striations in Molecular Gas Discharges" Physical Review A 10:922-44 (1974)

71. Padial, N. T., G. D. Meneses, F. J. da Paixao, G. Csanak, and D. Cartwright, "Electron-Impact Excitation of the Lowest Four Excited States of Argon" Physical Review A 23:2194-2212 (May 1981)

72. Pitchford, L. C. and A. V. Phelps, "Multi-Term Boltzmann Analysis of Electrons in N_2." Joint Institute for Laboratory Astrophysics, AFWAL-TR-81-2035, (1981)

73. Pringle, D. H., and W. E. Farvis, "Screened Probe Measurements in the Helium Negative Glow" Proceedings of the Physical Society B, 68:836-848 (1955)

74. Rapp, D. and D. D. Briglia, "Total Cross Sections for Ionization and Attachment in Gases by Electron Impact II Negative Ion Formation" Journal of Chemical Physics, 43:1480-9 (September 1965)

75. Rapp, D. and P. Englander-Golden, "Total Cross Sections for Ionization and Attachment in Gases by Electron Impact. I Positive Ionization" Journal of Chemical Physics 43:1464-1479 (September 1965)

76. Rapp, D., T. E. Sharp, and D. D. Briglia "Large Isotope Effect in the Formation of H^- or D^- by Electron Impacat on H_2, HD, and D_2" Physical Review Letters, 14:533-5 (April 1965)

77. Sakai, Y., H. Tagashira, and S. Sakamoto, "The Development of Electron Avalanches in Argon at High E/N Values, I. Monte Carlo Simulation.", Journal of Physics D: Applied Physics, 10:1035-49 (May 1977)

78. Schultz, G. J. "Cross Sections and Electron Affinity for O^- Ions from O_2, CO, and CO_2 by Electron Impact" Physical Review 128:178-186 (October 1962)

79. Segur, P., M. Yousfi, and E. Marode "A Self Consistent Microscopic Study of the Cathodic Zone of a Helium-Mercury Discharge" Proceedings of the 6th International Conference on Gas Discharges. Edinburgh, IEE Conference Publication 189, 2:56-59, (1980)

80. Spence, D. and G. J. Schultz "Cross Sections for Production of O^- and C^- by Dissociative Electron Attachment in CO_2: An Observation of the Renner-Teller Effect" Journal of Chemical Physics 60:216-220 (January 1974)

81. Spencer-Smith, J. L. "Negative Ions of Iodine. I Probe Measurements" Philosophical Magazine 19:806-23(1935)

82. Schaper, M. and H. Scheibner, "Absolutbestimmung der Gesamtanregungsquerschnitte der Edelgase durch Elektronenstoss" Beiterung Plasma Physik 9:45-57 (1969)

83. Specht, L. T., S. A. Lawton, and T. A. DeTemple, "Electron Ionization and Excitation Coefficients for Argon, Krypton, and Xenon in the Low E/N Region" Journal of Applied Physics, 51:166-170 (January 1980)

84. Thompson, J. B. "Electron Energy Distribution in Plasmas IV Oxygen and Nitrogen" Proceedings of the Royal Society of London, A262:503-518 (1961)

85. Thompson, J. J. and Thompson, G. P., Conduction of Electricity Through Gases, Vol II, 3rd ed. Cambridge: Unversity Press (1933)

86. Tran Ngoc An, E Marode, and P. C. Johnson, "Monte Carlo Simulation of Electrons Within the Cathode Fall of a Glow Discharge in Helium." Journal of Physics D: Applied Physics, 10:2317-28 (1977)

87. Ul'yanov, K. "Theory of a Normal - Glow Discharge at Intermediate Pressures" High Temperature 10:841-7 (September - October 1972) Translation Teplofizika Vysokikh Temperatur (USSR) 10:931-8 (September-October 1972)

88. von Engel, A. "A Theory of the Anode Fall in Glow Discharges" Philosophical Magazine 32:417-26 (1941)

89. von Engel, A. Ionized Gases 2nd ed. London: Oxford University Press, (1965)

90. von Engel, A. and M. Steenbeck, Electrische Gasentladungen Berlin: Springer (1932)

91. Wadehra, J. M. and J. N. Bardsley, "Vibrational and Rotational State Dependence of Dissociative Attachment in e-H_2 Collisions", Physics Review Letters, 41:1795-8 (December 1978)

92. Ward, A. L., "Calculations of Cathode-Fall Characteristics" Journal of Applied Physics 33:2789-94 (September 1962)

93. Weston, G. F. Cold Cathode Discharge Tubes, London: Iliffe (1968)

94. Williams, W., S. Trajmar, and A. Kupperman, "Angular Distributions in the Electron Impact Excitation of Xe at 20 eV" Journal of Chemical Physics, 62:3031-5 (April 1975)

95. Willis, S. L., and M. R. C. McDowell, "Electron Impact Excitation of Helium at Intermediate Energies" Journal of Physics B: Atomic and Molecular Physics 14:L453-9 (1981)

96. Woolsey, G. A. "Studies of Electronegative Plasmas" PhD Dissertation, Physics Department, Queen's University Belfast (1963)

97. Ziesel, J. P., G. J. Schultz, and J. Milhaud "S^- Formation by Dissociative Attachment in OCS and CS_2" Journal of Chemical Physics, 62:1936-40 (March 1975)

98. Zimmerman, G. Zeitshrift fur Physik, 91:767 (1934)

Appendix A: Review of Negative Ion Formation

In order to provide continuity in the descriptions of the models, the mechanisms and important features of negative ion formation are reviewed. Several reactions occur which form negative ions and these are listed and described below:

$X + e^- \rightarrow X^- + h\nu$	radiative capture
$X + e^- + M \rightarrow X^- + M$	3 body electron capture
$XY + e^- \rightarrow X + Y^-$	dissociative attachment
$XY + e^- \rightarrow X^+ + Y^- + e^-$	ion pair formation

(X = an atom, e^- = an electron, $h\nu$ = a photon, M = an electron or an atom, XY = a molecule made of atoms X and Y)

Dissociative Attachment

The most common process of forming negative ions is dissociative attachment. In this case, an electron collides with a molecule XY and dissociates the molecule into a neutral atom X and a negative ion Y^-. To aid the visualization of transitions between states, dissociative attachment can be divided into 3 cases using molecular potential energy curves. These three cases will be discussed next. The discussion will include the influence of vibrational excitation on dissociative attachment.

In all three cases represented in Fig A-1a, b, c, the heavy solid line refers to the ground state of the neutral molecule XY. The nuclear separation oscillates then between R_1 and R_2. The thinner

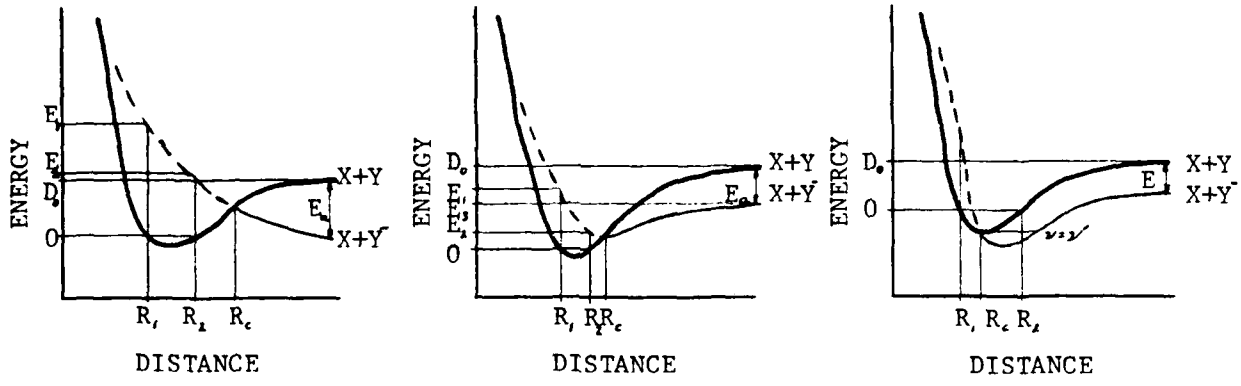

Fig A-1

Potential Energy Curve Allowing Dissociative Attachment

curve refers to the molecular ion state XY^- which at infinite separation ($X + Y^-$) tends to a limit which lies below the potential energy curve of the neutral molecule by an amount of energy equal to the electron affinity (E_a) of atom Y. The solid region represents the range over which the negative ion state is stable. The dashed region represents the range over which the negative ion state is unstable. In this region the negative ion may give up the electron and return to a ground state neutral molecule XY, via autodetachment. If $\Gamma(R)/\hbar$ is the rate (sec^{-1}) for autodetachment, then the energy in this unstable region is uncertain by an amount $\Gamma(R)$ and the dashed line actually should be a band with a width $\Gamma(R)$. The molecular ion state curve crosses the ground state curve at R_c. Applying the Franck-Condon principle to the transition from the ground molecular state to the

Table A-1. Threshold for Dissociative Attachment and Ion Pair Production

Molecule	E_a (eV) (ref. 8)	D_o (eV) (ref. 51)	E_{DA} (eV)	E_i (eV) (ref. 51)	$E_{i\ mole}$ (eV)	E_{Th} (eV)
HgI	3.06-I	.35	0.	10.43-Hg		7.73
HgBr	3.36-Br	.71	0.	10.43-Hg		7.78
HgCl	3.61-Cl	1.04	0.	10.43-Hg		7.86
F_2	3.45-F	1.60	0.	17.42-F	15.69	15.57
HgF	3.45-F	1.8	0.	10.43-Hg		8.78
IBr	3.36-Br	1.82	0.	10.44-I	9.85	8.89
	3.06-I		0.	11.84-Br		10.59
I_2	3.06-I	1.54	0.	10.44-I	9.31	8.92
ICl	3.61-Cl	2.15	0.	10.44-I	10.08	8.98
	3.06-I		0.	13.01-Cl		11.8
Br_2	3.36-Br	1.971	0.	11.84-Br	10.52	10.45
BrCl	3.36-Br	2.23	0.	11.84-Cl	11.1	10.71
	3.61-Cl		0	13.01-Br		11.63
FO	3.45-F	2.23	0.	13.61-O	12.79	12.39
	1.46-O		.77	17.42-F		18.18
Cl_2	3.62-Cl	2.48	0.	13.01-Cl	11.5	11.8
BrO	3.36-Br	2.40	0.	13.61-O		12.65
	1.47-O		.93	11.84-Br		12.77
IF	3.45-F	2.52	0.	10.44-I		9.51
	3.06-I		0.	17.42-F		16.58
BrF	3.45-F	2.548	0.	11.84-Br	11.78	10.94
	3.36-Br		0.	17.42-F		16.60
ClO	3.61-Cl	2.75	0.	13.61-O	11.0	12.76
	1.47-O		1.29	13.01-Cl		14.30
HgH	.75-H	.37	0.	10.43-Hg		10.05

Table A-1. (cont.)

Molecule	E_a (eV)[2] (ref. 8)	D_o (eV)[2] (ref. 51)	E_{DA} (eV)	E_i (eV) (ref. 51)	$E_{i\ mole}$ (eV)	E_{Th} (eV)
HI	3.06-I	3.05	0.	13.60-H	10.38	13.59
	.754-H		2.79	10.44-I		13.23
IO	1.47-O	1.8	.34	10.44-I		10.78
	3.06-I		0.	13.61-O		12.05
HBr	3.36-Br	3.76	.40	13.60-H	11.67	13.99
	.75-H		3.0	11.84-Br		14.84
HCl	3.61-Cl	4.43	.82	13.60-H	12.75	14.42
	.75-H		3.68	13.1-Cl		16.69
SH	2.08-S	3.55	1.47	13.61-H	10.43	15.09
	.75-H		2.80	13.60-S		16.39
HF	3.45-F	5.94	2.49	13.60-H	16.06	16.08
	.75-H		5.18	17.42-F		22.6
OH	1.47-O	4.45	2.99	13.60-H	12.91	16.58
	.75-H		3.70	13.61-O		17.31
O_2	1.47-O	5.12	3.65	13.61-O	12.07	17.26
H_2	.75-H	4.48	3.73	13.60-H	15.43	17.33
HD	.75-H	4.51	3.75	13.60-D	15.45	13.35
SO	1.47-O	5.36	3.89	10.36-S	10.29	14.25
	2.08-S		3.28	13.61-O		16.90
NO	1.47-O	1.5	5.03	14.54-N	9.26	19.57
CN	1.27-C	7.76	6.49	14.54-N	14.17	21.03
CO	1.47-O	11.09	9.63	11.26-C	14.01	20.89
	1.27-C		9.82	13.61-O		23.44

E_a = Atomic Electron Affinity
D_o = Molecular Dissociation Energy
E_{DA} = Threshold for Dissociative Attachment
E_i = Atomic Ionization Potential
$E_{i\ mole}$ = Molecular Ionization Potential
E_{Th} = Threshold Ion Pair Formation

AD-A138 100 INVESTIGATION OF SHEATH PHENOMENA IN ELECTRONEGATIVE GLOW DISCHARGES(U) AIR FORCE INST OF TECH WRIGHT-PATTERSON AFB OH SCHOOL OF ENGINEERING G L DUKE 3/3

UNCLASSIFIED DEC 83 AFIT/DS/PH/83-6 F/G 20/3 NL

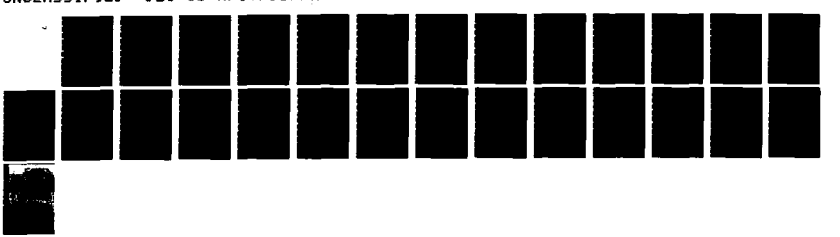

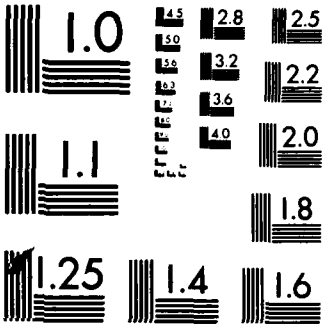

negative ion state leads to a final state represented by some point lying between a and b on the potential energy curve. The threshold for dissociative attachment, E_{DA}, is the difference between the molecular dissociation energy D_o and the electron affinity, E_a, of the negative atomic ion. Thresholds have been tabulated for several molecules and they are

$$E_{DA} = D_o - E_a \tag{A-1}$$

compared to thresholds for ion pair formation shown in Table A-1.

The competition between autodetachment and dissociation in molecular negative ions leads to a strong dependence of the cross section on the mass of the nuclei and the rotational and vibrational states of the neutral molecule. In case I represented in Fig 1a, first suppose autodetachment did not occur. Then all transitions from the ground state to the ion state would result in dissociation into an atom X and ion Y^- with a relative kinetic energy between E_1 and E_2. If autodetachment is allowed to occur at some internuclear separation R at a rate $\Gamma(R)/\hbar$, then after the transition to the negative ion state, the atomic nuclei begin to separate with a relative velocity V(R), and the fraction of negative ion molecules remaining (ref 8) or "surviving" is

$$F(R) = \exp - \int_{R}^{R_c} \frac{\Gamma(R')}{\hbar V(R')} dR' \tag{A-2}$$

If the separation between the atomic nuclei reaches R_c before autodetachment takes place, then the neutral molecule dissociates into $X + Y^-$. The cross section for this process can then be approximated by

$$\sigma_a(R) = \sigma_c \exp - \int_R^{R_c} \frac{\Gamma(R')}{\hbar V(R')} dR' \qquad \text{(A-3)}$$

where σ_c is the cross section for the initial capture (ref 8). Because heavy atomic nuclei typically oscillate more slowly than lighter nuclei, the heavier nuclei spend more time near the turning points and have steeper potential wells. This increases the probability that the internuclear separation R of the molecular ion will exceed R_c before it autodetaches. Typical peak cross section values from the ground vibrational state for dissociative attachment range from $10^{-20}cm^2$ for light molecules such as H_2, HD, and D_2 to 10^{-14} or $10^{-15}cm^2$ for heavy molecules such as HI, and I_2. (See Table A-2).

In case II represented in Fig 1 (b), only electrons with energies between E_1 and E_3 can dissociate the molecule and produce atomic negative ions through the dissociative attachment process. The resulting negative ion Y^- and atom X thus will have relative final energy ranging from 0 to E_1-E_3. Electrons with energies between E_2 and E_3 can be captured, but they will form excited molecular negative ions XY^-. These molecular ions will eventually autodetach unless the excess energy can be absorbed through a collision. Thus the total attachment cross section for this case will be independent of pressure for pressures greater than some critical pressure, but will be proportional to the pressure for pressures less than the critical pressure. The critical pressure occurs when the average time for the vibrationally excited molecule to transfer its excess energy to a gas molecule is comparable to the time for autodetachment.

Table A-2. Thresholds and Peak Cross Section Values for Dissociative Attachment

Process Diatomic Molecules	Threshold (eV)	Peak (cm^2)	Energy at Peak (eV)	Reference
$e^- + F_2 \rightarrow F^- + F$	0.	8.0_{-15}	0.	23
$e^- + I_2 \rightarrow I^- + I$	0.	3.1_{-15}	.01	19
$e^- + Cl_2 \rightarrow Cl^- + Cl$	0.	2.02_{-16} 2.79_{-18} 4.84_{-18}	0. 2.6 5.8	57
$e^- + HI \rightarrow$ Neg Ions	0.	2.3_{-14}	0.	24
$e^- + HBr \rightarrow Br^-_r + H$	.395	2.71_{-16}	.293	64
$e^- + DCl \rightarrow Cl^- + D$	.55	1.25_{-17}	.836	16
$e^- + HCl \rightarrow Cl^- + H$	.8236	2.2_{-17}	.85	33
$e^- + O_2 \rightarrow O^- + O$	3.65	2.0_{-18}	6.45	25
$e^- + HCl \rightarrow H^- + Cl$	3.68	5.2_{-19}	7.0	16
$e^- + H_2 \rightarrow H^- + H$	3.73	1.6_{-21}	3.73	17
$e^- + H_2 \rightarrow$ Neg Ions		1.23_{-20} 1.23_{-20}	10.4 13.9	76 76
$e^- + HD \rightarrow$ Neg Ions	3.75	6.34_{-21} 1.46_{-20}	10.4 13.9	76 76
$e^- + D_2 \rightarrow D^- + D$	3.83	3.0_{-24} 2.73_{-21} 9.88_{-21}	3.83 10.6 14.	17
$e^- + CO \rightarrow O^- + C$	9.6	2.43_{-19}	10.2	78
$e^- + CO \rightarrow$ Neg Ions	9.6	2.02_{-19}	10.	74
$e^- + NO \rightarrow$ Neg Ions	5.03	1.12_{-18}	8.1	74

Table A-2. (cont.)

Process Diatomic Molecules		Threshold (eV)	Peak (cm^2)	Energy At Peak (eV)	Reference
Triatomics					
$e^- + N_2O$	$O^- + \ldots$	.20	3.57_{-18}	1.4	25
			1.03_{-17}	2.39	25
$e^- + OCS$	$S^- + \ldots$	.6	3.12_{-17}	1.24	97
$e^- + CS_2$	$S^- + \ldots$	2.6	3.75_{-19}	3.35	97
			3.02_{-19}	3.68	97
$e^- + CO_2$	$O^- + \ldots$	3.2	1.48_{-19}	4.3	74
			4.29_{-19}	8.1	74
$e^- + H_2O$	Neg Ions	5.3	4.9_{-18}	6.4	22
$e^- + H_2O$	$H^- + \ldots$	5.7	6.95_{-18}	6.62	30
$e^- + CO_2$	$C^- + \ldots$	14.	2.0_{-21}	18.5	80
Polyatomics					
$e^- + SF_6$	Neg Ions	0.			55
$e^- + NF_3$	$F^- + \ldots$	.7	5.98_{-17}	1.82	47
$e^- + NH_3$	Neg Ions	.79	5.7_{-18}	2.47	31
$e^- + NF_3$	$NF^-_2 + \ldots$	.9	5.99_{-17}	1.89	23
$e^- + NF_3$	$F^-_2 + \ldots$	1.0	6.0_{-17}	1.87	23
$e^- + CF_4$	$CF^-_3 + \ldots$	5.	$4._{-19}$	6.89	97

In case III represented in Fig 1 (c), negative ion molecules with vibrational states $\nu<\nu'$ are stable, but those with $\nu>\nu'$ are unstable and can result in autodetachment. These states may be stabilized through collisions similar to the process described for case II. Similarly, the cross section for attachment will exhibit resonance maxima which are associated with the vibrational levels with $\nu>\nu'$, provided the lifetime of the excited vibrational state is long compared to its period. This situation occurs in O_2 and NO, resulting in the production of O^-_2 and NO^- after collisions with other gas molecules. Table A-2 tabulates experimental data for thresholds and cross section peaks for several attaching molecules.

Increased vibrational excitation enhances the dissociative attachment cross section for all three cases since electron capture can generally occur at larger and larger values of R. Thus the molecular negative ion is more likely to "survive", the closer R approaches R_c through vibrational excitation. Rotational excitation can also enhance the cross section for dissociative attachment due to the centrifugal stretching occurring in the excited states, but in a less dramatic manner than vibrational excitation. Bardsley and Wadehra (ref 17, 91) have shown that the magnitude of the dissociative attachment cross section from the $\nu = 5$ level in H_2 and D_2 increases three to four orders of magnitude. Allan and Wong (ref 12) have measured similar increases in their experiments with HCl. The change in the "survival factor" is thought (ref 91) to be more important than the change in the Franck Condon factor in explaining this dramatic effect. If the lifetime of the vibrationally excited molecule is long compared to the period of vibration, the attachment probability will contain resonance

peaks. This is a result of the initial electron capture cross section σ_c exhibiting resonance peaks due to the ratios of populations in the various vibrational levels. Experimentally this variation with respect to rotational and vibrational population appears as a temperature dependence.

The remaining processes, including radiative capture, three body capture, and ion pair formation are generally less important than dissociative attachment and will be discussed only briefly.

Radiative Capture:

Radiative capture is the simplest process for creating negative ions. Electrons are captured directly by neutral atoms with the excess energy being dissipated in radiation. The amount of energy released by this process is equal to $E + E_a$ where E is the kinetic energy of the incident electron and E_a is the electron affinity of the atom. This capture process produces a continuous emission spectrum extending indefinitely from the long wavelength limit at

$$\lambda = \frac{hc}{E_a} \qquad \text{(A-4)}$$

A typical magnitude for this process is on the order of 10^{-22} cm^2 with a large peak near zero impact energy (ref 8). This is two orders of magnitude smaller than the smallest cross section for dissociative attachment. The relatively large low energy peak occurs because the electron spends a longer time within the range of the atomic field at lower incident energies.

Three Body Electron Capture:

In three body electron capture the energy released by the process is converted, not into a photon, but into kinetic energy of the third body. The magnitude of the attachment cross section for this process can be determined by arguments based on two body collisions. The third body will be effective in absorbing energy only if it makes an effective collision with the capturing atom, when the electron is also within an atomic radius ($r_o \simeq 10^{-8}$cm) of the capturing atom. If λ is the mean free path for effective collisions between the atom and a single third body, then the probability for an effective collision is to a good approximation r_o/λ . This results in an effective three body attachment cross section that can be approximated by the following expression in terms of an effective cross section per unit concentration of the third body.

$$\sigma \approx r_o^2 \frac{r_o}{\lambda} \qquad \text{(A-5)}$$

Thus it remains to determine λ , which varies considerably depending on the nature of the third body. Two cases will be considered:

1) when electrons are third bodies, and

2) when atoms and molecules are third bodies.

When electrons are the third body, the effective cross section for energy transfer is on the order 10^{-16}cm^2, and the mean free path for a unitary third body density simply becomes

$$\lambda = 10^{16}\text{cm} \qquad \text{(A-6)}$$

and the third body attachment cross section is on the order of

$$\sigma_a = 10^{-40}\text{cm}^2 \qquad \text{(A-7)}$$

In comparison to dissociative attachment, an electron number density greater than or equal to $10^{20}cm^3$ would be required to produce a comparable number of negative ions per sec. For most purposes this is an exceptionally large electron density.

When atoms or molecules are the third body, two cases exist: resonant and non-resonant energy transfer. In the resonant case, the energy transferred is absorbed totally as internal energy in the third body. The cross section for this process is known to be quite large on the order $10^{-14}cm^2$ or greater(ref 8). This yields a mean free path and effective attachment cross section of

$$\lambda = 10^{14}cm \qquad \sigma_a = 10^{-38}cm^5 \qquad \text{(A-8)}$$

Thus third body densities of $10^{18}cm^{-3}$ or larger would be necessary to make three body attachment comparable to that of dissociative attachment. Thus molecules possessing several internal degrees of freedom are the most effective as third bodies. However, energy transfer into vibrational motion often is not as efficient as transfer into rotational motion.

Ion Pair Formation:

The last process to be discussed which forms negative ions is ion pair formation or polar excitation. During this type of collision, an electron excites a molecule (XY) to an unstable electronic state which dissociates spontaneously.

$$XY + e^- \rightarrow X^+ + Y^- + e^- \qquad \text{(A-9)}$$

This process differs from the previous processes in that the electron is not captured during the collision, but corresponds to an inelastic collision in which the electron acts as a source of energy for

electronic excitation. Thus polar excitation occurs at much higher electron energies than the capture processes. Minimum threshold energies, E_{th} usually range from 10 to 25 eV.

A typical potential energy curve for this process is depicted in Fig A-2.

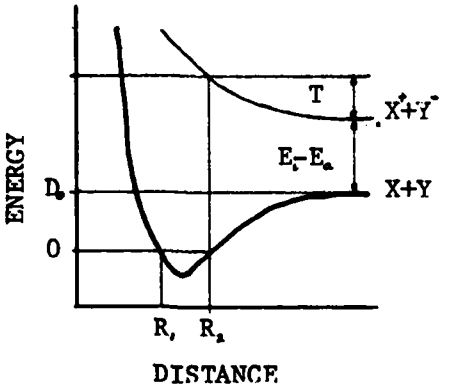

Fig A-2. Potential Energy Curve For Ion Pair Formation

Again the heavy solid line refers to the ground state of the neutral molecule. The thinner line refers to an unstable electronic state which dissociates spontaneously into ions. The energy at infinite nuclear separation tends to a value of $E_i - E_a$, where E_i is the ionization energy of X and E_a is the electron affinity of Y. The final relative kinetic energy (T) of the ions is given by the following equation:

$$T = E_{Th} + E_a - E_i - D_o \qquad \text{(A-10)}$$

where D_o is the dissociation energy of the ground state. Thresholds for ion pair formation for several diatomics are previously listed in Table A-1.

The shape of the cross section for polar dissociation differs from the previous capture process. Actually it resembles the shape of other electronic excitation processes and thus is typified by a sharp rise

near threshold to a maximum on the order of 10^{-16}-10^{-17} cm^2 at 2 to 4 times the threshold energy, after which it declines. The decline being inversely proportional to the energy or more slowly if optical transitions are allowed between the ground state and the excited state (ref 68:497).

Appendix B. Parameters for GLOW Code Calculations

This appendix describes the parameters used to characterize the ionization, attachment, diffusion, and ion-ion recombination coefficients as well as the ion drift velocity. Most of the data for the rare gases was taken from the literature. Effort was given to obtain the best parameters for HCl from drift tube measurements of Davies (ref 33:31-55).

The parameters for the rare gases are summarized in Table B-1. A, B, and s refer to the parameters in equation III-38 and were taken from Ward (ref 95:2790). The transverse diffusion coefficient was obtained from data tabularized by Dutton (ref 39:6491 (He), 651 (Ar), 654 (Xe)). The mean free path λ was estimated using the formula:

$$\lambda = \frac{1}{N\sigma} \qquad \text{(B-1)}$$

where σ is the momentum transfer cross-section. Momentum transfer cross-sections have been tabulated by Kieffer (ref 54:2(He), 13 (Ar), 17

Table B-1

Parameters Used to Describe Rare Gas Processes in the GLOW Code

	A	B	s	$D_e p$	λ	r	k_+
	$\frac{1}{\text{cm torr}}$	$\frac{\text{Volt}^{\frac{1}{2}}}{\text{cm}^{\frac{1}{2}}\text{torr}^{\frac{1}{2}}}$		$\frac{\text{cm}^2\text{torr}}{\text{sec}}$	cm		$\frac{\text{cm}^{\frac{1}{2}}\text{torr}^{\frac{1}{2}}}{\text{volt}^{\frac{1}{2}}\text{sec}}$
He	4.4	14.	½	1.35E6	.052	8.E-3	4.1E4
Ar	29.22	26.64	½	3.6E6	.311	3.32E-3	8.25E3
Xe	65.3	36.08	½	1.64E6	.124	5.E-3	4.0E3

(Xe)). The value of the momentum transfer cross section at 1eV was used. This energy is representative of electrons diffusing radially in the positive column region of a discharge. The value of r was also taken from the data given by Ward (ref 92:2791) for v_+ and v_e.

The ion-ion recombination rates were estimated using the approximate scaling formula developed by Hickman (ref 49:4875). The formula is given by

$$k_r = \frac{1}{4.38E4 \left(\frac{T}{300°K}\right)^{\frac{1}{2}} m^{\frac{1}{2}} (E.A.)^{\frac{3}{2}}} \qquad \text{(B-2)}$$

where T is the gas temperature in degress Kelvin, m is the reduced mass of the diatomic molecule in a.u., and E.A. is the electron affinity of the negative ion in eV. The values of these parameters and the resulting ion-ion recombination rate for a 300°K gas is given in Table B-2.

Table B-2

Parameters for Calculating Ion-Ion Recombination Rates

	m (a.u.)	E.A. (Cl^-) (eV)	K_r (cm/sec)
He	4.	3.613	7.2E-6
Ar	39.95	3.613	3.15E-6
Xe	131.3	3.613	2.59E-6

The ionization and attachment coefficients for HCl were curve fit from the experimental data of Davies (33:33). Using equation III-38, both values of s = ½ and s = 1 were tried. The value s = 1 gave the best fit, which also yielded values for A = 14.34 and B = 243.94. In order to model the attachment coefficient over the complete range, both

equations III-39 and III-40 had to be used. A fifth order (n=5) polynomial was used for E/p < 90v/cm-torr with the following values for coefficients

a_0 = -.748878814,
a_1 = .1274582651,
a_2 = -.0052731662,
a_3 = 9.48227228E-5,
a_4 = -7.86191615E-7, and
a_5 = 2.46552683E-9.

For E/p $\geq$ 90v/cm-torr, the best fit was given by C = .254193623029, D = 9.14964650482E-3, and t=1. This concludes the data inputs used for the GLOW code except for the discharge parameters, such as current, pressure, and electrode separation which are discussed in the Chapter III with the results of the calculations.

Appendix C. Parameters for SHEATH Code Calculations

This appendix describes the parameters used in the SHEATH code. The initial values of code parameters will be summarized first followed by a description of the electron impact cross-sections used in calculating the electron distribution function.

The discharge parameters are summarized in Table C-1. The anode was placed just outside the cathode fall region where the electric field leveled off to a constant value. This was done to keep the energy step size as small as possible, less than 1.6eV, in order to maximize the energy resolution in calculating the distribution function. With this step size limitation, lengthening the electrode distance was not feasible since most of the storage space on a Cyber 74 was already being used. For 100% He, the electrode distance was 2.2 cm and for the remaining He/HCl mixtures the electrode distance was 2.1 cm due to the contraction that accurred. J is the discharge current density and γ is the secondary emission coefficient. The distribution of electrons

Table C-1

Discharge Parameters Used in the SHEATH Code

Mixtures	D (cm)	J (amp/cm^2)	γ
He/HCl	2.1-2.2	16	.2
Ar/HCl	1.15	10	.0417
Xe/HCl	.87	10	.004

leaving the cathode was the same as that used by Long (ref 60) and is displayed in Fig C-1. The x axis is plotted in terms of energy bins which were typically 1. - 1.6eV in width depending on the gas mixture. This distribution is higher in energy than the one used by Boeuf et al. (ref 14) which was a flat isotropic energy distribution over the range of 0 to 5eV. Boeuf and Marode (ref 13) later used a narrower distribution which was isotropic and flat between 4 and 5eV.

The gas parameters are summarized in Table C-2. The gas density was constant throughtout the discharge and was determined from the gas pressure, p_o and temperature, T_o. The positive ion mobility, k_+ was obtained from Ward (ref 92:2791) and was the same as that used in the equilibrium analysis. Q_{max} determined the point at which the code transforms from energy space to spatial coordinate as described earlier. It was varied so the coordinate transition was as close as possible to the minimum of the electric field within the bounds of equation IV-11.

Table C-2

Gas Parameters Used in the SHEATH Code

Mixtures	p_o (torr)	T_o (^oK)	k_+ cm -torr / volt sec
He/HCl	1	300	4.1E+4
Ar/HCl	1	300	8.25E+3
Xe/HCl	1	300	4E+3

The cross sections for He, Ar, Xe, and HCl which were used in the SHEATH code calculations are discussed next. The most important cross

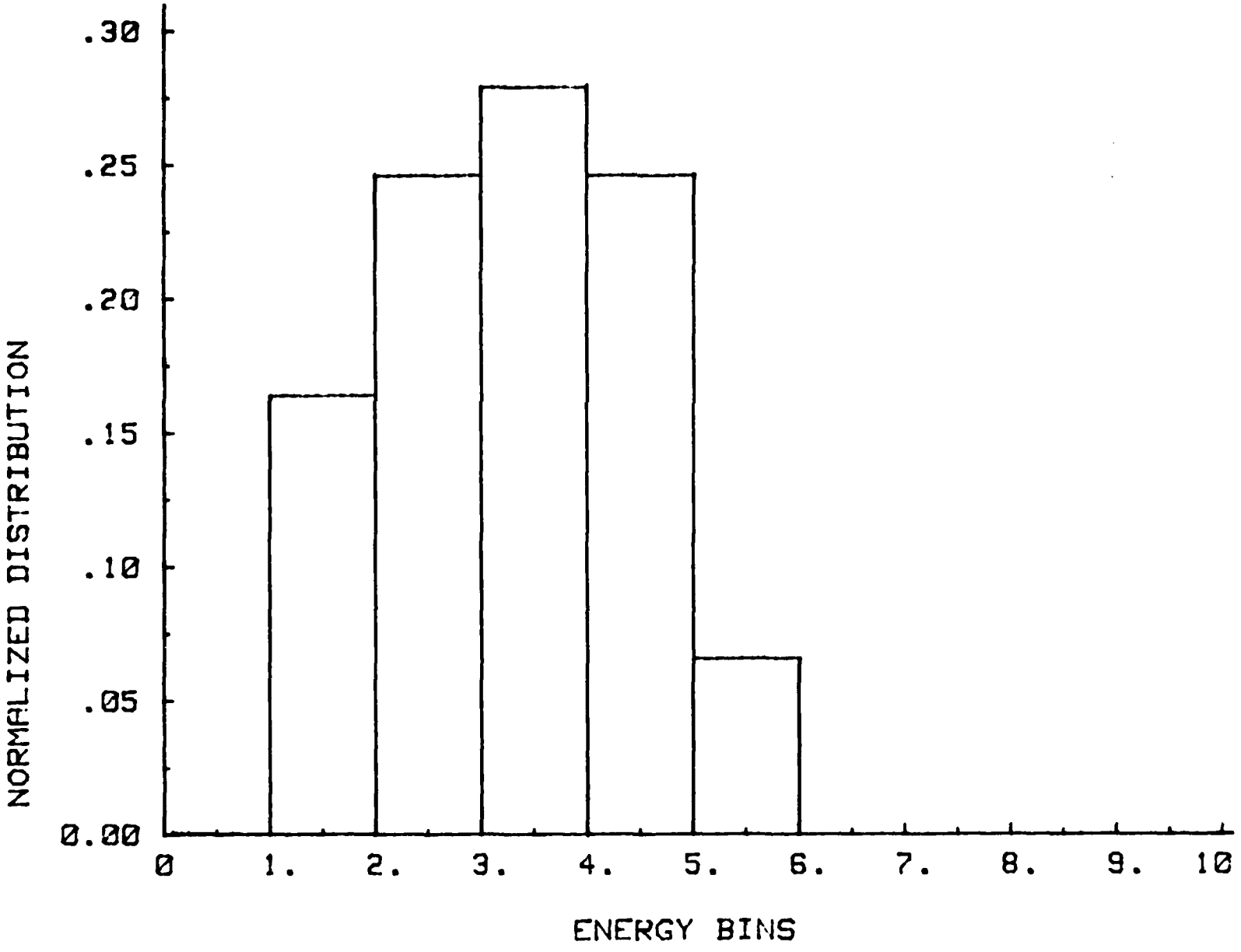

FIG C-1 ELECTRON ENERGY DISTRIBUTION AT THE CATHODE

sections in the calculations are the ionization cross sections of the rare gases. This cross section determines how quickly the electrons multiply, and thus directly effects n_e and dE/dx in Poisson's equation. For the rare gases, the ionization cross section was obtained from measurements by Rapp et al. (ref 75) over the complete range. The ionization cross section for HCl had to be extended above 100eV. Since HCl was used in small concentrations and the mean electron energy in the HCl mixtures was always less than 87 eV, any error in the approximation should be negligible. More specifically the peak electron mean energy ranged in He mixtures from 59eV to 99eV in pure He, for Ar mixtures it ranged from 20.5eV to 21.eV, and for Xe mixtures it ranged from 25.4eV to 25.9eV.

The six cross sections used to model the electron kinetics in He are plotted in Fig C-2. The threshold and references for each range are listed in Table C-3 below. The electronic cross sections were extended using the formulas listed under the reference column.

The cross section for Ar are plotted in Fig C-3 and the references and thresholds are given in Table C-4. The three electronic cross sections were derived using a standard technique of backing out cross section from transport data using a code which solves the equilibrium Boltzmann equation. Ratios between these cross sections were obtained from data of Eggarter (ref 41)), Ganas, etal (ref 44), and Chutjan (ref 28). Keeping the ratios constant, the sum of the three cross sections was then varied and the predicted electron drift velocity and Townsend ionization rate were compared with transport data listed in Dutton (ref 39) and Specht, et al. (ref 83). Up to 20eV, the agreement with transport data is within 9% and the total electronic cross section

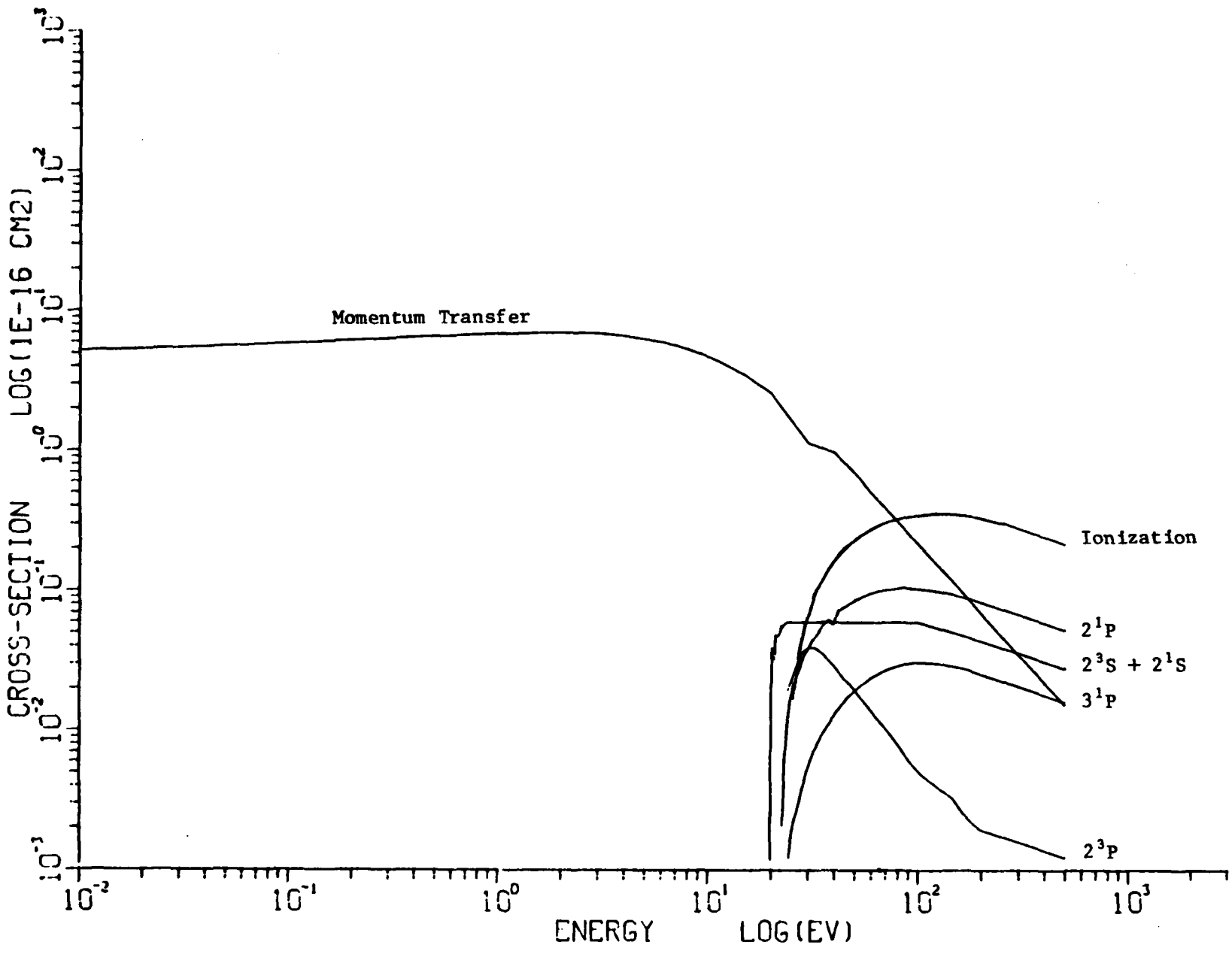

FIG C-2 ELECTRON IMPACT CROSS SECTIONS IN He

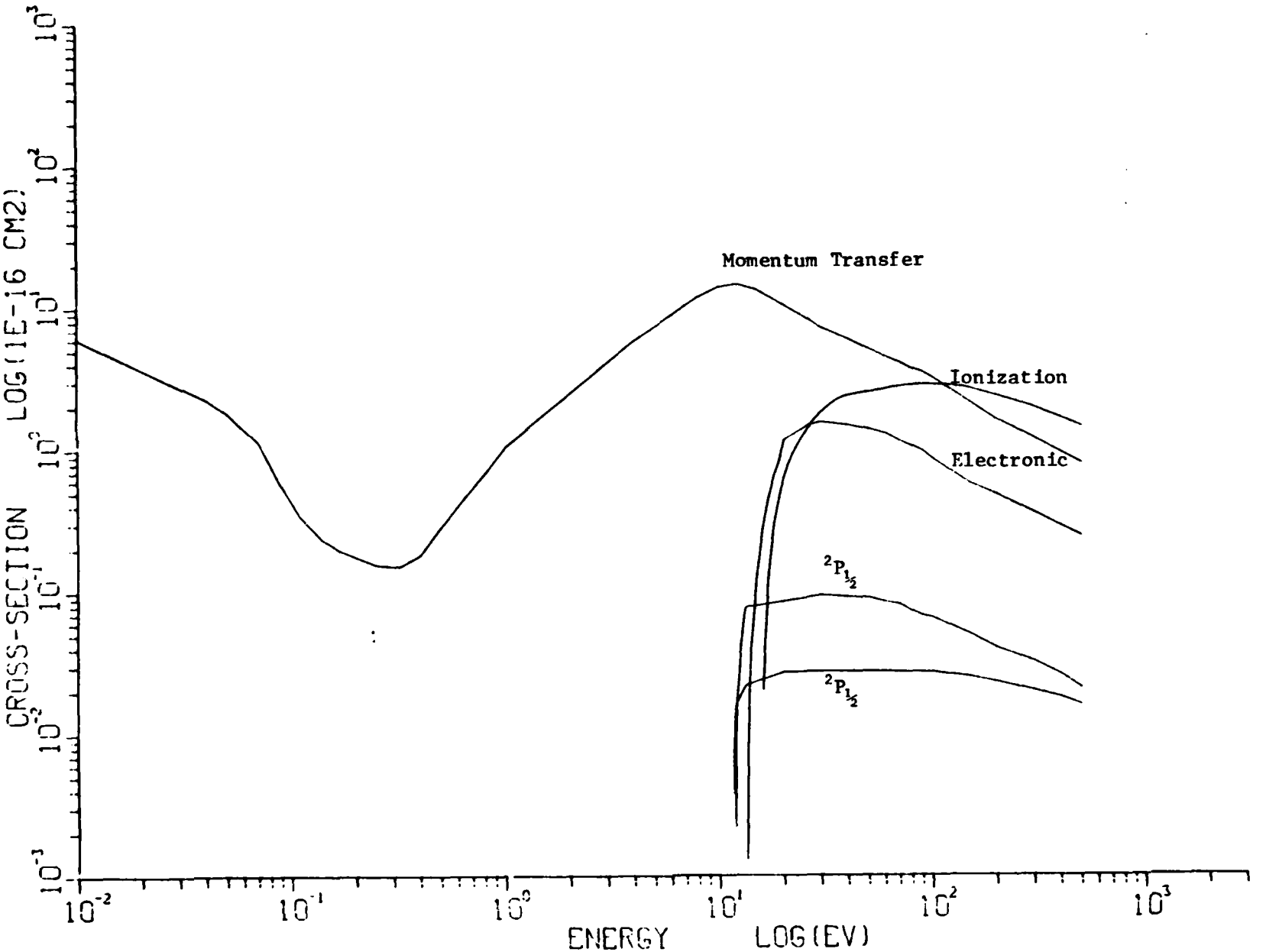

FIG C-3 ELECTRON IMPACT CROSS SECTIONS IN Ar

Table C-3

Electron Impact Cross Sections in He

Process	Threshold (eV)	Range (eV)	References
Momentum Transfer	0.	0.-6. 6.-500.	Kieffer (ref 54) Hayashi (ref 48)
Electronic			
$2^3S + 2^1S$	19.805	0.-23.54 24.-100 100.-500.	Kieffer (ref 54) Constant $\sigma = .624/\epsilon^{\frac{1}{2}}$
2^3P	20.949	0.-199.6 200.-500.	Kieffer (ref 54) $\sigma = .02755/\epsilon^{\frac{1}{2}}$
2^1P	21.203	0.-196.1 200.-500.	Kieffer (ref 54) $\sigma = 1.179/\epsilon^{\frac{1}{2}}$
3^1P	23.071	0.-207.8 210.-500.	Kieffer (ref 54) $\sigma = .3605/\epsilon^{\frac{1}{2}}$
Ionization	24.586	0.-500.	Rapp, et al. (ref 75)

Table C-4

Electron Impact Cross Sections in Ar

Process	Threshold (eV)	Range (eV)	Reference
Momentum Transfer	0.	0.-30. 30.-500.	Kieffer (ref 54) Long (ref 60)
Electronic			
$^2P_{3/2}(3p^5)$	11.6	0.-500.	Derived
$^2P_{1/2}(2p^5)$	11.8	0.-500.	Derived
Remaining Electonic	13.2	0.-500.	Derived
Ionization	15.759	0.-500.	Rapp, et al. (ref 75)

agrees well with Jacob and Mangano (ref 53) up to 17eV where their cross

section stopped. The shape of the total electronic cross section for higher cross energies was obtained from de Heer, et al. (ref 35).

The cross sections for Xe are plotted in Fig C-4 and the references and thresholds are given in Table C-5. As for Ar, the electronic and a section of momentum cross section for Xe were derived by backing them out of transport data.

Table C-5

Electron Impact Cross Sections in Xe

Process	Threshold (eV)	Range (ev)	Reference
Momentum	0.	0.-6.5	Kieffer (ref 54)
Transfer		6.5-20.	Derived
		20.-500.	Hayashi (ref 48)
Excitation	8.32	0.-500.	Derived
Ionization	12.13	0.-500.	Rapp, et al. (ref 75)

The momentum transfer cross section was lowered in the region from about 6.5 to 20eV in order to get the drift velocity to agree within 20% of that measured by Huang (ref 50) and the data listed in Dutton (ref 39). Huang found that the electron mobility for fields above 4Td remained constant, given by μN = 5.5E21 molecules/(v-sec-cm)$^{\frac{1}{2}}$. The shape of the electronic cross section below 11eV was taken from Dowell's unnormalized data (ref 37). The ionization rate predicted

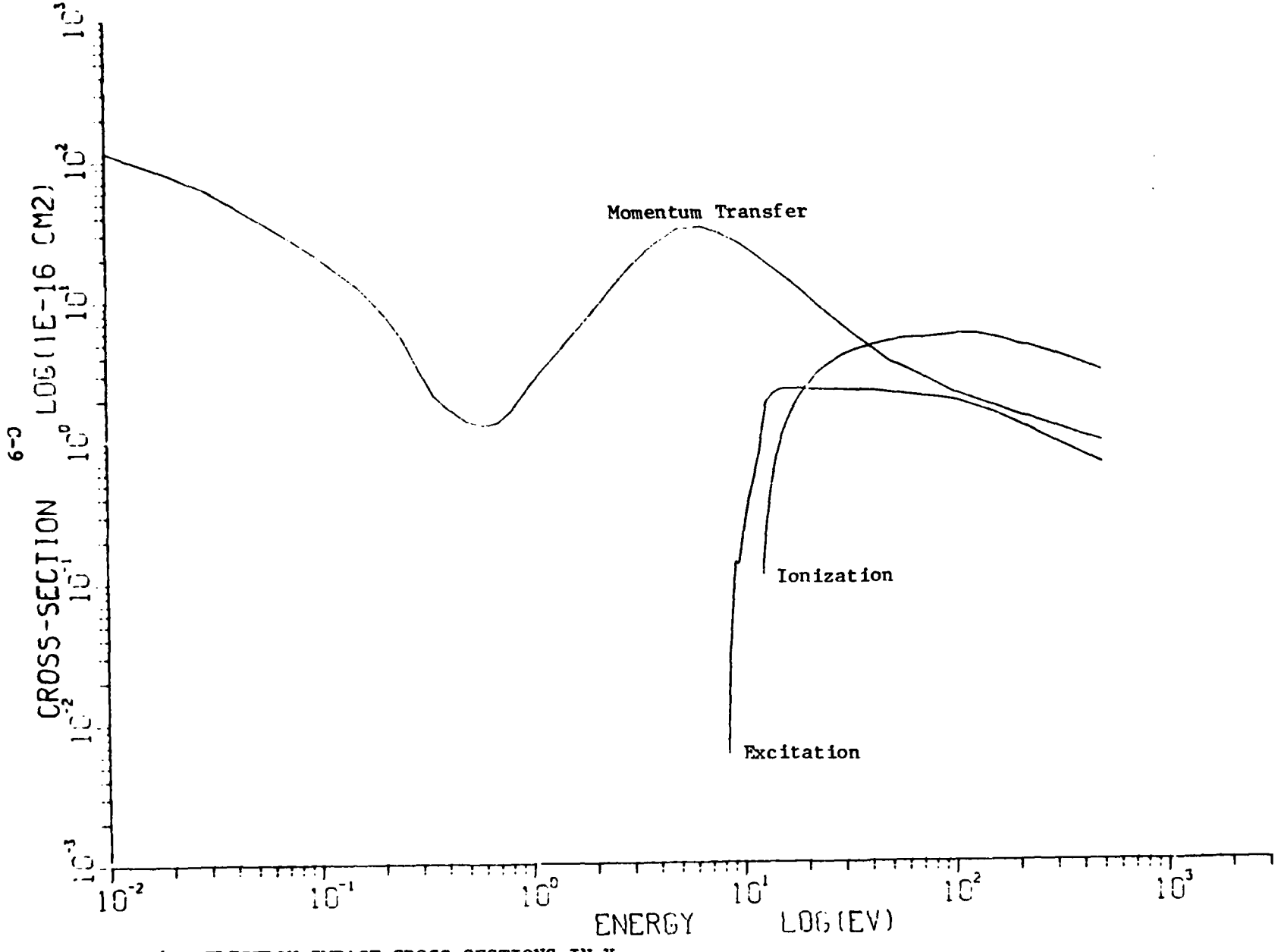

FIG C-4 ELECTRON IMPACT CROSS SECTIONS IN Xe

from the Boltzmann code agreed within 20% with the data in Dutton (ref 39) up to 60Td using this electronic cross section up to 20eV. The shape at higher energies was obtained from Ganas, et al. (ref 44) and de Heer et al. (ref 35) and normalized to the value derived for 20eV.

The cross sections for HCl are plotted in Fig C-5 and Fig C-6. The thresholds and references for each range are listed in Table C-6. The electronic cross section for the Band C state was assumed to have a peak at 100eV which is slightly less than the energy of the peak of the ionization cross section. The cross section was assumed to decrease according to the formula $\sigma = 18./\varepsilon^{\frac{1}{2}}$. The shape of the ionization cross section from Compton, et al. (ref 79) was used over the range 100-280eV and normalized to Davies' data. At higher energies the shape of the ionization cross section for O_2 (ref 75) was used which also peaks at the same energy. It was normalized to the HCl ionizaton at 280eV. This concludes the discussion of the data inputs used for the SHEATH code.

Table C-6
Electron Impact Cross Sections in HCl

Process	Threshold (eV)	Range (eV)	References
Momentum Transfer	0.	0.-100.	Davies (ref 33:45)
		100.-500.	Logrithrimic extrapolation
Vibration			
v = 1	.36	0.-7.	Davies (ref 33:46)
v = 2	.70	0.-7.2	Davies (ref 33:47)
Attachment			
Cl^-	.67	0.-2.7	Davies (ref 33:47)
H^-	5.6	0.-12.	Davies (ref 33:48)
Excitation			
A	5.5	0.-11.	Davies (ref 33:47)
B + C	9.3	0.-100.	Davies (ref 33:48)
		100.-500.	Derived
Ionization	12.74	0.-100.	Davies (ref 33:48)
		100.-500.	Derived

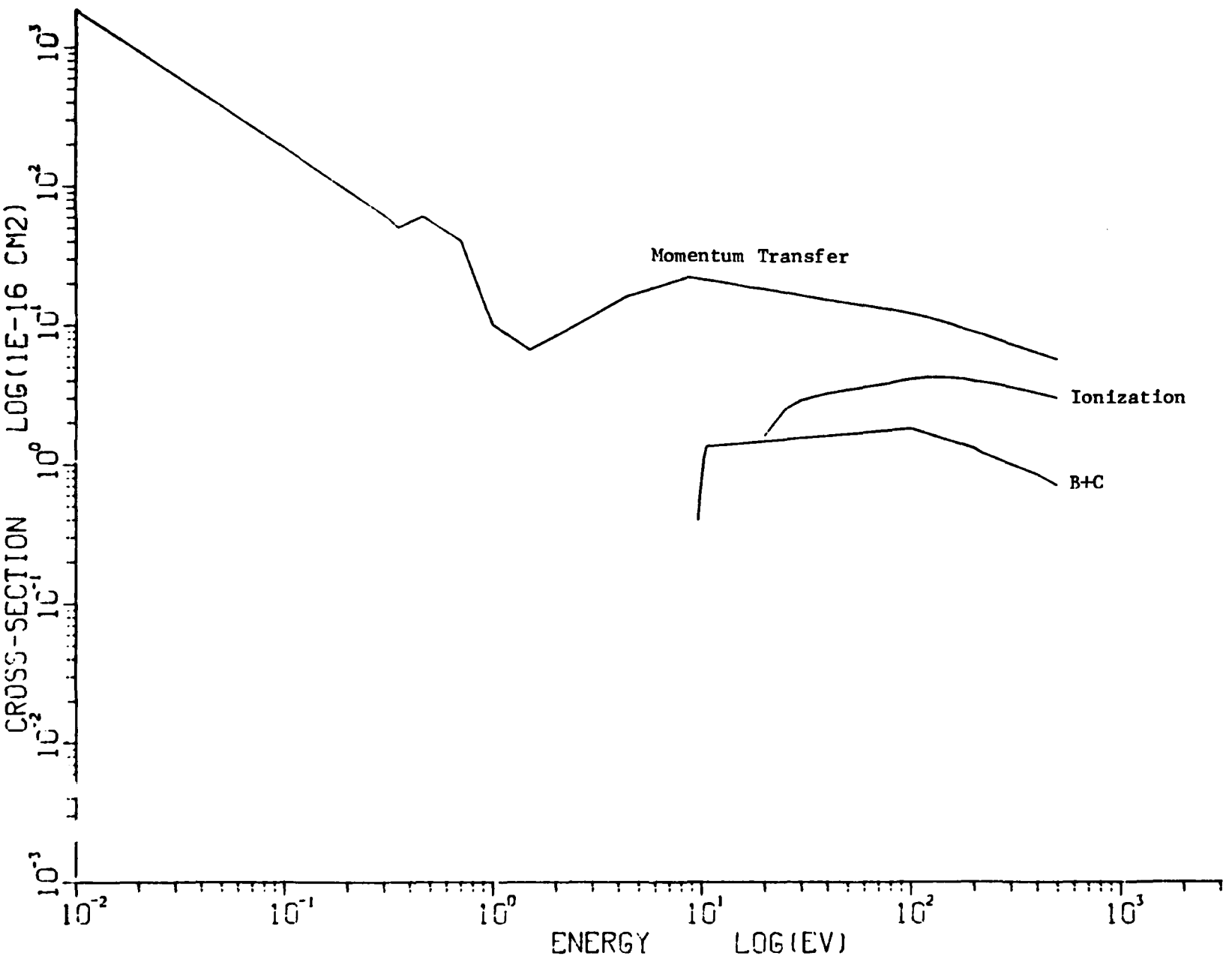

FIG C-5 HIGH ENERGY ELECTRON CROSS SECTIONS IN HC1

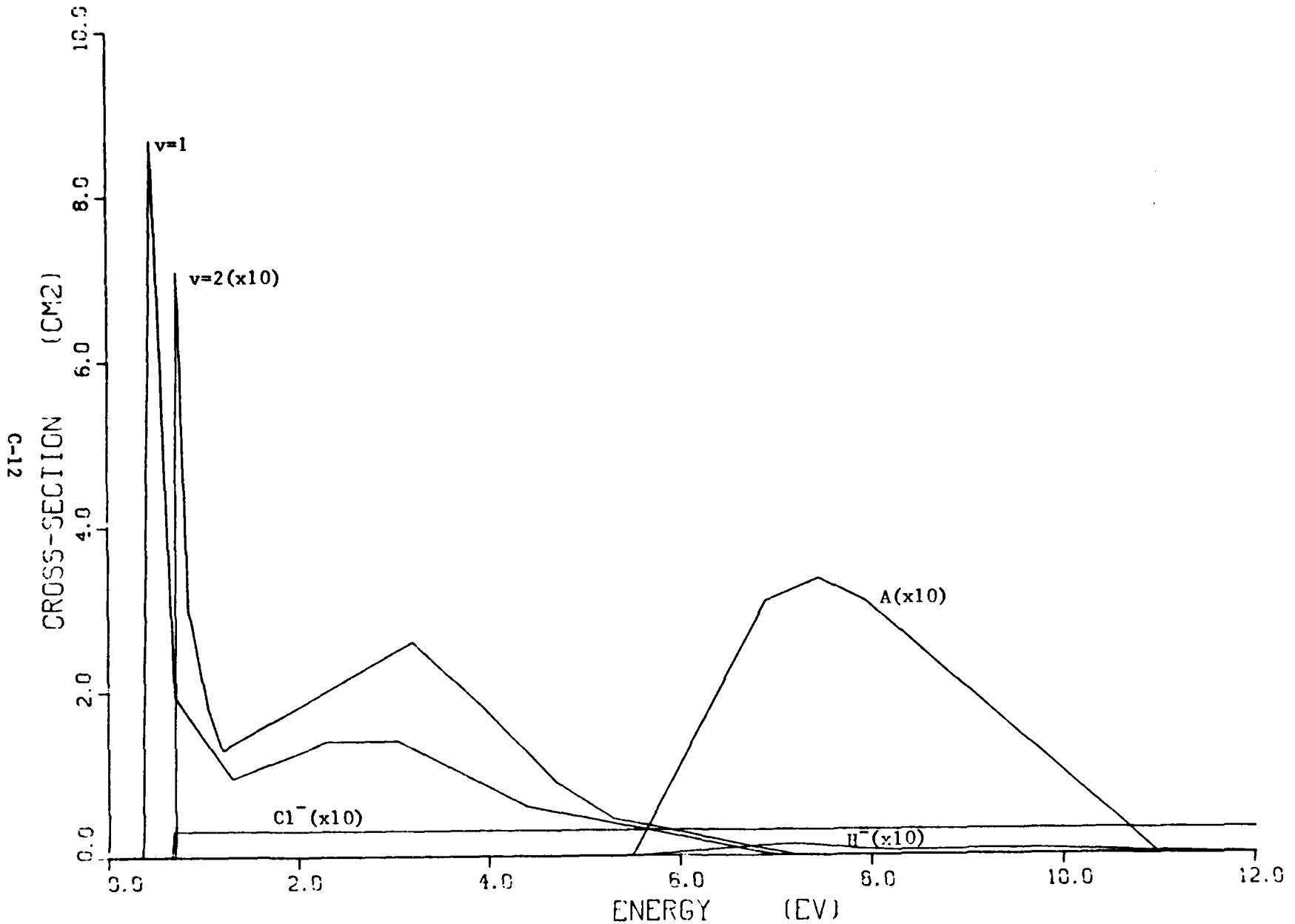

FIG C-6 LOW ENERGY ELECTRON CROSS SECTIONS IN HCl

VITA

Capt Duke was born 9 April 1949 in Canton, IL. He was raised on a farm in midwestern Illinois and graduated from Northwestern High School in 1967. He was a foreign exchange student to Sweden with the American Field Service during the summer of 1966. In 1971 he received a bachelor's degree in both physics and economics from Grinnell College and was commissioned a Second Lieutenant through the Air Force Reserve Officers' Training Corps. He obtained an educational delay and attended the University of Missouri-Rolla and received a Master of Science degree in physics in 1973. In August 1973 he was assigned to the 4000th Aerospace Applications Group (SAC) at Offutt AFB, Omaha, NE. Initially as group system controller, he commanded and controlled the realtime operations of Air Force weather satellites (DMSP). Later, as group mission planner, he developed, produced, and distributed operational messages for the command and control of weather satellites through a computer network.

Capt Duke attended the Air Force Institute of Technology from July 1977 to July 1980. After completing the course requirements for a doctoral degree in physics, he was assigned as the Technical Area Manager of the Plasma Physics Group in the Aero Propulsion Laboratory. He assumed his present duties as Executive Officer of the Aero Propulsion Laboratory in November 1982 and also completed the requirements for his doctoral degree.

Capt Duke is married to the former Mary Wenski of Kansas City, MO. They have two sons, Brian and Eric.

Permanent address: 7199 Chadbourne Drive

Dayton, Ohio 45424

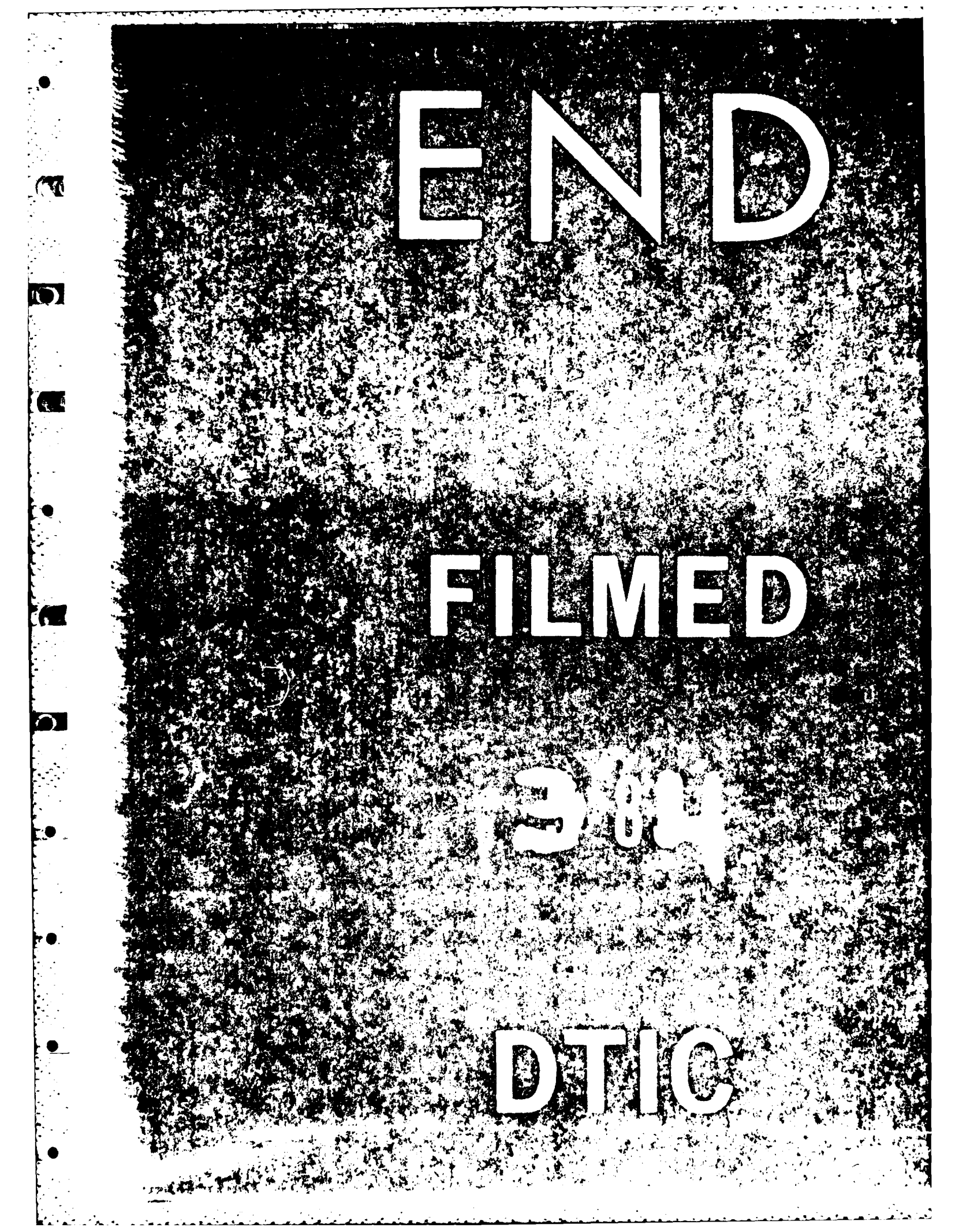
END
FILMED
3-84
DTIC